

Alma Mater Studiorum – *Università di Bologna*

DOTTORATO DI RICERCA IN SCIENZE VETERINARIE

Ciclo XXXIII

Settore Concorsuale: 07/H1

Settore Scientifico Disciplinare: VET01

*A preclinical study of spinal cord injury focused on cellular
and molecular modifications as potential targets for
innovative therapies*

*Presentata da: **Andrea Bighinati***

Coordinatore Dottorato
Prof. Arcangelo Gentile

Supervisore
Prof.ssa Luciana Giardino

Co-supervisore
Prof.ssa Laura Calzà

Esame finale anno 2021

Index

LIST OF ABBREVIATIONS.....	1
ABSTRACT	2
1. INTRODUCTION	4
1.1. THE SPINAL CORD	5
1.1.1. Spinal cord anatomy in human	7
1.1.2. Spinal cord anatomy in quadrupeds: cat and laboratory rodents	32
1.2. SPINAL CORD INJURY IN HUMAN MEDICINE	38
1.2.1. Etiology and epidemiology.....	38
1.2.2. SCI symptoms and clinical classification	39
1.3. SPINAL CORD INJURY IN VETERINARY MEDICINE.....	43
1.4. SPINAL CORD INJURY PATHOPHYSIOLOGY.....	45
1.4.1. Vascular disruption	47
1.4.2. Ion unbalance and oxidative stress.....	47
1.4.3. Metabolic collapse	48
1.4.4. Glutamate excitotoxicity.....	49
1.4.5. Inflammation	50
1.4.6. Phagocytosis activation	54
1.4.7. Cell death	55
1.4.8. Astrogliosis.....	57
1.4.9. Demyelination and remyelination.....	60
1.4.10. Other endogenous repair attempts	62
1.4.11. Chronic SCI	63
1.5. SCI THERAPIES	63
2. AIM OF THE THESIS	67
3. MATERIALS AND METHODS	70
3.1. ANIMALS AND SURGERY	71
3.1.1. Scaffold implantation.....	72
3.1.2. PRV injections.....	73
3.2. SCAFFOLDS PREPARATION	73
3.2.1. Materials.....	74
3.2.2. Scaffold characterization	74
3.2.3. In vitro drug release	74
3.3. LOCOMOTION ANALYSIS	74
3.3.1. BBB scale.....	74

3.3.2.	<i>Catwalk</i>	75
3.4.	CELL CULTURE EXPERIMENTS	75
3.4.1.	<i>Primary neural stem cells-derived OPCs</i>	76
3.4.2.	<i>Conditioned medium preparation</i>	76
3.4.3.	<i>Cytokine assay</i>	77
3.5.	FLOW CYTOMETRY	77
3.6.	SYNAPTOSOME PREPARATION, GLUTAMATE, AND GABA ASSAY.	77
3.7.	RT-PCR ANALYSIS	78
3.8.	WESTERN BLOT	80
3.9.	BIOINFORMATIC DATA ANALYSIS	81
3.10.	HISTOLOGY	82
3.11.	IMMUNOFLUORESCENCE	83
3.12.	IN-SITU HYBRIDIZATION	84
3.13.	STATISTICAL ANALYSIS	85
4.	RESULTS	92
4.1.	OUTLINE OF THE PRESENTED RESULTS	93
4.2.	CHARACTERIZATION OF THE SCI ANIMAL MODEL	101
4.3.	PRV TRACING IN THE CNS: THE EFFECT OF THE VIRUS ON MRNA TRANSCRIPTION AND PROCESSING IN THE INFECTED NEURONS	112
4.4.	TIME-COURSE CHANGES OF EXTRACELLULAR MATRIX ENCODING GENES IN THE SPINAL CORD FOLLOWING CONTUSION INJURY: A DATA-DRIVEN APPROACH	129
4.5.	A TIME-COURSE STUDY OF THE EXPRESSION LEVELS OF SYNAPTIC PLASTICITY-ASSOCIATED GENES IN A RAT MODEL OF SPINAL CORD INJURY: FOCUS ON UNLIONED BRAIN AND SPINAL CORD AREAS	150
4.6.	IMPROVED FUNCTIONAL RECOVERY IN RAT SPINAL CORD INJURY INDUCED BY A DRUG COMBINATION ADMINISTERED WITH AN IMPLANTABLE POLYMERIC DELIVERY SYSTEM	171
4.7.	WHITE MATTER AND NEUROPROTECTION IN ALZHEIMER'S DEMENTIA	184
4.8.	NGF AND ENDOGENOUS REGENERATION: FROM EMBRYOLOGY TOWARD THERAPIES	199
5.	GENERAL CONCLUSIONS	223
	REFERENCES	225

LIST OF ABBREVIATIONS

CNS	<i>Central Nervous System</i>
SC	<i>Spinal Cord</i>
SCI	<i>Spinal Cord Injury</i>
BSCB	<i>Blood Spinal Cord Barrier</i>
OPCs	<i>Oligodendrocytes Precursor Cells</i>
OLs	<i>Oligodendrocytes</i>
MDM	<i>Monocytes-Derived Macrophages</i>
ROS	<i>Reactive Oxygen Species</i>
GFAP	<i>Glial Fibrillary Acidic Protein</i>
NGF	<i>Nerve Growth Factor</i>
DPL	<i>Days Post Lesion</i>
BBB	<i>Basso, Beattie & Bresnahan Score</i>
PRV	<i>Pseudorabies Virus</i>
PLLA	<i>Poly(L-lactide) Acid</i>
Ibu	<i>Ibuprofen</i>
T3	<i>Triiodothyronine</i>

ABSTRACT

Spinal Cord Injury (SCI) is a devastating condition for human and animal health. It is mainly caused by traumatic damage to the spinal cord that leads to the deafferentation of the spinal structure below the lesion site and the formation of a glial scar in the highly specialized central nervous system tissue. Moreover, spinal lesions are very heterogeneous, with various grades of inability after the primary damage. The primary level of the injury initially causes this high level of variability in the spinal cord, which dictates the patients' functional inability. Besides, the lesion is rapidly evolving in the week following the initial trauma; particularly, the activation of a robust inflammatory response causes the amplification of cellular damage and cytotoxic products' release. The secondary cascade of SCI can be divided into immediate, acute, sub-acute, and chronic phases, each fundamental in determining the final extension of the spinal cord lesion and the level of patient inability. Typically, the immediate and acute phases are characterized by a substantial elevation in cellular death caused by the initial traumatic damage and the release of excitotoxic neurotransmitters and Reactive Oxygen Species. During the sub-acute and chronic phases, the inflammation response and astrogliosis act as the primary obstacle to tissue repair and regeneration. In particular, neurons, oligodendrocytes precursor cells, and mature oligodendrocytes are highly vulnerable to the toxic microenvironment after the SCI and susceptible to the elevated levels of noxious stimuli. These modifications hence, cause the death by necrosis and apoptosis of these vulnerable cells, leading to an expansion of the lesion to the surrounding unlesioned tissue with a significant impact on the neuronal conduction. In particular, oligodendrocytes' death leaves many unmyelinated fibers in the spinal cord slowing or blocking the conduction of information from or to the brain. The creation of an astrocytic barrier around the primary lesion site blocks the regenerative attempt neuronal regrowth and creates a physical barrier for all the cells in the lesioned microenvironment. Among these cells, the oligodendrocytes' precursors cells typically maintain myelin's homeostasis in the CNS and respond to damage differentiating in myelinating oligodendrocytes. The presence of a glial scar and the ECM composition modifications lead the oligodendrocytes precursor cells to a block of differentiation and the mature oligodendrocytes to a loss of functional myelinating capacity. Thus the regenerative response of the organism in case of SCI is significantly reduced, and only little spontaneous amelioration is observed in spinal lesioned patients during the early phases of the pathology.

This work mainly focuses on studying and characterizing the modification induced by the SCI in a preclinical animal model. We investigated the ECM composition in the spinal cord segments surrounding the primary lesion site at a gene expression level. The primary aim was to identify crucial genes participating in the onset of the secondary degeneration cascade in the spinal cord segments

not directly involved in the primary lesion. We found Timp1 and CD44 as a crucial hub in the secondary cascade of SCI in both spinal cord segments surrounding the lesion site. Interestingly, a temporal and anatomical difference in gene expression, indicating a complex regulation of ECM genes after SCI that could be used as a tool for regenerative medicine.

We also investigated the modification in synaptic plasticity-related gene expression in spinal and supraspinal areas involved in motor control. We confirmed the anatomical and temporal difference in gene expression in spinal cord tissue and identified the motor cortex as the area more invested by the lesion-related modifications. This analysis suggests that a molecular mapping of the lesion-induced modification could be a useful tool for regenerative medicine.

In the last part, we evaluated the efficacy of an implantable biopolymer loaded with an anti-inflammatory drug and a pro-myelinating agent on the acute phase of SCI in our preclinical model. We found a consistent reduction of the inflammatory state in the spinal lesion site and the cord's surrounding segments. Moreover, we found increased preservation of the spinal cord tissue with a related upregulation of neuronal and oligodendroglial markers after lesion. Our treatment showed effective ameliorating functional outcome and reducing the lesion extension in the chronic phase. This proof of concept study investigated in a preclinical model of SCI the efficacy of novel treatments to target specifically the acute phase of the lesion and reduce the alteration induced by the secondary cascade.

1. INTRODUCTION

1.1. The Spinal Cord

The spinal cord anatomy is described in humans, in the cat because of the wide use of this specie in neurophysiology and neuroanatomy studies that provided the basic principles of spinal cord functional anatomy, and rat, the laboratory animal species used for the experimental part of this thesis.

The spinal cord's general characteristics are shared between the phylum of vertebrates, but the length, some structure, the specific neuronal composition, and nomenclature differ between different species. The spinal cord is hosted in the vertebral canal, formed by repeated bone structures called vertebrae, derived from the paraxial mesoderm that gives origin to the sclerotome structure in embryo ¹. During embryogenesis and under the influence of segmentation and homeotic genes, the vertebral column acquires specific regionalization depending on the position of each vertebra along the rostrocaudal axis of the body: cervical, thoracic, lumbar, sacral, and coccygeal having different shapes and characteristics ¹. During embryogenesis, the vertebral column organization, such as of the other parts of the central nervous system, is dictated by the expression of different Hox genes along the rostrocaudal axis, a pattern of gene expression known as "Hox Code" ². The vertebral column's axial domain shows a high variation in the number of the vertebrae for each domain among vertebrate taxa, and each species has its axial formula that defines the composition of the vertebral column ¹.

The spinal cord is the anatomical part of the body that allows the conduction of sensory and proprioceptive information from the body's periphery to the central nervous system, transferring inputs from the brain to the periphery in the form of motor actions. Moreover, it allows maintaining the organism's body homeostasis, the appropriate reaction to sensory stimuli from the surrounding environment, and voluntary movement. The spinal cord is generally described as a continuous ovoidal/cylindrical shape tube extending from the medulla oblongata. The cord's most caudal part is named *conus medullaris* and extends as *filum terminale*, mainly composed of glia, nerve fibers, and ependymal cells. The spinal cord comprises a sequence of segmental components laterally delimited by the emergence of spinal nerve ^{3,4}. The spinal cord is a symmetric structure, defined by two median fissures, one in the dorsal part, called *dorsal median fissure*, and the other in the ventral part of the cord and called *ventral median fissure*, where the pia makes a double fold between the two parts. In the dorsal part of the cord are presents two minor sulci, named *dorsal intermediate sulcus*, that indicates two white matter pathways, the *fasciculus gracilis* running between the *dorsal median fissure* and the *dorsal intermediate sulcus*, and the *fasciculus cuneatus* located between the *dorsal intermediate sulcus* and the *dorsolateral sulcus* ^{3,4}.

The spinal cord's primary anatomical division is between the external white matter, composed mainly of axons and glial cells forming the axon-myelin unit ⁵. The internal gray matter is formed principally by neuron cell bodies, glial cells, and in a minor percentage of poorly myelinated axons. The gray matter in the spinal cord is an H-shaped (sometimes referred also as "butterfly structure"), symmetric structure and is divided into ventral and dorsal horns. The central canal is located at the center of the gray matter and is filled with cerebrospinal fluid and direct continuity with the brain's fourth ventricle. This canal is encircled first by a layer of ependymal cells and then by the second layer of glial cells called *substantia gliosa* ^{3,4}. The gray matter is classically distinct in a ventral (ventral horn) and a dorsal (dorsal horn) part. In the ventral horn resides the cell body of motoneurons (alpha- and gamma-motoneurons) innervating muscles. These motoneurons are somatotopically organized, which means that the neurons controlling the axial and trunk muscles are placed more medially, whereas neurons innervating limbs are located laterally. Moreover, the motoneurons innervating the limb's proximal part are located medially from motoneurons innervating the distal parts of the limbs ⁶. Extensor and flexor motoneurons also show a somatotopic distribution, with extensor motoneurons placed more ventrally and flexor motoneurons located more dorsally in the ventral horns ^{3,4}.

The white matter is organized in the ventral, dorsal, and two lateral columns or funiculi divided by the internal gray matter. The tracts of white matter near the median fissures are called ventral and dorsal commissure and contain crossing fibers (decussation). The white matter region near the dorsal horns and in direct contact with the pial surface is the *dorsolateral fasciculus* (tract of Lissauer). In this tract are located primary afferent fibers which ascend or descend the spinal cord for a few segments before entering the dorsal horns. The dorsal column in the spinal cord enlarges through the rostrocaudal axis due to the increase of the central process of dorsal root ganglion cell transmitting sensory information from the periphery. The fibers from the more caudal structures (sacral, lumbar, and lower thoracic ganglia afferents) are located more medially in the dorsal column, whereas fibers from the rostral structures (high thoracic and cervical ganglia afferents) are located more laterally. The lateral and the ventral column of the white matter contains almost all the ascending and descending pathways of the spinal cord and the propriospinal system of the cord. The principal ascending tracts include the spinothalamic, spinocerebellar, and spinotectal tract and their functions are to transmit inputs from the periphery to the appropriate region of the brain. The descending tracts are the corticospinal, vestibulospinal, tectospinal, and reticulospinal tracts. The descending tracts are mainly involved in locomotor and reflex pathways. The proportion between white and gray matter is not constant through all the length of the spinal cord but vary in the different segments, having a higher quantity of white matter in the thoracic and sacral segments,

while in the cervical and lumbar segments, especially in enlargements, the percentage of white matter compared to gray matter is inferior^{3,4}.

1.1.1. Spinal cord anatomy in human

In humans, vertebrae numbers along the vertebral column are 7 cervicals, 12 thoracics, 5 lumbar, 5 sacral, and 4 coccygeal. All vertebrae share a typical structural pattern composed of the body of the vertebra, a dorsal arch, and the lateral process (pedicles and laminae) which connect these two structures; at the dorsalmost portion, each vertebra has its spinal process, which is peculiar for the respective spinal level (Fig. 1). This conformation forms a central cavity defined *spinal canal* where the spinal cord is physically protected. The thoracic vertebrae have one particular structure called *costal facet* situated lateral to the vertebral body that allows the protrusion of the rib from the vertebral column⁷. In humans and other bipedal species (avian) at the sacral level, a structure called *sacrum* is formed by the fusion of five vertebrae. This structure has a wide-body curved shape and a triangular foramen with the ventral (pelvic) surface concave. The foramen on the ventral surface are oriented in an anterolateral direction and allow the sacral nerve and arteries' passage. The sacrum's dorsal surface is convex and has a crest formed by the fused spinous processes in the middle. The *sacrum* is in direct contact with the L5 vertebra above and the *coccyx* below. It also contacts the iliac bone at its sides and articulates with it through the *sacroiliac joint*. In humans, the vertebral canal terminates with a peculiar structure called the *coccyx*, composed of three to five triangular rudimental vertebrae fused. The *coccyx* is the residual of the tail structure from the ancestor animal reabsorbed during the embryo development. All coccygeal vertebrae lack spinous processes, and only the first three coccygeal vertebrae have a short transverse process. The last coccygeal vertebra is a mere nodule of bone.

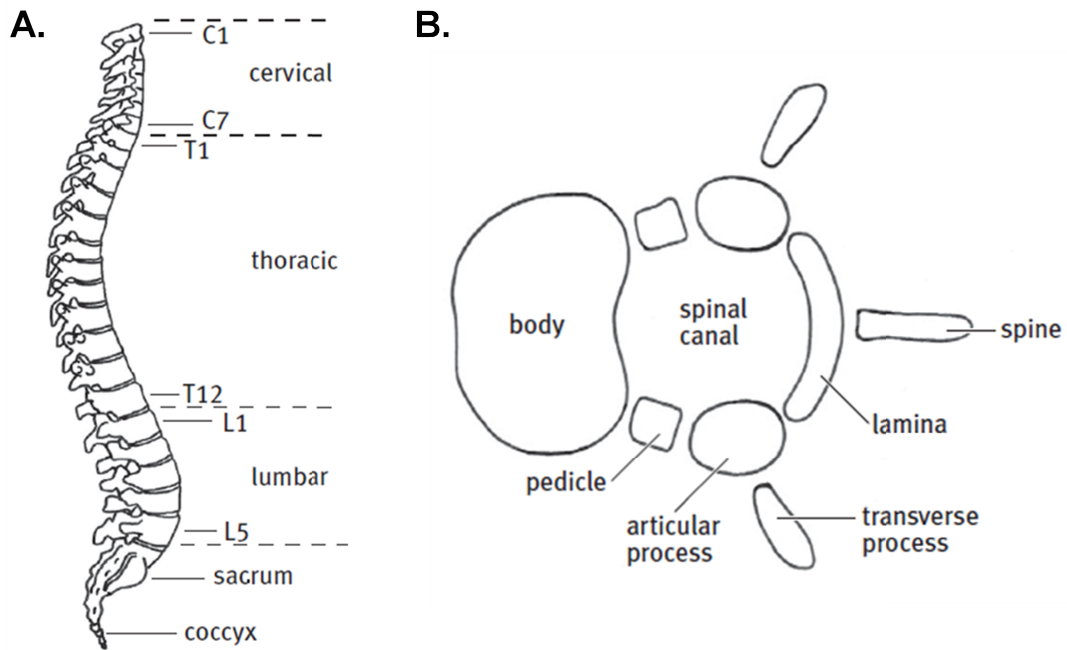


Fig. 1: Structure of the vertebral column. Panel A illustrates the entire vertebral column in the human. Panel B illustrates the structure of a single vertebra. Image from ⁸.

Each vertebra is linked to the next by a structure called an *intervertebral disc*, a fibrocartilaginous structure that prevents the two adjacent vertebrae from rubbing and damaging the respective body. The *intervertebral disc* comprises two parts; the external called *anulus fibrosus* that anchors the two bodies of the vertebrae, and an inner part called *nucleus pulposus*, which has a gel-like consistency resisting compression in weight lifting maneuver and during extension or torsion of the back.

The vertebral column organization is finally fixed by the ligaments that keep all the vertebrae in line with the surrounding. There are three main medial ligaments designed to limit the extension of movement of the vertebral column. The *anterior longitudinal ligament* is in the anterior (ventral) side of the column and, together with the *posterior longitudinal ligament*, located on the posterior (dorsal) side of the column, protect the vertebrae from hyperextension movements. The last ligament is the *supraspinous ligament*, which runs upon each vertebra's spinous process and grants resistance during forwarding bending movements together with intervertebral ligaments named *ligamentum flavum* (from their yellow color) ^{6,9}. The *lateral spinal ligaments* are present only in human and in bipedal avian species and are fundamental for maintaining the erect posture.

The spinal cord is wrapped in three layers of meningeal sheets covering the cord's entire length and protecting the rootlets of the ganglia entering the spinal cord (Fig. 2). The most external meninge called *dura mater* is the most resistant of the three and envelopes the ganglionic and root ganglia extending from the spinal cord. The dura layer is separated from the spinal canal by the *subdural space*, which is virtual in physiological conditions ^{6,10}. The *arachnoid* and the *pia mater* are the sheets

underneath the dura mater. Together, they are called leptomeninges, and the subarachnoid space containing the cerebrospinal fluids between them ¹⁰.

The blood to the meninges and the spinal cord is supplied mainly by two *posterior spinal arteries (PSA)* and one *anterior spinal artery (ASA)*. Their ramification at the intervertebral foramen creates the segmental spinal arteries, which fed blood to the ganglion and root nerves. The blood drainage is carried mainly by two veins, one posterior and one anterior to the spinal cord (Fig. 4) ¹¹.

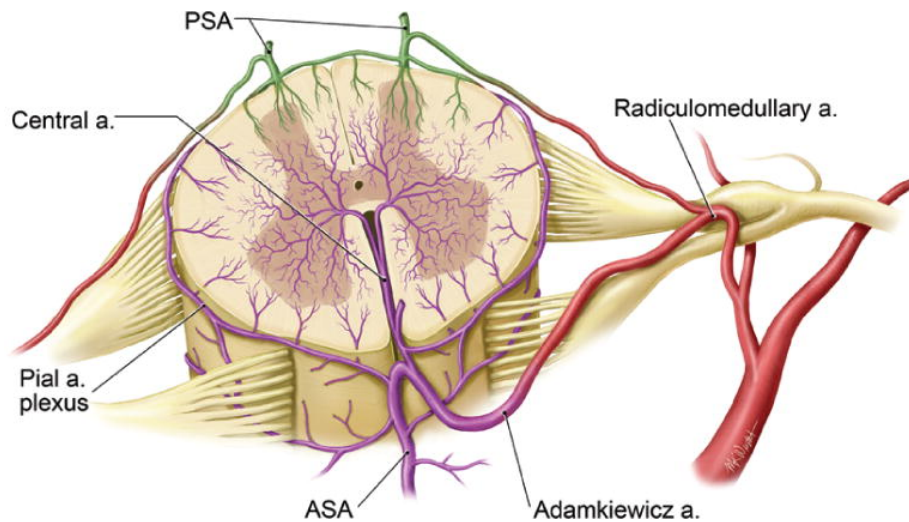


Fig. 2: Anatomical representation of the arterial and venal drainage in the spinal cord. Abbreviations: PSA, Posterior Spinal Artery; ASA, Anterior Spinal Artery. Image from ¹².

In humans, the spinal cord extends until the first lumbar vertebra; thus, the spinal cord's total length is shorter than the vertebral canal's length. At L2, a single sacral nerve forms the *cauda equina*. The length of the spinal cord in humans is 43-45 cm in males and 42-43 cm in females ³. The spinal cord is divided into 8 cervicals, 12 thoracics, 5 lumbar, 5 sacral, and 1 coccygeal segment, which sends a total of 31 pairs of nerve roots from the spinal cord to the periphery of the body. Except for the C1 spinal nerve, which lacks the sensory component, all other spinal nerves are composed of pairs of afferent, sensory (dorsal) and efferent, motor (ventral) nerves ³. Generally, each spinal cord segment corresponds to its vertebral process, except for C8, which lacks a corresponding vertebra. Hence the spinal nerves in the cervical region exit from the spinal cord above the corresponding vertebrae, and C8 exit above the T1 vertebra. From level T1, the spinal nerve exit route from the spinal cord is below the corresponding vertebrae. Due to the shortened length of the spinal cord with respect to the vertebral column, the spinal level and the vertebral level are not associated. Therefore the spinal nerve starting from the lumbar level of the spinal cord has to travel more distance to exit in correspondence of their vertebral process, forming the cauda equina structure (Fig. 3) ³.

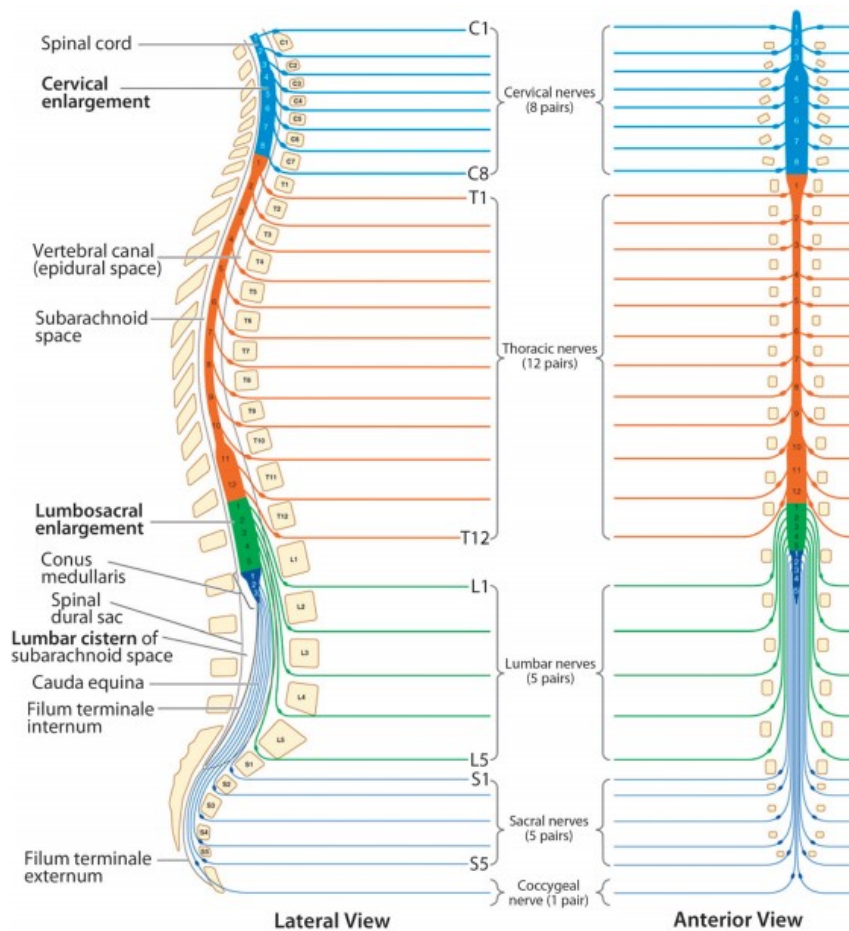


Fig. 3: Representation of the spinal cord's lateral and anterior view with the vertebral column (light orange squares). Light blue represents the cervical, orange represents the thoracic, and dark blue coccygeal tracts of the spinal cord. Image adapted from ⁶.

Spinal cords receive inputs from peripheral structures (skin, subcutaneous tissues, and viscera) through the dorsal nerve roots, fixed to the dorsolateral sulcus of the cord by a series of rootlets in line. This structure is called the *dorsal root entry zone (DREZ)* and contains from 6 to 8 rootlets for a length of 10 to 12 mm. The cell bodies of these sensory neurons lie in the dorsal root ganglia (DRGs), an enlarged and oval structure outside the spinal cord and within the intervertebral foramina ³. DRGs are larger in cervical segments of the spinal cord, then decrease in the thoracic segments. In the lumbar segments, the dimension of ganglia increases and decrease newly from S1 levels. S2, S3, and coccygeal DRGs are found within the vertebral canal and sometimes in the form of scattered nerve cells rather than DRG ³.

The neurons located in the DRGs are pseudo-unipolar neurons that send an axonal branch toward the body's peripheral organs (peripheral branches) and a branch in the spinal cord (central branches). Histologically, the DRGs are divided into "small dark" and "large light" neurons based on their staining properties. The first class of neurons is poor in neurofilaments and generates nociceptive A δ and unmyelinated C fibers. Whereas the "large light" neurons are rich in

neurofilaments and send myelinated A α , A β , and A δ mechanoreceptive fibers. This different type of fibers convey different information to the Central Nervous System (CNS), in particular, “large light” neurons relays low threshold mechanical and proprioceptive stimuli, and “small dark” neurons convey high threshold stimuli ^{3,8}. Axons travel in the sensory bundle of nerves in each segment’s dorsal part and synapses on the dorsal horn neurons. The dorsal root is somatotopically organized, and the fibers with larger diameters (Ia and Ib), heavily myelinated that receive information of muscles stretch, and reflexes are in the center of the bundle. The thinly myelinated fibers A β travels medially in the bundle and transmit mechanoreception from the skin and the joints. Lastly, in the external position of the afferent spinal bundle, poorly myelinated A δ and unmyelinated C fibers are located, which receive noxious and thermal stimuli ¹⁰. As a general rule, the thick myelinated fibers project in the dorsal and ventral horns’ deep layers. The exception to this rule is represented by some thin unmyelinated fibers that project to laminae V, VII, and X. Whereas C-fibers of somatic and visceral origin typically send projection to superficial laminae in the dorsal horns (I and II). Some visceral afferent composed of small, rapidly conducting myelinated axons reach deeper laminae in the gray matter (V). Information about nociception from the skin is carried by myelinated A α and A β fibers ending in laminae I to V and thin unmyelinated C fibers ending in laminae I to III ^{3,8}.

Through the ventral root, the axons of both alpha- (extrafusal innervations) and gamma-motoneurons (intrafusal innervations) of the ventral horns exit the spinal cord and travel through the peripheral nerves until their striated, target muscle ³. The fibers of the ventral root exit from the spinal cord from an elliptical region named the *anterior root exit zone (AREZ)*. The ventral roots also contain thin autonomic unmyelinated pre-ganglionic motor fibers from the intermediolateral column within the efferent somatic motor fiber. It is estimated that 25% of the ventral root’s total fibers are unmyelinated and carry nociceptive information in humans. These unmyelinated fibers do not directly enter the spinal cord through the ventral root, but project to the CNS using the ventral root and then loop back into the dorsal root.

The spinal nerves exiting from the spinal cord are mixed fibers containing both sensory and motor neuron axons after the union of the dorsal and the ventral root. After leaving the CNS through the intervertebral foramen, spinal nerves divide in a *sinuvertebral* branch that innervates the *posterior longitudinal ligament*, the *anulus fibrosus*, the epidural blood vessel, the ventral *dura mater*, and the *dorsal vertebral periosteum*. After this first division, the spinal nerves bifurcate in a large ventral ramus and a small dorsal ramus, both composed of mixed fibers. The dorsal rami of spinal nerves supply the muscles, fascia, ligaments, and skin of the dorsal part of the body (not the limbs), is divided into a medial and a lateral branch, except for the first cervical, fourth and fifth sacral, and all the coccygeal nerves. The ventral rami of the spinal nerves supply the muscle, fascia, ligaments body’s ventrolateral part, the limbs, the *perineum*, and also contains the neurons for the skin’s

sympathetic innervation. The ventral ramus of spinal nerves also receives a *gray ramus communicans* from the associated sympathetic ganglion. The ventral rami in all mammals form plexuses and exchange fibers in the cervical, lumbar, sacral, and coccygeal regions.

The parasympathetic system's fibers originate from the neurons in the intermediolateral cell column in the sacral S2-S4 segments of the spinal cord and leave the CNS through the corresponding spinal nerves' ventral root remaining in the ventral rami. After exiting the sacral foramina, the autonomic pre-ganglionic parasympathetic nerves separate from the ventral rami to form the *splanchnic nerves* and contact the pelvic parasympathetic ganglia. Sympathetic pre-ganglionic efferent fibers originate from the same spinal cord nuclei of the parasympathetic pre-ganglionic neurons from all thoracic and the upper two or three lumbar levels of the spinal cord. The myelinated axons of these neurons leave the spinal nerves and form the white rami communicantes entering the sympathetic chain. The sympathetic chain in humans runs along the vertebral column's entire length on both sides of it. It is formed by 22 paravertebral ganglia divided into 3 cervical, 11 thoracics, 4 lumbar, and 4 sacral ^{3,8}.

The different neuron types in the spinal cord gray matter were classified according to morphological and anatomical characteristics in ten distinct laminae by Bror Rexed in the cat at the beginning of the 50s ¹³. The dorsal horn contains the laminae from I to V, whereas in the central part of the spinal cord are presents lamina VI and VII in the lateral part and lamina X around the central canal. The motoneuron pools in the ventral horns are contained in the lamina IX, placed in the ventralmost position, surrounded by lamina VIII (Table 1, Fig. 4) ¹⁴. The Rexed's spinal cord classification is useful, especially for the dorsal horns. Still, for the lateral column and the motoneuron pools, the columnar organization of neurons sharing the same functions is usually preferred (Table 1, Fig. 4) ^{9,14}. In terms of functional anatomy, dorsal horns contain cell bodies of secondary sensory neurons that receive innervations from the primary sensory neurons located in the dorsal root ganglia. Secondary neurons send axons to the spinal interneurons or loop in relay circuits to motoneurons controlling reflexes. Neurons located in lamina I-II receive axonal projection carrying information from the external surface body (temperature, touch, pain), whereas lamina V neurons receive information about proprioception or deep self-sensation and participate in muscle reflexes ⁶. The central part of the gray matter in cervical and thoracic segments until L2 contains sympathetic pre-ganglionic neurons that control the Autonomous Nervous System (ANS, sympathetic innervations of visceral organs and glands). In contrast, neurons located from S2 to S4 provides the parasympathetic innervations ¹⁰.

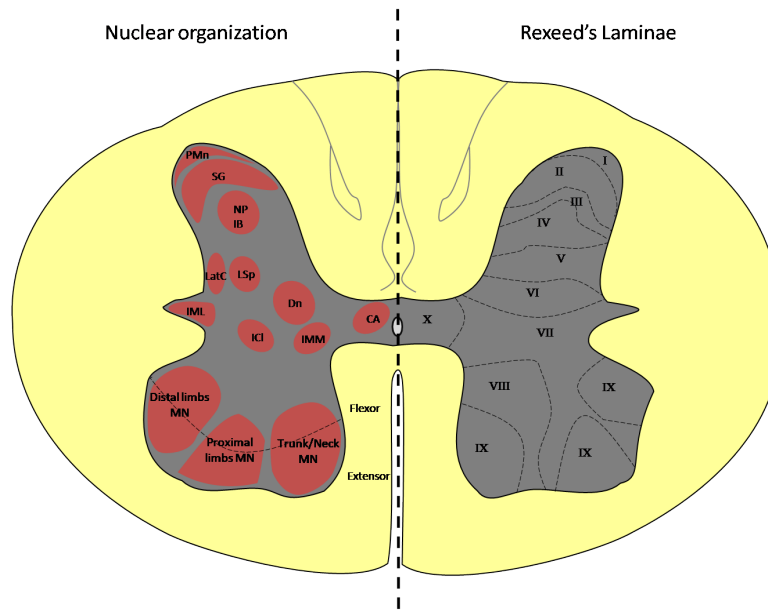


Fig. 4: the picture reports a schematic coronal representation of the human spinal cord at the lumbar level. On the right side of the picture is reported the Rexed laminae division of the gray matter. The left side reports the principal nuclei in the gray matter and their location in the laminae of Rexed. Abbreviations: PMn, Nucleus Posterior Marginalis; SG, Substantia Gelatinosa; NP, Nucleus Proprius of the posterior horns; IB, Internal Basilaris nucleus; LatC, Lateral Cervical nucleus; LSp, Lateral Spinal nucleus; Dn, Dorsal Nucleus; IML, Intermediolateral nucleus; ICI, Intercalated nucleus; IMM, Intermediomedial nucleus; CA, Central Autonomic area; MN, motoneurons.

Lamina I is the most superficial part of the dorsal horn and is also known as *nucleus posterior marginalis*. It is characterized by a reticulated structure composed of the myelinated axons penetrating this layer. This layer has a low density in neurons, and the principal cells vary in form and size. The most common type of neurons is large fusiform neurons oriented parallel (*Waldeyer cells*) and small or medium-sized neurons with scant cytoplasm. In human lamina I, are present also small multipolar neurons. The dendrites orientation is principally parallel to the surface of lamina I but are also present ventral dendrites that penetrate lamina II to IV. Neurons in lamina I respond mainly to nociception, particularly to noxious mechanical or heat stimuli and innocuous thermal stimuli. The principal fibers arriving in lamina I are C and A δ fibers from the skin, viscera, muscles, and joints via Lissauer's tract. Lamina I also receives innervations from supraspinal zones, in particular hypothalamus and brainstem, and then neurons in lamina I project to deeper laminae. This circuit is involved in the discriminative aspect of pain and temperature sensation. Neurons in lamina I also project to the contralateral brain and cross the midline before ascending. The principal targets in the brains are *lateral parabrachial area*, *nucleus accumbens* and *septal nuclei*, the *nucleus of the solitary tract*, *hypothalamus*, the *lateral reticular nucleus*, the *ventrolateral medulla*, and the *cuneiform nucleus*. Neurons in lamina I also have an intraspinal projection to intermediolateral, intermediomedial and intercalated nuclei³.

Underneath lamina I is located Lamina II, also known as *substantia gelatinosa*, for its typical translucent appearance due to lack of myelinated fibers. It is thickest compared to lamina I, and it does not have a uniform thickness, being larger in the cervical and lumbosacral enlargements. This layer's neuronal density is high and can be divided into the outer (2o) more dense and inner (2i) less dense layer based on the cell density. The neurons in this layer are small round or slightly elongated fusiform neurons extending in the rostrocaudal direction. The neuronal type can also be distinguished in islet, filamentous, curly, and stellate cells. The islet cells have a long dendritic tree with a rostrocaudal extension and did not extend their dendrites or axons outside lamina II. The filamentous cells represent 20% of the lamina II neurons and have a characteristic fine expansion of their terminal dendrites and usually extend them in a dorsoventral way. Curly cells are not so abundant in lamina II and have a circular dendrite structure extending in the sagittal plane with very few branches. The stellate cells grow their dendritic tree in all directions reaching laminae I and III.

The axons of these cells penetrate deeper laminae III and IV. Neurons in lamina II can also be divided into projecting neurons (Golgi type I) and local interneurons (Golgi type II). Most lamina II neurons project into lamina II itself. Only a few neurons project supraspinally through the dorsolateral or lateral fasciculus. Lamina II is the main site of A δ and C fibers afference carrying nociceptive information. The lamina II is topographically organized, e.g., the 2o zone receives C fibers only, whereas the 2i zone receives both C and A δ fibers. Moreover, a somatotopic organization is present with afferents from the cutaneous ventral medial line of trunk and limbs projecting to the medial part of lamina II, whereas cutaneous afferent from the dorsal median line projecting in the lateral part of this lamina. Lamina II integrates and modulates nociceptive inputs at a segmental and suprasegmental level, modulating ascending projections in the surrounding laminae. Most lamina II neurons are inhibitory interneurons containing GABA and glycine, but also excitatory interneurons are present in lamina II³.

Lamina III is surrounded laterally by lamina II and medially by the white matter. This lamina is thicker than the precedent laminae and is distinguishable from lamina II for the presence of myelinated fibers forming a longitudinal arrangement. Moreover, neurons in lamina III are larger and less dense compared to lamina II. The shape of neurons in lamina III is principally rounded or slightly elongated, and the distribution of these different neuron types is homogeneous. The lamina III neurons' dendritic trees are asymmetric, with a more pronounced development in the dorsal side, reaching lamina II and diffusing in the sagittal and transverse planes. Neurons in lamina III receive inputs principally from A β and A δ fibers from cutaneous sources and integrate these signals with the information receiving from upper laminae. The integration of proprioception information is mediated by projection in the spinocervical tract and the postsynaptic dorsal column pathway. Still, studies

have identified neurons in lamina III projecting into spinothalamic, spinohypothalamic, spinoparabrachial, and spinoreticular paths. The major part of neurons in lamina III contains GABA³.

Lamina IV is twice as thick as lamina III and is considered the head of the dorsal horn. Moreover, it is the base of the *nucleus proprius* of the dorsal horns. This lamina contains the internal basilar nucleus (IB) in the segments to C1 to C6 and the dorsal nucleus in the thoracic and upper lumbar levels. The boundaries of lamina IV are not clear but distinguishable from the surrounding laminae for a lower neuronal density and larger neurons. The neurons in this layer are principally round, triangular, or multipolar in shape. The neurons' dendritic tree branching is principally mediolateral but presents neurons that extend their dendrite rostrocaudal and dorso-ventrally, reaching lamina I. The neurons' connections in lamina IV are similar to those in lamina III, except that the lamina IV neurons receiving integration also from lamina I neurons. Principally, lamina IV neurons integrate light mechanical stimuli³.

Lamina V is also called the dorsal horn's neck and is divided into a reticulated lateral zone and a homogeneous dense medial zone. The medial part of lamina V contains medium-sized, fusiform, or triangular-shaped neurons, whereas medium multipolar neurons are localized in the lateral zone. The neuron's dendrites in this layer extend mainly dorso-ventrally in a symmetrical way, reaching the laminae II-III dorsally and VII ventrally. The neurons in lamina V are mostly multireceptive wide dynamic neurons that can receive direct inputs from A β and A δ fibers and polysynaptic inputs from C fibers from both cutaneous and visceral origin. This lamina, like lamina I, is a site of convergence of somatic and visceral inputs. The other types of neurons in lamina V include nociceptive cells, with similar multireceptive and mechanoreceptive cells with less dendritic arborization. The majority of supraspinal projecting neurons from lamina V are located in the medial part. Projections are principally contralaterally running in spinocerebellar, spinoreticular, spinomesencephalic, spinoparabrachial, and spinocervical pathways. Instead, neurons in the lateral reticular region projects in propriospinal pathways, particularly in the pre-ganglionic spinal neurons. Lamina V receives inputs from the *red nucleus* in the brain through rubrospinal fibers³.

The lamina VI is present only at the spinal enlargements and is defined as the dorsal horns base. Its boundaries are not distinguishable from the surrounding laminae V and VII. Lamina VI is divided, like lamina V, in a medial and a lateral part. The types of neurons in the two parts of lamina VI are different; the medial zone contains mainly medium-sized neurons elongated or triangular with a high cellular density. In the lateral part are instead present large multipolar neurons at a low cellular density. The dendrites of neurons in lamina VI are mainly oriented dorso-ventrally, with the significant extension in the cord's dorsal side reaching laminae II and III. In contrast, in the ventral

part, dendrites extend principally in lamina VII. Predominantly, lamina VI is composed of propriospinal neurons and interneurons receiving inputs from the collateral axons of Ia muscle spindle afferent, cutaneous, and nociceptive inputs from dorsal laminae. Moreover, a descending input derives from the *red nucleus*. The principal projection of neurons in lamina VI are spinal neurons in lamina VII and few connections with supraspinal targets in the *cerebellum* and *dorsal reticular nucleus* of the *medulla* ³

Lamina VII occupies the central gray in the spinal cord and extends into the ventral horns in concomitance of the cervical and lumbar enlargement. Moreover, from T1 to L3 segments, lamina VII also comprises the gray matter's lateral horn. Lamina VII contains a different nuclear column of gray matter, including the *central cervical nucleus (CeCv)*, the *nucleus dorsalis*, the *thoracic nucleus*, the *intermediomedial nucleus (IMM)*, the *intermediolateral nucleus (IML)*, and the *sacral parasympathetic nucleus (SPSy)*. The *IML* and *SPSy* contain the pre-ganglionic neurons of the sympathetic and parasympathetic systems. These neurons are located in the *IML* of the spinal level L5-S1 and the *SPSy* at the S2-S4 spinal level. Lamina VII contains a homogeneous cellular distribution mainly composed of medium-sized interneurons, fusiform, multipolar, and triangular. The arborization of the dendritic tree of lamina VII interneuron is principally mediolateral, extending through all the spinal cord's gray matter. A particular class of interneurons located in the central part of this lamina (*Renshaw cells*), and contacting the motoneurons pool, have short ventral dendrites. Most of the neurons in lamina VII are premotor interneurons receiving inputs from the descending motor pathways. In this lamina, the interneurons have a somatotopic organization that follows the motoneuron's distribution in the lamina IX. The interneurons contacting the trunk musculature motoneurons are located more medially, whereas interneurons reaching the limb motoneurons are located more laterally. Neurons in lamina VII receive inputs also from the upper laminae controlling the propriospinal reflex pathway. The principal projections of lamina VII are the motoneurons in lamina IX and other neurons in lamina VII at different spinal levels. Neurons in the lateral part of lamina VII also project to supraspinal targets, including the *amygdala*, *hypothalamus*, *cerebellum*, *contralateral superior colliculus*, *parabrachial nucleus*, *periaqueductal gray*, and the *pontomedullary reticular formation*. The supraspinal afferents for lamina VII neurons are the brain's motor areas, including the motor cortex and red nucleus ³.

The neuron composition of lamina VIII, located at the ventral horn base, is very heterogeneous. Neurons in lamina VIII vary in size ranging from small to moderately large, and are triangular or multipolar in shape, resembling motoneurons. The dorsal trees' arborization in lamina VIII is mainly dorso-ventrally oriented, with the dorsal branches extending to the lamina VII or the ventral gray commissure, whereas the ventral dendrites reach lamina IX. Lamina VIII is principally constituted by

propriospinal interneurons involved in the coordination of locomotor activity. Neurons in this lamina connect the cervical and the lumbar enlargement and modulate the coordination between hindlimbs and forelimbs. Moreover, spinal commissural neurons project to the contralateral lamina VIII modulating the coordination between left-right limbs. Only a few neurons in the lamina VIII project are supraspinal targets, including the *medullary reticular formation, periaqueductal gray, thalamus,* and contralateral *cerebellum* ³.

The lamina IX is not continuous like the other laminae but is composed of different columns formed by motoneurons innervating the body's somatic muscles. The motoneurons are the largest neurons in the spinal cord and have a multipolar shape with a long axon exiting the CNS via the ventral root. Based on the dimension of the neurons, large motoneurons (65%) also called α -motoneurons, supplying the extrafusal fibers of striated muscles, intermediate size motoneurons (25%), corresponding to the γ -motoneurons, innervating principally intrafusal fibers of striated muscle, and small neurons (10%) corresponding to the β -motoneuron innervating both intra and extrafusal fibers and interneurons in lamina IX are distinguishable. The α -motoneurons have a large and myelinated axon and a high activation threshold firing at high frequency innervating fast-twitch fatiguable-type muscles (type II). In contrast, γ -motoneurons have slightly myelinated axons, low threshold, fire frequency, and innervate low-twitch fatigue-resistant muscles (type I). β -motoneuron are really few in the lamina IX and have not been well characterized. Each α -motoneuron column receives inhibitory inputs from the Renshaw cell in lamina VII, limiting the motoneuron's firing and preserving the muscles from damage. Lamina IX is divided into medial, central, and lateral cell columns innervating different muscles with a somatotopic organization. The medial column is present for the entire spinal cord's length except for L5-S1 segments and innervates the body's epaxial muscles. The central column is present in the cervical (C1-C6), lumbar (L4-L5), and sacral (S1-S3) levels and contains the neurons of the phrenic nucleus and the spinal nucleus of the accessory nerve. The lateral column of lamina IX is present only at the level of the spinal cord's enlargements. It contains the motoneurons innervating the limbs' dorsal part, whereas the medial column supplies the ventral part of the limbs. At the S1-S2 level in the lateral column is present a specialized nucleus called *Onuf's nucleus* that provides innervations to the perineum. A further subdivision in lamina IX is the neurons' organization in motoneurons pool innervating an individual muscle in the periphery. The pool of motoneurons' innervating flexor muscles are located in the dorsal part of the lamina instead pool innervating extensor muscles situated in the lamina's ventral part. The arborization of dendritic trees in motoneurons is mainly longitudinal, and the dendrites of a single neuron often form branches with the dendrites of other motoneurons to create longitudinal bundles. These longitudinal bundles allow motoneurons innervating specific groups of muscles to synchronize their function. An

exception for this type of regulation is the dorsolateral column's motoneurons, which have very short dendrites and few contacts with adjacent neurons. Neurons in lamina IX receive afferents from the cerebral cortex, brainstem through the vestibulospinal, reticulospinal corticospinal, and rubrospinal pathways³.

Lamina X, also referred to as *area 10*, is the central part of the central canal's gray matter. The neurons in this area are small-medium sized and are multipolar, triangular, and spindle-shaped. This lamina has a low neuronal density and is confined by the *IMM*, which is often embedded inside the lamina. The principal nuclei in this lamina are the *intercalated nucleus (central autonomic area)* and the *cholinergic central canal cluster*. Neurons in the middle and rostral part of lamina X have a dendritic tree extending dorso-ventrally reaching laminae VI and VIII. In contrast, in the ventral part of lamina X, neurons grow their dendrites bipolar rostrocaudal. Inputs in *area 10* are from visceral afferent A δ and C fibers conducting nociceptive and mechanoreceptive information and from ascending propriospinal axons. Lamina X neurons project to the dorsal column and form the postsynaptic dorsal column pathway. It has been demonstrated that some of the neurons in lamina X also project supraspinally to the *lateral parabrachial nucleus*, the *nucleus of the solitary tract*, the *amygdala*, the *medullary and pontine reticular formation*, *periaqueductal gray*, the *thalamus*, and *hypothalamus*. Lastly, *area 10* receives supraspinal inputs from the *brainstem*, mediating the inhibition of the nociceptive transmission³.

In addition to Rexed's classification of the gray matter's laminae, particular aggregations of neurons in the spinal cord share the same function and receive information from a specific area of the brain, forming a discrete nucleus. Some of these nuclei present in the rat or in the cat spinal cord are not yet identified in the human. The next paragraph reports the principal nucleus in the human spinal cord, and table 1 contains a general description and organization of the nuclei in the spinal cord (Fig. 4)³.

The *central cervical nucleus (CeCv)* is situated in the C1-C4 levels of the spinal cord and is located in the lamina VII of the gray matter, laterally to the *IMM*. The neurons in this nucleus are principally large and multipolar, with dendrites elongating dorsolaterally. This nucleus receives afferents from the neck muscles and joints and sends efferents to the contralateral *cerebellum* and the *vestibular nuclei*, controlling the tonic neck reflexes.

The *lateral cervical nucleus (LatC)* is situated in the upper cervical segments (C1-C3) and located in the dorsal part of the *lateral funiculus*. Neurons in this nucleus are small in size and round in shape, and their dendrites extend longitudinally in the spinal cord. This nucleus's principal afferents are the spinocervical pathway originating from neurons in laminae I to V. *LatC* project to supraspinal

periaqueductal gray and contralateral *thalamus* and transmit information regarding hair movement, noxious cutaneous mechanical and thermal stimulation.

The *dorsal nucleus*, also called *Clarke's column*, is present at the base of the dorsal horns embedded in lamina VII of the spinal segments from C8 to L2. The neurons in this nucleus are medium to large in dimension and round in shape. The dorsal nucleus receives information from the lower limbs regarding proprioception from muscle spindles and joints, and the axons of this nucleus project to the *cerebellum* via the uncrossed spinocerebellar tract.

The *intermediomedial nucleus (IMM)* is located in lamina VII and lamina X and is present at all spinal cord levels. The neurons in this nucleus are principally medium-sized and triangular-shaped. The neuron's principal role in this nucleus is to integrate signals from the autonomic fibers from the visceral organs. It receives innervations from the nucleus of Barrington in the *brainstem* and sends efferents to the *IML*.

The *intermediolateral nucleus (IML)* belongs to the autonomic nuclei together with the *sacral parasympathetic nucleus* and the *intercalated nucleus*. The *IML* is situated in the lamina VII in the zone between the dorsal and the gray matter's ventral horns. The extension of this nucleus starts from C8 or T1 and ends at L1 spinal segment. This nucleus contains the pre-ganglionic sympathetic neurons innervating the visceral autonomic system. Receive innervations from the *Barrington's nucleus* and the *IMM*.

The *intercalated nucleus (ICI)* is located in lamina VII and forms a bridge between the *IML* and the *central autonomic area* in lamina X. Neurons in this nucleus are propriospinal neurons and do not project to supraspinal targets.

The *sacral parasympathetic nucleus (SPSy)* is present in the lamina VII of the S2-S4 segments of the spinal cord. The neurons in this region are parasympathetic pre-ganglionic neurons innervating the viscera and receive inputs from the *brainstem*.

The *sacral dorsal commissural nucleus (SDCom)* is located in the laminae 2i, 3-7 of the S1-S5 segments of the spinal cord. This nucleus receives somatic afferent from muscles but is mainly involved in mediating nociception from pelvic visceral organs.

Table 1: Laminae and columnar structures in the spinal cord gray matter. Based on: ^{3,4,8}

Lamina	Afferences	Efferences	Column	Function
I	C and Aδ fibers from skin, muscles and viscera. Supraspinal innervations from the hypothalamus and brainstem	Sends innervations to laminae II, IV, V and VI	Nucleus posterior marginalis	N/A
II	C and Aδ fibers from skin, muscles and viscera. Fibers from lamina I and II	Innervate mainly other neurons in lamina II	Substantia gelatinosa	N/A
III	Aβ and Aδ fibers from cutaneous sources	Innervates thalamus, hypothalamus, reticular formation of the brainstem	Lateral Cervical Nucleus (LatC)	Located in C1-C3 segments in the lateral horns. Receives inputs from spino-cervical tract starting in laminae I from IV and sends information to PAG and thalamus contralaterally.
IV	Aβ and Aδ fibers from cutaneous sources. Fibers from lamina I	Innervates thalamus, hypothalamus, reticular formation of the brainstem	Nucleus Proprius of the posterior horns (NP) Internal Basilar Nucleus (IB)	The first CNS neurons composing the spinothalamic tract sending information of pain and temperature. Runs across the entire length of the spinal cord. Located in the C1-C6 segments Receive inputs from the median and ulnar nerves and transmit the information in the thalamus. Receive also innervations from the motor cortex.
V	Aβ, Aδ and C fibers from cutaneous, visceral and muscles. Fibers from laminae I and V. Supraspinal innervations from the red nucleus	Innervate cerebellum, dorsal column nuclei, thalamus, parabrachial nucleus, periaqueductal gray, pontomedullary reticular formation, lateral cervical nucleus, nucleus of the solitary tract, and the superior colliculus. Propriospinal connection with pre-ganglionic spinal neurons and lamina V neurons	Same structures of lamina IV	
VI	Inputs from the Ia muscle spindle afferent and laminae I, II, III, V, and VI. Supraspinal innervations from the red nucleus	Propriospinal connection with lamina VI neurons. Innervate cerebellum and dorsal reticular nucleus of the medulla	Nucleus dorsalis (Clarke's column)	Located in the C7-L3 segments, receive afferents from muscle spindles and tendon organs transmitting proprioception information. It is the main component of the spinocerebellar tract contacting the cerebellar cortex.
VII	Supraspinal innervations from the motor cortex and red nucleus. Few propriospinal inputs from laminae IV, V, and VI	Motoneurons in lamina IX with somatotopic innervations	Central Cervical Nucleus (CeCV)	Located at C1-C4 spinal segments. Receive afferents from cervical muscles and control tonic reflex in the neck area projecting to the contralateral cerebellum.
			Intermediolateral nucleus (IML)	Located in the most lateral part of lamina VII and extending from T1 to L3 spinal segments, it is organized in column of neurons extending their

conveys information from the upper trunk and limbs and is present only in the cervical and thoracic segments above T6, lining laterally to the *Gracile fasciculus*. These fasciculi are formed by highly myelinated fibers from the DRGs neurons ascending ipsilaterally to the *gracile* and *cuneate* nuclei. They synapse onto second-order sensory neurons crossing the midline and sending their axons to upper brain regions, including the thalamus. These fibers show limited somatotopic organization in laminae, with fibers from lower spinal cord segments located more medially and with many overlapping fibers. No overlap has been reported between fibers from the two fasciculi. The final target of the direct dorsal column pathways is the ventro-posterolateral nucleus of the *thalamus*. This nucleus receives innervations from the *gracile* and *cuneate* nuclei through the internal *arcuate* fibers, which cross the midline in the *medial lemniscus*. This pathway is also called the dorsal column medial lemniscus pathway and transmits proprioceptive, tactile, and vibratory information ³.

The postsynaptic dorsal column pathway runs together with the direct dorsal column pathway in the *gracile* and *cuneate fasciculi*. Neurons of the postsynaptic dorsal column pathway reside in laminae III to V, VII, and X at all spinal cord levels and receive primary afferent from visceral organs. Also, these pathways contact the *gracile* and the *cuneate nuclei* in the *medulla* with a somatotopic organization. Then axons from the *gracile* and *cuneate nuclei* decussate in the *lemniscus* and contact the contralateral *thalamus* supplying visceral nociceptive stimuli. The postsynaptic dorsal column pathway is considered the principal afferent pathway for transmitting nociceptive stimuli from visceral organs ³.

The spinothalamic tract is divided into a ventral part named paleospinothalamic, and a lateral part called neospinothalamic tract. This pathway conveys nociception, temperature, pressure, touch (crude, non-discriminative) to the thalamus's somatosensory region. The ventral spinothalamic tract is located in the white matter's ventral funiculus and conveys crude touch and pressure sensation. The lateral spinothalamic tract is located in the ventrolateral funiculus and transmits pain and temperature sensation. Those two distinct pathways are separated for all the spinal cord's length, then merge in the *medulla* to form the *spinal lemniscus*. It has been demonstrated that fibers conveying pain and temperature sensation in the lateral spinothalamic tract are separated, and the fibers for the pain are located more ventrally in this tract. The specific location in the spinal cord of the neurons participating in the spinothalamic tract is not well known in humans. Still, in primates and other mammals, this tract originates from neurons in laminae I, IV, V, VII, VIII, and X. These neurons are mainly contralateral in respect to the termination of this pathway and are located primarily on upper cervical segments. The dorsolateral spinothalamic tract is principally constituted by neurons residing in laminae I to V. Lamina I neurons receive innervations from A δ and C fibers transmitting noxious, mechanical, and thermal stimuli. Their axons ascend in a bundle of nerve in the middle of the lateral funiculus forming the lateral spinothalamic tract. Neurons in laminae IV and V constitute another essential part of the spinothalamic tract. These neurons are wide-dynamic range cells

and receive different inputs from interneurons in lamina II. The neurons in laminae IV and V integrate these signals and send information regarding innocuous and noxious tactile stimuli. The neurons in the dorsal laminae I to V constituting the spinothalamic tract project in the lateral *thalamus* and send information about pain's sensory discrimination. Whereas neurons from deeper laminae VII to X project in the medial and intralaminar nuclei of the *thalamus*, mediating aversive behavior responds to pain. Usually, the spinothalamic tract fibers are large and coarse, except the most dorsal part of the tract with fine and homogeneous fibers. The fibers' decussation is in the same segment of the spinal cord for the lateral spinothalamic tract, whereas in the ventral spinothalamic tract, fibers decussate one or more segments rostrally. This pathway also shows a somatotopic organization, with fibers from the caudal segment in a lateral position and fibers from a cranial segment in a medial position. The spinothalamic tract project to the *ventral posterolateral nucleus*, the *ventral posteromedial nucleus*, the central lateral nucleus of the *intralaminar nuclei*, and the posterior nuclear group of the *thalamus*. The projections to the central lateral nucleus play a fundamental role in the motivational affective response to pain, whereas projections to the lateral *thalamus* are involved in the sensory response to pain. Moreover, the spinothalamic tract has other supraspinal targets involved in affective responses or pain modulation, including the *medullary reticular formation*, the *parabrachial area*, the *periaqueductal gray*, and the *nucleus accumbens*. A dysregulation or damage to the spinothalamic tract is involved in chronic pain in patient ³.

The spinocervico-thalamic tract arises mainly from neurons in lamina IV of the cervical enlargement. Still, some contribution to this tract derives also from neurons in laminae I, II, III, and V. Axons of these neurons ascend ipsilaterally in the spinal cord's dorsolateral white matter synapse on neurons in the *LatC* nucleus in cervical segments. Axons of the *LatC* nucleus continue to ascend in the spinal cord and decussate in the ventral white commissure to terminate in the contralateral ventroposterolateral nucleus and the medial part of the *thalamus*. This pathway conveys information from cutaneous and hair sensory receptors, particularly regarding movement, mechanical and thermal innocuous stimulation. It has been shown that many spinocervico-thalamic neurons also respond to noxious muscle stimulation indicating potential participation in nociceptive transmission together with the spinothalamic tract. Under physiological conditions, the spinocervico-thalamic tract neurons are under tonic inhibitory control of descending pathways from the *periaqueductal gray* and *raphe magnus* ³.

The spinoreticular tract is located in the ventrolateral part of the white matter. It originates from neurons in lamina VII and VIII mainly, with some other contribution from the reticulated part of lamina V. The axons of the spinoreticular tract cross the midline in the same segment of the spinal cord from which they start the ascension and run in the ventrolateral funiculus intermingled to spinothalamic fibers. The principal supraspinal target is the *brainstem's reticular formation*, where they target lateral, dorsal, and *gigantocellular nuclei*, the *oral and caudal pontine reticular nuclei*, the dorsal and lateral

paragigantocellular nuclei, the *raphemagnus*, and the *central reticular nuclei*. This pathway is involved in controlling the descending modulation of the motivational affective aspect of pain and motor response to pain. Like the spinothalamo-cervicocollic pathway, this tract receives tonic inhibition from the *periaqueductal gray* and the *raphe magnus*³.

The spinoolivary tract is located between the ventral and lateral funiculi in the white matter. Neurons that give origin to this tract are situated mainly in the intermedial part of the *nucleus proprius* and the *CeCv*. Their axons decussate in the same segment of origin of the spinal cord. The spinoolivary tract projects to the primary olivary nucleus and the medial and dorsal accessory olivary nuclei. These regions, in turn, send efferent to *Purkinje cells* in the cerebral cortex. This pathway is involved in transmitting proprioceptive information from muscle spindles and joints and is involved in controlling the locomotor functions³.

The spinomesencephalic tract is located in the ventral funiculi of the white matter. It includes several projections to different midbrain areas, and the spinotectal tract is included together with the spinomesencephalic pathway. This tract originates from neurons located in all laminae of the gray matter except for lamina IX, with a smaller contribution of the neurons in *area 10*. The midbrain's principal regions targeted by the spinomesencephalic tract are the *periaqueductal gray*, *cuneiform nucleus*, *intercollicular nucleus*, *superior colliculus*, *nucleus of Darkschewitsch*, *pretectal nuclei*, *red nucleus*, *Edinger-Westphal nucleus*, and the *interstitial nucleus of Cajal*. A somatotopic organization in the termination of this tract is present, with cervical axons terminating in more rostral structures of the midbrain and lumbar axons terminating in more caudal structures. Due to the many targets in the brain of the spinomesencephalic tract, this pathway is involved in multiple aspects of sensory discrimination, including the motivational aspect of pain (projection to the *periaqueductal gray*), motor control (projection to the *red nucleus*), noxious and innocuous response to mechanical stimuli (projection to *periaqueductal gray* and *pretectal nuclei*). The spinotectal tract fibers are located ventral to the spinomesencephalic pathway and terminate primarily in the *superior colliculus* and *intercollicular nucleus*. This tract transmits information regarding reflex movements of the head and the response to visual stimuli³.

The spinohypothalamic tract is located in the lateral funiculus of the white matter. Neurons that give origin to this tract are situated through the cord's whole length principally in lamina I and laminae III, IV, and X. The supraspinal targets are different hypothalamus regions, including *lateral* and *dorsal hypothalamic areas* and the *dorsomedial*, *suprachiasmatic*, *paraventricular*, and *supraoptic nuclei*. Most of the fibers of this tract (around 70%) decussate in the *hypothalamus* and give rise to collateral connection in the *thalamus*. This tract transmits information regarding noxious stimuli to muscles and visceral organs and is involved in autonomic response to pain³.

The spinocerebellar tract is located in the lateral funiculus. It can be divided into dorsal and ventral spinocerebellar tract in the lumbar and lower thoracic segments of the cord and cuneocerebellar and rostral spinocerebellar tract in the upper thoracic and cervical part of the cord. The dorsal spinocerebellar tract neurons and its homolog, the cuneocerebellar tract, reside in lamina VII, specifically in the dorsal nucleus for the dorsal spinocerebellar tract. The axons of these pathways project ipsilaterally to the *vermis*, the *paravermal region* of the *cerebellum* (dorsal spinocerebellar tract), and the *inferior cerebellar peduncle* (cuneocerebellar tract). The dorsal and rostral spinocerebellar tract neurons are located in lamina V-VII of the lumbar and cervical enlargements and project to the ipsilateral *cerebellum*. Only a few percentages of fibers project ipsilaterally directly. In contrast, most dorsal and rostral spinocerebellar fibers decussate immediately in the spinal cord and ascend to the *bulbs* and the *pons* and recross the midline to contact the ipsilateral *cerebellum*. These pathways convey proprioceptive and cutaneous information from Golgi tendon organs and muscle spindles and are involved in the limbs' coordination and posture ³.

Table 2: spinal cord ascending pathways and brain targets.

Ascending Tract	Secondary neurons	Brain target	Functional anatomy
Gracile fasciculus	Ipsilateral Gracile nucleus	Controlateral thalamus, ventroposterolateral nucleus	Transmit touch, deep pressure, proprioception, stereognosis, and vibration information from all the body, mostly lower limbs.
Cuneate fasciculus	Ipsilateral Cuneate nucleus	Controlateral thalamus, ventroposterolateral nucleus	Transmit touch, deep pressure, proprioception, stereognosis, and vibration information from all the body, mostly lower limbs.
Spinothalamic tract	The ipsilateral spinal cord, laminae I, III-VII, and X, mainly from C1-L5 segments of the cord	Controlateral thalamus, ventroposterolateral nucleus	Transmit information regarding pain and the association between motivational-affective responses to pain; this tract also carries non-discriminative touch and temperature information.
Spinoreticular tract	Ipsilateral spinal cord, laminae V, VII and VIII	Bilateral reticular formation in the brainstem	Control the eliciting of pain response, have a high threshold for noxious stimulation, and inhibit nucleus raphe magnum and bulbar reticular formation.
Spinomesencephalic tract	Ipsilateralspinalcord, laminae I, IV, VI, and X	Controlateralperiaqueductalgray	Controls of nociception and motivational-affective response to pain transmit spinovisual reflexes.
Spinoparabrachial tract	Ipsilateralspinalcord, laminae I, II, III, V, VII and X	Controlateralparabrachialnucleus	Carry information for somatic and noxious stimuli in the visceral organs is also associated with motivational-affective, autonomic, and endocrine responses to pain.
Spinohypothalamic tract	Ipsilateralspinalcord, laminae I, III, IV, and X	Contralateral hypothalamus	Send information regarding noxious mechanical stimulation with a high threshold responding to autonomic pain.
Spinocervical tract	The ipsilateral spinal cord, mainly in laminae IV	Controlateral thalamus	Transmit innocuous sensory stimuli from the skin, the hair, and muscles.
Spinovestibular	Ipsilateral spinal cord C1-C4, mainly in laminae VII	Controlateral and ipsilateral vestibular nucleus	Controls the tonic and postural reflexes of the neck.
Spinoolivary tract	Ipsilateralspinalcord, laminae III, IV	Contolateralaccessoryolivarynucleus	Transmit information about unconscious proprioception and segmental motor control
Dorsal spinocerebellar tract	The ipsilateral spinal cord, mainly from Clarke's column in L3-L4 segments	Ipsilateral cerebellum	Transmit signals from muscle spindles and tendon's organs for the proprioceptive elaboration of spatial movement of posterior limbs.
Ventral spinocerebellar tract	Ipsilateralspinalcord L3-6, laminae VII, IX	Ipsilateralanteriorcerebellum	Transmit signals from muscle spindles and tendon's organs for the proprioceptive elaboration of spatial movement of posterior limbs.
Cuneocerebellar tract	Ipsilateralspinalcord C1-8, laminae I, V and VII	Ipsilateralcerebellum	Transmit signals from muscle spindles and tendon's organs for the proprioceptive elaboration of spatial movement of anterior limbs.
Rostral spinocerebellar tract	Ipsilateralspinalcord C5-8, laminae V and VII	Ipsilateralcerebellum	Transmit signals from muscle spindles and tendon's organs for the proprioceptive elaboration of spatial movement of anterior limbs.

The descending tracts traveling in the spinal cord contain axons originating from f the cerebral cortex and *brainstem nuclei* involved mainly in motor function control and coordination and the regulation of autonomic functions. Descending tracts are localized in the ventral and lateral funiculus. The central descending tract is the corticospinal tract originating from pyramidal neurons in the motor cortex, often referred to as the pyramidal tract for the level of decussation of axons in the *medullary pyramid*. This tract is the primary way to carry voluntary movement information from the brain to the secondary motoneuron in the spinal cord and then to the peripheral muscles. Generally, all descending fibers decussate in the

caudal medulla and travel through the spinal cord to innervate the target neurons; only a few numbers of fibers remain uncrossed ⁶. Even though motoneurons are located in the spinal cord's lamina IX, the descending pathway's primary targets are interneurons or secondary pre-motoneurons in the dorsal horns and intermediate gray matter. However, in humans, direct monosynaptic connections (20% of the total corticospinal axons) are formed by the primary motoneurons (*motor cortex*) on secondary motoneurons in lamina IX. Fig 5 illustrates the principal descending pathway in the spinal cord and Table 3 summarizes the main features.

The corticospinal tract in humans originates primarily from pyramidal neurons (*Betz cells*) of lamina V located in the *primary motor cortex (area 4)* and *premotor cortex (area 6)*. Only 20% of the corticospinal tract's fiber derives from the somatosensory cortex's limb and trunk areas. More than one million axons form the corticospinal tract, and 70% of those are myelinated. The majority of the axons (80%) have a diameter inferior to 2 mm, whereas the remainder varies from 5 to 22 mm, with a tiny percentage (3,5) of axons larger than 20 mm. The majority of fibers descend through the *cerebral peduncle* and the *basilar pons* and decussate in the *caudal medulla* to form the lateral corticospinal tract. Only 15% of fibers descend ipsilaterally and decussate in the ventral white commissure forming the ventral corticospinal tract. Both lateral and ventral corticospinal tracts run along with the entire spinal cord extension. Still, most fibers end in the cord's cervical segments with a progressive decrease in corticospinal fibers' number along the craniocaudal axis. Corticospinal fibers principally terminate in lamina V-VII and on the interneurons in lamina IX. It has been reported that a small percentage of corticospinal fibers ends directly on motoneurons forming a direct cortico-motoneuronal connection. In humans, around 20% of corticospinal fibers create this direct connection. In contrast, in the monkeys, only 5% of fibers displayed this cortico-motoneuronal route. This difference is due to the increasing dexterity in the movements and fine grasping of objects. The corticospinal tract gives rise to many collateral pathways contacting different ascending and descending system. The collaterals to the dorsal column are essential for the coordination of distal movements and manual dexterity. In humans, the corticospinal tract is the last pathway to develop. Axons of this pathway reach their most lumbar target at 24 weeks post conception. Myelination starts at 40 weeks post conception and is complete after the second or third year ³.

In humans, the rubrospinal tract is rudimentary, less developed than in other monkeys and carnivores species. The neurons of origin are 150-200 large-sized neurons in the *magnocellular part of the red nucleus* projecting mainly to the contralateral cervical laminae V-VII. Only a few axons are terminating in the lumbar segments of the cord. The regression of the rubrospinal tract in humans is due to the substitutive function carried out by the corticospinal tract. The principal role of the rubrospinal tract is to activate flexor muscles and inhibit extensor muscles ³.

The vestibulospinal tract originates from neurons located in the *hindbrain's vestibular nuclei*, the dorsolateral part of this nucleus project to the lumbosacral spinal cord, whereas the rostro-ventral part sends efferent to the cervical and thoracic segments. Based on the fibers' origin in the vestibular nuclei, the vestibulospinal tract is divided into a more prominent lateral part and a small medial part. The lateral vestibulospinal tract runs for all the spinal cord ipsilaterally and contacts directly the α and γ motoneurons in lamina IX. This tract's principal function is to facilitate the activation of extensor muscles and the inhibition of flexor muscles. The medial vestibulospinal tract runs in the ventral column in the area called *sulcomarginal fasciculus*. This tract extends only to the cervical segments and innervates interneurons primarily in laminae VII and VIII, with few direct connections with motoneurons. The primary function is to control the movement of the head, neck, and upper body ³.

In humans, the reticulospinal tract is not a continuous descending tract but is intermingled with propriospinal fibers in the spinal cord. This pathway arises from the *reticular formation* of the *pons* and the *medulla oblongata*, which in turn receives somatic innervations from vestibulospinal, tectospinal, and motor inputs from motor areas. Even if it is not continuous in the spinal cord, the reticulospinal tract is present at all cord segments, and it shifts posterolaterally as it descends. The fibers run ipsilaterally in the white matter's ventral and lateral columns and synapse on neurons in laminae VI-IX. This tract can be divided into medial and lateral reticulospinal tracts. The medial reticulospinal tract originates from the *medial tegmental field* of the *pons* and the *medulla*. Whereas, lateral reticulospinal tract originates from the medial part of the *gigantocellular reticular nucleus* in the *pons*. The reticulospinal tract is essential for transmitting preparatory movements, postural control, and the modulation of sensory, autonomic response information. Moreover, it participates in the diffuse noxious inhibitory control phenomena involved in blocking the voluntary movements in the presence of a noxious stimulus ³.

The tectospinal tract originates from the *superior colliculus*, and the fibers project mainly contralaterally in the upper cervical segments. There are also few ipsilateral projecting fibers arising from the anteromedial part of the *colliculus*. This tract runs in the ventral funiculus near the ventral median fissure and synapse on neurons located in laminae V-VIII. This pathway is mainly involved in controlling neck and head postural reflexes movements in response to visual stimuli ³.

The solitariospinal tract in humans is formed by a few fibers originating from the *nucleus of the solitary tract*. The principal spinal targets of these fibers are the *phrenic nucleus* in the C4-C6 segments and motoneurons in the thoracic segments of the spinal cord. This pathway is involved in controlling the respiratory functions and vomiting reflex ³.

The descending autonomic fibers originate from the *hypothalamus* and other regions in the *brainstem*. These pathways descend in the dorsal part of the spinal cord and synapse on neurons in laminae I, II, VI, VII,

IX, and X. Specific targets of this tract are the *IML* and *SPSy* in the lumbosacral segments. The descending autonomic fibers are essential in controlling the body's autonomic functions, including blood pressure, stress response, and micturition ³.

Projections from the *locus coeruleus* are located in the ventral funiculus and the dorsolateral funiculus. These two different projections originate from the noradrenergic cell group A4 and A5 in the *locus coeruleus* and the group A7 in the *nucleus subcoeruleus*, respectively. These fibers travel in the spinal cord ipsilaterally and contact neurons in laminae I-III, VII, and the *SPSy* in the sacral cord. This tract modulates information transmission regarding autonomic regulation, motor function, and reproductive and excretory systems ³.

Projections from the *raphe complex* are located close to the corticospinal tract in the dorsolateral fasciculus. These fibers arise from serotonergic neurons in the *raphe magnus* and the *gigantocellular reticular formation* and terminate in the spinal cord's dorsal horns, targeting neurons in laminae I, II, and V. These projections modulate autonomic, reproductive, and excretory system. There is also a non-serotonergic component of the raphespinal tract involved in modulation of nociception and a direct projection to motoneurons in the ventral horns modulating motor function ³.

Table 3: Principal descending pathways, their targets in the spinal cord, and their functions.

Descending Tract	Primary neurons locus	Spinal cord target	Functions
Corticospinal tract	Pyramidal neurons in the primary motor, premotor, and somatosensory cortical areas.	Controlateral lamina III-VI neurons, lamina IX neurons (only primates). Fibers arriving at sacral levels of the cord.	Controls of limbs and trunk muscles and active motion
Descending autonomic fibers	Hypothalamus, brainstem	Mainly in controlateral laminae I of the pre-ganglionic sympathetic and parasympathetic cell column (IML)	Autonomic regulation of blood pressure, circadian rhythms, and response to stress
Rubrospinal tract	Caudal magnocellular region in Red nucleus	Controlateral laminae V, VI, and VII in the cervical and lumbar enlargement. Some monosynaptic contact in lamina IX	Control of muscles, integration of corticospinal tract signals
Tectospinal tract	Superior colliculus	Controlateral laminae V, VII, and VIII of cervical levels of the cord	Movement of the head and response to auditory and visual stimuli
Cerebellospinal tract	Cerebellar nucleus	Controlateral lamina VII interneurons in the cervical segments	Not clear function
Reticulospinal tract	Medial reticular formation of the rhombencephalon	Both contralateral and ipsilateral fibers contacting interneurons in laminae V, VI, VII, and IX	Control of posture, preparation of movements, and modulation of autonomic functions
Vestibulospinal tract	Lateral and medial vestibular nucleus	Ipsilateral dorsal horns at all levels of the cord, especially in the cervical segments	Control of head position, initiation of extension of the limbs, and postural coordination of the trunk.
Raphespinal tract	Gigantocellular reticular formation in Raphe structures	Bilateral dorsal horns (gigantocellular reticular formation) and motoneurons (Raphe obscures and pallidus)	Control of pain sensation and integration of gait control in the autonomic and somatomotor system
Solitarispinal tract	Solitary tract nucleus	Controlateral ventral horns of cervical and thoracic levels	Controls of respiratory function and vomiting reflex

The last class of fibers in the spinal cord's white matter comprises propriospinal neurons that innervate and connect different spinal cord segments. The propriospinal system refers to the set of neurons that stay inside the spinal cord boundary with both the cell body and their axons^{15,16}. This system was not well characterized in the past and considered less important than the ascending and descending pathways. However in the last decades, with the improvement of tracing techniques, it was defined that almost 44% of the axons in the spinal cord white matter belongs to the propriospinal system¹⁷. Typically propriospinal neurons are interneurons that modulate mainly the functions of motoneurons in lamina IX. Thus propriospinal neurons are located in all laminae of the gray matter¹⁶. The Propriospinal system has an assortment of roles in the body's physiology, and the principal is the fine coordination in motor function acting directly on motoneurons pools. Moreover, the propriospinal system can modulate the descending tract's inputs to central pattern generators (CPGs) and regulate the interaction between the nociception system and reflex pathways and affect the respiratory cycle and the autonomic system^{18,19}. From a clinical point of view, these interneurons are fundamental for the recovery after acute trauma in the spinal cord because they could anatomically overcome the primary lesion site and activate the secondary route of signal transmission in the lesioned cord, connecting the supra- and sub-segments. Moreover, propriospinal neurons connect the cervical and the lumbar enlargements participating in the coordination between upper and lower limbs¹⁶. Propriospinal fibers in the spinal cord's white matter do not have a dedicated tract as the ascending or descending pathways. Instead, they mesh together with these tracts. Table 4 reports the principal types of propriospinal fibers within the spinal cord.

Table 4: Propriospinal pathway and a brief description of their functions in the spinal cord ^{16,17}.

Subgroup of propriospinal fibers	Type of fibers	Principal function
Short axon propriospinal projections	Limb segment	Located in the enlargements of the spinal cord at all levels of the gray matter excluding lamina IX. Sends their axons intra-segmentally or inter-segmentally (no more than 2 spinal levels) in the motoneuron pools controlling their functions or transmitting direct information from the descending pathways.
	Short thoracic	Located mainly in segments T6-8 of the cord in all the laminae but IX. These propriospinal neurons' axons ascend or descend for 1 to 5 segments of the spinal cord and synapse principally with interneurons in laminae III-VIII, and X. Controls axial musculature and position of the body.
	Thoracic respiratory interneurons	Modulate respiratory signals from the medulla to intercostals and abdominal motoneurons subgroups. Also, integrate nociceptive information from the skin and visceral organs to couple them with respiratory function.
Long axon propriospinal projections	Descending propriospinal tract	Neurons are located in the segment C4-6 in laminae IV, V, VII, and VIII. The projection of these propriospinal neurons finds its target in the lumbar enlargement's motoneuron pools, coupling cervical motoneurons' activity to the lumbar motoneurons. The principal function is the coordination of the movement of the limbs.
	Ascending propriospinal tract	Neurons are located in the cord's lumbosacral segments in laminae IV, V, VII, and VIII. Their axons contact the motoneurons in the cervical enlargements. The function is the same as the descending propriospinal neurons.
	Upper cervical inspiratory projections	Located in the C1 and 2 segments of the spinal cord. Principally ends in the phrenic motoneurons at C4-5 levels, but some fibers run down the cord and low thoracic levels. Mainly controls in a monosynaptic manner the respiratory rate acting on phrenic motoneurons. Moreover, the lower projection of these propriospinal neurons works in a multisynaptic way on costal motoneurons.

1.1.2. Spinal cord anatomy in quadrupeds: cat and laboratory rodents

As mentioned in the preceding paragraph, most information regarding the spinal cord's anatomical structure and connections derived from studies on experimental animals, principally cats and rats^{4,13}, then extended to humans and other primates thanks to the improvement of imaging techniques²⁰. Even if the spinal cord's general structure is highly conserved in all vertebrates, slight differences exist between different species. This paragraph will illustrate the principal differences in the spinal cord between humans, cats, and rats. A brief description of the structures observed in the cat and rats but not in the human will be included.

The main difference in spinal cord structure between quadrupeds and bipeds, as mentioned before, it is relative to the segmentation profile. In the rat, the spinal cord is divided by the emerging spinal nerves into 34 segments: 8 cervical, 13 thoracics, 6 lumbar, 4 sacral, and 3 coccygeal for a total length of around 9 cm. In the cat, the segmentation profile includes 38 segments: 8 cervical, 13 thoracics, 7 lumbar, 3 sacral, and 7 coccygeal with a total length of cord around 30 cm. The vertebral column's segmentation profile is different between these species, but in most mammalian species, the sum between thoracic, lumbar, and sacral vertebrae is 22. The vertebral column's significant increase in cat and rat is given by the coccygeal components forming the tail. In particular, in the rat, the vertebral column's axial formula is 7 cervical, 13 thoracics, 6 lumbar, 4 sacral, and 27 to 30 coccygeal vertebrae. Whereas in the cat, there are 7 cervicals, 13 thoracics, 7 lumbar, 3 sacral, and 21 to 23 coccygeal vertebrae^{4,8}. Moreover, in animals with a quadruped

posture, the vertebral bodies are usually wedging in their ventral side, whereas humans and other avian species with bipedal posture are wedging dorsally⁸.

The spinal cord's general structure in both cat and rat is very similar to the human spinal cord, with only a slight difference in the gray matter's dorsal horns. The dorsal horns are more spindle in the human spinal cord, especially in cervical segments, compared to the cat and rat's dorsal horns. Moreover, the lumbosacral enlargement in the rat starts in the L2 segments ending at the L6, whereas in humans, the lumbosacral enlargements end at the second sacral segment. The gray matter's lamination in all the spinal cord is very similar in all three species, and all laminae are distinguishable in the gray matter. Table 5 reports the principal differences in laminae composition for cats and rats. However, each lamina's characterization is complete in animals, and some neuronal nuclei have been identified in cats and rats but not in the human spinal cord.

Table 5: principal differences in Rexeed's laminae in rat and cat spinal cord.

Lamina	Rat	Cat
I	Contains very few synaptic glomeruli. 80% of nociceptive neurons possess NK-1 receptor.	Axons from this lamina form 50% of the spinothalamic tract.
II	No filamentous cells. In the 2o layer, there are no curly cells, but neurons called stalked for their dendritic extension covered with dendritic spines giving a cone shape. 1/3 of neurons is GABAergic; those neurons are principally islet cells.	In the 2o layer, there are no curly cells, but neurons called stalked for their dendritic extension covered with dendritic spines giving a cone shape.
III	This lamina has a medial deflection, and the cells are similar in size and morphology to those in lamina II. Axons from this lamina form spinothalamic, spinohypothalamic, spinoparabrachial, and spinoreticular tracts.	Constituted by a heterogeneous population of non-nociceptive cells.
IV	This lamina has a medial deflection. Axons from this lamina form the spinocerebellar, spinohypothalamic, spinothalamic, and spinomesencephalic tracts. Supraspinal targets include nucleus accumbens, septal nuclei, lateral parabrachial area, and reticular nuclei.	Axons from this lamina form the spinocerebellar, spinohypothalamic, spinothalamic, and spinomesencephalic tracts. Supraspinal targets include nucleus accumbens, septal nuclei, lateral parabrachial area, and reticular nuclei.
V	The medial and lateral zone are more distinguishable basing on the cell density.	The medial and lateral zone are more distinguishable basing on the cell density.
VI	The distinction between medial and lateral zones only in the lumbar segments.	No differences.
VII	Different distribution of neuronal nuclei. Mainly composed of small neurons with short dendrites.	Different distribution of neuronal nuclei.
VIII	Receive afferents from supraspinal periaqueductal gray and collaterals from interstitiospinal, vestibulospinal, and reticulospinal tracts.	Receive afferents from supraspinal periaqueductal gray and collaterals from interstitiospinal, vestibulospinal, and reticulospinal tracts.
IX	Dendrites of motoneurons extend to laminae III and IV. Dendritic bundles extending in the transversal plane cross the midline and contact contralateral motoneurons.	This lamina is composed of 30% small neurons. Different neuronal columns form bundles of dendrites. Dendritic bundles extending in the transversal plane cross the midline and contact contralateral motoneurons.
X	No morphological distinction between neurons. This lamina is homogeneous in its appearance.	No morphological distinction between neurons. This lamina is homogeneous in its appearance.

The nuclear subdivision of the gray matter is very similar between human and cat; whereas, in the rat, some nuclei are shifted caudally compared to the human position. For example, *Clarke's column* is located in T1-L3 segments and mainly in laminae IV, and V and the IML have the same extension but are located in lamina VII in the rat. Moreover, *SPSy* is confined to S1, 2 segments, and *SDCom* extending from L6 to S4. Nevertheless, in both rats and cats, more nuclei in the gray matter have been identified than the human spinal cord.

The *internal basilar nucleus (IB)* is located in the C1-6 segments of the spinal cord, mainly at the base of the dorsal horn in lamina IV. This nucleus receives innervations from DRGs neurons forming the median and the ulnar nerves. Moreover, *IB* also receives projections from the sensory-motor cortex. Efferent fibers from this nucleus project mainly to the contralateral *thalamus*^{4,8}.

The *lateral spinal nucleus (LSp)* is present at all spinal cord levels in both rats and cats. *LSp* is mainly localized in the white matter, ventrolateral to the lateral edge of the dorsal horns. Neurons in this nucleus have three patterns: the first group of neurons contacts the lateral gray matter. The second group extends longitudinally in this nucleus. Finally, a third group contacting the reticulated portion of laminae IV and V. The primary afferents received by *LSp* derives from *medullary and pontine reticular formation* and collaterals from the dorsal column. In turn, *LSp* neurons project mainly bilaterally to the *hypothalamus, thalamus, amygdala, nucleus accumbens, parabrachial nucleus, the nucleus of the solitary tract, and tractus solitaries nucleus*. The neurons of this nucleus are also involved in the propriospinal system. *LSp* neurons in the thoracic segments project to *LSp* neurons in the cervical segments. Efferent from this nucleus synapse even neurons of the sympathetic preganglionic column. The neurons of the *LSp* nucleus transmit information regarding nociception in both somatic and visceral compartments^{4,8}.

Another nucleus described in the rat and cat but not yet identified in humans is the *lumbar dorsal commissural nucleus (LDCom)*. This nucleus is included in lamina VII of the L1-2 segments of the spinal cord in the dorsal gray commissure. *LDCom* neurons are preganglionic autonomic cells which show sexual dimorphism with a larger dimension in male respect to female. The projections from this nucleus are directed to the hypogastric nerve and pelvic ganglia^{4,8}.

The *Stilling's sacral nucleus*, also called *sacral precerebellar nucleus (SPrCb)*, has been described only in the rat and not in the cat and human spinal cord. This nucleus is located in lamina VII of the S1-4 segments and is composed of large multipolar neurons. Initially, the *SPrCb* nucleus was treated as a continuation of the *dorsal nucleus*, but their projection profile is different. *SPrCb* sends axons to the contralateral *cerebellum*, in contrast to the ipsilateral projection of the *dorsal nucleus*, moreover some neurons in the *SPrCb* project to the *thalamus*. The principal function of the *SPrCb* nucleus is to send information regarding cutaneous and muscular nociception, but the connections with the thalamus are involved in spatial orientation of the tail.

In the L1-L3 segment of the spinal cord is present another nucleus similar to *SPrCb* in structure and function. This nucleus, called the *lumbar precerebellar nucleus (LPrCb)*, is less characterized than the sacral nucleus^{4,8}.

The white matter organization in both cats and rats presents differences compared to the human spinal cord. The descending tract that supplies motor information for locomotion and limb coordination has a different location and target than human corticospinal innervations. At the same time, the origin of the motor inputs in the brain has a similar localization for many vertebrate species, the descending pathway, i.e., the corticospinal tract synapses on interneurons located in the dorsal horns, especially in laminae III to VII in both cat and rat. This innervation is substantially different from the innervations in primates and humans, where corticospinal tract fibers terminate mainly in the ventral horns. Moreover, unlike in humans, in non-primate mammalian species, very few direct connections with motoneuron in lamina IX have been observed²¹. The corticospinal tract position in humans and primates is shifted dorsolaterally compared to other mammalian species. In the rat but not in the cat, most of the corticospinal tract fibers are located in the white matter's dorsal funiculus (Fig. 6).

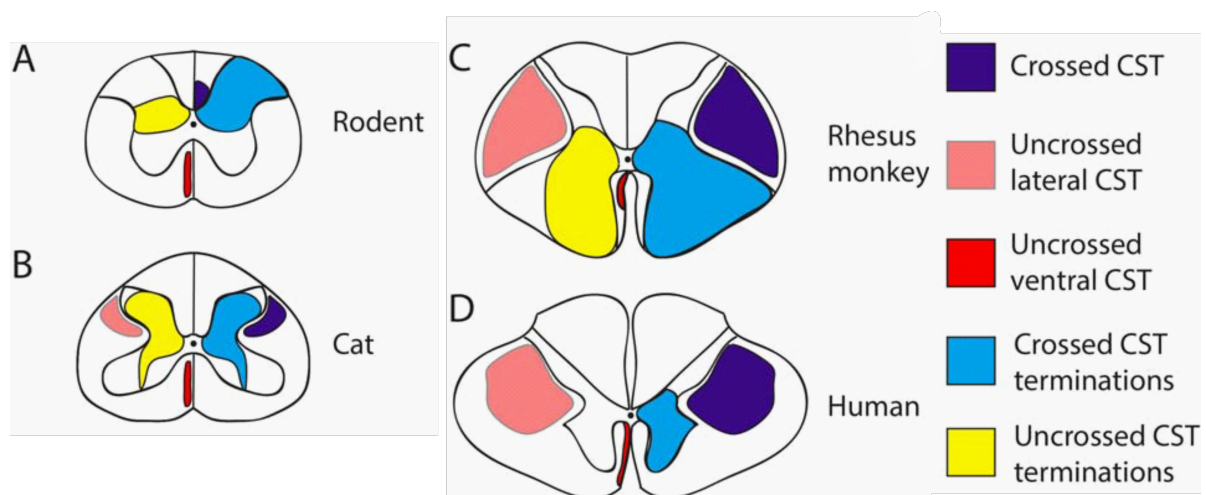


Fig. 6: localization of CST fibers in the spinal cord of different mammalian species (A-D). The location of the CST has switched from dorsal to ventral during the evolution. Also, the CST fibers' termination is located more ventrally in humans and primates than other mammalian species. In particular, in the cat and rat, no direct, or very rare, monosynaptic connection with lamina IX motoneurons have been observed. Figure adapted from²¹.

Together, the ventralization and the appearance of direct corticomotoneuron connection in humans are involved in the organization and coordination of more complex movements, including the forelimbs' increasing dexterity. Moreover, in rats, cats, and other non-primate mammalian species, the corticospinal fibers are thin and less myelinated than the human corticospinal tract, and 40% originate from parietal areas of the cortex. Thus, the movement coordination in non-primate mammalian species is mediated by integrating descending inputs carried by different white matter pathways, including the rubrospinal, vestibulospinal, and reticulospinal tract^{4,8,21}.

A direct hypothalamospinal tract has been characterized in cats and rats and not in the human spinal cord. This tract of fibers originates from different nuclei in the *hypothalamus*, mainly the ipsilateral *paraventricular nuclear*. The principal termination of these hypothalamic fibers is on lamina I and preganglionic neurons of the sympathetic and parasympathetic column at all spinal cord levels. The hypothalamospinal pathway is involved in different autonomic functions, including regulating blood pressure and stress response ^{4,8}.

Other descending pathways in both cats and rats' spinal cord share many similarities with humans and primates. Table 6 reports the principal differences.

Table 6: principal differences in descending white matter pathways in rat and cat spinal cord.

Tract	Rat	Cat
Rubrospinal	This tract is located immediately ventral to the dorsal horn's junction and the spinal cord's periphery. Termination presents at cervical and lumbar enlargements in laminae V-VII. Monosynaptic contact with lamina IX motoneurons in cervical regions have been described.	The termination is mainly on last order interneurons in lamina VII. Monosynaptic contact with lamina IX motoneurons in cervical regions have been described.
Vestibulospinal	Primary studies on this tract are made on the cat, but presumably, the rat's organization is similar.	It presents a caudal vestibulospinal tract from the caudal part of the spinal, medial, and group F nuclei of the vestibular nuclear complex. These fibers are located in the ventrolateral white matter and terminate in lumbar segments of the cord, supplying motor information for tail muscles.
Tectospinal	No relevant differences.	This descending tract is more developed in carnivorous species. In cat is composed of more fibers with respect to the human.
Solitariospinal	Some fibers extend for all the length of the spinal cord.	No relevant differences.

The ascending tract organization in the cat and rat spinal cord is similar to humans and other primates. The main differences are in the numbers of fibers and their myelination, but almost all ascending tracts originate from the same cells. They are localized in the same place of the spinal cord in all vertebrates. Table 7 contains a brief description of the principal differences in cats and rats ascending tracts. As for other spinal cord structures, in cats and rats, two ascending tracts not described in humans have been mapped.

The spinoparabrachial pathway in humans is often described as part of the spinomesencephalic or spinoreticular tract. This tract originates from neurons localized in the laminae I, II, V, VII, X, and *LSp* nucleus in the cervical, thoracic, and lumbar segments of the spinal cord. The projections are principally in the controlateral *parabrachial nuclei*, but ipsilateral projections from cervical laminae II and V have been described. The projections to the *parabrachial nuclei* are somatotopically organized, with neurons in laminae I and II from the cervical level projecting to the external lateral *parabrachial subnucleus*. In comparison, neurons from dorsal horns of thoracic and lumbar segments project to the parabrachial nuclei's central zone. Projections from lamina V and *LSp* of all spinal levels are directed to the internal

parabrachial subnucleus. Also, some projections to the *thalamus* have been described. This tract's neurons respond principally to somatic and visceral noxious stimuli and are involved in the motivational affective, autonomic, and endocrine response to pain ^{4,8}.

Another ascending tract well described in both cats and rats but not identified in humans is the spino-vestibular tract. This pathway originates from neurons in the *CeCv* in C1-C4 segments of the spinal cord and runs in the ventral funiculus to project in the vestibular nuclei. The projection to supraspinal targets are bilateral, originating from ipsilateral projecting neurons in the medial part of the dorsal horns and contralateral projecting neurons in the *CeCv* and lamina VIII. This tract conveys information from neck muscles, joints, and ligaments and controls reflexes, particularly the neck, the cervicovestibulospinal, and postural reflexes ^{4,8}.

Table 7: principal differences in ascending white matter pathways in rat and cat spinal cord.

Tract	Rat	Cat
Direct dorsal pathway	Presence of a third dorsal column for the tail, the column of Bishoff. Only 23% of the fibers are myelinated.	Presence of a third dorsal column for the tail, the column of Bishoff. 71% of the fibers are myelinated.
Postsynaptic dorsal column	Neurons are located more dorsally.	No relevant differences.
Spinothalamic	It is also present a dorsolateral spinothalamic tract. Neurons are located mainly in laminae IV and V in cervical and lumbar levels. Are present ipsilaterally projecting neurons in cervical lamina VIII. 9500 neurons form this tract.	It is also present a dorsolateral spinothalamic tract. Neurons are located mainly in laminae VII and VIII in cervical and lumbar levels. Are present ipsilaterally projecting neurons in cervical lamina VIII. 6000 neurons form this tract.
Spinocervico-thalamic	This tract contains only 300-500 neurons in all the spinal cord located in the LatC nucleus.	No relevant differences.
Spinoreticular	Neurons are also located in the LPs column.	Neurons are also located in the LPs column.
Spinoolivary	No relevant differences.	5 different routes carry sensory information to the primary olivary nucleus, and this tract is involved in segmental motor control.
Spinomesencephalic	Neurons are located in laminae I, IV, VI, and X. The majority of projections arise from the lumbosacral segments. 75% of neurons project contralaterally.	Neurons are located in laminae I, IV, VI, and X. The majority of projections arise from the lumbosacral segments. 75% of neurons project contralaterally.
Spinocerebellar	In sacral and coccygeal segments is present the Stilling's nucleus. Projection arises mainly from the dorsal nucleus in L3-L4 segments.	Projection arises mainly from the dorsal nucleus in L3-L4 segments.

1.2. Spinal cord injury in human medicine

Spinal cord injury (SCI) is one of the most devastating and limiting conditions for human health. SCI affects primarily the person who experiences this dramatic status, both at a physical and emotional level. In 40% of cases, patients with SCI need constant and specialized care for their daily routine, even for the exploitation of their physiological needs. Thus they must have caregivers that follow them and helps in their tasks. SCI also concerns the patients' parents and caregivers, which follows the injured from the spinal lesion day for the rest of their life. The spinal cord injury's functional consequences are related to the spinal cord's anatomy, where the lesion can impact both the grey and the white matter.

Historically, spinal cord injury cases were reported since ancient Egypt and were described as conditions that could not be treated, characterized by the inability to move all four limbs, the absence of sensation of the body, and the inability to control bowel function²². The description of the patient's condition after a spinal lesion was made only on physical symptoms, but it was very accurate and described the clinical status of a lesioned spinal cord perfectly.

1.2.1. Etiology and epidemiology

Traumatic spinal cord lesion is caused in 90% of cases by motor vehicles accident or falls. Other spinal cord injury sources comprehend violence, sports injuries, and pathologies (infections and tumors). The overall incidence of SCI by single cause varies depending on the country's economic and sociologic status. In the poorest countries, SCI cases due to violence or war are increased with respect to more industrialized countries where street accidents or falls are the primary causes. This different distribution and categorization of SCI render difficult a correct estimation of this condition's incidence worldwide.

Moreover, in the less developed countries, it is not available a national register of patients with SCI; thus, the global incidence tends to be down-estimated²³. Anyway, recent epidemiologic studies assessed the global incidence of SCI and categorized injuries based on the cause. SCI is a life-lasting condition and affects over 27 million patients worldwide, with an incidence rate of 350 new cases per 100000 population (Fig. 7)²⁴. Another critical factor for the patients with this condition is the cost of life after spinal cord lesion, in fact, the need for specialized cares (caregivers and special equipment like wheelchair or rollators) and lifelong treatments for rehabilitation and the management of secondary problems/pathologies with an estimated cost of life per patient of 2 million dollars²⁴.

As mentioned above, the SCI condition is a lifelong condition; this is very important because most injuries occur during the second to third decade of life, with a different distribution between men (mainly third decade) and women (second decade). The onset of the spinal cord injury showed a bimodal age-peak, with the second period in the sixth and seventh decades of life, where an increased incidence is observed²⁵. Moreover, it presents a different distribution of SCI incidence between men and women at a young age with a ratio of 2:1, attributed to different lifestyles and occupations. The incidence rate in old age has a similar distribution between the two sexes²⁴.

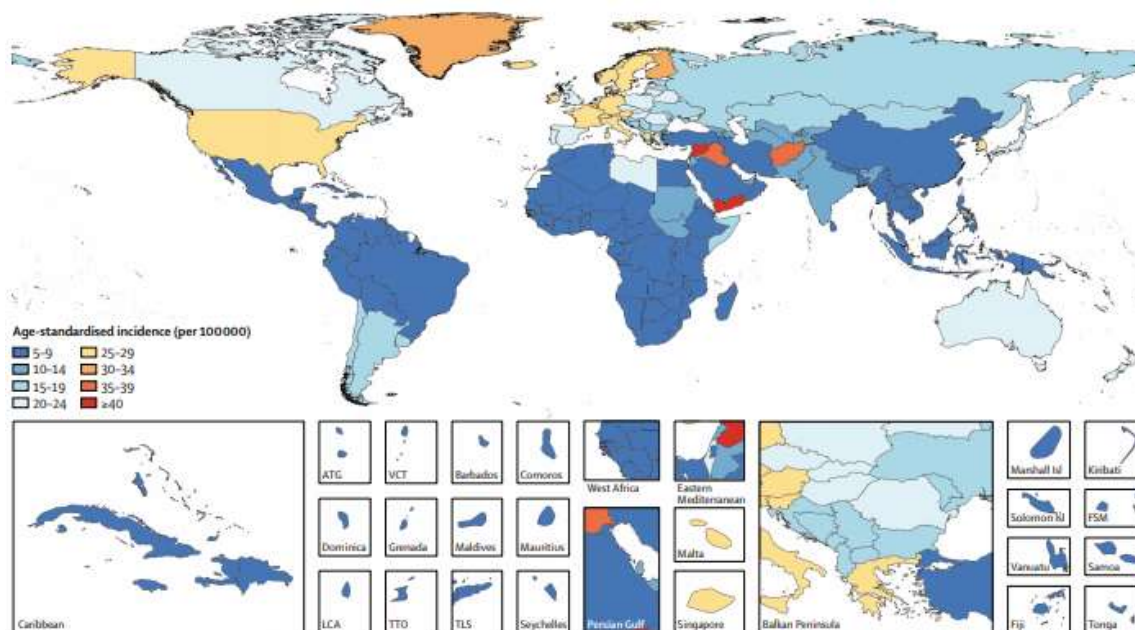


Fig. 7: Age-standardized incidence per country of Spinal Cord Injury. Image from James et al., 2019.

Another complication for a reliable and accurate estimation of the traumatic spinal cord injury cases is the different types of spinal cord syndromes and non-traumatic spinal cord injuries (NTSCI) that develop at a late age or, consequently, a pathological condition. In term of etiology, Central cord syndrome is the most common compression syndrome of the spinal cord and have an exceptionally high incidence in the elderly. Central cord syndrome occurs after a hyperextension of the cord's cervical tract and results in an intense motor weakness of the arms ²⁶. Another spinal cord syndrome is the Brown-Sèquard syndrome or cord hemisection; this condition is more uncommon and is caused by a perforating injury ²⁷. This condition is characterized by an ipsilateral loss of motor function and proprioception coupled to a controlateral loss of pain and temperature sensation. Thus, spinal cord syndromes are quite heterogeneous in terms of the anatomy of the damage, usually affecting one or two segments of the cord, resulting in loss of locomotor and sensory capacity in different region of the body according to the lesion anatomy ²⁸.

1.2.2. SCI symptoms and clinical classification

The primary clinical manifestation of SCI is the partial or complete loss of voluntary movement and sensation in the body segments below the injury level. After spinal cord injury, symptoms depend on the level, the type of the primary injury, and its extension. Moreover, an assortment of secondary pathologies and conditions are elicited after a spinal cord lesion affecting the clinical course and functional outcome.

The advancement in clinical practices and patients follow up in the last decades led to a reduction of the death rate after the initial trauma. The first advancement in managing SCI patients was the introduction and diffusion of intensive care units for early patient management. A second advancement came from the opening of specialized centers (“spinal cord injury units”), where intensive rehabilitation programs are dedicated to functional recovery (when and how possible). Moreover, alternative strategies for patient

autonomy and internal medicine problems (intestinal, urinary and sexual function, respiratory and autonomic functions, skin pressure ulcers, etc.) are designed for these patients.

In general, cervical lesions result in more severe conditions with complete paralysis of the arms, legs, and body, defined as tetraplegia. Also, the loss of sensory perception associated with the respiratory function complications often requires assisted breathing and hemodynamic regulation due to neurogenic shock in the lesion's acute phase. The most common lesion level is the spinal cord's cervical tract, which accounts for almost 50% of all spinal injuries; the segment mainly involved is the C5 ²⁹. A lesion in the spinal cord's thoracic part can cause either tetraplegia or paraplegia, depending on the primary injury level. High thoracic lesions (from T1-2) are often associated with tetraplegia and symptoms similar to cervical injury. On the contrary, low thoracic lesions (below T3 level) result in paraplegia and the loss of sensation below the injury level. Lumbar and sacral lesions are the less severe condition, with only the posteriors limbs involvement and less associated complication.

Although the primary symptom is the loss of sensory and motor control of the limbs, which is caused in the initial days after the lesion by the phenomenon called Spinal Shock, patients with spinal cord lesions often present a dramatic clinical situation. Among the secondary conditions after injury, the circulatory system's involvement represents one of the crucial points in the patients' clinical outcome. One of the first and most dangerous complications after SCI is the neurogenic shock that develops in the cervical and high thoracic lesion (T4-T6). Neurogenic shock is caused by the loss of sympathetic nervous system regulation below the level of the injury. In a patient with SCI at the thoracic level, the tone of the parasympathetic nervous system (which travels through the Vagal nerve) is not counteracted by the sympathetic tone because of the lesion of the sympathetic descending paths in the spinal cord. The results are vasodilatation, bradycardia, bronchoconstriction, and dry skin. One of the major complications in the first weeks after injury above the T6 level is autonomic dysreflexia, a condition characterized by increased blood pressure and the destabilization of the cardiocirculatory system, including cardiac arrhythmias, that can lead to stroke, seizures, and death of the patient ³⁰. Moreover, Deep Vein Thrombosis (DVT) is often associated with spinal cord lesions. The initial immobility, age, the concomitant presence of fractures, and other pathological conditions favor the evolution of a thrombotic situation. Hence, anticoagulant therapy must be administered to SCI as early treatment ³¹.

Another vital system compromised after a spinal cord lesion is the urodynamic system. Patients with SCI experience the loss of control of micturition and the inability to sense the bowel's status after the injury due to an interruption in communication between the bladder, the sphincter's muscles, and the Pontine Micturition Center (PMC) in the brain. Thus, there is an augmentation in urine retention, which requires catheterization and antibiotics drugs to prevent infection to the urinary tract, which are among the main causes of death after SCI, especially in low-income countries ³². Immediately after SCI, male patients could display an erection or priapism induced by the injury's neurogenic shock.

Pain is a common manifestation after the spinal cord lesion. It presents in patients immediately after the injury as a direct consequence of the initial damage and in later phases, often associated with neuropathic dysfunctions. Severe pain is registered in 53% of patients with SCI³³ and includes both neuropathic (above, at the level of SCI or three segments below the level) and nociceptive pain (where are present nociceptive receptors in muscles). Patients are treated with painkillers and specialized care, but in most of the cases unsuccessfully.

Other symptoms related to pain in SCI patients are involuntary contraction and spasms. Those episodes are manifested late after the injury and are caused by a lack of communication between the above-below levels of the spinal cord, a dysregulation of the propriospinal network, and supraspinal (reticulospinal) descending noradrenergic fibers and residual corticomotor fibers. Besides, modification in neurotransmitters receptor abundance (in particular receptors for Gamma-Aminobutyric Acid, GABA). Patients are treated with GABA agonists (Gabapentin) or glutamate antagonists (Pregabalin) to control pain and spasms³⁴.

Another clinical complication in SCI patients is skin pressure ulcers due to immobility. The development of ulcers is also associated with the patients' lifestyle (age, weight, diabetes, smoke) and the care in hospitalization and after the hospital's demission. Thus this point is one of the most expensive for the patients and his family³⁵. The psychological aspect of a spinal injury has a significant impact on patients' clinical evolution. SCI modifies and changes the life of a person with this condition forever. It is considered that the incidence of SCI is higher in young adults with an increased life expectancy. Patients after SCI need continuous psychological support and re-adjust their way of life, from the most straightforward to the more complicated tasks.

Among other complications, heterotopic ossification is a condition with abnormal soft tissue bone formation around joints below the spinal cord injury level that occurs in 20-30% of patients with spinal cord injury³³. It is symptomatologically evident in 1-6 months after the injury (average of two months). Commonly affected joints are the hips (70-97%), knees, shoulders, and elbows. Heterotopic ossification limits the range of joint movements and can therefore have a significant impact on functional outcome. Moreover, the rate of relapse after surgical removal is very high.

Spinal cord injury patients need a personalized diagnostic framework. The first step is identifying the spinal level subjected to the primary lesion and determination of its extension. Successively, the definition of the lesion status as complete, characterized by a complete absence of sensory and motor function below the Neurological Level of Injury (NLI); or incomplete defined by the retention of some sensory or motor function below the level of injury, depending on the severity of the primary lesion³⁶. The first classification of spinal injury was proposed in 1969 by Frankel and named "Frankel Grade"³⁷. This classification was very easy to perform and assigned a score, from A to E, where E represented the healthy patient and A patients with a complete SCI and no motor or sensory function below the NLI. Despite the simplicity of this

evaluation score and the diffuse use in the 70s and 80s, this classification failed to discriminate between low-severity lesion, particularly between grade C and D patients. Moreover, this grading system did not account for the recovery of motor function after the initial phase of the injury, so it was difficult to predict the recovery of patients and communicate the final level of inability²⁵. In the following years, other grading systems were proposed to classify SCI (Bracken Scale, UMNI, Yale Scale)³⁸⁻⁴⁰.

However, all these classification systems were difficult to perform in clinical practices since the high subjectivity and the consequent inter-operator variability. They did not account for the recovery after the initial trauma. In 1984, the American Spinal Injury Association (ASIA) developed a new rating scale system for SCI classification (Fig. 8), named ASIA scale⁴¹. This scale stratifies in 5 grades the neurological deficit, assigning a letter to the severity of SCI. A (AIS A) indicates a complete loss of sensory and motor function below the NLI, and E (AIS E) represents a normal sensation and motility. The intermediate levels correspond to the incomplete lesion with different severity and clinical outcome based on the patient's lesion and function loss.

The physician often refers to NLI as "the most caudal neurological level at which all motor and sensory function are normal"⁴². This definition is important in particular for lesions with a classification of AIS B, C, or D, which represents incomplete lesion with retaining of some sensory and motor function below the NLI in dermatomes and myotomes that remains partially innervated below the NLI in an incomplete SCI, defined as Zone of Partial Preservation (ZPP)⁴². The evaluation with the ASIA scale allows quantifying the neurological damage in patients with SCI and associating with a possible recovery in the lesion's successive phases with a right prediction of each patient's recovery rate, depending on the initial type and extension of the spinal cord damage. Although the improvement in SCI evaluation, the patients' initial status with spinal lesion often does not consent the physician to obtain a good evaluation of the AIS scale due to spinal shock condition. A series of guidelines for the clinical management of SCI patients is updated with the new methodologies in clinical practices, and AIS evaluation has become the gold standard for spinal lesion classification⁴³.

ASIA INTERNATIONAL STANDARDS FOR NEUROLOGICAL CLASSIFICATION OF SPINAL CORD INJURY (ISNCSCI) **ISCOS**

Patient Name _____ Date/Time of Exam _____
 Examiner Name _____ Signature _____

RIGHT

MOTOR KEY MUSCLES

UER (Upper Extremity Right)

- Elbow flexors C5
- Wrist extensors C6
- Elbow extensors C7
- Finger flexors C8
- Finger abductors (palm finger) T1

LER (Lower Extremity Right)

- Hip flexors L2
- Knee extensors L3
- Ankle dorsiflexors L4
- Long toe extensors L5
- Ankle plantar flexors S1

(VAC) Voluntary Anal Contraction (Yes/No)

RIGHT TOTALS (MAXIMUM)

UERS: + UEL: = UEMS TOTAL: (50)

LEMS: + LEL: = LEMS TOTAL: (50)

• Key Sensory Points

LEFT

MOTOR KEY MUSCLES

UEL (Upper Extremity Left)

- Elbow flexors C5
- Wrist extensors C6
- Elbow extensors C7
- Finger flexors C8
- Finger abductors (palm finger) T1

LEL (Lower Extremity Left)

- Hip flexors L2
- Knee extensors L3
- Ankle dorsiflexors L4
- Long toe extensors L5
- Ankle plantar flexors S1

(DAP) Deep Anal Pressure (Yes/No)

LEFT TOTALS (MAXIMUM)

UERS: + UEL: = UEMS TOTAL: (50)

LEMS: + LEL: = LEMS TOTAL: (50)

SENSORY KEY SENSORY POINTS

Light Touch (LT) Pin Prick (PP)

SENSORY SUBSCORES

LTR: + LTL: = LT TOTAL: (112)

PPR: + PPL: = PP TOTAL: (112)

NEUROLOGICAL LEVELS

1. SENSORY LEVEL: R: L:

2. MOTOR LEVEL: R: L:

3. NEUROLOGICAL LEVEL OF INJURY (NLI):

4. COMPLETE OR INCOMPLETE? (Incomplete - Any sensory or motor function in S4-5)

5. ASIA IMPAIRMENT SCALE (AIS):

ZONE OF PARTIAL PRESERVATION (If complete, ignore this field)

Sensory: R: L:

Motor: R: L:

This form may be copied freely but should not be altered without permission from the American Spinal Injury Association. REV 1/15

ASIA Impairment Scale (AIS)

A = Complete. No sensory or motor function is preserved in the sacral segments S4-5.

B = Sensory Incomplete. Sensory but not motor function is preserved below the neurological level and includes the sacral segments S4-5 (light touch or pin prick at S4-5 or deep anal pressure) AND no motor function is preserved more than three levels below the motor level on either side of the body.

C = Motor Incomplete. Motor function is preserved at the most caudal sacral segments for voluntary anal contraction (VAC) OR the patient meets the criteria for sensory incomplete status (sensory function preserved at the most caudal sacral segments (S4-S5) by LT, PP or DAP), and has some sparing of motor function more than three levels below the ipsilateral motor level on either side of the body.
 (This includes key or non-key muscle functions to determine motor incomplete status.) For AIS C – less than half of key muscle functions below the single NLI have a muscle grade \geq 3.

D = Motor Incomplete. Motor incomplete status as defined above, with at least half (half or more) of key muscle functions below the single NLI having a muscle grade \geq 3.

E = Normal. If sensation and motor function as tested with the ISNCSCI are graded as normal in all segments, and the patient had prior deficits, then the AIS grade is E. Someone without an initial SCI does not receive an AIS grade.

Using ND: To document the sensory, motor and NLI levels, the ASIA Impairment Scale grade, and/or the zone of partial preservation (ZPP) when they are unable to be determined based on the examination results.

Fig. 8: ASIA table for sensory and mobility evaluation for SCI patients with the classification for each grade of the scale (right box). From: www.asia-spinalinjury.org

With improved clinical imaging techniques, a series of evaluations can be performed on patients with SCI at their arrival in the hospital. These imaging techniques include Computed Tomography (CT), X-Ray Imaging, and Magnetic Resonance Imaging (MRI) helps the physician to define the extension of the primary lesion to the spinal cord and to assess other possible complications at the level of bone fractures and ligament compromised between different vertebrae. Moreover, MRI can identify possible hemorrhage after the initial trauma and lead the clinician to decide when to perform an initial surgery to limit the secondary damage⁴⁴.

1.3. Spinal Cord Injury in Veterinary Medicine

SCI is a devastating condition not only for humans but also for companion animals' health. Like for the human, spinal cord injured animals have to face the massive loss of function after the lesion and the related symptoms including bowel dysfunction, respiratory, gastrointestinal tract, and circulation impairments⁴⁵. The causes of SCI in companion animals are similar to those in humans, but especially for dogs and cats, one of the principal causes of spinal cord damage is Intervertebral Disc Herniation (IVDH)⁴⁶, with an incidence of 34% in dogs and 8% in cats⁴⁵. Other causes for SCI in animals are similar to those in humans, having a 7% incidence due to traffic accidents and a 2% from penetrating injuries, and a less prominent percentage of cancer-related non-traumatic SCI.

Although the significant improvement in cares and veterinary practice for the management of little animals with SCI, at the time is not present nor a global nor a national register for the evaluation of the cases of SCI, so the incidence of the spinal lesion in company animals is calculated by every single veterinary clinic that follows up spinal injured animals. From the clinical point of view, SCI symptoms in animals are very similar

to those developed in humans after a spinal lesion; thus, spontaneous SCI in pets has been used for many years as a translational medicine research field ⁴⁷.

Anyway, classification for the SCI severity and prognosis after the injury is difficult for pets since sensory and pain evaluation, as used in humans, requires patients collaboration. Three different evaluation scales are used to define SCI severity in companion animals (Modified Frankel Scale, 14-Point Motor Scale, and the Texas Spinal Cord Injury Score for Dogs) ⁴⁸⁻⁵⁰. However, there is no clinical consensus on which of them is the most appropriate to evaluate SCI severity. The management of lesioned animals in clinical practices starts from identifying the primary lesion site and then stabilizing the patient in a recumbency position that allows further examinations. As for humans, the first cares are to reduce the spinal shock provoked by the lesion and contain the respiratory impairment with the administration of oxygen through a mask and limit the hemodynamic decompensation with resuscitative fluids administration ⁵¹. This initial management of companion animals by the veterinary is defined Airway, Breathing, Circulation (ABC) ⁴⁵ and is aimed at reducing the initial complication following SCI.

In recent years, accessibility to imaging technology has improved the definition of the initial damage to the spinal cord and lesion type. It is also common in veterinary practice to have a CT or MRI of the spinal cord to help the veterinarian decide on the animal's clinical situation.

1.4. Spinal cord injury pathophysiology

The primary event (or primary damage) can be distinguished in traumatic or non-traumatic. The first type is characterized by the displacement of tissues like bone, ligaments, or disc materials, that penetrate the spinal cord or cause a closed trauma (without skeletal component displacement). The second type is induced by malignant formation, vascular problems, infection, or severe demyelinating conditions.

For the traumatic spinal cord injury, four primary injury types have been defined: I) contusion coupled with compression, II) contusion alone, III) distraction and IV) partial laceration or complete transection^{25,52}. The first type is the most common in human medicine and is caused mainly by traumatic fractures of the vertebral canal and the spine that produce bone fragments entering the spinal cord. Contusive lesions without bone fractures are less common and usually observed in individuals with other cervical spine diseases that cause hyperextension of the spine^{25,52}. The damage caused by distraction (two adjacent vertebrae are pulled apart, stretching and tearing the spinal cord and relative vascularization in the axial plane) is often non-recognizable by conventional X-ray examination. It requires functional Magnetic Resonance Imaging (fMRI) or Diffusor Tensor Imaging (DTI). The dissection/transection type is caused by a missile injury, mainly the external part's projection (like bullets) in the spinal cord. The severity of these lesions varies depending on the percentage of the spinal cord transected by the missile passage, and hence the patient's outcome could be a minor lesion to the spinal cord or a complete transection.

The primary lesion is then followed by the so-called "secondary injury" or "secondary degeneration", a complex and long-lasting cascade of cellular and molecular events triggered by the primary event, the extension of which is not always proportional to the primary lesion extension. This secondary degeneration determines the patient's clinical and functional outcome and invests both the grey and the white matter. Neurons, oligodendrocytes (OLs), and oligodendrocyte precursor cells (OPCs) are all highly vulnerable to the tissue microenvironment derived from primary and secondary degeneration.

The extension of the primary injury is fundamental in determining the clinical and functional outcome of the patient. During the primary insult, the damage involves mainly the gray matter of the spinal cord⁵², but the secondary cascade's onset after the insult extends the damage to the white matter rapidly, especially to the more vulnerable OLs and OPCs^{53,54}. The secondary damage's extension spreads more rapidly in the white matter than the gray matter, as confirmed by DTI⁵⁵. The loss of myelin sheaths starts after few hours from the initial damage leading to a progressive impairment of nerve conduction velocity in the segments surrounding the primary lesion.

The secondary cascade was first described in 1911 by Allen⁵⁷ as a mixture of biochemical factors that causes more damage to the spinal cord tissue after the cords' initial dissection in experimental animals. The

significant advancement in molecular biology, morphological and tissue imaging techniques has allowed to characterize the secondary cascade of spinal cord injury at both biochemical and cellular levels, also distinguishing between different time-related events that temporally classify the secondary cascade in: I) immediate events (until 2 hours from the primary event), II) acute phase (the first two days after injury), III) sub-acute phase (the first two weeks after SCI) and IV) chronic phase (Fig. 9)⁵⁶⁻⁵⁸. Moreover, it has been highlighted that secondary degeneration spread around the lesion epicenter, investing intact tissue not directly affected by primary trauma, thus leading to a physical enlargement of the lesion over a long period of time.

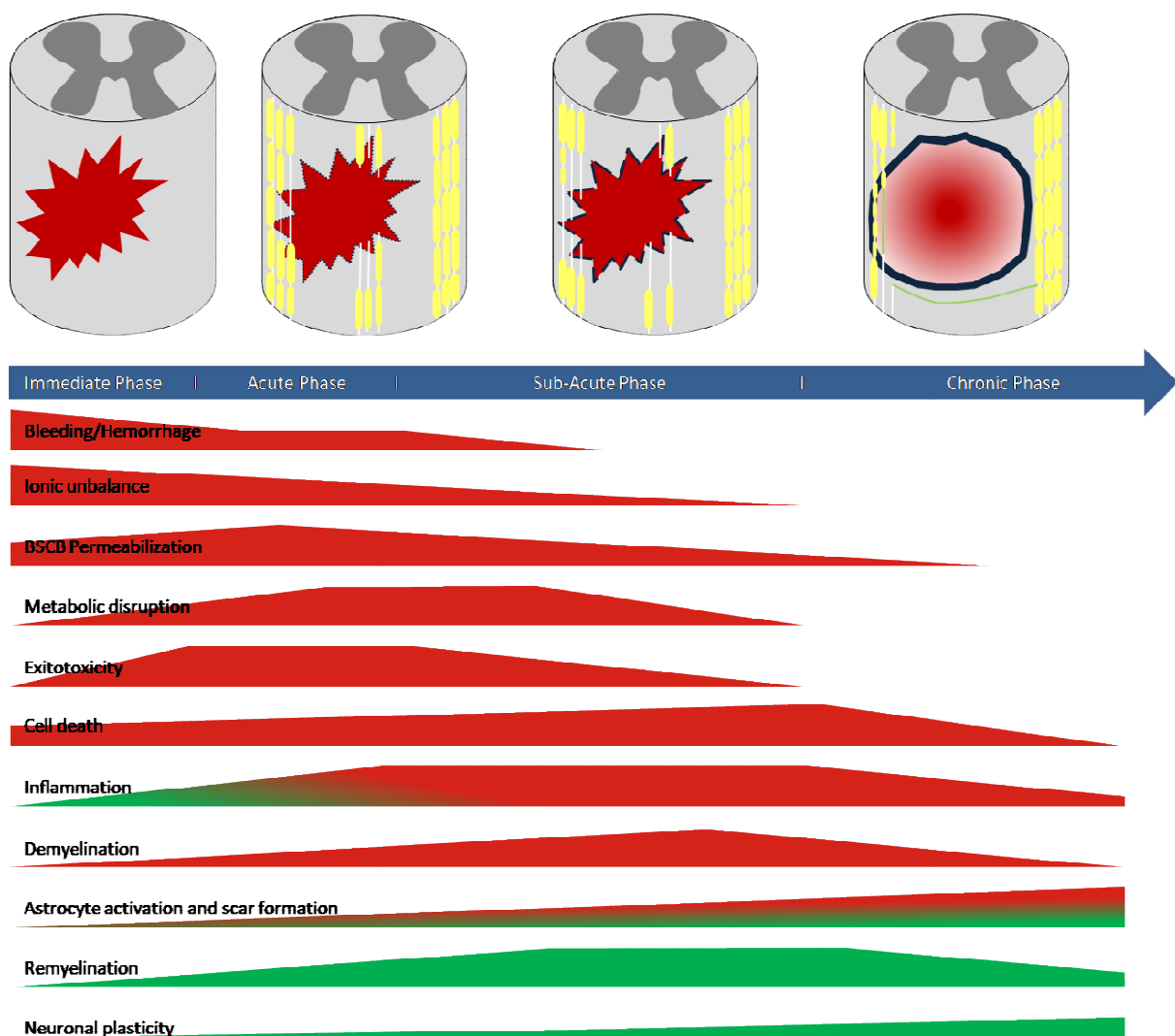


Fig. 9: The illustration reports a schematic evolution of the SCI during the injury's secondary phases. The red dot represents the initial damage to the spinal cord. White lines represent axons, and in yellow are illustrated myelin sheaths. The blue line surrounding the lesion epicenter from the acute phase represents astrocytic scar development. Green lines represent newly formed axons in the chronic injured spinal cord. The second panel of the picture reports the principal modification after SCI and their time course during the lesion evolution. In red are labeled the negative factors altering the spinal cord microenvironment, whereas labeled in green are the positive factors. Note that some processes cause both negative and positive modifications to the injured spinal cord.

1.4.1. Vascular disruption

After the initial trauma, the tissue undergoes immediate modification in structure and anatomy. Most of the immediate events are bleeding and disruption in the spinal cord's microcirculation, leading to hemorrhage, impaired blood perfusion, and tissue hypoxia-ischemia⁵² (Fig. 10). Tissue hypoxia is further worsened by the systemic hypotension of the patient when associated with neurogenic shock^{25,59}. Tissue hypoxia, bleeding, and hemorrhage release in the parenchyma red blood cells and leukocytes from the peripheral system bypassing the blood-spinal cord barrier (BSCB) deleterious for both the gray matter and the white matter. In fact, the grey matter is highly vascularized, and neurons are glucose-dependent cells; the white matter cell OLs and OPCs are highly vulnerable to hypoxia and inflammation⁵⁹.

The hypoxia and necrotic tissue in the primary lesion site trigger the activation of inflammatory cells infiltrated after the breakdown of the blood-spinal cord barrier with the production of cytokines (IL-1 β and TNF- α among others) that enhance the pro-inflammatory activation of microglia and astrocytes, leading to increased cellular damage and death⁶⁰⁻⁶². Moreover, the extensive production of free radicals and Reactive Oxygen Species (ROS) mainly by nitric oxide synthases and the following calcium-mediated activation of phospholipases, xanthine oxidases, and the Fenton and Haber-Weiss reactions⁵² causes oxidative stress to neurons and glial cells, leading to the block of mitochondrial respiratory chain enzymes, glycolysis inactivation, inhibition of Na⁺/K⁺ ATPase and sodium membrane channels. The final event is the calcium overload of the cells^{52,63}. Lipid peroxidation is the most dangerous consequence of the ROS secondary damage after SCI, being a cascade reaction started by ROS or reactive nitric species (RNS) with one polyunsaturated fatty acid. This reaction produces a lipid peroxy radical that reacts with other polyunsaturated fatty acids present in the cell membrane until their exhaustion or quenched by other radical species. The termination of this lipid peroxidation chain generates two toxic products named: 4-hydroxynonenal (HNE) and 2-propenal^{59,64,65}. Together with the other lipid peroxy radicals, these products compromise cellular membranes' integrity again, particularly in the mitochondria, amplifying the damage and creating a loop where the initial ionic imbalance and ATP depletion are the cause and the effect of the lipid peroxidation reaction. Moreover, the oxidation of proteins and the subsequent carbonylation of amino acids and DNA alteration occurs, leading to apoptotic or necrotic cell death⁶⁶. OLs are very vulnerable to ROS damage because of their high quantity of lipids in their membrane enveloping the axons.

1.4.2. Ion unbalance and oxidative stress

Cells surviving the initial mechanical damage and immediate events have to face a new microenvironment characterized by an imbalance of the principal ions and ROS presence. The mitochondrial compartment is rapidly overloaded with noxious stimuli; thus, a metabolic impairment occurs in both neurons and OLs, which are both highly demanding of ATP and energy to sustain neuronal transmission and membrane repolarization, as well myelination. Mitochondria in neurons produce the energy mainly through oxidative

reactions that generate ROS, then eliminated by enzymes (coenzyme Q and cytochrome C) to finally obtain ATP and a proton gradient in the mitochondria membrane^{67,68}. Besides, in normal conditions, mitochondria in the cells serve as a storage compartment for calcium, controlling this ion's concentration in the cytosolic compartment⁶⁷. After SCI, the ionic imbalance causes an increase in cytosolic Ca⁺⁺ in the first minutes to hours. Mitochondria sequester more Ca⁺⁺ in their internal compartments leading to increased ATP production and an augmentation in the oxidative chain reaction with the production of ROS⁶⁹. The ionic imbalance and the concurrent excitotoxicity lead to mitochondrial failure in the first days after SCI^{70,71}. Moreover, mitochondrial permeabilization causes the influx of water, and the swelling of this cellular compartment definitively blocking the ATP production and the concurrent efflux of ROS in the cytosolic compartment. ROS activates several enzymes, including the poly-ADP ribose polymerase (PARP), which blocks glycolysis and causes cell death⁷²⁻⁷⁴. Permeabilization of the mitochondrial membrane causes the release of pro-apoptotic factors like AIF and ferrous ions from oxidative chain complexes. Thus, after SCI, mitochondrial failure is one of the most critical events in the early phases post-injury in inducing neuronal and glial death and amplifying the secondary degeneration cascade in the lesion to the spinal cord.

1.4.3. Metabolic collapse

Following ROS activation's cascade, damaged cells die, releasing the cytoplasmic content (neurotransmitters, especially glutamate, ATP, ions, and other cellular debris) in the extracellular space. Actually, several different cellular and molecular events contribute to altered microenvironment homeostasis and cell death in secondary degeneration. For example, there is a local increase in pressure in the primary lesion site due to the rupture of microvasculature, hemorrhage, vasospasm, and the activation of thrombosis pathways leading to the formation of edema in the spinal cord (Fig. 10). This mechanism is also called vasogenic shock, and the accumulation of liquids in the extracellular space causes tissue swelling and contributes to cell death. The mitochondrial membrane disruption from lipid peroxidation, amplifies the ATP depletion and hence the disruption of the Na⁺/K⁺ gradient between intra- and extracellular space⁷⁵. Moreover, the uncontrolled influx of Na⁺ from the extracellular space triggers the passive influx of Cl⁻ through chloride channels and water through aquaporins leading to cell swelling, disruption of cytoskeletal structure finally leading to cell death⁵⁹.

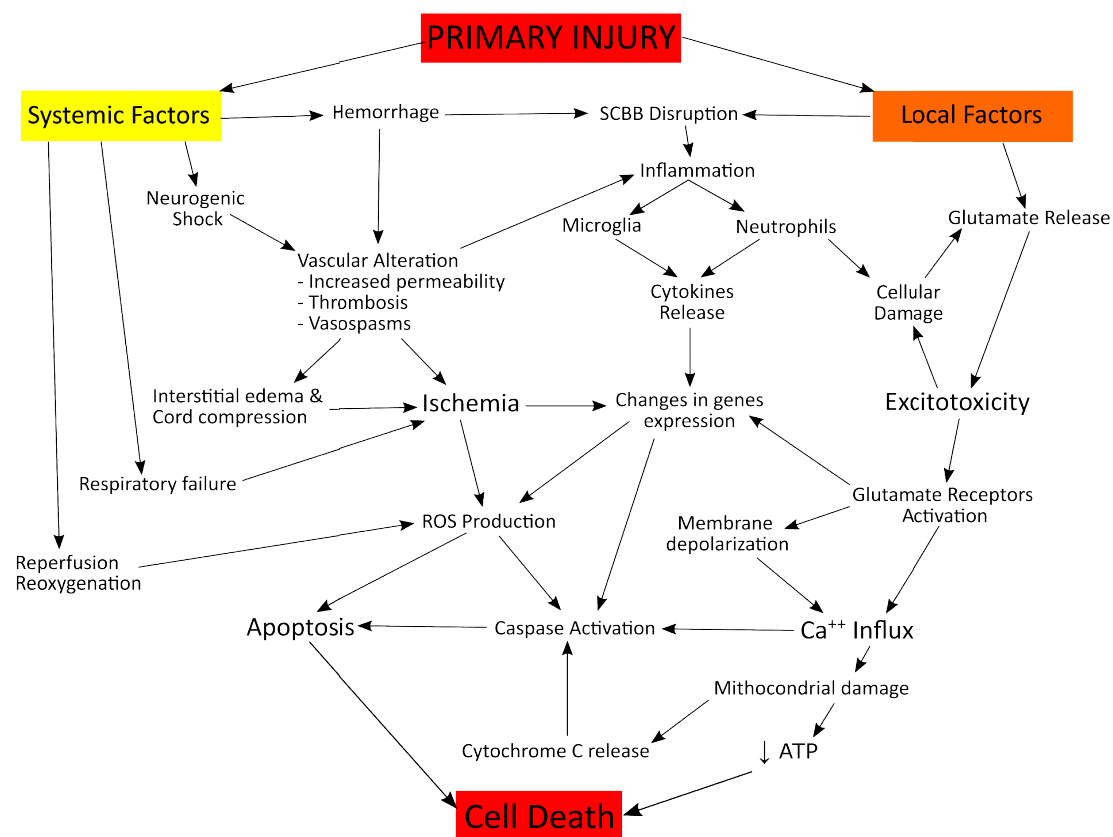


Fig. 10: this schematic drawing reports the initial secondary degeneration mechanism developing in the injured spinal cord. The early phase of the SCI produces many nocive signals that ultimately lead neurons and glial cells to activate cell death pathways. The extensive activation of calcium influx in the cells after SCI is the principal cause of cell death, especially in neurons and OLs.

1.4.4. Glutamate excitotoxicity

Another important event in the early phase is the release of excitatory amino acids (EAAs), namely glutamate, in the extracellular space (Fig. 10). A different mechanism mediates the release of glutamate from the synaptic vesicles. The physical rupture caused by the traumatic events, which is amplified by the ionic imbalance and secondarily the ATP depletion, causes the inhibition of the glutamate reuptake from the extracellular space. Thus, overstimulation of glutamate receptors stimulates its release via Ca-dependent mechanism⁵⁶. A ten-fold increase in glutamate concentration is demonstrated in the injured spinal cord, starting from 15 minutes post-lesion^{76,77}, and this toxic concentration is maintained for at least two hours after SCI^{77,78}.

During this time, glutamate act through ligand-receptor interaction on neurons and glial cells^{79,80}. Glutamate has two types of receptors, the metabotropic and the ionotropic type (the latter including AMPA, NMDA, and kainate receptors). After glutamate release, the excitotoxicity is mediated mainly by the activation of ionotropic type receptors, particularly the NMDA receptor, which causes a massive influx of Na^+ and Ca^{++} in the cells contributing to the ionic imbalance and stimulating the activation of apoptotic pathways^{59,81,82}. The influx of Na^+ and Ca^{++} also activate metabotropic receptor acting on the membrane

potential, displacing the magnesium gradient, leading to Ca^{++} overloading and the activation of metabolism of inositol phospholipids via the PI-3K pathway. This leads to an increased availability of the arachidonic acid substrates that become targets of inflammatory enzymes and ROS^{56,63,81,83}. The final result of the massive glutamate release in the first hours after SCI is the massive Ca^{++} mobilization across different compartments of the neurons and glial cells, this augmentation in calcium levels cause a delayed death (from 1 to 7 days) in the cells surrounding the primary lesion site⁵⁹. The rise in calcium levels caused by both EAAs overload and ionic imbalance after SCI has ultimately been defined as “the final common pathway for cell death”⁸⁴. Moreover, Ca^{++} acts as a second messenger, activating various enzymatic pathways leading to a metabolic depletion. The initial damage and the immediate events start the cascade of secondary events in the first hours after SCI leading to uncontrolled necrotic cell death and the spreading of the damage to the healthy tissue causing more axonal damage, neuronal and glial death.

1.4.5. Inflammation

One of the significant events in SCI's secondary cascade is the recruitment and activation of inflammatory and immune cells and the subsequent production of pro-inflammatory molecules (Fig. 11). In literature, more than 3 thousand published papers are focusing on the inflammation process after SCI. Even if it is generally associated with a poor prognosis after SCI, it has also been demonstrated that inflammatory cascade activation has a fundamental role in limiting the spinal cord's damage after injury and promoting myelin repair when limited in intensity and time⁸⁵. Especially during the initial phases of the secondary cascade of SCI, the correct activation of inflammatory components is crucial to limit the tissues' damage. Instead, aberrant activation of pro-inflammatory cells coupled with the release of cytokines and chemokines is usually observed after SCI. Although activation of inflammation is a physiological process after damage to any body organs, traumatic SCI induces a very high level of immune cells activation and a potent neuroinflammatory response with the extension to other organs, particularly kidneys and liver^{59,86}. Moreover, it has been demonstrated that the neuroinflammation caused by the same type of lesion in the brain or the spinal cord elicits different responses, having a more robust activation and cellular recruitment in the spinal cord with respect to the brain⁸⁷. Thus spinal cord lesions require the activation of an inflammatory cascade with proper timing and a correct intensity with a correct balance between resident microglia and the recruitment of peripherally derived inflammatory cells. This situation is often difficult due to the early modification and the continuous presence of pro-inflammatory stimuli derived from the surrounding necrotic tissue. Nonetheless, the great interest in the inflammation onset after SCI in the early phases is driven by the so-called “therapeutic windows”, particularly by the possibility of shaping the inflammatory response to limit the damage and enhance neuronal protection and remyelination. The remodeling of the inflammatory cascade is targetable principally in the immediate and acute phases of SCI.

In subsequent phases, the sequelae of events have already shaped the microenvironment in a pro-inflammatory way.

1.4.5.1. Cytokines production

During the acute phase of SCI, multiple factors, including the intracellular material poured in the extracellular space, debris derived from the primary lesion, tissue hypoxia, and hemorrhage, concur in the activation of the inflammatory/immune system's response. The first signals detected from resident and circulating cells are the alarmins proteins release by necrotic and damaged cells. Among those alarmins are ATP, IL-33, and HMGB1⁸⁸. These alarmins are sensed by the spinal cord's resident cells, especially microglia, via the Patterns Recognition Receptors (PRRs) that stimulate the production of cytokines and chemokines. The recruitment of inflammatory cells is then prompted by the rise of these inflammatory markers after SCI, especially starting from the following hours after injury and in the acute phase. The principal cytokines produced after SCI are IL-1 β , IL-6, and TNF- α , which are the most potent activator of inflammation. Whereas the principal chemokines produced are CXCL1 and CXCL2⁸⁸. The rise in cytokine levels starts within minutes from the primary damage and is sustained for all the successive phases of injury, with a change in cells that produce the inflammatory signals. In the primary phases, as already mentioned, cytokines are mainly produced by resident cells that, in turn, activate peripheral immune cells (macrophages and lymphocytes), increasing the production of pro-inflammatory cytokines⁸⁸. The evidence of the importance of inflammatory status after SCI is rising every year in the research and clinical field. As a matter of fact, the concentration of inflammatory markers in the cerebrospinal fluid (CSF) has a prognostic value in evaluating the severity of the functional loss in the evolution of SCI^{62,89}.

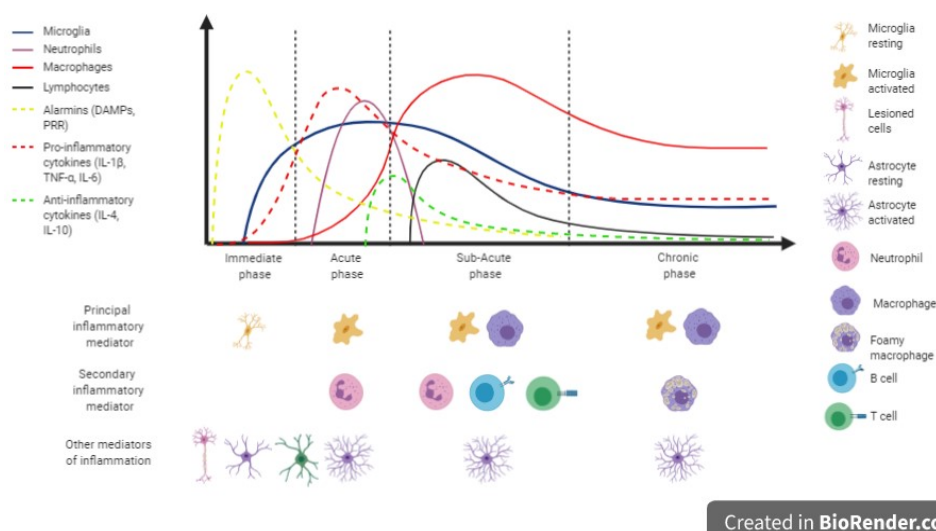


Fig. 11: The picture illustrates the timeline of cellular and cytokines involved in developing inflammation after SCI. The inflammatory cascade starts in the early phases of SCI with the release of DAMPs and alarmins from damaged cells, which stimulates the production of cytokines and chemokines from resident cells. The first inflammatory cell type activating after SCI is microglia, followed by the invasion of peripheral neutrophils, macrophages, and lymphocytes. Pro-inflammatory cytokines' production reaches a peak in the acute phase and remains sustained for all the successive phases. Anti-inflammatory cytokines are also secreted in the acute phase, but their levels are downregulated successively. Illustration created with BioRender.com

1.4.5.2. Inflammatory cells activation

In the traumatized spinal cord, the first inflammatory response after the initial trauma is given principally by the resident cells, the microglia, which respond to the molecules and debris produced by the immediate events after SCI (Fig. 11) ^{59,60,90}. Usually, resting microglia in the CNS has a ramified structure and is distinguishable from peripheral macrophages by the low expression of the CD45 marker⁹¹. In the spinal cord lesion, after the activation mediated by inflammatory cytokines and other stimuli (ATP, ROS, NO), the microglia retract its cytoplasmic processes and assume an ameboid shape becoming indistinguishable from peripheral macrophages, and also the membrane markers CD45 is upregulated at the levels of hematogenous cells ⁹¹. In the first 30 minutes from the SCI, microglia becomes activated and migrate in the proximity of the primary lesion site, forming a boundary between the spared tissue and the injury epicenter, avoiding the initial spreading of the damage^{91,92}. This initial migration and sealing of the primary lesion have neuroprotective effects mediated by the release of a high quantity of ATP in the extracellular microenvironment, which is sensed by the microglia through the P2Y purinergic receptor⁹³. The cytokine burst produced by microglia (CXCL1, CCL2, and CXCL2 especially) acts as a potent homing signal for peripheral inflammatory and immune cells, but secondarily, the IL-1 β and TNF- α produced has also a detrimental effect on neurons and OLs ^{94,95}. Moreover, the high cytosolic concentration of Ca⁺⁺ in the tissue surrounding the lesion enhances phospholipase activation that generates the arachidonic acid, the substrate for Cyclooxygenase (COXs) enzymes, that in turn is converted by the activated microglia in pro-inflammatory prostanoids (prostaglandin, prostacyclins, and thromboxanes) ^{96,97}. After SCI, have been reported a high increase in COX2 mRNA and protein expression ⁹⁸, which leads to the production of prostanoids that act on microcirculation, altering the already compromised vasculature in the tissue. Moreover the presence of ROS and the activation of the iNOS in the microglia increase ROS and RNS, creating an inflammatory microenvironment and enhancing the death of the neurons and glia ⁹².

The first type of cells invading the spinal cord in response to trauma are neutrophils (Fig. 11) ^{25,59,60,90,99}. The presence of neutrophils in the injured spinal cord is detectable starting from 3 hours after injury and reaching a peak at 24 hours, then rarely found later post-injury ^{100,101}. CCL2 mainly mediates the recruitment of neutrophils, CXCL1 and CXCL2, expressed by astrocytes and microglia ¹⁰², and the subsequent activation of these cells contribute to phagocytosis of debris and death cells. Despite neutrophils are classically associated with tissue inflammation and neurodegeneration with the production of pro-inflammatory cytokines and myeloperoxidases ^{59,60,90,100}, in SCI, it has also been observed that the total depletion of neutrophils worsens both the anatomical and the functional recovery ¹⁰³. This could be due to the elimination of the growth factors (VEGF, FGF, BMPs) produced by these cells that stimulate the reparation of the spinal cord after trauma ¹⁰³. Thus, controlling the neutrophils' response in the acute phase of SCI can improve the lesion's functional and physiopathological output.

Starting from the third day post-lesion, the peripheral monocyte-derived macrophage (MDM) invades the spinal cord parenchyma and accumulates in the lesion epicenter, responding to the homing clues produced by the spinal cord tissue. About a week from the lesion, MDM has become the predominant inflammatory cell in the injured spinal cord (Fig. 11) ¹⁰⁴⁻¹⁰⁶. In contrast to MDM, activated resident microglia in the first week after SCI reduces its phagocytic activity and becomes less active in producing cytokines. Moreover, microglia are slowly displaced from the lesion epicenter by MDM, which can actively modulate their function ^{105,107}. After the MDM entrance in the spinal cord, the presence of these cells in the lesion epicenter is sustained in all the secondary lesion phases and are detectable after long times following SCI. For instance, some studies report that after three months from the primary lesion, the percentage of macrophages in the lesion epicenter is diminished by 50% ¹⁰⁶. MDM in the lesion epicenter secretes many pro-inflammatory cytokines (IL-1 β , IL-6, TNF- α , NO, MMP9) ¹⁰⁸ that hampers the regenerative capacity of the surrounding neurons and glia and stimulate the proliferation of macrophages and monocytes from the periphery, creating a loop of inflammatory recruitment ^{106,108} and stimulating the activation of the astrocytes in the primal lesion site ¹⁰⁹. Another important event for the inflammation process in the SCI sub-acute phase is the infiltration of lymphocytes in the spinal cord's parenchyma. This event starts around the first week after SCI and continues for the next month (Fig. 11) ²⁵. Although the presence of lymphocytes in the cord after the lesion is not as high as the infiltrating MDM, these cells play a fundamental role in sustaining the inflammatory environment after SCI. Lymphocytes are classically divided into T and B cells, where the first cells actively kill the infected cells and secrete inflammatory markers, and the second type of cell controls the humoral immune response secreting antibodies ¹¹⁰. After SCI, there is a strong activation of an autoimmunity response mediated in particular by B cells with the production of auto-antibodies against DNA and RNA released in the extracellular space ¹¹¹. Autoreactive cytotoxic T cells also participate in the killing of neurons and glia in the spinal cord ¹¹¹. Moreover, the balance between effector cytotoxic T cells (Foxp3⁻) and helper T_{reg} (Foxp3⁺) is disrupted after SCI leading to reduced production of IL-10 from T_{reg} cells that lead to continuous activation of cytotoxic T cells and macrophages ¹¹². Also, the inflammatory cell polarization is unbalanced and shifted towards an M1 inflammatory cell type compared to the normal activation of the inflammatory cascade in the other body's other organs ^{59,113}. The polarization of macrophages is one of the most important mechanisms that dictate an inflammatory process's resolution and subsequent repair of the damaged tissues. Macrophages can respond to T helper 1 stimuli, IFN- γ , activating their machinery to produce pro-inflammatory cytokines (IL-12, IL-23, IL-1 β , and TNF- α), becoming more active in phagocytic and antigen-presenting activity ^{91,107}. Alternatively, they can respond to the prototypical signals of T helper 2, IL-4, and reduce the expression of pro-inflammatory cytokines and the killing activity ^{25,110}. These two different types of activated macrophages are called M1 or "classically" characterized by the expression of CD86 marker and M2 or "alternatively" macrophages expressing the CD206 marker ^{110,113}. In animal models of SCI, a marked increase in the M1 polarization in the first week

post-injury and a strong reduction of CD206+ M2 macrophages have been observed. This increase correlates with the non-resolving condition of inflammatory SCI ¹¹⁴. The presence of an unbalanced microenvironment with a prominence of pro-inflammatory cues stimulates the MDM to differentiate in M1 type cells producing more inflammatory cytokines and causing neuronal and glial cell death ¹¹⁵. Moreover, M1 macrophages contain 17 times higher levels of chondroitin sulfate proteoglycans (CSPGs) than the M2 type and express the repulsive guidance molecule A (RGMA) and Nogo-A, factors involved in the inhibition of axonal regrowth and regeneration after injury ¹¹⁶⁻¹¹⁸. On the other hand, M2 macrophages produce anti-inflammatory cytokines such as IL-4, IL-10, and TGF- β and stimulate the recovery phase and down-regulate the principal inflammatory cellular mediator like NF- κ B and cytokines stimulating immune suppression ¹¹⁰. Moreover, it has been demonstrated that M2 macrophages enhance neurite extension in vitro ¹¹⁵. In vivo study of transplantation of M2 macrophages in an injured spinal cord showed that these cells cannot maintain their M2 polarization in the injured cord starting to shift to M1 as early as 2 days post transplantation, with a shift of 50% at one week post implant ¹¹⁵. This non resolving inflammatory state have as result the incomplete capacity of the tissue to initiate the repair mechanism and to regenerate after a lesion.

1.4.6. Phagocytosis activation

The activation of microglia, neutrophils, and macrophages increases these cells' phagocytic activity towards cell debris and apoptotic cells. Usually, phagocytosis is guided by different signals that drive professional phagocytic cells to eliminate the apoptotic cell. Namely, these signals are a first secreted "find me" signal from the apoptotic cell, which activates the phagocytic cell and induces the change in shape and migration toward the site of production. A second signal is the "eat me" ligand on the apoptotic cells, which is recognized by the receptor on the phagocytic cells and activates the internalization process. The last signal is the "digest me" cascade in the phagosome inside the phagocytic cell ¹¹⁹. In the healthy CNS, phagocytosis is a fundamental process in shaping the neuronal dendritic tree, eliminating synapses and removing apoptotic cells, especially in the aging process. Phagocytosis in SCI has been described as both a positive and a negative factor during the secondary injury. After SCI, there is an increase in the release of "find me" factors from apoptotic cells, particularly ATP, UDP, and CX3CL1 (also known as fractaline). Microglia and macrophage respond to "find me" factors exposed on the apoptotic cells and the debris through the TREM2, CXCR3, and P2Y6/12 receptors, removing them from the lesion site and enhance reparative process^{120,121}. In particular, myelin debris removal is associated with an improvement in axonal growth and remyelination since myelin contains growth inhibitory factors. Removal of myelin is mediated by the complement's C3 component, which acts as an "eat me" signal on debris, recognized by the engulfment receptor C3R on microglia and macrophages. It has been described that after myelin phagocytation, microglia/macrophage cells assume a "foamy morphology" increasing the expression of anti-inflammatory

cytokines (IL-10 and IL-4) and promote the limitation of inflammation in the spinal cord in both in vitro and in vivo ¹²². Moreover, removing myelin from the lesion site stimulates the differentiation of OPCs in OLs and improves remyelination ¹²⁰. Anyway, it has been demonstrated that the elevated level of pro-inflammatory cytokines (TNF- α especially) and the microenvironment in the lesion site hamper the capacity of phagocytosis of myelin debris, reducing the level of CR3, especially in the macrophages ¹²⁰. Also, macrophages but not microglia show a long retention time of myelin debris inside their cytoplasm, blocking myelin debris's adequate clearance during the secondary cascade and thus stimulating a pro-inflammatory environment ¹²³. The continuous inflammatory microenvironment leads to an overactivation of the phagocytosis acting on the TLR receptor expressed on microglia and macrophages cell. Moreover, the inflammatory microenvironment reduce the expression of "don't eat me" signals like CD47 and CD200 on neurons and OLs ^{121,124}.

1.4.7. Cell death

The initial traumatic event and the continuous inflammatory stimuli cause the loss of many cells in the spinal cord through both necrosis and apoptosis cell death. Both types of cell death have been registered in laboratory animals and humans as well ^{125,126}. The primary lesion disrupts the tissue and causes immediate death, mainly by necrosis. On the other hand, apoptosis is usually detectable starting from the acute phase, reaching the highest peak after two weeks and then diminishing but constantly remaining present throughout all the phases of SCI ^{90,125}. During SCI evolution, cells undergo different cell death types: necrosis, necroptosis, and apoptosis.

Necrosis is the first type of cell death in SCI. It is induced directly by the primary injury and involves all the cell types in the lesioned area. Necrosis of cells is a direct consequence of extensive disruption of the cell membrane's integrity or the exposition to an unbalanced microenvironment with abnormal variations compared to normal homeostasis¹²⁷. Usually, necrosis is limited to the first hours after SCI and involves primarily the cells in the lesion epicenter directly invested by the primary damage. Besides, the release of a massive amount of glutamate and ROS after the damage drives partially damaged cells to death through necrosis. This secondary necrotic cell death wave is fundamental because the principal cell types involved are neurons, OLs, and OPCs, which express high levels of NMDA and AMPA receptors ¹²⁷.

Necroptosis is a variation of necrotic cell death that requires the activation of intrinsic factors in the cells. This type of cell death has been recently described after SCI, particularly in neurons, OLs, and astrocytes¹²⁸⁻¹³⁰, especially during the acute phase of SCI. Necroptosis is activated in cells partly damaged by the primary injury and exposed to the microenvironment modification. Unlike necrosis, necroptosis requires cellular receptors' activation from extracellular clues, particularly the pro-inflammatory cytokine TNF- α . Contrary to the apoptotic pathways, necroptosis does not require the activation of the caspase pathway for causing cell

death. In damaged cells, the interaction of TNF- α with its receptor TNFR1 activates the protein kinases RIPK1 and 3, which in turn phosphorylate MLKL, the direct effectors of cell death forming the necrosome¹³¹. It has been observed that necroptosis is more pro-inflammatory than the other regulated cell death pathways, this observation is fundamental in understanding the impact of inflammation in SCI. Necroptosis is induced by inflammation but at the same time is a cause of inflammation, resulting in a loop amplifying the damage to tissue surrounding the primary lesion site and expanding the lesion area during the secondary degeneration.

The apoptotic pathway is an organized event requiring cellular pathway activation to terminate the cells undergoing this mechanism effectively. Apoptosis differs from necrosis and necroptosis principally because it is associated with low inflammation levels after cell death. The principal cell types undergoing apoptosis after SCI are neuron, OLs, and OPCs, and these events are present in all phases of SCI and at a very distant level in the spinal cord from the primary lesion site. The apoptotic pathway requires the initial recruitment of several initiator complexes (FasL, iNOS, TNFR1) in an ATP dependent way, followed by the caspase 8 pathway's activation that leads to cell shrinkage and nuclear fragmentation in an ordinate procedure. Typically the apoptotic cells express "eat me" signals on their membrane for the phagocytation without the activation of inflammatory mediators^{119,127,132}. After SCI, apoptosis occurs mainly in OLs near the lesion epicenter, which reaches the higher mortality rate at one week post-injury¹³³ and involves neurons and microglia, especially at the lesion epicenter¹³⁴. This first wave of cell death occurring from hours to days after SCI contribute to different effect in the injured epicenter, first of all, the enhancement of inflammation through microglia cell death, secondarily impairment of neuronal conductance and lastly starting of local demyelination through neuronal and oligodendroglial death^{57,58,125}. The second wave of apoptotic cell death occurs in the first weeks after SCI and is triggered by excitotoxicity and inflammation. It is not restricted to the lesion epicenter but spreads through the adjacent segments of the cord, affecting mostly OLs¹²⁵, which respond to the Fas and TNF- α through the specific receptors on their membrane¹³⁵.

Another mechanism linked to cell damage that causes neuronal degeneration is the acute axonal degeneration (AAD)^{59,136}, which occurs in the first 48 hours after SCI. This mechanism is mainly mediate by the excess of Ca⁺⁺ in the axonal cytoplasm that opens pores in the axonal membrane¹³⁷, and represent a targetable point for therapeutic intervention in the preservation of axonal state after SCI. At the end of the AAD, the transected axons severed by their neuron body (distal end) will undergo a degenerative process called Wallerian Degeneration that destroys the severed axon the first days after SCI^{138,139}. The severed axons' proximal end instead reorganize in a growth bulb bearing the structures for the axonal elongation and regeneration. However, the external microenvironment and the presence of inflammatory cells and myelin debris (including proteins inhibiting axonal regrowth like Nogo-A, MBP, OMgp, and MAG)¹⁴⁰ convert the axon tip into retracting bulbs which recede from the injury site^{141,142}.

1.4.8. Astrogliosis

Astrocytes constitute an essential component of glial cells in the CNS and have multiple functions in the healthy brain and spinal cord, including: I) homeostatic balance of the surrounding cells; II) elimination and reuptake of the ECM neurotransmitters in the synaptic cleft (especially GABA and glutamate); III) provide metabolic and trophic support to neurons; IV) regulation of endothelial cells and blood flow; V) modulation of synaptic function and neuronal transmission¹⁴³. Astrocytes respond to all negative stimuli in the CNS and react immediately to activate different cellular processes to control the ongoing pathological event. The reaction of astrocytes to traumatic damage or other noxious mechanism is called astrogliosis¹⁴³. It is composed of a series of modifications in astrocyte structure and functions which is variable and heterogeneous depending on the type of damage and the local level of inflammatory stimuli^{144,145}. In the context of SCI, astrocytes activate early after the initial damage supporting the microglia in controlling the modification in the homeostasis due to the release of a high quantity of ions and EAAs in the extracellular space and respond to the cytokines secreted through a series of membrane receptors (IL1R1, TNFR1-2, TGF β 2, TLR2, TLR3, TLR4) starting the modification in gene expression leading to changes in morphology and ultimately to the hypertrophy of the astrocytes¹⁴⁴⁻¹⁴⁷. Astrocytes also produce a series of cytokines and chemokines that act as recruitant and activator for the immune cells, among those molecules are IL-1 β , MCP-1, CCL2, CXCL1, and TNF- α ^{148,149}. Moreover, they can increase their expression of adhesion molecules that enhance the recruitment of immune cells and modify the extracellular environment composition, in particular IL-1R1, ICAM, and VCAM^{102,148}. Although the principal effect of astrocytes in the acute phase is the activation of pro-inflammatory cells through secretion of IL-1 β and TNF- α , it has been reported that there is also the production of anti-inflammatory cytokines as TGF- β and IL-10 mediating the M2 polarization of macrophages and switching the response to pro-regenerative/repairative^{25,149}. Moreover, in response to cytokine gradient, astrocytes start to proliferate and migrate toward the primary injury site¹⁵⁰, constituting a heterogeneous pool of differently activated cells. Experiments in vivo demonstrate that astrocytes can switch from an activated form to a quiescent one if transplanted in a non-injured spinal cord¹⁵¹, meaning that the signals arriving at these cells constitute a substantial factor in response to noxious stimuli. Even if it is not a uniform process, astrocytes' activation has some common characteristics that allow distinguishing between resting and reactive cells. The first signal is the overexpression of intermediate filament proteins like GFAP, Nestin, and Vimentin, and secondly, the loss of the radial shaped morphology and the assumption of an aligned morphology toward the primary lesion site^{144,146}. At the lesion epicenter, the activated astrocytes and the migrating one form a dense border containing the primary damage and isolate the noxious microenvironment from the healthy surrounding tissue. This barrier is maintained by the active proliferation of astrocytes at the lesion border mediated by STAT3 signalling^{152,153}. The formation of this barrier in the lesioned spinal cord is called glial scar and is composed of many cell types (Fig1 12), but astrocytes play a significant role in the formation and sealing of the

primary injury site and closing the meningeal leakage and ultimately with the creation of the insulating barrier.

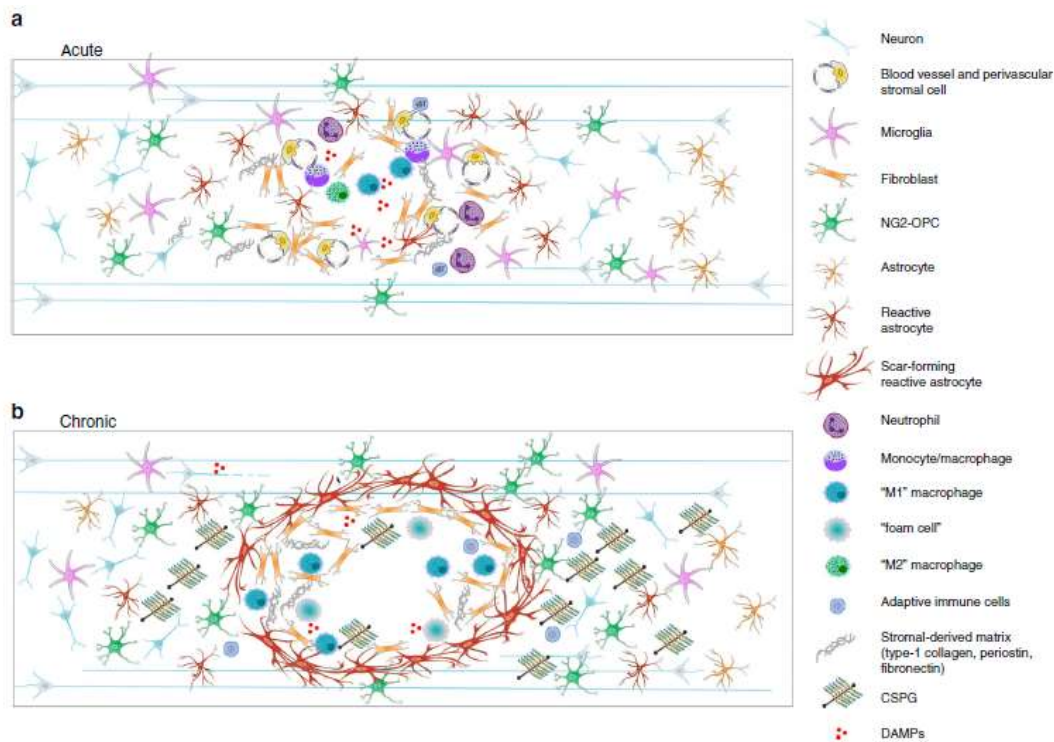


Fig. 12: The picture illustrates the cells' activation and development of the glial scar after SCI. Note that the chronic scar is composed of many different types of cells, particularly activated astrocytes in the lesion border, limiting the extension of the necrotic damage caused by the inflammation. Inflammatory cells are confined inside the glial scar and continue to produce pro-inflammatory cytokines. The scar shapes the surrounding spinal cord tissue modifying the composition of the ECM in particular. The glial scar is often associated with poor functional outcome, but the complete ablation worsens the SCI condition in experimental animals. Image from ¹⁵⁰

Although astrocytes are the principal liable cells for the glial scar formation during the sub-acute phase of SCI, the scar is composed of other cells that directly participate in its maturation and evolution during the sub-acute and chronic phase of the SCI. Usually, astrocytes reside in the lesion border and the perilesional healthy tissue of the lesioned spinal cord, whereas other cell types populate the interior of the scar and shape the surrounding microenvironment (Fig. 12) ¹⁵⁰. The main cell types in the astroglial scar are the resident microglia and immune cells that, as mentioned above, stimulate an inflammatory microenvironment after SCI and reside in the primary lesion site producing pro-inflammatory cytokines and mediating the removal of cellular debris. The containment of the microglia/MDM population positively affects the surrounding tissue, preventing the abnormal distribution of these reactive cells ^{60,150}. Another cell type that migrates and differentiates in the glial scar is the fibroblastic-like cells ¹⁵⁰. Usually, these cells in the spinal cord are associated with the vasculature endothelium and participate in the generation of stroma and other ECM components, principally Fibronectin and Collagen I ¹⁵⁴. The fibroblast-like cells become isolated from the healthy tissue by the astrocytic scar, preventing the outspread of the stroma produced by those cells. The last cell type that composes the glial scar is the OPCs; as mentioned before, these cells are fundamental in the remyelination process after SCI but can also respond directly to the

damage and became hypertrophic, producing great quantity of NG2, a CSPG associated to axonal regrowth inhibition¹⁵⁵. In the glial scar NG2⁺ cells intermingle with the reactive astrocytes at the injury border¹⁵⁰. It has been reported that some OPCs in the glial scar are positive to the astrocyte marker GFAP and capable of differentiating in functional astrocytes¹⁵⁶. Although this capacity, the role of OPCs in the glial scar is not well clear still¹⁵⁰. The interaction between all the cells types in the injured cord form a novel environment constituted by a central degenerating area composed mainly of activated immune cells and degenerating neurons and glia and a peripheral zone composed of astroglial cells and fibroblast-like cells. A strong network of cytokines and other soluble factors is present in the lesion epicenter and influence the maturation and the function of all the cells composing the astroglial scar. Thus this stormy microenvironment contributes to the continuous activation of all cells type of the astroglial scar leading to a non effectively resolve pathology¹⁵⁰. On the other hand, the glial scar's presence is fundamental in limiting the spreading of the degenerative signals in the healthy tissue and containing the majority of inflammatory signals within the primary lesion site. It has been observed that complete ablation of the glial scar after SCI is deleterious for functional recovery and worsens the spinal cord's anatomic integrity, leading to a spreading of the damage to surrounding healthy tissue¹⁵⁰.

Another critical aspect of the glial scar is its composition in terms of non-cellular components, particularly the ECM proteins and molecules that constitute the external microenvironment of the glial scar and interact with all the cell types in the lesioned spinal cord. In the healthy spinal cord, the ECM composition is rich in glycoproteins and proteoglycans like Aggrecan, Brevican, and Neurocan bound together to a hyaluronan scaffold's backbone intermingled with linker proteins known as Tenascin¹⁵⁷. The structure of ECM spinal cord tissue is composed of: I) a basement membrane, mainly formed of collagens, laminins, and fibronectins; II) an interstitial space, which has a relatively loose structure composed of hyaluronan (HA) and CSPG; and III) a perineuronal net (PNN) composed of a tight structure of CSPG, HA, and tenascin which wrap densely synaptic boutons¹⁵⁸. As mentioned above, the principal constituent of ECM in the spinal cord are glycosaminoglycans (GAGs), principally composed of linear polysaccharide chains of chondroitin sulfate (CS), heparan sulfate (HS), and HA. Except for HA, the other classes of GAGs are typically bounded to an amino acid residue of a core protein to form a proteoglycan (PG)¹⁵⁹. Hyalectans like versican (CS/DSPG), aggrecan (CS/KSPG), neurocan (CSPG), and brevican (CSPG) are expressed in the spinal cord. Another component is Tenascin (R, C, X), which is highly elastic and can bind to HA, PG, and other cell surface proteins to establish a substrate for the cells and extracellular molecules, creating a reticulate structure in ECM, particularly at the levels of PNN. Tenascin-R is expressed in healthy and adult CNS by OLs and motoneurons. Other components like collagens and laminins are involved in maintaining the basement membrane between the endothelial cells and parenchyma¹⁵⁸. After SCI, the primary lesion disrupts the organized structure of the ECM and alters cellular composition. During the secondary phase, the glial scar

and the inflammatory infiltrate modifies the ECM composition, particularly the production of CSPGs by astrocytes. This dramatic CSPGs enhancement protects the CNS resident cells at the primary stages of the lesion but, in the chronic phase, often inhibits both regenerations of axons and remyelination by OLs and altering OPCs differentiation¹⁶⁰. The fragmentation of the HA backbone also causes the release of pro-inflammatory molecules (CD44, low molecular weight HA, MAG, OMgp) from the ECM itself, which are recognized by microglia macrophages, increasing the tissue inflammation¹⁵⁷. Lastly, the alteration of ECM composition alters its stiffness, rendering the primary lesion site and the surrounding tissue involved in secondary degeneration stiffer than normal spinal cord parenchyma, thus disadvantaging cellular differentiation and process elongation for both neurons and OLs¹⁶¹. The nature of modification in ECM after SCI enhances the expression of molecules inhibitory to axonal regrowth and restrict neurite plasticity.

1.4.9. Demyelination and remyelination

As mentioned in the previous paragraph, OLs are mostly affected by the consequences of modification in normal homeostasis after SCI. The microenvironment following SCI contains many noxious molecules and inflammatory mediators and a lack of the normal oxygenation that allows the proper levels of O₂ in tissues. OLs, on the other hand, express a series of receptors that can ligate many of the molecular messengers released from the microenvironment and transmit signals that bring those cells to death through the necroptotic or apoptotic pathway in the first 24 hours post-injury¹⁶². Among these pro-apoptotic signals, the elevation of EAAs, particularly glutamate, has a deleterious effect on OLs since these cells express all the ionotropic receptors for glutamate and respond with a burst influx of Ca⁺⁺, leading the cell to apoptotic death^{79,163}. As described in the previous section, other noxious stimuli for the survival of OLs after SCI derives from the release of high levels of pro-inflammatory cytokines, oxidative stress, and loss of trophic support from degenerating neurons¹⁶⁴. In addition to OLs death, the precursors of OPCs represent a class of cells undergoing the necrotic and apoptotic process after SCI. OPCs are very sensitive to the modification of the microenvironment and, in particular, to the levels of nutrients (glucose) and state of oxygenation and inflammation of the tissue¹⁶⁵. Moreover, OPCs express the purinergic receptors for the capitation of ATP levels and are sensitive to the perturbation in the concentration of the second messengers in the extracellular space, causing the activation of pro-apoptotic pathways¹⁶⁶. The final result of SCI on OPCs is the activation of cell death programs and a block of their differentiation process due to the presence of myelin debris, activation of inflammatory cells, and astrocytes.

As a whole, these mechanisms are deleterious for the endogenous remyelination of nude axons and constitute the first depletion of mature OLs during the first stages of SCI^{54,167,168}. The death of OLs continues for the first month after SCI and spreads in the adjacent segments of the primary lesion site, arriving at 4 segments of distance in some cases^{59,169}. The depletion of myelinating OLs has a significant impact on the state of axonal myelination due to their ramified structure and the capacity to myelinate

multiple axons. For instance, the death of one OLs could leave without myelin sheath multiple axons spared from the initial damage or the secondary degeneration and hence compromising the conduction of the electric impulses in the spared white matter⁵⁹. Therefore, the demyelination of the spared tract of white matter and the impaired remyelination contribute to developing the functional deficit in the patient with SCI¹⁷⁰. The functional restoration of locomotion in SCI patients could be improved by enhancing the remyelination of the demyelinated but spared axons in the spinal cord passing in the lesion epicenter's proximity. Another potential therapeutic target is the limitation of the initial death of OLs and OPCs and the stimulation of the endogenous differentiation of the latter cell type¹⁷⁰⁻¹⁷². The associated secondary neuronal death is a successive event and starts mainly after 24 to 48 hours from SCI. The state of myelination of axons is fundamental to neuronal survival and conduction of the information through the spared neuronal tissue. Progressive demyelination that follows OLs cell death exposes "nude" axons to a deleterious microenvironment and reduces the axons' metabolic supply. The presence of axo-myelinic synapse has been described as supplying metabolic support to long axons of nerves, especially in the spinal cord. The disruption of this axo-myelinic synapse after the death of the OLs exposes axons to a toxic microenvironment and pro-apoptotic factors, including myelin debris. Successively neurons undergo modification in axonal cytoskeletal proteins, especially the neurofilaments, causing a reduction in the axons' diameter and, in the end, a complete truncation. Moreover, modification in the axons' structural proteins associated with a reorganization of the ionic channels along the entire length of the cells reduces the capability to transmit electrical signals and eliminate the salutatory conduction¹⁶⁴.

The only repair capability of the CNS is remyelination. Unlike neurons, it is well known that OPCs can proliferate and differentiate in functional OLs even in adult life with a very efficient mechanism under physiological conditions resulting in continued myelination of the CNS¹⁷³. OPCs respond to the SCI with their activation and start to proliferate as soon as 24 hours post-lesion, continuing their proliferation for the first weeks post SCI. The factor prompting the OPCs activation is the presence of unmyelinated axons, cytokines and growth factors secreted by the astrocytes and microglia cells. Among these, there are IGF-1, BDNF, FGF, EGF, PDGF, IL-10, and neuregulin 1^{174,175}. It is noteworthy that neuregulin 1 is the principal marker associated with remyelination and is secreted and upregulated by neurons in the first week of SCI¹⁷⁶. Neuregulin 1 is also a pro differentiating signals for the OPCs, together with other growth factors like IGF-1, BDNF, EGF, and CNTF, and starting from 2 weeks from SCI in animal models has been observed the presence of newly formed OLs in the spinal cord¹⁷⁵.

Despite the initial expansion of OPCs after SCI, functional remyelination is not very efficient in the injured spinal cord. Experimental studies demonstrated that newly formed myelin sheaths are sparse and often composed of Schwann cells instead of functional differentiated OLs¹⁷⁴. The poor remyelination observed after SCI is mainly caused by different factors, particularly the presence of the astroglial scar and the

inflammatory microenvironment. The first obstacle to effective remyelination is the decreased capacity of OPCs to differentiate in functional OLs. This mechanism requires many factors presented to the OPCs in an ordinate way. One of the principal obstacles in OPCs differentiation after SCI is the presence of high levels of IL-1 β , CSPGs, and myelin debris. On the other hand, the low level of pro differentiating factors like T3 hormone limits the capacity of OPCs to produce functional OLs ^{174,177}. Another factor limiting effective remyelination is the limited capacity of newly formed OLs to recognize the “nude” axons and expand their cellular membrane to enwrap the axons. Moreover, the same inhibitory clues that act on axonal elongation also block the expansion of OLs membranes. In particular, myelin debris and CSPGs are recognized by LAR, and RPTP- σ receptor activates the RhoA/Rock pathway in the OLs ¹⁷⁴. Compared to neuronal rewiring, remyelination is more efficient in the context of SCI, and many authors claim that the endogenous repair of the spinal cord after a traumatic insult is mainly composed of the remyelination of “nude” axons. The partial functional recovery in patients with SCI could be affected by the spinal cord tissue's capacity to activate OPCs and generate functional myelinating OLs. In both animals (experimental and companion) and humans has been observed spontaneous remyelination which is also active after a long time from the traumatic event ^{174,175}.

1.4.10. Other endogenous repair attempts

All the modifications described in the previous paragraph produce principally negative effects after SCI, and those negative effects are translated into a poor functional outcome after a lesion. Anyway, to some extent, in both animals and humans with SCI, a certain grade of spontaneous recovery is observed in locomotor function. This spontaneous amelioration is often associated with the intrinsic reparative/regenerative capacity of the spinal cord. An increasing number of studies in the literature focus on enhancing endogenous regeneration with different therapies acting on neuronal cells. The rationale for targeting these cells is that after SCI is present spontaneous axonal elongation and dendrite sprouting in the perilesional site. After SCI, endogenous neuronal elongation is a very rare and poorly efficient mechanism, observed mainly in animals study but not described in humans ¹⁷⁸. The reorganization of the surviving axons in the perilesional zones or supraspinal targets is a more efficient mechanism known as neuronal circuitry plasticity. This mechanism is characterized by neurons' spontaneous ability to detect the loss of connection with their target and send a collateral projection to another neuron. These collateral projections are mainly directed to propriospinal neurons in the spinal cord to create a relay circuitry to bypass the lesion site ¹⁷⁸. The formation of new synaptic contacts is anyway limited to short distances and cannot overcome the damaged tissue in a diffuse lesion. Moreover, due to a robust inflammatory microenvironment after SCI and the glial scar containing anti regrowth factors like NogoA, CSPG, myelin debris, the efficacy of neuronal rewiring is very poor, often leading to maladaptive plasticity.

1.4.11. Chronic SCI

The SCI's final stage is the stabilization of the glial scar with the consolidation of all the previous modifications discussed above. Overall the last phase of SCI is called the chronic phase and is the life-lasting condition that the patients have to face after the traumatic lesion to the spinal cord. During the previous phases, the modification creates a non-resolving pathology that leads to functional loss and the creation of a scar in the spinal cord tissue. The ultimate modification of the lesioned spinal cord in the chronic phase is the enlargement and the cavitation of the glial scar formed in the precedent phases. This process is mostly driven by the apoptotic death inside the glial scar; the permanent inflammation is driven by M1 macrophages stimulating the death of astrocytes in the scar border through activation of TLR4/MyD88 pathway¹⁷⁹. The exact mechanism of cavitation of the glial scar is not well understood, even though many secondary processes are involved in this phenomena and actively remodel the glial scar. Among these mechanisms are: ischemia, hemorrhage, lysozyme activity, and pulsative hydrodynamics⁵⁹. One of the most common consequences of the cyst formation after SCI is the development of syringomyelia, which is a progressive accumulation of CSF in the spinal cord that augments the pressure and causes compressive damage to the surrounding healthy tissues⁵⁹. Clinical manifestations of syrinx formation in the patient are pain and the aggravation of neurological deficit. The creation of the syrinx is a complex process and mainly derived from the SCI's immediate events, like the hemorrhage and the CSF circulation alteration, but also edema and inflammation play an essential role in this pathological event⁵⁹.

1.5. SCI Therapies

The devastating condition of a spinal cord injury has driven research in more recent years toward developing clinical and pharmacological interventions to treat patients with this ailment. The creation of novel surgical techniques, such as the laminectomy procedure, helped physicians manage spinal cord injury and reduce the disabilities that follow this condition¹⁸⁰.

In the last decades, many improvements have been made in the managing of patients (humans and animals) with a spinal cord injury, starting from their initial recovery at the specialized center or hospital and clinical intervention in order to control and ameliorate the general health of these patients that many times suffers from polytrauma. Despite these advancements, spinal cord injury is an incurable condition classified as "Orphan disorder by Orphanet (ORPHA:90058) and by EMA (EU/3/19/2153).

The only practicable intervention on the patients after SCI is the surgical intervention to reduce the compression caused by edema and bleeding. Moreover, surgery can be necessary in case of spine fractures that need stabilization. In the last decades, the timing of initial surgery for SCI decompression has been investigated as a primary factor in reducing the spinal cord's damage and improving the patient's functional recovery in the successive months. As for the ischemic strokes, where an early surgery is more effective in limiting damage and function loss ("time is brain")¹⁸¹, the concept of timing for the intervention and

therapy in spinal lesioned patients has driven the clinician to the concept of “Time is Spine”¹⁸². Many independent studies¹⁸³ and a multicenter study called Surgical Timing in Acute Spinal Cord Injury Study (STASCIS)¹⁸⁴ compared early surgical intervention (24-72 h) to late (after 72 h) surgical intervention for the decompression of SCI. The results of these studies demonstrated that early surgical intervention improves the functional recovery in spinal cord injury patients, and hence the early admission of the patients in specialized centers is critical for the outcome of this condition.

According to this lack of a therapeutical plan for SCI, a pharmacological intervention to target the destructive molecular and cellular events in the spinal cord after a lesion is an urgent need to improve the patients' functional outcome. Actually, there is no “gold standard” in human or animal medicine to treat SCI. In the past was used diffusely the Methylprednisolone Sodium Succinate (MPSS), a steroidal anti-inflammatory which acts as a glucocorticoid receptor agonist and function as antiedema. MPSS was thought to promote neuroprotection acting on the mechanism of peroxydation of the neuronal membranes in the early secondary cascade of the spinal cord injury¹⁸⁵. However, its clinical practice usage has been abandoned because NASCIS studies were strongly disputed in the last years due to biases in the trial design. In particular, NASCIS I did not compare the effects of MPSS with a placebo group and did not define a therapeutic dosage with a dose-response study¹⁸⁶. The study design for NASCIS II was then implemented with the insertion of a placebo group and the definition of a therapeutical range of concentration of MPSS¹⁸⁷. Even with this implementation, the application of MPSS in SCI patients failed to reach a significant improvement in locomotor function. However, a successive re-examination of patients' stratification based on the timing of administration of MPSS found an amelioration in functional recovery of 4.8 points in the motor scale in patients receiving MPSS until 8 hours after the injury¹⁸⁸. NASCIS III study was aimed to define whether a more prolonged administration of MPSS induced more neuroprotection than the standard 24 hours scheme of administration¹⁸⁷. The study identifies that patient who received the first bolus of MPSS after 8 hours has higher functional recovery if the administration of MPSS was maintained for the next 48 hours. The limitation of this drug delivery protocol is the increase in complications like severe pneumonia and sepsis due to the high regime of immunosuppression. The evidence of inefficacy of MPSS lead to its discontinuation from clinical practice, and the high risk of developing essential side effects with this therapy leads to the recommendation to suspend all the treatment with cortisonal drugs at the admittance of the patient to the clinic. Several clinical trials, reported in table 8, were performed with other putative drugs aimed to improve functional recovery in SCI based on their efficacy on pre-clinical models. None of those clinical trials highlighted significant positive results; only some treatments were effective in a limited cohort of patients showing little benefit for the functional recovery¹⁸⁶. It is essential to mention that now there are different clinical trials for innovative strategies to target SCI in human and animal medicine. Among them, Minocycline was classically used for its properties as antibiotics, which stimulated neuroprotection in the lesioned spinal cord preventing OLs and microglia apoptosis¹⁸⁹. A phase II clinical

trial with Minocycline in SCI patients showed an improved ASIA scale for cervical injury and no effect on thoracic injuries ¹⁹⁰. From these results, a phase III clinical trial for Minocycline is ongoing to improve the therapeutic range and administration and reduce side effects (ClinicalTrials.gov NCT01828203) ¹⁸⁶. Other clinical trials for novel therapies in SCI include antibodies targeting specific axon regrowth inhibitory molecules like Nogo-A, which directly blocks axon elongation and is strongly expressed after SCI ¹⁹¹⁻¹⁹³. Riluzole is an anticonvulsant drug approved for treating Amyotrophic Lateral Sclerosis (ALS) and is involved in a SCI clinical trial (ClinicalTrials.gov NCT00876889) ¹⁸⁶ for its property of Na⁺ channel blocker and inhibitor of glutamatergic excitotoxicity ¹⁹⁴⁻¹⁹⁶. Cethrin is a recombinant C3 transferase that blocks specifically the RhoA protein ¹⁹⁷, and it is actually on a phase I/IIa clinical trial (ClinicalTrials.gov NCT02669849) ^{186,198}. In SCI, the blockage of RhoA activity enhances axonal elongation and regrowth ¹⁹⁹. The latest clinical trials involve biomaterials and stem cell implantation in the lesioned spinal cord for the regeneration of neuronal tissue and enhance white matter sparing. INSPIRE is the clinical trial (ClinicalTrials.gov NCT02138110) ¹⁸⁶ for Neuro-Spinal Scaffold of poly-lactic-co-glycolic acid coupled with poly-L lysine (PLL-PLGA). Stem cells used in clinical trials for SCI includes derived neuronal/glial progenitors from Human Embryonic Stem Cells (hESC) like OPC (ClinicalTrials.gov NCT02302157), fetal forebrain human neuronal stem cells (ClinicalTrials.gov NCT01321333); but also non-neuronal cells like adipose-derived mesenchymal stem cells (AD-MSCs, ClinicalTrials.gov NCT03308565) ¹⁸⁶. The stem cell clinical trials are still in the early phases of recruitment and the definition of eligibility criteria, and we will have the results in the next years.

Table 8: The table reports the most relevant clinical trials in SCI therapy. From ¹⁸⁶.

Drug	Therapeutic plan	Control group	Primary goal	Results
MPSS (NASCIS I)	High dose 1000 mg i.v. bolus and daily for 10 days	Low dose 100 mg i.v. bolus and daily for 10 days	NASCIS motor and sensory score	No differences in functional recovery. More infection in the high dose group
MPSS (NASCIS II)	30-mg/kg i.v. bolus then 5.4- mg/kg/h infusion for 23 h	Placebo	NASCIS motor and sensory score	Improved sensation and motor function for patients treated within 8 h from SCI
MPSS (NASCIS III)	5.4-mg/kg/h i.v. infusion for 48 h	5.4-mg/kg/h i.v. infusion for 24 h	ASIA Score	Significative locomotor improvement for patients treated after 8 hours with MPSS. Nonsignificant trend for motor improvement at 6 weeks
GM1 ganglioside	100 mg i.v. for 18-32 doses 300 mg i.v. then 100 mg daily for 56 days 600 mg i.v. then 200 mg for 56 days	Placebo	Frankel grade ASIA score Benzel grade	Significantly greater improvement in ASIA motor Score with GM1 versus placebo. No difference in the fraction of patients exhibiting marked recovery at 26 weeks with high-dose versus low-dose versus placebo.
Thyrotropin Releasing Hormone (TRH)	0.2 mg/kg bolus i.v. and 0.2 mg/kg/h for next 6 hours	Placebo	NASCIS motor score	No efficacy for complete injuries. Partial effect on incomplete injury
Nimodipine	0.015 mg/kg/h for 2 hours followed by 0.03 mg/kg/h for 7 days	No treatment	ASIA scale	No significant differences among the treatment groups.
Gacyclidine	0.005mg/kg, 0.01mg/kg or 0.02 mg/kg i.v. twice at an interval of 4 h	Placebo	ASIA scale	No significant differences among the treatment groups.

2. AIM OF THE THESIS

The thesis's present work was aimed to study the changes in the CNS after acute traumatic damage and evaluate the modification during the secondary phase of the trauma. The present work mainly focuses on the traumatic SCI and the evolution of the spinal cord's microenvironment after a contusive trauma. The principal goal is to understand the pathophysiological alteration following SCI to identify a possible target for enhancing the organism's endogenous reparative process. Moreover, the possibility of acting on the secondary degeneration in the early phases of trauma was investigated extensively to identify potential therapeutic windows for the limitation of the inflammatory activation in the lesioned spinal cord.

The relevance of identifying an effective treatment for SCI is crucial for both human and animal medicine. This experimental work is indeed realized in an optic of "One Health" ²⁰⁰ for improving the condition of lesioned patients without any specie distinction.

The present work of the thesis is divided into 5 sections to investigate the SCI induced modifications and effects on the spontaneous repair. The last two sections present a detailed review of myelin pathology in the CNS and axonal regrowth stimulated by NGF. The first section focuses on establishing a reliable animal model of contusive SCI for the successive experimental procedures. The principal goal of this part of the work is to realize a contusive lesion at the vertebral T9 level that is reproducible and shows the principal characteristic of the SCI evolution during the time. Moreover, in this phase, the wellness criteria of the lesioned animal and the functional test were also selected to evaluate locomotor deficit. The secondary goal was to identify the best analysis for defining the total lesion volume in the injured spinal cord with histological techniques.

The second section of the thesis regards a methodological consideration for tracing experiments in the CNS. The primary goal of this section was to evaluate the possibility of coupling in-situ hybridization with Pseudo Rabies Virus (PRV) as a retrograde tracer for the characterization of neuronal circuits in the CNS. The secondary goal was to analyze the inflammatory response in the spinal cord of animals traced with PRV in the early phases of infection.

The third section of the present work focuses on studying the extracellular matrix components modification in the segments surrounding the lesion epicenter at different time points. This part of the work's principal goal was to investigate the gene expression changes induced by the lesion in the spinal cord segment not directly involved in the primary event. We also selected 3 different time points to evaluate gene expression following the secondary degeneration timeline to perform a longitudinal study. The secondary goal of this section of the thesis was the identification of essential genes involved in the modification induced by the SCI with a bioinformatics approach.

The fourth part of the thesis investigates the changes in gene expression involved in synaptic plasticity in different areas of the CNS, including the supraspinal connection of motoneurons in the spinal cord. This approach is firstly aimed to evaluate the plasticity of the motor system in the rat after a contusive lesion of the spinal cord. Also for this section, we selected 3 times points crucial in the secondary degeneration evolution to study the modification in synaptic plasticity with a longitudinal approach. The principal aim was to understand the extension of the modification in synaptic plasticity and the principal site of the CNS involved in these modifications.

The fifth section of this work is focused on the stimulation of the endogenous repair capacity in the spinal cord and the limitation of the extensive inflammatory microenvironment after the injury. The principal goal of this part was the testing in vivo of therapeutical implantable biomaterials loaded with different drugs combination to stimulate remyelination (T3) and reduce inflammation (Ibuprofen). This strategy is used to overcome adverse reaction problems commonly present in SCI systemic treatment and increase the concentration of drugs in the primary lesion site bypassing the BSCB. The secondary goal was to improve locomotion in animals treated with the implantable scaffold loaded with drugs than the animals receiving the unloaded scaffold.

The sixth section of the thesis regards myelin pathology in the CNS, primarily focusing on several aspects of OPCs biology. Among the function of OPCs, this review concerns the histology and role in the neurovascular-neuroglial unit in preclinical and clinical studies on Alzheimer's Disease (AD). Moreover, the susceptibility of OPCs to hypoxia-ischemia is studied in this part of the thesis, being a common cause of death in many CNS pathologies/conditions, including SCI.

The last section of the present work of the thesis aims to describe the effect of the Nerve Growth Factor (NGF) on the repair capacity of the CNS, Peripheral Nervous System (PNS), and other body districts. Moreover, the interaction between NGF and the OPCs/OLs pool in neurodegenerative conditions is described.

3. MATERIALS AND METHODS

3.1. Animals and surgery

CD-Sprague Dawley female rats of 8 weeks of age (200-250 gr.) were used to create the spinal cord injury model. All animals had free access to food and water with no diet restriction during the experimental period. Animals were housed in pairs to reduce the stress and stimulate recovery after the surgical procedure. Preoperative antibiotics (Enrofloxacin 5 mg/kg, s.c.) and painkillers (Tramadol 5 mg/kg, s.c.) were administered one hour prior surgical procedure. Bladders were manually expressed before anesthetizing the animals with isoflurane (1–3%) in O₂; the anesthetic plane was maintained for all the surgery duration. Heart rate and respiratory rate were used as indicators of the deep anesthetic plane, whereas pinching response and pupillary reflex were used as indicators of the light anesthetic plane. Contusive lesions of the spinal cord were performed at the vertebral T9 level (T12 spinal level). To obtain a reproducible in vivo model of SCI, all surgical procedures were standardized in young adult female animals. Rats were placed on the adapted stereotaxic table for SCI surgery, and their backs were shaved and sterilized with Betadine solution. A longitudinal, median dorsal incision in the skin, with a length of 4 cm starting from the midline between the scapulae and arriving at the last fluctuating rib, was made using a 10 scalpel exposing the superficial muscles layers. To expose the vertebral column, the fat tissue covering the muscle layer was carefully removed using iris scissor, and two incisions, parallel to the body axis, were made on the vertebral column's sides in the underlying spinotrapezius muscle. After the ligaments of the latissimus dorsi were cut and the vertebral column separated from the deep muscle layers at both sides to expose the transverse process of the vertebrae. In the end, the processus spinosus of T7–T11 vertebrae were freed from the overlying remaining muscles. For identifying the T9 vertebra, we used the shape and the edge of the spinous process as tactile and were possible visual markers. Once the T9 vertebra was identified, the T8 and T10 transverse processes were mounted and fixed on the stereotaxic modified brackets to block the vertebral column and avoid movement during the spinal contusion. The laminectomy procedure was used to expose the spinal canal. Briefly, using a Rongeur, the pedicles of the T9 vertebra were cut, and all the *lamina* were removed using a clamp to expose the spinal canal and spinal dura. Before spinal cord contusion, the dura mater was carefully cut with a 25G needle to avoid the spinal cord's compression due to hemorrhage. Spinal cord injury was performed using Impact One Impactor (Leica Biosystems, Wetzlar, Germany) at the vertebral T9 level using a round tip of 1.5 mm or 2 mm in diameter. To standardize the spinal cord's contusive lesion and obtain a mild/moderate contusion, we used fixed-parameters, a force of 1 N (0.75 m/s), and 0 s of stance time after the impact. The depth of impact was 1.5 mm or 2 mm to reach ventral horns of grey matter and spare the underlying white matter tracts. After the contusive lesion, hemorrhage was gently stopped using a sterilized cotton bandage then the overlying back muscles were sutured using a 3/0 resorbable wire. The skin incisions were closed with wound clips. After the surgery, all animals receive 1 ml s.c. of sterile physiologic solutions, and bladders were manually voided.

Then rats were placed in their house cages and monitored until the full recovery from anesthesia. For pain management and avoid infections after the surgery, rats were treated for 3 days twice a day with antibiotics and painkiller therapy (enrofloxacin 5 mg/kg and tramadol 5mg/kg s.c.). Since the spinal lesion causes a severe functional loss compared to healthy uninjured animals and the only laminectomy procedure) did not recapitulate the locomotor impairment observed in the injured animals (data not showed), as control group unlesioned and healthy age-matched animals were used.

Animal wellness was evaluated mainly monitoring daily body weight increase/loss after the surgical procedure, using the animals' weight on the day of surgery as the baseline. We then integrate the bodyweight information with clinical parameters, including physical appearance, behavior/activity, clinical signs, lesion/autotomy, and cyst/tumors. The integrated score was evaluated daily for the first two weeks after injury, then once a week until the day of sacrifice. This integrated score represents the general status of the animal and defines wellness after the contusive lesion. Animals with a score greater than 20 were euthanized and excluded from the analysis ²⁰¹. In case rats showed urinary retention or difficulty in spontaneous voiding after the lesion, bladders were manually expressed 3 times a day until spontaneous micturition reflex was present.

All animal protocols described here were carried out According to the European Community Council Directives 2010/63/UE, and approved by the Italian Ministry of Health (D.Lgs 26/2014, authorization n°574/2015-PR). Moreover, animal protocols were carried out in compliance with the ARRIVE guidelines and the NIH Guide for the Care and Use of laboratory animals.

For neuronal tracing analysis, a total of 9 adult female Lewis rats were investigated in this study [LEW/OrIRj (Lewis); weight, 200-230 g; purchased from Janvier, France]. The rats were housed in groups of 3per cage, and food (rat chow) and water were provided *ad libitum*. Rats were maintained on a 12:12 h light: dark cycle (light on from 6:00 A.M. until 6:00 P.M.). All experimental procedures were conducted following ethical guidelines and were approved by the Veterinary Office of the Canton of Zurich, Switzerland (license 136/17).

3.1.1. Scaffold implantation

Animals underwent a contusive spinal cord lesion at the thoracic level T9 described before using the features to obtain a mild/moderate spinal cord contusion. After performing spinal cord lesions, PLLA scaffolds, either conjugated or unconjugated with drugs, with a surface of 0.75 cm², were locally implanted upon the contused spinal cord. To avoid moving the PLLA implant, tissues were coated with surgical adhesive glue (BioGlue, CryoLife, Kennesaw, GA), forming a bridge between the two adjacent vertebrae to reduce the possibility of the implanted scaffold to be removed from the spinal canal.

3.1.2. PRV injections

Animals were initially anesthetized in 5% Isoflurane (Piramal Healthcare, Digwal, Telangana, India) in air, and anesthesia was maintained with an intramuscular injection of a triple-combinatorial preparation of Medetomidine (Dormitor, 0.105mg /kg body weight, Provet AG), Midazolam (Dormicum®, 1.4mg /kg bodyweight, Roche) and Fentanyl (0.007mg /kg bodyweight, KantonsapothekeZürich). The urethra was exposed with a 2cm long incision into the skin above the lower abdomen. Using a 10uL microsyringe (Hamilton, VWR International GmbH) attached to a 33G needle (NanoFil, World Precision Instruments), four injections of 1µL PRV614 (2.03×10^9 pfu/mL) each were performed on the ventral and lateral sides of the EUS. Animals were then sutured and allowed to recover on a heat blanket for 45min before subcutaneous application of the antidote (Antisedan, 0.75mg /kg bodyweight, Provet AG and Anexate, 1mg /kg body weight, Roche). Analgesics (Rimadyl, 2.5mg /kg bodyweight, Pfizer) and antibiotics (Bactrim, 15mg /kg body weight, Roche) were applied immediately after surgery and daily until the end of the experiment. Two animals did not receive any PRV injections and were used as a reference.

Scaffolds preparation

The electrospinning apparatus (Spinbow Srl, Italy) comprised a high-voltage power supply, two glass syringes containing the polymeric solutions, each one connected to a stainless-steel blunt-ended needle (inner diameter 0.51 mm), positively charged and positioned on the opposite sides of a grounded aluminum drum-type collector (diameter 5 cm) rotating at 75 rpm. Needle-to-collector distance was fixed at 20 cm. This kind of apparatus enabled the co-electrospinning of two different polymeric solutions, whose feed rates were independently controlled by two syringe pumps, and to collect the corresponding fibers evenly distributed on the rotating drum. The delivery system containing T3 and Ibu was produced by co-electrospinning the following two PLLA polymeric solutions: (i) PLLA 20% w/v dissolved in DCM:DMF 70:30 (v/v), with the addition of a suitable amount of Ibu to give a 5wt% of the drug in the final fibers, and (ii) PLLA 20% w/v dissolved in DCM:MetOH 70:30 (v/v), with the addition of a suitable amount of T3 to obtain a 0.6 wt% of the drug in the final fibers. The applied voltage was 18 kV, and the solution feed rates were set at 1.2 ml/h. An electrospun control sample was produced by co-electrospinning the aforementioned described polymeric solutions not-loaded with drugs. All scaffolds were produced at RT and relative humidity of 30% by co-electrospinning the polymeric solutions for a period of 3 h and a half hours, giving samples with a thickness range of 170-200 µm. Scaffolds were sterilized using γ-rays (25 KGy) before implantation.

3.1.3. Materials

PLLA (RESOMER® L 206 S, inherent viscosity = 0.8-1.2 dL/g) was purchased from Evonik Industries. N, N-Dimethylformamide (DMF), dichloromethane (DCM), Methanol (MeOH) were purchased from Sigma Aldrich. 3,3,5-Triiodo-L-thyronine sodium salt (T3) ≥95% (HPLC) was purchased from Sigma Aldrich. Ibuprofen (Ibu) was purchased from Sigma Aldrich.

3.1.4. Scaffold characterization

Fiber morphology was observed using a Leica Cambridge Stereoscan 360 Scanning Electron Microscope (SEM) operating at 20 kV. The samples were sputter-coated with gold before the examination. For determining each scaffold's fiber diameter distribution, 100 fibers were measured, and the results plotted as the mean diameter ± standard deviation.

3.1.5. In vitro drug release

For the determination of drugs release from scaffolds were used rectangular electrospun samples of approximately 3 cm² using 10 mL of phosphate-buffered solution (PBS, 0.1 M, pH = 7.4) as media for drugs release. Samples were incubated in an SW22 Julabo shaking water bath for a maximum period of 15 days. Daily, the PBS was removed entirely and replaced with fresh buffer. Aliquots were analyzed using HPLC and mass spectrometry to determine Ibu and T3 cumulative release, respectively. The concentration of Ibu released in the PBS buffer was measured using an HPLC system equipped with two mobile phase delivery pumps (LC-10ADvp, Shimadzu, Japan) and a UV-Vis detector (SPD-10Avp, Shimadzu, Japan). Samples were accurately weighted and solubilized in ACN:DMSO (3:1 v/v) then added to ACN:PBS (PBS 0.1M pH 7.4) in a ratio 1:4:5 v/v, heated up, and sonicated for 15 minutes. Finally, the samples were centrifuged for 10 minutes at 10000 r.p.m., filtered through a syringe filter NY 0.2µm, and analyzed by HPLC-UV. T3 was measured using a UPLC-MS/MS system. 3 mg of PLLA were extracted three times with 1 mL of methanol and left in an ultrasonic bath for 10 minutes. The three extracts were pooled and evaporated under N₂ stream to the volume of 1mL in the volumetric flask before analysis in UPLC-MS/MS.

3.2. Locomotion analysis

3.2.1. BBB scale

Hind limb locomotor function and spontaneous recovery after spinal cord injury were evaluated using the Basso, Beattie, and Bresnahan (BBB) Scale²⁰². This 21 point scale goes from 0, representing the complete immobility of the posterior limbs, to 21, associated with a healthy animal. This scale correlates the spinal lesion's severity to the locomotor impairment; thus, higher percentages of tissue spared from the spinal lesion are directly associated with a better performance in the BBB Scale. Evaluation of hind limb functional

locomotor loss was performed before lesion to discard animals with spontaneous locomotor deficit, then three days post-lesion, this time point was chosen to avoid to cause too much stress to the animals in the first days after surgery. Then animals were observed once a week until the day of sacrifice. For evaluation of hind limb performance, animals were taken from their home cage and put in a transparent arena with a smooth floor surface to avoid scratching the abdomen. Two independent operators observed the animals' spontaneous locomotion for 4 minutes and evaluated the capacity of hind limb simple movements or the ability to perform stepping and gait. If the animals did not move during the test, they were gently lifted from the tail and repositioned at the arena's opposite side. After 4 minutes of observation, animals were returned to their home cage. The observations were converted into a single paw score; then, to obtain the BBB Score was made the mean between the single paw scores rounded down. The final BBB Score is constituted by the mean of BBB Scores from each operator rounded down. Animals receiving a score greater than 8 at 3 days post lesion (DPL) were discarded from the study. The number of animals included in each experiment is indicated in the results section and the captions.

3.2.2. Catwalk

Gait analysis was performed using the CatWalk (Noldus) automatized system. Animals were trained to walk repeatedly along with the platform before surgery, then tested two days before spinal cord lesion and at 14, 28, and 49 DPL to avoid habituation to the tests and poor performances. All animals performed 5 compliant runs, as defined by the instrument parameters (run duration from 0.5 s to 7s), for each time point, and the mean values of all parameters were calculated using the CatWalk software. Gait analysis was performed using 11 different parameters, divided into 4 categories: spatial parameters (print area, maximum contact area, the base of support); kinetic parameters (stand time, swing time, swing speed, single stance); comparative parameters (stride length, step cycle); coordination parameters (duty cycle, step sequence regularity index). All parameters were analyzed for both hind paws and front paws (shown as a mean of the right paw and the left paw).

3.3. Cell culture experiments

The murine macrophage cell line RAW 264.7 was purchased from the American Type Culture Collection (ATCC® TIB-71™). Cells were grown at 37°C in DMEM high glucose medium (Thermo Fisher Scientific) supplemented with 10% heat-inactivated fetal bovine serum (FBS - Thermo Fisher Scientific), 1% penicillin/streptomycin (100 U ml⁻¹/100 µg ml⁻¹, Thermo Fisher Scientific), in a humidified incubator of 5% CO₂. When 70-80% confluence was reached, cells were detached mechanically with the scraper and subcultured in 75 cm² flasks.

3.3.1. Primary neural stem cells-derived OPCs

Fetal neural stem cells (NSCs) were isolated from E.13.5 rat forebrain as already described, with some modifications. Briefly, tissues were incubated in a non-enzymatic dissociation buffer (Sigma-Aldrich, Saint Louis, MO, USA) at 37°C for 15 minutes and then mechanically dissociated by pipetting. Cells were resuspended in culture medium (DMEM/F12 GlutaMAX 1 x; 8 mmol/L HEPES; 100 U/100 µg Penicillin/Streptomycin; 0.1 x B27; 1 x N-2; 20 ng/mL bFGF; 20 ng/mL EGF; Thermo Fisher Scientific, Waltham, MA, USA) and plated in suspension, at a density of 10 cells/µl. Neurospheres were allowed to proliferate until they attained a diameter of about 100µm.

In order to obtain oligospheres, primary neurospheres were centrifuged at 300 x g for 5 minutes. The pellet was mechanically dissociated by pipetting, and cells were counted and plated again at a density of 10 cells/µl in OPCs medium (DMEM/F12 GlutaMAX 1x; 8 mmol/L HEPES; 100 U/100 µg Penicillin/Streptomycin; 0.1x B27; 1x N-2; 20 ng/mL bFGF; 20 ng/mL PDGF; Thermo Fisher Scientific). Oligospheres were centrifuged, and the pellet was mechanically dissociated to obtain a single-cell suspension. After cell count, cells were plated at a density of 3000 cells/cm² on poly-D, L-ornithine (50µg/ml)/laminin (5µg/ml; Sigma-Aldrich) coating in OPC medium.

In order to induce oligodendrocyte differentiation and maturation, after 3 DIVs OPC medium was replaced with the oligodendrocyte differentiation medium (DMEM/F12 GlutaMAX 1x; 8 mmol/L HEPES; 100 U/100 µg Penicillin/Streptomycin; 0.1x B27; 1x N-2; Thermo scientific) and divided into three groups: i) standard T3-mediated differentiation induction (50 nM T3; 10 ng/ml CNTF; 1x N-acetyl-L-cysteine – NAC; Thermo Fisher Scientific); ii) exposed to PLLA electrospun; iii) exposed to PLLA electrospun loaded with ibu and T3. Electrospun were mounted in 24-wells specific rings, submerged in the culture medium without direct contact with cells. The differentiation phase lasts 12 days.

3.3.2. Conditioned medium preparation

To evaluate the bioactivity of ibuprofen and T3 released from electrospun PLLA fibers conditioned medium was prepared as described below. Sterilized samples (1,5 cm x 0,5 cm) of the scaffolds conjugated with the drugs and blank scaffolds were immersed in 1 ml of complete growth medium for 3 days at 37°C with shaking (50 rpm). Medium with Ibu at a final concentration of 200 µM and T3 at 250 nM with blank PLLA electrospun scaffolds were incubated under the same conditions and served as control. At the end of the incubation, cells were seeded on a 24-well plate with a density of 12000 cells/well. After 3 days, confluent cells were treated for 24 h with conditioned medium and lipopolysaccharide (LPS) at the final concentration of 500 ng/ml to stimulate inflammation. Three samples/group were analyzed.

3.3.3. Cytokine assay

Cell supernatants were centrifuged at 4000xg for 10 min at 4°C before being processed for TNF α quantification by using the Bio-PlexPro Mouse Cytokine kit (BioRad, CA, USA) and following manufacturer's instructions.

3.4. Flow cytometry

A 10-mm spinal cord segment enclosing the injury site was processed for flow cytometry at 1 DPL, and 8 DPL for both groups of animals implanted with PLLA alone or PLLA conjugated with drugs. In brief, animals were sacrificed and perfused with 100ml of Dulbecco's modified PBS (dPBS, Lonza, Basel, Switzerland) to remove circulating inflammatory cells and improve the performance of cell sorting. Cells were isolated with Adult Brain Dissociation Kit solutions in GentleMACS Octo Dissociator (Miltenyi Biotec, Bergisch Gladbach, Germany) before removing myelin debris using the Debris Removal solution (Miltenyi Biotec). This step is fundamental to obtain a sample with only live cells and avoid contamination from necrotic or damaged cells and their debris. At least 2×10^5 cells were resuspended in DPBS. Cell populations were marked respectively with CD11b-PE-Vio770 (1:10), CD45-APC-Vio770 (1:10), GLAST-PE (1:10), CD32-APC (1:10) and CD86-VioBright-FITC (1:10) for the identification of macrophagic (CD11+CD45+), microglial (CD11+CD45-), lymphocytic (CD11-CD45+), astrocytic (GLAST+) and M2 lineages (CD32-/CD86-), respectively. To distinguish live cells, DAPI staining solution (0.1 μ g/ml) was used. All antibodies and DAPI solution were purchased from Miltenyi Biotec. Immunolabeled cell count analysis was performed using FlowLogic software (Miltenyi Biotec).

3.5. Synaptosome preparation, glutamate, and GABA assay.

This procedure was carried out on animals of the 1 DPL and 8 DPL cohorts to study the effect of PLLA loaded with drugs on synaptosomal glutamate release after spinal cord injury. In brief, on the day of sacrifice, 5 animals per group were lethally anesthetized, and their spinal cords were dissected at the level of spinal injury (1 cm length) then inserted in a vial containing cold (4°C) Krebs' solution (mM: NaCl 118.5, KCl 4.7, CaCl₂ 1.2, KH₂PO₄ 1.2, MgSO₄ 1.2, NaHCO₃ 25, glucose 10; gassed with 95% O₂ and 5% CO₂). The vial was then transferred into a freezer set at -80°C for slow freezing and kept until synaptosome analysis. On the day of the experiment, cryopreserved rat spinal cords were slowly thawed at 25°C. after that, a crude synaptosomal (P2) fraction was prepared as follows: the tissue was suspended in ice-cold buffered sucrose solution (0.32 M, pH 7.4) and homogenized. The homogenate was centrifuged for 10 minutes at 2500 rpm at 4°C to remove nuclei and debris, and then synaptosomes were isolated from the supernatant by centrifugation at 9500 rpm for 20 minutes at 4°C. The P2 pellet was then resuspended in 7 ml of Krebs' solution.

Following preparation, identical aliquots of synaptosomal suspension were distributed on microporous filters (0.5 ml/filter), placed at the bottom of a set of parallel superfusion chambers maintained at 36°C and perfused with aerated (95% O₂/5% CO₂) Krebs solution (0.3 ml/min). After 30 minutes of superfusion, to equilibrate the system, 5 minutes fractions were collected from the 30th to the 65th minute (seven samples). The initial three samples were used to assess basal glutamate and GABA release. Synaptosomes were then depolarized with 15 mM K⁺ (substituting for an equimolar concentration of NaCl) for 90 seconds. Following the stimulation period, the synaptosomes were perfused with the original medium until the end of the experiment. Glutamate and GABA were measured by HPLC with fluorimetric detection. In brief, 25 µl was transferred into glass micro vials and placed in a temperature-controlled (4°C) Triathlon autosampler (Spark Holland, Emmen, The Netherlands). Thirty µl of o-phthalaldehyde/mercaptoethanol reagent were added to each sample, and 30 µl of the mixture was injected onto a Chromsep analytical column (3 mm inner diameter, 10 cm length; Chrompack, Middelburg, The Netherlands). The column was eluted at a flow rate of 0.48 ml/min (Beckman 125 pump; Beckman Instruments, Fullerton, CA, USA) with a mobile phase containing 0.1 M sodium acetate, 10% methanol, and 2.2% tetrahydrofuran (pH 6.5). Glutamate and GABA were detected using a Jasco fluorescence spectrophotometer FP-2020 Plus (Jasco, Tokyo, Japan). The retention times of glutamate and GABA were ~3.5 and ~15.0 min, respectively.

Spontaneous glutamate and GABA levels in each sample were expressed in pmol/5 min/mg of protein. The effects of K⁺ stimulation on endogenous glutamate levels during the third fraction were reported and expressed as percentage changes of basal values, as calculated through the two fractions collected before treatment.

3.6. RT-PCR Analysis

Rats were sacrificed at different time points to investigate gene expression modification caused by the SCI in the acute phase, the subacute phase, and the chronic phase. The time points chosen were respectively 1, 8, and 45 DPL. On the day of sacrifice, rats were euthanized with chloral hydrate (37%) administered i.p. The animals' death was ascertained when no heart pulsation and respiration were observed. For gene expression and western blot analysis, the spinal cords were withdrawn and dissected in 3 pieces of 1 cm length. The spinal cord segments were the cervical segment (SC-Cer) corresponding to cervical enlargement and spinal level C5-C8, the spinal cord's rostral segment from the lesion corresponding to spinal level T7-T10, and the caudal segment from the lesion, corresponding to spinal level L2-L5 bearing the lumbar enlargement. The cervical segments were used as an internal control for analysis and investigated the modification in a distant spinal cord area from the lesion epicenter. Tissues of interest were dissected, weighed, and immediately snap-frozen with liquid nitrogen, then stored at -80°C till use. Segments of spinal cord were homogenized in 1 ml of Qiazol solution (Qiagen, Hilden, Germany), according to

manufacturer instruction, in ice using a mechanical Ultra Turrax homogenizer (Ika, Staufen, Germany) until the lysates were uniformly homogeneous. Total RNA was extracted from homogenized tissues using RNeasy Plus Universal Mini Kit (Qiagen). Briefly, after lysis homogenates were kept at room temperature for 5 minutes, then were added 100 μ l of gDNA eliminator solution to each sample and shaken vigorously for 15 seconds. For partitioning of RNA, 180 μ l of chloroform were added and mixed to the homogenates for 15 seconds; then samples were centrifuged at 12000 x g for 15 minutes at 4°C. After centrifugation 3 distinct phases were formed in the homogenates, the overlying aqueous phase containing the RNA was collected from each sample and put in a new tube. Precipitation of RNA was obtained by adding 600 μ l of 70% ethanol. The samples were passed in an RNeasy Mini Spin column (Qiagen), placed in a 2 ml tube, and centrifuged at 10000 x g for 15 seconds at room temperature to retain the total RNA in the membrane of the RNeasy Mini Spin column. For purification of the eluates, 700 μ l of RWT buffer (Qiagen) were added to the column and centrifuged at the conditions mentioned above. Then 2 washes of the membrane were made, adding 500 μ l of RPE buffer (Qiagen) and centrifugation of the sample after adding the washing buffer. Total RNA was then eluted in 40 μ l of RNase-free water. After RNA extraction, we quantified the total RNA for each sample and verified the purity of the RNA through the absorbance ratio of 260/280 nm (Nanodrop 2000 spectrophotometer, Thermo Scientific). All samples carried a sufficient amount of RNA, and no contamination from genomic DNA or proteins was detected. For cDNA synthesis, were used 5 μ g of pooled RNAs from each experimental group. The strategy of pooling RNA samples before retrotranscription allowed us to use less material from each sample and reduce the variability between samples from the same group. cDNA was synthesized using the RT² first strand kit (Qiagen). Pooled RNAs from each group were incubated in GE buffer solution for 5 minutes at 42° C to eliminate enzymatically any possible genomic DNA contamination. Then were added 4 μ l of 5X BC3 buffer, 1 μ l of Control P2, 2 μ l of RE3 Reverse transcriptase mix, and 3 μ l of RNase free water to each pool. Incubation protocol was 15 minutes at 42°C for retrotranscription and 5 minutes at 95°C for reverse transcriptase inactivation with an automatic Biometra T-gradient thermal cycler (Analytic Jena, Jena, Germany). At the end of reverse transcription, 91 μ l of RNase-free water were added to each sample.

We used the Qiagen PCR array technology to investigate ECM and SP-related gene expression changes after spinal cord injury. The Qiagen PCR arrays are reliable and sensible technology that consent to investigate several genes involved in a specific function or pathology at the same time and in the same sample. The plate also contains the internal control for the amplification reaction and 5 different housekeeping genes to reduce variability in data interpretation. The panels of genes contained in the PCR arrays are reported in tables 9 and 10. Eighty-four genes involved in the Extracellular matrix were analyzed using the RT² Profiler Extracellular matrix and Adhesion molecules PCR Array (Qiagen, PARN-013ZD), whereas 84 genes involved in SP were studied using the RT² Profiler Synaptic Plasticity PCR Array (Qiagen, PARN-126ZD). According to

the manufacturer's protocol, real-time PCR master mix was prepared adding 1350 μ l of 2x RT2 SYBR® Green Mastermix and 1248 μ l of RNase free water cDNA samples. Then 25 μ l of PCR master mix were added to each well in the PCR array plate using an 8-channel pipette. The amplification and fluorescence collection was obtained with CFX96 Touch Real-Time PCR Detection System (Bio-Rad, California, USA) protocol was the following: 10 min at 95°C for polymerase activation followed by 45 cycles composed by 15 sec at 95°C, 30 sec at 55°C, and 30 sec at 72°C for amplification and data collection.

RT-qPCR analyses were performed on both cell lysates and segments of the spinal cord. Short oligonucleotide sequences were designed ad hoc using primer Basic Local Alignment Search Tool (BLAST, NIH) and used as primers for molecular biology analysis, and primers were synthesized by IDT (Coralville, IA, USA). Table 11 reports all primers' characteristics and gene entry sequence used in this study. We used a different strategy from pooling for single-gene analysis. All data obtained are derived from a single animal to verify if the differences between groups are statistically significant. cDNAs were retrotranscribed from the RNA of every single animal for each group. 1 μ g of single sample RNA was retrotranscribed using iScript gDNA Clear cDNA Synthesis Kit (Bio-Rad), according to the manufacturer's protocol, at each sample were added 2 μ l of DNase master mix (Bio-Rad). Then samples were incubated at 25°C for 5 minutes and immediately at 75°C for 5 minutes for enzyme inactivation. After the genomic elimination step at each sample were added 4 μ l of iScript Reverse Transcription Supermix (Bio-Rad) and samples were cycled at 25°C for 5 minutes (priming phase), 40°C for 20 minutes (reverse transcription phase), and 95°C for 1 minute (reverse transcription inactivation) using the Biometra T-gradient thermal cycler (Analytic Jena). One sample of RNA was processed without adding the reverse transcriptase and used as no RT control for the RT-qPCR analysis in order to discriminate aspecific amplification. A total of 10 ng per sample of cDNA was used for each RT-qPCR for single genes analysis. Amplification was performed by adding 10 ng of cDNA to 10 μ l of SsoAdvanced Universal SYBR Green Supermix (Bio-Rad), 1 μ l of primer mix (forward and reverse primer) 10 μ M, and 7 μ l of DNase free water. Amplification was obtained using the CFX96 Touch Real-Time PCR Detection System (Bio-Rad) with the following thermal profile: initial denaturation step (98°C, 3 min) and 40 cycles of amplification (95°C for 10 s and 60°C for 60 s). At the end of the amplification cycles, the amplified products' melting curve was performed according to the following temperature/time scheme: heating from 55°C to 95 °C with a temperature increase of 0.5°C/s. Primers efficiency values for all primers were 95–102%. The $2^{-\Delta\Delta C_t}$ method was used for the calculation of gene expression.

3.7. Western Blot

Western blot analysis was performed to quantify Timp1 protein expression in the spinal cord at 1,7 and 60 DPL. The rostral segments of the spinal cords were homogenized according to the RNeasy Mini Kit (Qiagen) protocol (with a ratio of mg of tissue to ml of lysis buffer, provided by the kit, equivalent to 1:10

weight/volume). Protein isolation was performed from the first flow-through of the spin column by precipitation in acetone. Briefly, four volumes of ice-cold acetone were added to the RNeasy spin column's flow-through, then incubated for 30 minutes at -20°C . After spinning at $15300 \times g$ for 10 minutes and removing the supernatant, the pellet was allowed to dry, then resuspended in RIPA buffer and protease inhibitor (1X Cocktail Sigma, 1nM of PMSF, 10nM of sodium fluoride, 1nM of sodium orthovanadate). Total protein concentration was estimated using a standard colorimetric method based on the Lowry assay (DC Protein Assay, Bio-Rad). For each sample, $40 \mu\text{g}$ of proteins and the marker protein (Precision Plus Protein Standards, Bio-Rad), diluted at a ratio of 1:100, was added to a solution of Leammli / β -mercaptoethanol, and after heating treatment (100°C , 5 minutes), the proteins were resolved in 4-20% Mini-PROTEAN TGX Stain-Free Gels (Bio-Rad). They were transferred to Amersham Protran 0.45 μm Nitrocellulose Blotting Membrane (Bio-Rad), blocked in Tris Buffer Saline solution containing 1% Tween20 (TBST) and 2.5% BSA, and finally incubated with the primary antibody (rabbit Timp1 Abcam ab61224, 1:500; mouse β -actin, Santa Cruz Biotechnology - Dallas, Texas, 1:200) overnight at 4°C . After washing three times in TBST, the membranes were incubated with HRP-conjugated secondary antibodies (swine anti-rabbit, Dako, 1:5000; swine antimouse, Dako, 1:5000) and HRP-conjugated protein for marker visualization (Precision Protein StrepTactin HRP-conjugate, Bio-Rad, 1:20000) for 1 hour at RT. The membranes were then washed three times with TBST. The immunoreactive signal was detected by incubating the membranes with Clarity Western ECL Substrate (Bio-Rad) for 5 minutes at RT in darkness and using the BioRad Chemi DOC MP imaging systems. Western blot signals were measured by densitometry using ImageJ (Fiji) software. The TIMP1 signals were normalized on β -actin in all the analyzed samples, and the ratio of lesioned (SCI +) to intact (SCI -) was calculated for each gel.

3.8. Bioinformatic data analysis

Data obtained from PCR Array were analyzed using GeneGlobe platform (Qiagen), all PCR arrays were normalized on the same housekeeping gene (Rplp1) as suggested by the software, and the cut-off for C_t was set at 35 cycles. Gene expression variation within the segment was calculated as ΔC_t between the gene and the housekeeping. $\Delta\Delta C_t$ for every gene was obtained subtracting the ΔC_t of the same gene between the spinal cord segment or brain areas, from lesioned groups and the same segment/area from the healthy control group. Gene expression was plotted on a clustergram using the C_t s values for each gene in the array. Clustergram plots enable to visualize changes in gene expression and the 2D clusterization of genes and groups based on the gene expression profile.

Relative quantification of mRNA was performed CFX96 Touch Real-Time PCR Detection System (Bio-Rad). As for the array, we calculate gene expression using the comparative cycle threshold method. $\Delta\Delta C_t$ with the

Bio-Rad CFX Manager Software. Values were collected for each gene analyzed and standardized on Rplp1 to avoid changes in the relative expression between PCR array analysis and RT-qPCR analysis.

Genes with a fold change of ± 2 or more were used for bioinformatic analysis. For biological function clustering of genes Panther software²⁰³ (www.pantherdb.org) was used. The Search Tool for the Retrieval of Interacting Genes (STRING V11) online database (<http://string-db.org>) can provide a critical assessment and the integration of PPIs, including experimental and predicted associations²⁰⁴. The STRING online database was used to outline protein-protein interactions (PPIs) of the Extracellular matrix (ECM) of all genes analyzed. Cytoscape v3.7.2²⁰⁵ is a standard open-source software tool to visualize complex networks with the ability to integrate any type of attribute data. Cytoscape was used to identify hub genes using genes expression profile overlaid to ECM network to eliminate nodes with fold regulation inferior to ± 2 to generate a specific network for each sample. The networks were continuously filtered based on degree parameters to have a maximum of 10 nodes. Then these genes were considered to further investigations.

3.9. Histology

For morphological analysis, animals were euthanized with chloral hydrate (37%) administered i.p. and then perfused transcardially with a sterilized physiologic solution at 37° C in order to remove blood completely from tissues and prevent coagulation of blood vessels, then with cold 4% paraformaldehyde and 14% picric acid in Sorensen Buffer 0.2 M (pH 6.9) for 20 minutes using an automatic peristaltic pump. To verify that the perfusion procedure was achieved optimally were observed several parameters: first, the tremor in the limbs and muscles of the animals; second, the absence of fixative solution dripping from the nose of the animals; in the end, the color of the extremities turning yellow from the presence of picric acid in all peripheral tissues and their progressive hardening for the reaction of formaldehyde with tissue proteins. The spinal cord was then post-fixed in the fixative solution for 90 minutes. After the post-fixation, spinal cords were washed in a 5% sucrose solution in Sorensen buffer 0.1 M (pH 7.4) for 48 hours, changing the washing solution every 24 hours. Washing the spinal cord in the sucrose solution prevents crio-damage during the freezing procedure.

Three to four days after viral injection, the rats were euthanized with an intraperitoneal overdose of pentobarbital (300 mg/mL, Streuli Pharma, Switzerland). All animals were transcardially perfused with 100 mL Ringer solution containing 1 % Heparin (B.Brown Medical Inc., Switzerland), followed by 350 mL of 4% paraformaldehyde (PFA, Sigma-Aldrich, Switzerland) in phosphate buffer (0.1M, pH 7.4) containing 5 % sucrose. Perfusion fixed spinal cords were dissected and post-fixed for 24 h at 4 °C in 4% paraformaldehyde. Afterward, spinal cords were transferred to a 30% sucrose solution in 0.1M phosphate buffer, pH 7.2, and stored for 3 days for cryoprotection. The lumbosacral cords were resected from the whole central nervous system, embedded in Tissue-Tek OCT compound, frozen in 2-methyl butane (Sigma-

Aldrich, Switzerland), cooled to -40°C with liquid nitrogen, and stored at -20°C until further processing. 14µm-thick L1-S3 spinal cord cross-sections were cut on a cryostat and collected free-floating in 0.1M phosphate buffer.

Spinal cord segments of 1.5 cm total length were dissected after tissue fixation. These segments included lesion core and unlesioned areas and were processed for histological analysis, embedded in paraffin and sectioned longitudinally (7 µm thick sections, 15 sections per level, one level every 160 µm). 5 animals per group of the 8 DPL and 60 DPL cohorts or were sectioned coronally (14 µm thick section, 20 sections per level, one level every 798 µm). The thickness of the section was 14 µm to guarantee the penetration of the solution (in particular the antibody solution) across the entire section. Slices were mounted on trigel specimen slides and stored at -20° C until the analysis. To visualize the spinal cord's gross structure after contusive injury, we used both hematoxylin/eosin (H/E) for inflammatory infiltrate and Toluidine Blue and Nissl staining for neuronal morphology to characterize the lesion extension at sub-acute and chronic time points. For the lesion area definition, longitudinal sections were captured with Nikon Microphot – FXA equipped with a CCD camera Nikon DXM1200F (Nikon) at a 4X magnification. Reconstruction of the entire spinal cord's entire longitudinal section was obtained using Photoshop's photo-merge function (Adobe). Lesion area was then determined for each reconstructed section with ImageJ software (NIH) as the number of pixels occupying the lesion site, and to obtain the ratio between the lesioned and healthy tissue, total section areas were measured for each section. 3D reconstruction was obtained to align different levels of the same spinal cord (sampling step 210µm).

3.10. Immunofluorescence

Only coronal sections were used for immunohistological analysis and labeled with primary antibodies (see the list in table 12) and secondary antibodies (table 13). For myelin analysis staining with Fuomyelin (Thermo Fisher) was performed. Briefly, sections were rinsed for 30 minutes in PBS then incubated O/N with the primary antibody in PBS/Triton 0.3% at 4° C. After the washing, sections were incubated with the proper secondary antibody in PBS/Triton 0.3% for 30 minutes at 37° C. Slides were then washed and mounted with a Phenilendyamine for photobleaching protection. Coronal sections were captured Nikon Eclipse E600 (Nikon, Italy) equipped with a QImaging Retiga 20002V digital CCD camera (QImaging, Surrey, BC, Canada) at a 10X magnification for atlas representation and a 20X magnification for quantification of immunoreactive area. The immunoreactive area was calculated using the NIS software (Nikon).

Free-floating sections were blocked and permeabilized in TNB blocking solution containing 0.3% Triton-X and 5% normal goat serum for 60 min at room temperature, before being incubated with the primary antibody (Table 4) diluted in TNB containing 0.05% Triton-X overnight at 4°C. The sections were then washed three times in 0.1 M PBS for 10 min each, incubated with secondary antibody (Table 5) for 2 hours

at room temperature, counterstained with 4',6-Diamidino-2-Phenylindole (DAPI), and ultimately washed three times in 0.1 M PBS and once in 0.05 for 10 min each. Sections were mounted on-slide, air-dried overnight at 4°C, and ultimately coverslipped with fluorescence mounting medium (Mowiol, Merck). Slides were stored at 4°C until imaging.

10-12 cross-sections of the spinal cord level between L1 and S2 were randomly picked and imaged with a fluorescent microscope (20x; Zeiss, Axio Scan.Z1). Exposure time was optimized during the first imaging and kept constant across all sections. Mosaic pictures were acquired and merged within the Zeiss software. Maximum intensity projections were created, and pictures were exported in TIFF format for investigation. Further analyses were performed with Fiji. Quantification of total NeuN particles was obtained with Fiji's automatic particles count and segmentation function after regulation of brightness/contrast threshold and binarization of each image. NeuN particles were then automatically grouped based on their area and perimeter in 100 subcategories based on their dimension. Data were represented as the total number of particles for NeuN count and a percentage of the total number of particles with a specific area or perimeter. Quantification of immunoreactivity for Iba1 and OX42 was obtained by measuring the fluorescence intensity in the lamina X and IML column of the lumbosacral spinal cord. Briefly, images were acquired with the same exposure time and brightness/contrast parameter and then binarized for the immunoreactivity analysis. An ROI of 162 x 130 µm was then used to quantify signal in the two areas of interest. Data were expressed as relative intensity on the area of the ROIs. For the analysis of dendritic length of Iba1 cells, were used the same ROIs. Briefly, ten single cells were selected in the ROIs, automatically skeletonized with Fiji Skeletonize function, and the total dendritic length and number of branches were measured. Quantification of OX42 single positive cell was made by manual counting the cell in the ROI used for the immunoreactivity analysis.

3.11. In-situ hybridization

Sequences of target, preamplifier, amplifier, and label probes are proprietary and commercially available (Advanced Cell Diagnosis). Here, we used probes against rat glutamic acid decarboxylase 2 (GAD2) and vesicular glutamate transporter 2 (vGluT2, Slc17a6). Experimental protocols were conducted according to guidelines from Advanced Cell Diagnosis. Briefly, spinal cord sections were mounted on slides (Huberlab, Superfrost), let dry in a sterile environment, and subsequently frozen at -20°C for 2 days. Then, the slides were thawed at room temperature for 15 min. Subsequently, slides were treated with hydrogen peroxide (Advanced Cell Diagnosis) for 10 min and washed twice in water for 2 min each, before incubation in target retrieval buffer (Advanced Cell Diagnosis) for 10 min at 98-100°C. Slides were washed first in water and then in 100% EtOH (Reuss Chemie). Then, protease treatment was applied for 30 min at 40°C in a HyBEZ oven (Advanced Cell Diagnosis). Subsequently, sections were incubated in a mix containing the two hybridization probes for 2 h at 40°C. After washing the slides twice in washing buffer (Advanced Cell

Diagnosis), the two probes were amplified consecutively, with two washing steps in washing buffer (Advanced Cell Diagnosis) in between each amplification step. Further amplification steps were performed with HRP detecting the specific channel of the different probes, always with washing steps with washing buffer (Advanced Cell Diagnosis) in between. The signals were developed with TSA Plus Cyanin3 and TSA Plus Cyanin5 (PerkinElmer, TSA Cy3, Cy5, TMR, Fluorescein Evaluation kit) for the probe targeting GAD2 and vGluT2, respectively. After the development of the last probe, sections were washed twice in washing buffer (Advanced Cell Diagnosis) and counterstained with DAPI (Advanced Cell Diagnosis) for 3 min at room temperature. Slides were coverslipped using fluorescence mounting medium (Merck, Mowiol) and let dry overnight in the dark. Afterward, they were stored at 4°C upon imaging.

Multiple cross-sections of the spinal levels L6 and S1 were randomly picked and imaged with a fluorescent microscope (20x; Zeiss, Axio Scan.Z1). Exposure time was optimized during the first imaging and kept constant across all sections. Mosaic pictures were acquired and merged within the Zeiss software. Maximum intensity projections were created, and pictures were exported in TIFF format for investigation. Further analyses were performed with Fiji. Briefly, images were acquired with the same parameter of exposure time and brightness/contrast, and representative ROIs of 162 x 130 μm were selected in lamina X of each slide of the spinal cord. Background (total integrate intensity/total area) was then subtracted from the ROIs, and images were thresholded in order to exclude any aspecific signal (3 times higher than background intensity). For in-situ signal quantification, the automatic analyze particles function of Fiji was used. Data are represented as total intensity/ROI total area.

3.12. Statistical analysis

All statistical analyses were made using GraphPad Prism (v 8.0) software (GraphPad Software). Student's t-test was used to compare two groups and ordinary one-way ANOVA and posthoc test to compare more than two groups. BBB scoring and animals' weight were represented as mean \pm SEM. BBB score and gait analysis data have been analyzed using the two-way ANOVA test. Results were considered significant when the probability of their occurrence due to chance alone was less than 5% ($P < 0.05$). For PCR Arrays analysis, data were reported as relative fold change expression. For mRNA expression analysis obtained with qPCR, data was reported as Log₂ of fold change, and P values were calculated using one-way ANOVA on the $\Delta\Delta C_t$ s from each single animals normalized on the mean of the ΔC_t of the respective group of intact spinal cord segment. Uncorrected Fisher's LSD post hoc analysis was used to compare the relative gene expression of each time points in the rostral and caudal from the lesion segment of the spinal cord. Statistical analysis was then confirmed with single Student's T-test between the rostral and the caudal segment for each time point. Dunnet's post hoc analysis was used to compare the relative genes expression of lesioned animals compared to intact. P values inferior to 0.05 were considered significant.

Table 9: List and position of the Extracellular Matrix and Adhesion molecules PCR Array genes (Qiagen).

Position	Unigene	Refseq	Symbol	Description
A01	Rn.7897	NM_024400	Adamts1	ADAM metalloproteinase with thrombospondin type 1 motif, 1
A02	Rn.86986	NM_001137622	Adamts2	ADAM metalloproteinase with thrombospondin type 1 motif, 2
A03	Rn.107051	NM_198761	Adamts5	ADAM metalloproteinase with thrombospondin type 1 motif, 5
A04	N/A	NM_001106811	Adamts8	ADAM metalloproteinase with thrombospondin type 1 motif, 8
A05	Rn.103790	NM_001007145	Catna1	Catenin (cadherin associated protein), alpha 1
A06	Rn.1120	NM_012924	Cd44	Cd44 molecule
A07	Rn.1303	NM_031334	Cdh1	Cadherin 1
A08	Rn.23200	NM_031333	Cdh2	Cadherin 2
A09	Rn.105829	NM_053938	Cdh3	Cadherin 3
A10	Rn.214089	XM_001061943	Cdh4	Cadherin 4
A11	Rn.21397	NM_057118	Cntn1	Contactin 1
A12	Rn.2953	NM_053304	Col1a1	Collagen, type I, alpha 1
B01	Rn.10124	NM_012929	Col2a1	Collagen, type II, alpha 1
B02	Rn.3247	NM_032085	Col3a1	Collagen, type III, alpha 1
B03	Rn.53801	NM_001135009	Col4a1	Collagen, type IV, alpha 1
B04	N/A	XM_001076134	Col4a2	Collagen, type IV, alpha 2
B05	Rn.121139	NM_001135759	Col4a3	Collagen, type IV, alpha 3
B06	Rn.117	NM_134452	Col5a1	Collagen, type V, alpha 1
B07	Rn.232118	XM_215375	Col6a1	Collagen, type VI, alpha 1
B08	Rn.53843	NM_001107100	Col8a1	Collagen, type VIII, alpha 1
B09	Rn.17145	NM_022266	Ctgf	Connective tissue growth factor
B10	Rn.214082	NM_001106598	Ctnna2	Catenin (cadherin associated protein), alpha 2
B11	Rn.112601	NM_053357	Ctnnb1	Catenin (cadherin associated protein), beta 1
B12	Rn.97792	NM_053882	Ecm1	Extracellular matrix protein 1
C01	Rn.99346	NM_001106710	Emilin1	Elastin microfibril interfacier 1
C02	Rn.17491	NM_022587	Entpd1	Ectonucleoside triphosphate diphosphohydrolase 1
C03	Rn.9375	NM_001127547	Fbln1	Fibulin 1
C04	Rn.1604	NM_019143	Fn1	Fibronectin 1
C05	Rn.50531	NM_019189	Hapln1	Hyaluronan and proteoglycan link protein 1
C06	Rn.12	NM_012967	Icam1	Intercellular adhesion molecule 1
C07	Rn.83597	XM_345156	Itga2	Integrin, alpha 2
C08	Rn.154664	NM_001108292	Itga3	Integrin, alpha 3
C09	Rn.12704	NM_001107737	Itga4	Integrin, alpha 4
C10	Rn.100796	NM_001108118	Itga5	Integrin, alpha 5 (fibronectin receptor, alpha polypeptide)
C11	Rn.34728	NM_031691	Itgad	Integrin, alpha D
C12	Rn.29975	NM_031768	Itgae	Integrin, alpha E
D01	Rn.14655	NM_001033998	Itgal	Integrin, alpha L
D02	Rn.54465	NM_012711	Itgam	Integrin, alpha M
D03	N/A	NM_001106549	Itgav	Integrin, alpha V
D04	Rn.25733	NM_017022	Itgb1	Integrin, beta 1
D05	Rn.42962	NM_001037780	Itgb2	Integrin, beta 2
D06	Rn.229225	NM_153720	Itgb3	Integrin, beta 3
D07	Rn.198908	NM_013180	Itgb4	Integrin, beta 4
D08	Rn.2807	NM_001108237	Lama1	Laminin, alpha 1

D09	N/A	XM_008758643	Lama2	Laminin, alpha 2
D10	Rn.10597	XM_003753026	Lama3	Laminin, alpha 3
D11	Rn.774	NM_012974	Lamb2	Laminin, beta 2
D12	Rn.49634	NM_001100841	Lamb3	Laminin, beta 3
E01	Rn.7145	NM_053966	Lamc1	Laminin, gamma 1
E02	Rn.9946	NM_133514	Mmp10	Matrix metalloproteinase 10
E03	Rn.11123	NM_012980	Mmp11	Matrix metalloproteinase 11
E04	Rn.33193	NM_053963	Mmp12	Matrix metalloproteinase 12
E05	Rn.10997	NM_133530	Mmp13	Matrix metalloproteinase 13
E06	Rn.10371	NM_031056	Mmp14	Matrix metalloproteinase 14 (membrane-inserted)
E07	Rn.165433	NM_001106168	Mmp15	Matrix metalloproteinase 15
E08	Rn.208361	NM_080776	Mmp16	Matrix metalloproteinase 16
E09	Rn.79007	NM_001134530	Mmp1	Matrix metalloproteinase 1a (interstitial collagenase)
E10	Rn.6422	NM_031054	Mmp2	Matrix metalloproteinase 2
E11	Rn.32086	NM_133523	Mmp3	Matrix metalloproteinase 3
E12	Rn.10282	NM_012864	Mmp7	Matrix metalloproteinase 7
F01	Rn.44474	NM_022221	Mmp8	Matrix metalloproteinase 8
F02	Rn.10209	NM_031055	Mmp9	Matrix metalloproteinase 9
F03	Rn.11283	NM_031521	Ncam1	Neural cell adhesion molecule 1
F04	Rn.138756	NM_203409	Ncam2	Neural cell adhesion molecule 2
F05	Rn.1878	NM_031591	Pecam1	Platelet/endothelial cell adhesion molecule 1
F06	Rn.30516	NM_001108550	Postn	Periostin, osteoblast specific factor
F07	Rn.10359	NM_138879	Sele	Selectin E
F08	Rn.10461	NM_019177	Sell	Selectin L
F09	Rn.10012	NM_013114	Selp	Selectin P
F10	Rn.185815	NM_001002023	Sgce	Sarcoglycan, epsilon
F11	Rn.98989	NM_012656	Sparc	Secreted protein, acidic, cysteine-rich (osteonectin)
F12	Rn.44057	NM_001271297	Spock1	Sparc/osteonectin, cwcv and kazal-like domains proteoglycan (testican) 1
G01	Rn.8871	NM_012881	Spp1	Secreted phosphoprotein 1
G02	Rn.216272	NM_001033680	Syt1	Synaptotagmin I
G03	Rn.1046	NM_053802	Tgfb1	Transforming growth factor, beta induced
G04	Rn.185771	NM_001013062	Thbs1	Thrombospondin 1
G05	Rn.165619	NM_001169138	Thbs2	Thrombospondin 2
G06	Rn.25754	NM_053819	Timp1	TIMP metalloproteinase inhibitor 1
G07	Rn.10161	NM_021989	Timp2	TIMP metalloproteinase inhibitor 2
G08	Rn.119634	NM_012886	Timp3	TIMP metalloproteinase inhibitor 3
G09	Rn.12723	NM_053861	Tnc	Tenascin C
G10	Rn.11267	NM_012889	Vcam1	Vascular cell adhesion molecule 1
G11	Rn.35666	NM_001170558	Vcan	Versican
G12	Rn.87493	NM_019156	Vtn	Vitronectin
H01	Rn.94978	NM_031144	Actb	Actin, beta
H02	Rn.1868	NM_012512	B2m	Beta-2 microglobulin
H03	Rn.47	NM_012583	Hprt1	Hypoxanthine phosphoribosyltransferase 1
H04	Rn.107896	NM_017025	Ldha	Lactate dehydrogenase A
H05	Rn.973	NM_001007604	Rplp1	Ribosomal protein, large, P1

Table 10: List and position of the Extracellular Matrix and Adhesion molecules PCR Array genes (Qiagen).

Position	Unigene	Refseq	Symbol	Description
A01	Rn.42924	NM_019254	Adam10	ADAM metallopeptidase domain 10
A02	Rn.214145	NM_001107239	Adcy1	Adenylate cyclase 1 (brain)
A03	Rn.10382	NM_017142	Adcy8	Adenylate cyclase 8 (brain)
A04	Rn.11422	NM_033230	Akt1	V-akt murine thymoma viral oncogene homolog 1
A05	Rn.10086	NM_019361	Arc	Activity-regulated cytoskeleton-associated protein
A06	Rn.11266	NM_012513	Bdnf	Brain-derived neurotrophic factor
A07	Rn.107499	NM_0129209	Camk2a	Calcium/calmodulin-dependent protein kinase II alpha
A08	Rn.10961	NM_133605	Camk2g	Calcium/calmodulin-dependent protein kinase II gamma
A09	Rn.23200	NM_031333	Cdh2	Cadherin 2
A10	Rn.6479	NM_024125	Cebpb	CCAAT/enhancer binding protein (C/EBP), beta
A11	Rn.6975	NM_013154	Cebpd	CCAAT/enhancer binding protein (C/EBP), delta
A12	Rn.89774	NM_012784	Cnr1	Cannabinoid receptor 1 (brain)
B01	Rn.90061	NM_031017	Creb1	CAMP responsive element binding protein 1
B02	Rn.102510	NM_001110860	Crem	CAMP responsive element modulator
B03	Rn.9765	NM_019621	Dlg4	Discs, large homolog 4 (Drosophila)
B04	Rn.9096	NM_012551	Egr1	Early growth response 1
B05	Rn.89235	NM_053633	Egr2	Early growth response 2
B06	Rn.44371	NM_017086	Egr3	Early growth response 3
B07	Rn.31998	NM_019137	Egr4	Early growth response 4
B08	Rn.229866	NM_001127319	Ephb2	Eph receptor B2
B09	Rn.103750	NM_0221970	Fos	FBJ osteosarcoma oncogene
B10	Rn.10368	NM_017295	Gabra5	Gamma-aminobutyric acid (GABA) A receptor, alpha 5
B11	Rn.11391	NM_013145	Gnai1	Guanine nucleotide binding protein (G protein), alpha inhibiting 1
B12	Rn.29971	NM_031608	Gria1	Glutamate receptor, ionotropic, AMPA 1
C01	Rn.91361	NM_017261	Gria2	Glutamate receptor, ionotropic, AMPA 2
C02	Rn.74049	NM_032990	Gria3	Glutamate receptor, ionotropic, AMPA 3
C03	Rn.10938	NM_017263	Gria4	Glutamate receptor, ionotropic, AMPA 4
C04	Rn.9840	NM_017010	Grin1	Glutamate receptor, ionotropic, N-methyl D-aspartate 1
C05	Rn.9710	NM_012573	Grin2a	Glutamate receptor, ionotropic, N-methyl D-aspartate 2A
C06	Rn.9711	NM_012574	Grin2b	Glutamate receptor, ionotropic, N-methyl D-aspartate 2B
C07	Rn.9709	NM_012575	Grin2c	Glutamate receptor, ionotropic, N-methyl D-aspartate 2C
C08	Rn.91209	NM_022797	Grin2d	Glutamate receptor, ionotropic, N-methyl D-aspartate 2D
C09	Rn.74240	NM_032069	Grip1	Glutamate receptor interacting protein 1
C10	Rn.87787	NM_017011	Grm1	Glutamate receptor, metabotropic 1
C11	Rn.9681	NM_001105711	Grm2	Glutamate receptor, metabotropic 2
C12	Rn.41715	NM_001105712	Grm3	Glutamate receptor, metabotropic 3
D01	Rn.89046	NM_022666	Grm4	Glutamate receptor, metabotropic 4
D02	Rn.29972	NM_017012	Grm5	Glutamate receptor, metabotropic 5
D03	Rn.10409	NM_031040	Grm7	Glutamate receptor, metabotropic 7
D04	Rn.44420	NM_022202	Grm8	Glutamate receptor, metabotropic 8

D05	Rn.37500	NM_031707	Homer1	Homer homolog 1 (Drosophila)
D06	Rn.22834 6	NM_178866	Igf1	Insulin-like growth factor 1
D07	Rn.9874	NM_017128	Inhba	Inhibin beta-A
D08	Rn.93714	NM_021835	Jun	Jun oncogene
D09	Rn.15806	NM_021836	Junb	Jun B proto-oncogene
D10	Rn.2398	NM_031135	Klf10	Kruppel-like factor 10
D11	Rn.34914	NM_053842	Mapk1	Mitogen activated protein kinase 1
D12	Rn.10209	NM_031055	Mmp9	Matrix metalloproteinase 9
E01	Rn.11283	NM_031521	Ncam1	Neural cell adhesion molecule 1
E02	Rn.2411	NM_00127671 1	Nfkb1	Nuclear factor of kappa light polypeptide gene enhancer in B-cells 1
E03	Rn.8395	NM_030867	Nfkbib	Nuclear factor of kappa light polypeptide gene enhancer in B-cells inhibitor, beta
E04	Rn.22168 5	NM_00127705	Ngf	Nerve growth factor (beta polypeptide)
E05	Rn.10980	NM_012610	Ngfr	Nerve growth factor receptor (TNFR superfamily, member 16)
E06	Rn.10573	NM_052799	Nos1	Nitric oxide synthase 1, neuronal
E07	Rn.16210 1	NM_00103419 9	Nptx2	Neuronal pentraxin 2
E08	Rn.10000	NM_024388	Nr4a1	Nuclear receptor subfamily 4, group A, member 1
E09	Rn.9715	NM_031073	Ntf3	Neurotrophin 3
E10	Rn.44225	NM_013184	Ntf4	Neurotrophin 4
E11	Rn.11246	NM_012731	Ntrk2	Neurotrophic tyrosine kinase, receptor, type 2
E12	Rn.23337	NM_022868	Pcdh8	Protocadherin 8
F01	Rn.24750	NM_053460	Pick1	Protein interacting with PRKCA 1
F02	Rn.34888	NM_017034	Pim1	Pim-1 oncogene
F03	Rn.10710 2	NM_013151	Plat	Plasminogen activator, tissue
F04	Rn.11243	NM_013187	Plcg1	Phospholipase C, gamma 1
F05	Rn.2024	NM_031527	Ppp1ca	Protein phosphatase 1, catalytic subunit, alpha isoform
F06	Rn.1495	NM_022498	Ppp1cc	Protein phosphatase 1, catalytic subunit, gamma isoform
F07	Rn.73852	NM_130403	Ppp1r14a	Protein phosphatase 1, regulatory (inhibitor) subunit 14A
F08	Rn.1271	NM_017039	Ppp2ca	Protein phosphatase 2, catalytic subunit, alpha isoform
F09	Rn.6866	NM_017041	Ppp3ca	Protein phosphatase 3, catalytic subunit, alpha isoform
F10	Rn.86669 3	NM_00110571	Prkca	Protein kinase C, alpha
F11	Rn.9747	NM_012628	Prkcg	Protein kinase C, gamma
F12	Rn.20472 4	NM_00110573 1	Prkg1	Protein kinase, cGMP-dependent, type 1
G01	Rn.44409	NM_013018	Rab3a	RAB3A, member RAS oncogene family
G02	Rn.19480	NM_199267	Rela	V-rel reticuloendotheliosis viral oncogene homolog A (avian)
G03	Rn.98353	NM_080394	Reln	Reelin
G04	N/A	XM_00375006 5	Kif17	Kinesin family member 17
G05	Rn.1892	NM_053453	Rgs2	Regulator of G-protein signaling 2
G06	Rn.859	NM_013216	Rheb	Ras homolog enriched in brain
G07	N/A	NM_00110762 7	Sirt1	Sirtuin (silent mating type information regulation 2 homolog) 1 (S. cerevisiae)
G08	Rn.1501	NM_00110930 2	Srf	Serum response factor (c-fos serum response element-binding transcription factor)
G09	Rn.42910	NM_021695	Synpo	Synaptopodin

G10	Rn.25754	NM_053819	Timp1	TIMP metallopeptidase inhibitor 1
G11	Rn.2275	NM_012675	Tnf	Tumor necrosis factor (TNF superfamily, member 2)
G12	Rn.2502	NM_013053	Ywhaq	Tyrosine 3-monooxygenase/tryptophan 5-monooxygenase activation protein, theta polypeptide
H01	Rn.94978	NM_031144	Actb	Actin, beta
H02	Rn.1868	NM_012512	B2m	Beta-2 microglobulin
H03	Rn.47	NM_012583	Hprt1	Hypoxanthine phosphoribosyltransferase 1
H04	Rn.10789 6	NM_017025	Ldha	Lactate dehydrogenase A
H05	Rn.973 4	NM_00100760	Rplp1	Ribosomal protein, large, P1

Table 11: Sequences and genetic loci of primers used for RT-qPCR analysis

Gene	Specificity	Genetic Locus	Forward Sequence (5'-3')	Reverse Sequence (5'-3')
Acan	rat	NM_022190.1	GTGAGATCGACCAGGAGCCA	TCGGGAAAGTGGCGATAACA
Agrin	rat	NM_175754.1	CCTGCAACATCTGCTTGATCC	GGATTCCAGGTTTGTAGTTGCTG
Bcan	rat	NM_001033665.1	GGACCTCACAAGTCTTCCAAGT	CTTTCAGGTCATCAGCGAGGG
Cd44	rat	NM_012924.2	AACTACAGCCTTGATGACTACCC	ATGACTCTGGACTCTGATGGTT
Cd44	mouse			
Cspg4	rat	NM_031022.1	AACAGGAAAAAGCACCCCA	ACCTGTCTTGTTCGCTTTGC
Fn1	rat	NM_019143.2	AAGACAGATGAGCTTCCCAA	TGAACTGTGGAGGGAACATCC
Gapdh	rat /mouse	NM_001113417.1	GGCAAGTTCAATGGCACAGTCAAG	CATACTCAGCACCAGCATCAC
Lgals1	rat	NM_019904.1	TTCAATCATGGCCTGTGGTCT	CTCTCCCCGAACTTTGAGACA
Ntn1	rat	NM_053731.2	AGGACTATGCTGTCCAGATCCA	TACGACTTGTGCCCTGCTTG
Postn	rat	NM_001108550.1	TGCAAAAAGACACACCTGCAAA	GGCCTTCTCTTGATCGCCTT
Rplp1	rat	NM_001007604.2	GGCAGTCTACAGCATGGCTT	GTTGACATTGGCCAGAGCCT
Sell	rat	NM_019177.3	ATCGCAGGAAAGGATGGATGAT	GGTTTTTGGTGGCGGTTGTT
Slit1	rat	NM_022953.2	CGCAAGGGCGCATCGT	GGGGCTATCTCCAGGTGCTAT
Slit2	rat	NM_022632.2	GGGGCCATAATGTAGCAGAGG	GACTGGTGACCTTCTCTCTCA
Tnc	rat	NM_053861.1	ATTGTCTACCTCTCTGGAATTGCTC	TTCCGGTTCAGCTTCTGTGG
Tnr	rat	NM_013045.1	CCTCAATGGGGAGTTAAGCCA	CTGGAAAACAATCCAGCCGC
Timp1-a	mouse	NM_011593.2	TGGGTGGATGAGTAATGCGTC	GGCCATCATGGTATCTCTGGT
Timp1-b	mouse	NM_001294280.2	CAACTCGACCTGGATGCTAA	ACTCTTCACTGCGGTTCTGG

Table 12: List of primary antibodies used for the immunofluorescence analysis

Antigen	Specie	Dilution	Supplier
GFAP	Rabbit	1:500	Dako
OX42	Mouse	1:250	Serotec
NF-200	Mouse	1:800	Sigma Aldrich
NeuN	Mouse	1:200	Millipore Merk
OX42	Mouse	1:500	Biosciences
Iba1	Rabbit	1:500	Wako
GFP	Chicken	1:500	Avés-Lab

Table 13: List of secondary antibody used for the immunofluorescence analysis

Specie Reactivity	Fluorophore	Specie	Dilution	Supplier
Rabbit	Rhodamine Red X (RRX)	Goat	1:100	Jackson Immuno Research
Mouse	Alexa Fluor 488	Goat	1:100	Thermo Fisher
Rabbit	Alexa Fluor 647	Goat	1:500	Jackson Immuno Research
Chicken	Alexa Fluor 488	Goat	1:500	Jackson Immuno Research
Mouse	Cy3	Goat	1:500	Jackson Immuno Research

4. RESULTS

4.1. Outline of the presented results

The three-year research project for this Ph.D. program focuses on the cellular and molecular substrate of the spinal cord injury evolution and stabilization, given possible novel therapeutic target identification. The following research projects have supported the activities:

- Italian Regenerative Medicine Infrastructure (IRMI), MIUR “cluster tecnologici nazionali (project CTN01_00177_888744)
- Step-by-Step, “Approccio integrato per il paziente con lesioni neurologiche acute”, POR-FESR Emilia Romagna 2014-2020 (<https://stepbystep-rer.it/>)
- Mat2Rep “Biomateriali multifunzionali per l'autoriparazione di tessuti e organi”, POR-FESR Emilia Romagna 2014-2020 (<https://mat2rep.it/>)

Results are presented in 4 manuscripts/published papers, integrated by a detailed description of the SCI model characterization. Moreover, two review articles dealing with the neurobiology of the CNS self-repair are also included.

In particular:

The first goal of the project was the establishment of a reliable and reproducible model of CNS traumatic lesions (see section 4.2). We chose traumatic spinal cord injury as the model better mimicking the human spinal cord traumatic injury. We performed a contusive lesion at the T9 level of the spinal cord to obtain a complete paralysis of the hind paws. To obtain a reproducible SCI model, we used an automated impactor with the possibility to define fixed parameters during the surgical procedure. Initially, we performed two different models of SCI based on the area of the primary damage. The first model was given by an impact with a 2 mm diameter tip with a depth of 2 mm in the spinal cord and defined as a “severe” lesion. The second model was performed with a reduced primary lesion diameter (1.5/1.5 mm diameter/depth) and denominated “mild” lesion.

In both SCI models, we found a locomotor dysfunction of the hind but not the front paws or trunk muscles. Both lesions cause a significant body weight loss in the first week after injury with a sustained loss in the severe lesion model from a clinical perspective. No other SCI nonrelated alterations were reported neither in the severe nor in the mild group. As described in the literature, in the severe SCI model, we observed the onset of the neurologic bladder (block of micturition) in the severe lesion model. This condition was spontaneously resolved in 6 to 10 days from the lesion.

The main difference between the two SCI models is the time for spontaneous partial locomotion recovery, being the animals in the mild group reach higher values in the BBB scale in a shorter time

than animals with the severe lesion (3 weeks vs. 4 weeks, respectively). In addition, gait parameters analyzed with automated CatWalk system revealed a general amelioration in the mild lesion compared to the severe lesion group.

From an anatomical point of view, we found that the initial damage in the severe lesion animals invested the descending reticulospinal tract controlling bladder and sphincters. The anatomical characterization of the two types of SCI demonstrated a significant difference in the ratio of damaged tissue to spared tissue at the chronic time point of 60 DPL. In the mild lesion, the rostrocaudal extension of the lesion is lower compared to the severe group. This reduced propagation of the lesion at late time points is essential for the functional recovery and the possibility to therapeutically act on the evolution of the lesion in the acute and subacute phases. This work allowed us to choose the severity of spinal cord lesions for subsequent drug delivery studies in the lesioned animals.

In paper number 1 (**section 4.3, manuscript in preparation**), we focused on the anatomical tracing of neuronal connectivity in the spinal cord using recombinant neurotrophic viruses and the characterization of labeled neurons' neurochemical phenotype in situ hybridization. This work has been carried out during the secondment period at the Institute for Regenerative Medicine under Prof. Martin Schwab. The primary motoneurons innervating peripheral muscles are the most targeted neurons for neuronal tracing studies, easily reachable with the injection of neuronal tracer in the innervated muscles. In the last decades, the improvement of viral tracing techniques has allowed the labeling of multi-synaptically connected chains of neurons starting from the peripheral neuron and reaching the brain's superior neurons. The specificity of viral labeling and the possibility of self-amplification of the signal allow to selectively identify the circuitry involved in motor function physiological functions. We used a recombinant Pseudorabies Virus (rPRV) with a cassette for the expression of eGFP to label the external urethral sphincter neuronal circuitry in the rat. This circuitry is responsible for micturition reflex and bladder voiding and, in SCI, for the neurologic bladder's onset. The purpose of this study was the evaluation of the modification induced by the infection of PRV to the neurons in the lumbosacral segments of the spinal cord involved in controlling the urethral sphincters. The pathological aspects of rPRV infections of the CNS are well described in the literature in terms of neuronal mortality and inflammation activation^{206,207}. We investigated the infection's effect on mRNA expression with the in-situ hybridization technique in the present work. We used two different time points (3 and 4 DPI) to evaluate the amount of mRNA in neuronal cells and two different mRNA types highly expressed in spinal neurons (vGlut2 and Gad2). Interestingly, we found a substantial reduction in the lumbosacral spinal cord segments mainly infected by rPRV, with a complete abolishment of these two mRNAs already at 3 DPI. This phenomenon is principally

given by the host shutoff mechanism activated by the viral particles in the infected neurons and a condition of stress induced by the inflammatory process's concomitant activation. We studied the disposition of the neuronal marker NeuN in the infected spinal cord and found a significant reduction of 30% in total NeuN particles at 4 DPI ($P=0.0157$; $F(2, 7)=7.965$), associated with neuronal stress and cellular death. Moreover, the remaining NeuN neurons at both time points showed a tendency in a dimension reduction, confirming a condition of stress for the infected neurons.

We then investigated the immune system's activation after the infection with rPRV to confirm the noxious microenvironment presented to the spinal neurons. We found that after infection, there is a potent activation of the spinal cord's resident immune cells, the microglia. We quantified this activation with immunoreactivity area in the lumbosacral area 10 and IMLs and found that microglia follow a time-dependent activation based on the time-dependent spreading of the virus. Especially at 4 DPI, the normalized immunoreactivity of Iba1 shows an increase of 10 times compared to naïve animals in all the areas in exams. Moreover, we determined the activation state of microglia/macrophage pool through their cellular process length and number. Accordingly, with the previous data on inflammatory cells activation, the number of dendrites on the microglia/macrophages cells was strongly reduced in the infected lumbosacral spinal cord segments at both time points (one-way ANOVA: lumbar segments, $P=0.0001$, $F(2, 7)=1.019$; sacral segments, $P=0.0002$, $F(2, 7)=34.56$). The remaining cellular processes in the immune cells analyzed were significantly shorter compared to the naïve animals' cells (one-way ANOVA: lumbar segments, $P=0.0006$, $F(2, 7)=0.7017$; sacral segments, $P=0.0004$, $F(2, 7)=8.139$). Ultimately, we determined the number of OX42 single-positive cells, representing the infiltrating lymphocytes in the infected spinal cord. OX42+ cells were undetectable in naïve animals, but we found a substantial increase after rPRV infection in a time-dependent fashion (3 vs. 4 DPI; t-test: lumbar segments, $P=0.0202$; sacral segments, $P=0.0083$).

Finally, data collected with the presented work show how the infection with neurotrophic viruses modifies the CNS microenvironment, altering the infected neurons' morphological status. Moreover, the strong effect of the rPRV on the transcription machinery prevents the expression of mRNA in the infected cells and did not allow to couple this tracer with in-situ hybridization for the characterization of the traced neurons even at early time points. Ultimately, the effect of infection in neurons and the strong inflammatory microenvironment elicited could modify the neuronal connectivity and alter animals' behavior.

We then characterized the time-course evolution of the molecular adaptation to the lesion in the spinal cord tissue and other CNS areas, focusing on extracellular matrix (**paper 2, section 4.4,**

manuscript submitted) and synaptic plasticity genes (**paper 3, section 4.5, manuscript in preparation**). We studied the longitudinal expression of a set of genes involved in producing proteins of the ECM in the spinal cord segment immediately continuous rostrally and caudally to the lesion epicenter. We used a data-driven strategy with a bioinformatic approach to identify the crucial genes involved in ECM modification after SCI. We then confirmed our data with both in-vitro and in-vivo experiments.

Briefly, we found a different expression pattern in the caudal and rostral segment of the spinal cord after the SCI on days 1, 8, and 45 after the lesion. Among the 100 genes analyzed, we identified Timp1 as a crucial gene involved in ECM modification after injury. The expression of Timp1 was highly upregulated after the lesion in both segments of the spinal cord at all the time points analyzed. Also, the bioinformatic approach confirmed the importance of Timp1 in the network of genes extrapolated from the expression analysis. Moreover, we also identified several other genes strongly modified by the lesion. Among these genes, we have distinguished those upregulated in the cord's rostral segment, namely Col1a1, Col3a1, Col8a1, Postn, and Tgfb1, from genes with an increased expression in both segments, CD44, Mmp12, Mmp13, Mmp8, Sell, and Tnc. The genes upregulated in both cord segments are principally involved in the inflammatory onset after the lesion, whereas the genes upregulated in the cord's rostral segment are principally involved in cellular adhesion and signal transmission.

We then confirmed the identification of Timp1 as a crucial hub in ECM modification with quantification of Timp1 protein in the rostral segment of the spinal cord after SCI at 1, 7, and 60 DPL. We found a significant time-dependent reduction in Timp protein after SCI and hypothesized that increased secretion of Timp1 mainly causes this downregulation in the ECM after SCI. Besides, the primary culture of astrocytes exposed to a cytokines mix showed an increased gene expression of both Timp1 and CD44, according to our data obtained from an in-vivo study.

We demonstrated that a bioinformatic approach is feasible and allows a substantial reduction in the number of experimental animals. Surprisingly, our data showed a different gene expression regulation between rostral and caudal segments of the spinal cord from the lesion epicenter. This is of fundamental importance for determining the organism's reparative capacity and the time-dependent development of the pathology).

In paper number 3 (section 4.5), we investigated the synaptic plasticity-related genes in spinal segments and supraspinal areas involved in motor control. The investigation of changes in synaptic plasticity-related genes is fundamental to understanding the early and late modifications in the locomotor circuit after SCI. As for the study of ECM gene expression, we used the same strategy for

grouping and pooling. We performed the same longitudinal study with 3 time points (1, 8, and 45 DPL) covering the principal phases of SCI to visualize the principal modification in synaptic plasticity-related genes. We selected the highly modified genes (± 2 fold change variation) in all the regions under investigation and plotted them as 2D clustergram to visualize the clusterization of both, spinal areas and supraspinal regions, involved in motor control. We found that in all spinal cord segments, the principal alteration in gene expression occurs at 1 DPL with the upregulation mainly of genes involved in inflammatory activation (Cebpd, Mmp9, Timp1, and Tnf) and the downregulation of neurotransmitter receptors and early response genes (Erg1-4, Gnai1, Grm8, Igf1, Nr4a1). Interestingly, in the spinal cord's thoracic segment, corresponding to the region's rostral segment, we found an early activation of Fos, Junb, and Ngf, lacking in the other segments of the spine after the lesion. In the end, in the spinal cord, the only gene with a consistent downregulation for all time points and all the segments was Nr4a1. This nuclear factor participates in the vascular response to injury.

The motor-related brain areas analyzed were the cerebellum, the basal ganglia, and the motor cortex. We did not observe a high level of gene expression modulation for the first two areas at all three time points. In the cerebellum, the only gene significantly upregulated at 45 DPL was Ngf, whereas Erg3 and Grin2c were downregulated at the same time point. Instead, in the basal ganglia, we found a consistent upregulation of the gene Reln at all time points. Reln encodes for Reelin, which is commonly involved in neuronal migration during the development and could result in reactivation of migratory cells after spinal injury. On the other hand, BDNF was highly downregulated at 45 DPL. The majority of gene modification was observed in the motor cortex, where 21 genes showed significant fold change variation at the three time points analyzed. In particular, we found transient downregulation at 1 DPL of neurotransmitters receptors and early phase gene, as for the spinal cord segment. Moreover, similarly to the spinal cord, Cebpd was upregulated at 1 DPL but also at 45 DPL in this brain region. The motor cortex showed a consistent downregulation of Ywhaq and Ntrk2 at all time points; the first gene encodes for a signal transduction protein that binds phosphoserine-containing proteins and is involved in apoptosis activation. Ntrk2 is the receptor of BDNF, and its downregulation could be harmful for the modification of the motor cortex's plasticity. Accordingly, we found also that Igf1 is consistently downregulated in the motor cortex; the gene is important for neuronal survival, and an excessive downregulation could impair motor function. On the other hand, the upregulation of Gria1 and Cnr1 at 45 DPL, two essential neurotransmitters receptors for the locomotor system's functionality, could balance the impairment caused by the downregulation of the genes as mentioned above.

We then attempted to pharmacologically interfere with the above described molecular and cellular events for a better functional outcome (**paper 4, section 4.6, published manuscript, J Neurotrauma, 37:1708–1719, August 1, 2020**). In particular, we use an innovative therapeutic solution (patent PTC/IT2018/000084) based on an implantable biopolymer conjugated with two drugs, one anti-inflammatory (Ibuprofen) and a pro-myelinating agent (T3). The presented study is a proof of concept study with great implications for the drug development for the treatment of acute neurotrauma. The principal goal of our implantable biopolymer was the reduction of the secondary injury of the SCI with the implantation of the scaffold loaded with drugs in the very immediate phase after the traumatic lesion. We expected a therapeutic effect in the animals receiving the PLLA-loaded scaffold as an amelioration of $\geq 20\%$ in functional outcome (gait analysis and BBB score). The initial phase of this work was the in-vitro quantification of drugs release from the electrospun biopolymer. We obtained a continuous release for both drugs for 14 days, with a 3.4 $\mu\text{g/ml}$ and 3.5 ng/ml daily release of Ibu and T3, respectively. The first event in the secondary cascade of SCI is the glutamate excitotoxicity elicited by the increased levels of these neurotransmitters after SCI. We found a significant and specific reduction in glutamate levels in animals implanted with our PLLA-drugs scaffold. In particular, the reduction of glutamate was significant at 24 hours from the lesion (3.72 – 0.66 pmol/5 min/mg of protein in the PLLA-drugs group vs. 6.63 – 1.35 pmol/5 min/mg of protein in PLLA group; $P < 0.05$), whereas showed a tendency in reduction at 8 DPL. Also, the K^+ evoked glutamate release from synaptosomes in the PLLA-drugs group was significantly lower at 8 DPL (153% vs. 205%; $P < 0.05$). Since the excitotoxicity and the onset of inflammation are the first hallmarks of the secondary injury, we then evaluated the number of inflammatory cells in the lesioned spinal cord with flow cytometry. We found an important reduction in the number of activated microglia/macrophages pool in the animals implanted with PLLA-drugs (PLLA, 4.83 – 0.85%; PLLA-Ibu-T3, 3.60 – 0.47%; $p < 0.05$) and a discrete reduction in the resting microglia at 8 DPL. The greatest modification observed was in the number of astrocytes identified with the GLAST marker. We found a significant diminishment of these cells at 1 and 8 DPL (PLLA= 36.43– 3.57%; PLLA-Ibu-T3, = 3.60 – 1.26%; $p < 0.0001$).

The locomotion capacity was measured with BBB scale and automated gait analysis with the CatWalk system. We observed a marked difference in BBB scoring between the two animals group starting from the third week (Two-way ANOVA $F(7,216) = 16.57$; $P < 0.0001$). Interestingly, at the latest BBB evaluation at 49 DPL, 60% of animals of the PLLA-drugs group received a score greater than 10, whereas only 20% of animals of the PLLA group reach this score. We confirmed the amelioration of gait parameters with automated measures using the CatWalk system. We observed a significant improvement in the Step Sequence Regularity Index, representing the correct alternation pattern of

paws during gait, in the animals implanted with PLLA-drugs ($P < 0.001$). These experiments demonstrated an overall recovery rate of locomotor function for our implantable treatment of 46%. We also analyzed the extension of the lesion and the total volume of the cavitation in the spinal cord and 60 DPL to correlate the improved recovery with an augmented sparing of the spinal cord tissue surrounding the lesion epicenter. We found a significant reduction in the lesion volume in animals treated with PLLA-drugs scaffold (two-way ANOVA, treatment effect, rostrocaudal, $F(1,105) = 6.854$, $P = 0.0101$; dorsoventral, $F(1,116) = 8.553$, $P = 0.0041$) accordingly with the improvement in locomotor function. In the end, we evaluated with IHC reactions the presence of long-lasting parameters for tissue inflammation, demyelination, astrocyte activation, and neuroprotection in the intact segments of the spinal cord surrounding the lesion epicenter. We observed a reduction of OX42 microglia/macrophages marker in the dorsal funiculus and the dorsal horns both caudally and rostrally to the lesion epicenter. This finding was in line with the observation of a reduced number of inflammatory cells obtained with flow cytometry analysis and suggest that our treatment can modulate the inflammatory response in the acute and the chronic phase of SCI. Also, for astrocyte activation determined by GFAP immunoreactivity, we obtained concordant results with our flow cytometry data. The immunoreactivity for GFAP was significantly lower in the gray matter of the caudal and rostral segments, confirming a reduced astrogliosis reaction in animals treated with PLLA-drugs scaffold. To confirm the enhanced sparing of the white matter and the reduced secondary degeneration of OLs elicited by our biopolymer, we analyzed the distribution of myelin with the lipophilic stain Fluoromyelin. We found that myelin distribution was more uniform in the white matter, and in particular, the lateral and ventral funiculus showed a significant sparing of myelin in the segments surrounding the lesion epicenter. In the end, we measured the potential axonal protection in the ventral funiculus with the quantification of NF200. Data obtained showed an increased positivity to NF200 in the caudal segment from the lesion in animals implanted with PLLA-drugs scaffolds, corresponding to fewer deafferented fibers.

Overall, the presented study demonstrated that multi-drug therapy with local delivery in the spinal cord is very effective in modulating the complex acute phase of SCI; in particular, our combination of drugs, Ibu+T3, is effective in modulating the secondary degeneration leading to an improvement in functional recovery and tissue sparing, acting principally on the inflammatory microenvironment but also the astrocyte reaction. This proof of concept study is well suitable for further amelioration and the application to other conditions characterized by inflammation and demyelination.

In papers number 5 and 6 (section 4.7 and 4.8, respectively), we discussed the issue of spinal cord injury repair in the context of the self-repair ability of the CNS, focusing on the white matter repair (**paper 5, published manuscript, *Molecules*, 25:503-517; 2020**) and the endogenous production of

the neurotrophic factor NGF (**paper 6, paper under review, *Advances in Experimental Medicine and Biology***). Myelin is the main component of the white matter of the central CNS, allowing the proper electrical function of the neurons by ensheathing and insulating the axons. The extensive use of magnetic resonance imaging has highlighted the early, extended, and regionally selective white matter alterations in several neurodegenerative diseases, including Alzheimer's dementia (AD) and other neurodegenerative diseases. Considering that an extensive white matter turnover occurs in adulthood and that myelin repair is currently recognized as the only true reparative capability of the mature CNS thanks to the presence of OPCs, the cells that differentiate in oligodendrocyte, we discussed white matter protection and repair as a potential target for neuroprotection. We reviewed several aspects of the OPC biology, including the anatomical and functional role of OPCs in the neurovascular-neuroglial unit, such as the OPC vulnerability to hypoxia-ischemia, neuroinflammation, and amyloid deposition. Finally, the position of OPCs in drug discovery strategies for dementia is discussed.

Lastly, in paper number 7 (section 4.8), we discussed the pleiotropic effects of NGF in the development, in the adult CNS and PNS, wound healing, and remyelination. The self-repair ability of tissues and organs in injury and disease is a fundamental biological mechanism and an important therapeutic target. The tissue plasticity and the presence of adult stem cell niches open a new path in pharmacological and non-pharmacological treatments development finalized to improve the intrinsic regeneration. In this context, Nerve Growth Factor (NGF) is widely studied for its capability of driving endogenous regeneration of ectoderm-derived tissues, directly acting on the cell targets and through the regulation of the stem cell niches. In fact, this growth factor is very promising for its crucial role in the development and the multiplicity of cellular targets. This chapter travels across the recent history of NGF pleiotropic role in ectodermal tissues generation and repairment, from embryonic development to skin wound healing, axonal regrowth, and remyelination. The better understanding of both the biological mechanisms underlying regeneration and the physiological role of NGF in development and injury response will open new therapeutic strategies, driven by the potential applications of this growth factor as an agent for improving endogenous regeneration processes.

4.2. Characterization of the SCI animal model, differences in the severity of the primary contusive lesion

Animal models in scientific research are fundamental for investigating complex conditions or diseases. The model used for research should be reliable, reproducible, and reflect human pathophysiology. The model must then be appropriately developed in the lab to standardize it, identify measurable end-points reflecting the longitudinal evolution of the condition, and be suitable for testing therapies.²⁰⁸

In the last decades, the use of animal models in research has increased conspicuously, partially explained by the extensive generation of transgenic lines, especially for mice, that replicate human condition²⁰⁹. On the other hand, the implementation of automatic or machine learning software for behavior study has pushed the research using live-recording sensors directly implanted or linked to the animal^{209,210}.

On the other hand, the rising public attention toward scientific research involving animals pushes against this tendency, favoring the improvements in the in-vitro system for replicating tissue and organs as with tissue “organoids” for drug screening and testing. Even if animal models' replacement with an in-vitro system is of great appeal, it is impossible to abolish animal experimentation completely. Principally, the in-vitro system cannot mimic and recapitulate the function and the physiological alteration caused by many diseases or conditions and the reciprocal modification within different organs in response to the primary damage or trauma²¹¹. Scientific research using animal models should respect the 3Rs rule to reduce the total number of animals to obtain relevant conclusions and minimize the harm caused to animals during the experimentation²⁰⁸.

In neuroscience, this technological advancement has allowed us to overcome a significant gap to study CNS and PNS pathology with a functional readout of the alterations in live animals. In particular, optogenetics and imaging techniques have prompted the utilization of animal models to investigate CNS connectivity and structure in normal and pathologic conditions^{212,213}. There are still many limitations for the recapitulation of neurodegenerative pathologies in animals models compared to the human disease. The principal obstacle is the absence of a reliable cognitive readout. Moreover, the impossibility of identifying all the cognitive alterations with behavioral tasks limits the utilization of animal models in neurodegenerative studies.

Conditions derived from neurotraumas are suitable and prone to scientific investigation using animal models. In particular, animals model with CNS traumas are very diffused in experimental neuroscience. The advantages of these models are the high similarity with the human condition from

an anatomical and pathological point of view. Moreover, all animal models of neurotrauma do not require genetic manipulation, and hence the alteration in their phenotype is caused only by the CNS trauma itself. In the end, CNS traumas are also crucial for veterinary medicine and not only for translational medicine. Besides, trauma to CNS like SCI occurs very frequently in companion animals (cat and dogs, mostly) and constitutes an essential veterinary medicine field.

It is noteworthy to consider that neurotrauma animal models need to be precise and accurate to replicate human conditions. CNS is the most complex system of the body and represents the major distinction between animals and humans. Hence, the site of the primary lesion in a neurotrauma model should be defined carefully. Moreover, the lesion's characterization in terms of volume and structure is of fundamental importance to investigate the functional deficits and correlate this loss of neuronal tissue to the phenotypic modifications. Lastly, it must be considered that humans and animals CNS are differently wired, and the functional compensation after a trauma is different and could cause misinterpretation of the results.

In the end, the model of neurotrauma should be easily reproducible and standardizable, with an established correlation between functional deficit and extension of the primary lesion. Moreover, pain and harm caused to the animal during the surgical procedure and the following experimental time should be avoided or reduced to a minimum, if possible ²¹⁴.

This section of this thesis work compares two rats contusive SCI models at the vertebral level T9 with different severity. The animal model is then characterized by locomotor tests and clinical scores to defining the most suitable lesion for the subsequent analysis. In the end, a reconstruction of the lesion volume in the spinal cord and its extension is evaluated to establish the correlation between functional deficit and the trauma in the spinal cord.

MATERIALS AND METHODS

All methods are extensively reported in the previous section of this thesis. For the following experiments were used young adults (>3 weeks) female CD Sprague Dawley rats. A total of 16 rats were used for the standardization of the lesion volume. Animals were divided into 2 groups (8 animals per group), one receiving the severe lesion (2x2 mm depth/diameter) and the other receiving the mild lesion (1.5x1.5 mm depth/diameter).

RESULTS

Clinical evaluation

After the surgical procedure, the general outcome is characterized by an initial worsening of animals' clinical condition in both groups, e.g., the severe lesion and the mild lesion group. Although this general trend, the severe lesion group showed a similar clinical score in the first days compared to the mild lesion group (Fig. 13 A). Despite this, the mild lesion group showed a shorter recovery from the lesion and surgery, with a complete disappearance of major symptoms (not related to SCI) in two weeks from surgery. On the other hand, the severe group showed longer recovery time after SCI and surgery, with complete recovery at the beginning of the third week. The primary indicator of animal health, the bodyweight, showed a statistical difference between the two groups with slower recovery in the severe SCI group (Fig. 13 B). In the mild lesion group, the complete recovery at the pre-surgical body weight was obtained in 2 weeks, while the severe lesion group was observed after three weeks. Moreover, animals in the severe lesion group showed more stress and ailment indicators like skin ulcers and a few autotomy cases of the anterior limb.

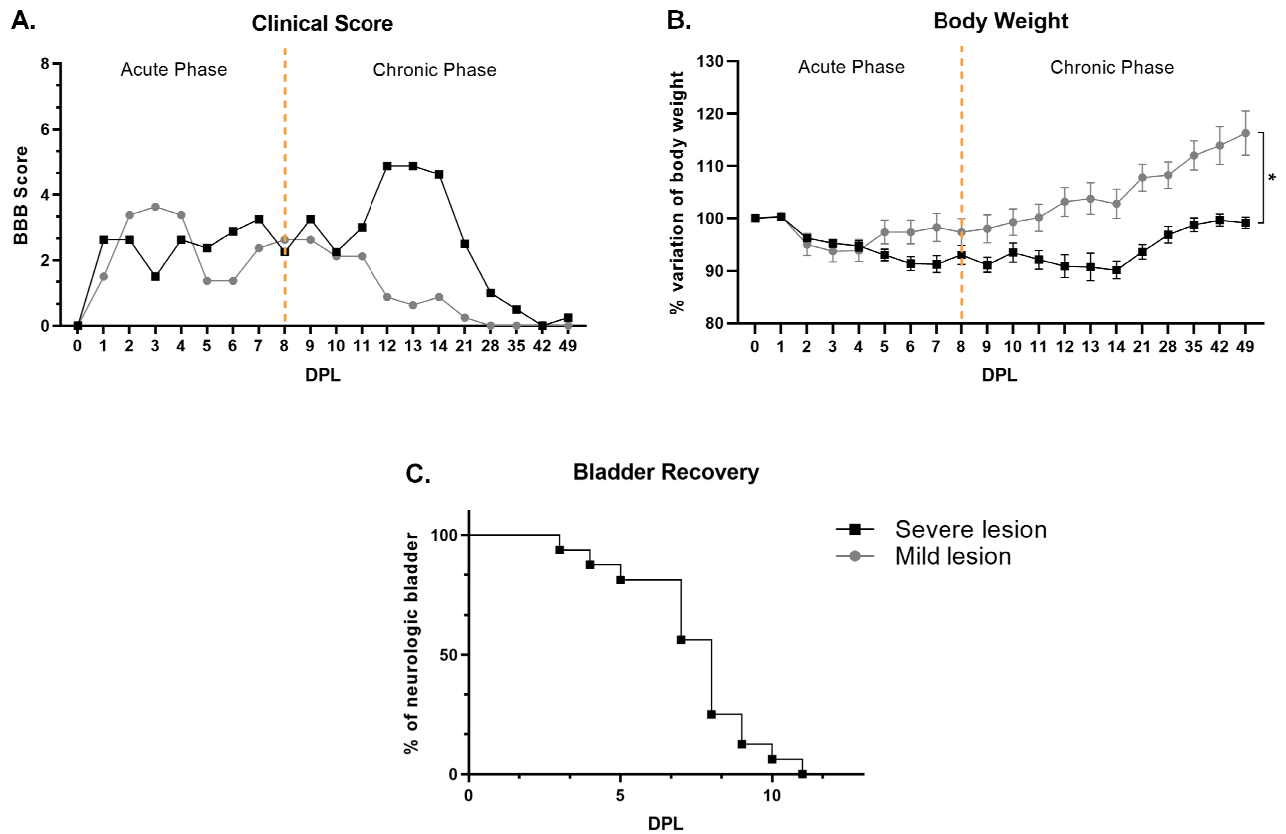


Fig. 13: Panel A reports the integrated clinical score curves based on different parameters for both groups of animals. In panel B are illustrated the variation in body weight expressed as a percentage of the weight on the day of surgery. Animals receiving the mild lesion of the spinal cord recover faster the weight loss in the first days post-injury (two-way ANOVA, $P=0.01$; $F(1, 14)=8.860$; $n=8$ animals per group). Panel C represents a survival curve for the evaluation of neurologic bladder recovery time after SCI. Micturition block resolves after 10 days in the severe lesion group.

Another clinical indicator of the different severity of the lesion is the development of the neurologic bladder in the first two weeks after the injury. All animals developed the neurologic bladder in the severe lesion group and spontaneously recovered after 6 to 10 days. In contrast, in the mild lesion group, no animals showed a complete block of the micturition, but only urine retain in the first hours after SCI (Fig. 13 C). In both groups, however, blood in urine was very frequent.

The intra-surgical mortality rate for both types of lesions was very similar and around 1.2%. Instead, the post-surgical mortality rate showed that the mild lesion group has a non-significative trend in lower mortality post-SCI than the severe lesion group.

Locomotion evaluation

Animals of both groups were evaluated with BBB observational score²⁰² and an automated CatWalk system for gait analysis²¹⁵. The BBB score was used as an indicator of the general recovery after the lesion, whereas the CatWalk system was also used to identify significant gait parameters for the following analysis. In general, both groups showed a spontaneous recovery after SCI in the first three weeks from the lesion measured with the BBB scale (Fig. 14), the extent of which is different between the mild and severe group. In particular, locomotion recovery started from the beginning of the second week in the mild group with an improvement of 11 points, compared to only 4 points increase in the severe lesion group. Then, the mild lesion group showed only a small improvement in locomotor capacity (1.4 points in the BBB scale), and the severe lesion group showed a slower recovery in the second week, reaching a higher performance at the end of the fourth week (7.6 points in BBB). The BBB score then reached a plateau showing an increment of only 0.8 points in the severe lesion group. At the latest time point of 49 DPL, the animals in the severe group were differently distributed in the BBB scale compared to the mild lesion group. The number of animals with a score higher than 10 (representing the ability to perform coordinated gait) was 3 in the severe group and 7 in the mild lesion group.

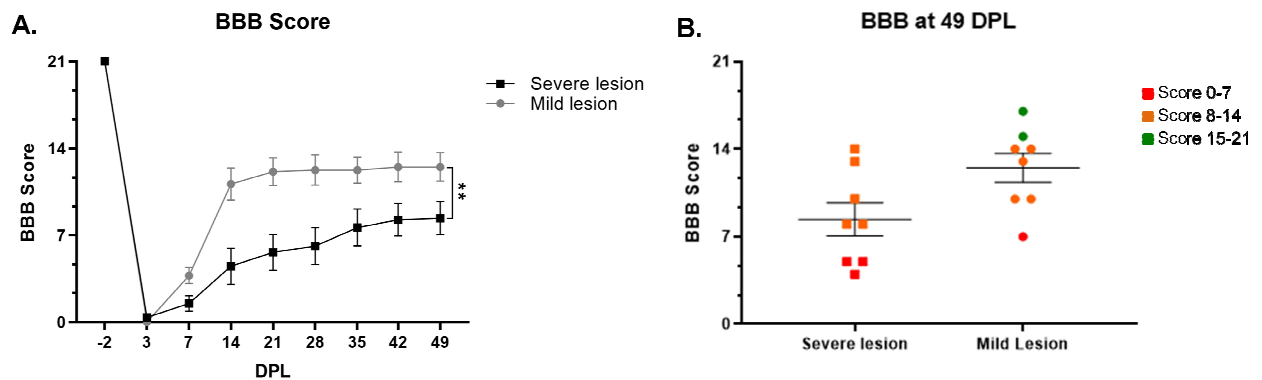


Fig. 14: Panel A reports the time course of the animal evaluation with the BBB scale. Animals in the mild group showed a significant improvement starting from the second week post-injury and reaching a plateau in the locomotor capacity during the third week. Animals in the severe group fail to reach the same locomotor recovery level even at the latest time point (two-way ANOVA, $P=0.0077$; $F(1, 14)=9.658$; $n=8$ animals/group). Panel B represents the distribution of the BBB score at the latest time point observed of 49 DPL. The severe group animals showed a BBB score spanning from 4 to 14 with no animals in the highest part of the scale. Animals in the mild lesion group span from 7 to 17, with two animals in the highest part of the scale.

CatWalk gait analysis showed a different recovery pattern and gait characteristic between the two groups (Fig. 15). Moreover, the stratification of the Catwalk parameters in 4 classes resulted in a definition of the best parameter to measure the locomotion deficit after SCI, possibly useful for evaluating the efficacy of novel therapies. The principal indicator of locomotor performance is the Step sequence regularity index illustrating the regular alternation between the four paws. In the mild

lesion group, we observed a regularity index significantly higher than in the severe lesion group. Among the other gait analysis parameters, we found a general typical modification pattern after SCI in all observed parameters. The lesion's severity modulates differently the spatial, kinetics, and coordination parameters but not the comparative parameters.

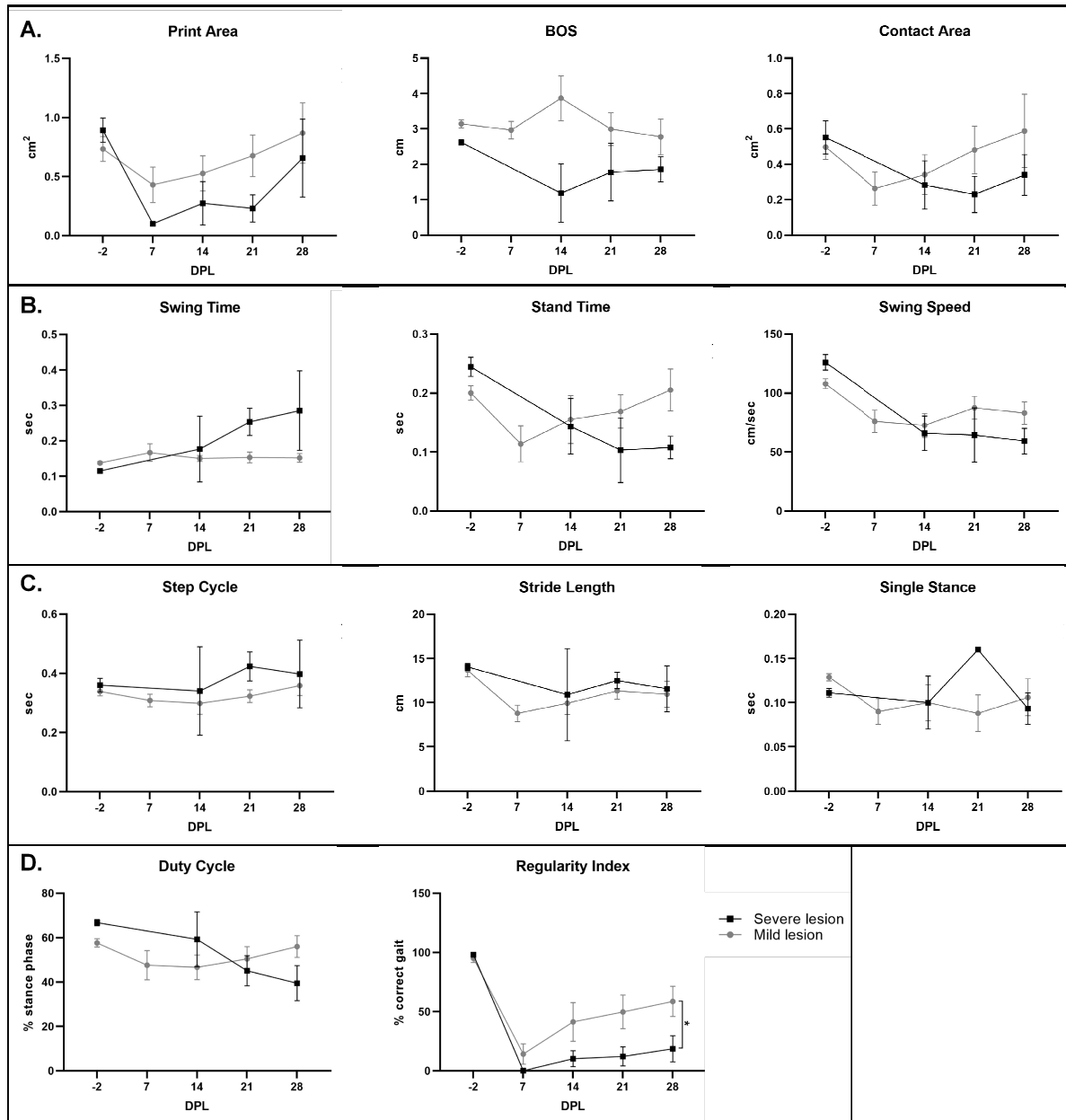


Fig. 15: The figure reports the selected parameters obtained from the CatWalk gait analysis of the two SCI models. In panel A are presented the spatial parameters describing the placing of the paws on the surface. Animals with mild lesions showed a nonsignificant trend in better improvement after SCI. Panel B reports the kinetics parameters, describing paws movements and stepping phases. Also, for these parameters, the mild lesion animals showed a better recovery trend than animals in the severe group. Panel C contains the comparative parameters of the gait, comparing each gait phase during the gait cycle. The severity of the lesion does not influence the recovery of these parameters. Panel D reports the coordination parameters, representing the correct step sequence during the gait. The step sequence regularity index showed a significant difference between the mild and the severe lesion groups (two-way ANOVA, $P=0.0477$; $F(1, 14)=4.708$, $n=8$ animals/group). Data are shown as the mean of the hind paws performance for each parameter.

Histological characterization of the lesion

We measured the volume and the total extension of the spinal cord lesion at 60 DPL to evaluate the enlargement from the acute to the chronic phase. We used H/E stained section in order to discriminate between inflammatory tissue and neuronal tissue. The lesion's full rostrocaudal extension was 5 and 4 cm at 60 DPL for the severe and mild lesion, respectively (Fig. 16). The lesion depth (dorsoventral) in the severe group invests almost all the spinal cord at the lesion level. Hence, the difference between the two groups is principally given by this factor. The lesion's total volume was reported as % of lesion area/total area of the section for each serial section of the spinal cord. The animals in the severe group showed a marked extension of the lesion area per section compared to animals in the mild group as reported in the graph in fig. 16 E. The longitudinal extension of the lesion in the severe group occupies 30% of the spinal cord tissue in the dorsal and central part of the spinal cord, with a reduction in the cord's ventralmost portion. Instead, the mild lesion showed a smaller extension with inclusion of roughly 15% of the total tissue in the dorsal and central part of the spinal cord.

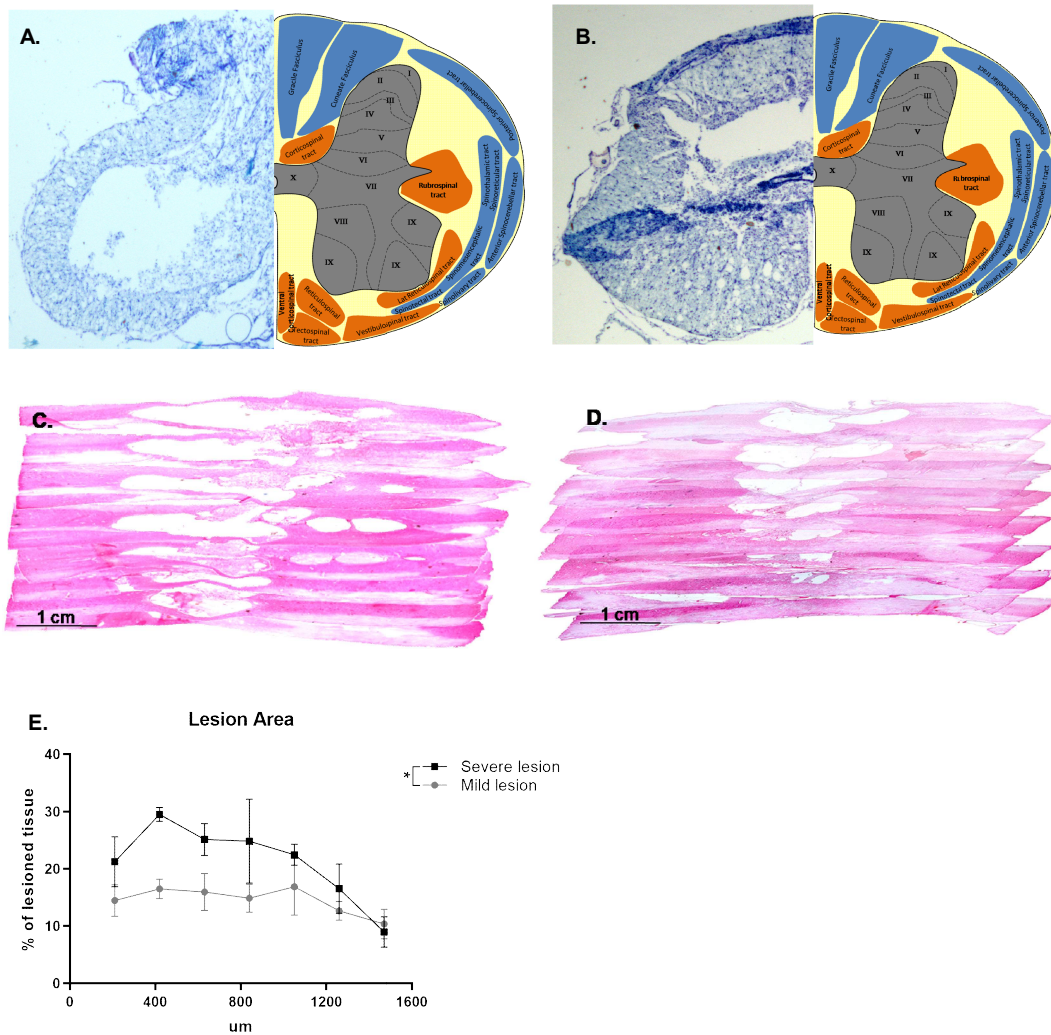


Fig. 16: The picture illustrates the anatomical characteristics of the two models of the lesion at 60 DPL. Panels A and B report schematic representation of a coronal section of the lesion epicenter in the severe (A) and mild (B) lesion. On the left is reported the spinal cord dyed with toluidine blue, and on the right a schematic representation of the white matter pathways and gray matter laminae. In panels C and D are illustrated a 3D reconstruction of the longitudinal segment of the cord embedding the lesion at 60 DPL in the severe and mild groups, respectively. The spinal cord's cavitation and the necrotic tissue surrounding the lesion epicenter are represented as a percentage of total tissue in panel E (two-way ANOVA, $P=0.0013$; $F(1, 28)=12.87$, $n=3$ animals/group).

DISCUSSION

A careful characterization of the animal model is fundamental to obtain robust and reproducible data from animal experiments. The first step in using animal models is identifying the best suitable model for the specific experimental aim. Firstly, we identified the contusive lesion as the type of lesion with the most similar characteristic to the principally diffused injury in human and veterinary medicine²⁵. Compared to the other experimental models of SCI, as transection and compression, SCI's contusive model follows the pathological progression of the lesion and represents the best model for translational medicine^{25,216}. In compliance with the 3Rs principles, we also defined the strain and gender as both well-known factors affecting SCI outcome^{217,218}. In particular, we decided to use the

CD-Sprague Dawley rat strain based on the faster functional recovery after SCI. Moreover, CD-Sprague Dawley rats showed a similar onset of pain and pain-related side effect compared to other strains of rats^{217,218}. From the review of the literature, we also noticed that there is a consensus that the feminine gender shows a better recovery after a CNS lesion. In particular, gonadal hormones estrogen and progesterone favors neuroprotection after neurotrauma²¹⁹. Based on this information in the literature and to respect the 3Rs rules, we chose to utilize young adult female CD-Sprague Dawley rats for our experiments and proceeded to characterize the SCI model.

We establish that the contusive lesion of the spinal cord at a vertebral T9 level was the most suitable type of lesion for our experiments. We then realized two different animal models of SCI based on the lesion's severity and characterized both models to identify the most suitable for the next experiments. The characterization of the model considered the initial difference in the primary lesion. In the severe model, the tip of the Impactor had a diameter of 2 mm and reached 2 mm of depth from the dorsalmost portion of the spinal cord. The mild model instead was realized with a 1.5 mm tip and a depth of 1.5 mm. For both models, the force of the impact and the dwelling time was the same, respectively, of 0.75 N and 0 seconds. For both lesion types, the lesion's depth was sufficient for the complete lesion of the white matter's dorsal corticospinal tract. We then followed the animals' clinical evolution with the SCI and found that no statistical differences were present in the clinical score between the two groups of animals, although the mild lesion group showed a tendency in a better recovery. The monitoring of the body weight after the lesion showed a reduction in the first week for both groups, with the animals in the severe group losing more weight after the surgical procedure and showing a slowest recovery of the weight lost compared to the animals the mild lesion group. These data show that both types of SCI contusion are similar in the clinical evolution of the symptoms after the surgery. Anyway, it is possible to distinguish between the two groups observing the weight loss after SCI. Another specific indicator of the lesion severity is the development of the neurologic bladder in the severe lesion group and the almost complete absence in the mild group. The neurologic bladder is principally caused by the spinal shock in the first hours after SCI and successively derives from a block in transmitting the information from the brainstem to the sacral and lumbar IML (sympathetic chain)^{220,221}. The information regarding the voiding reflex is conveyed in the spinal cord through the reticulospinal pathway, traveling in the ventral funiculus adjacent to the ventral horns. In the severe SCI model, the primary lesion directly invested the reticulospinal tract, whereas in the mild model, the tip of the impactor does not reach the ventral funiculus, sparing the reticulospinal tract from the initial damage. The dimension of the primary lesion in the rat spinal cord is directly involved in developing the neurologic bladder in the severe

group. Accordingly with the present literature on SCI models, the block of micturition in the severe SCI is only temporary with a spontaneous resolution after 6 to 10 days^{25,220}.

For the definition of the functional deficit in the two models of SCI, we used the widely diffused observational scoring system BBB scale²⁰² and an automated gait analysis²¹⁵ to identify the parameters mostly modified by the lesion over a time of 60 days from experimental injury. Interestingly, the severe lesion group showed an utterly different locomotion recovery from the mild lesion group in the first two weeks, evaluated with the BBB scale. Starting from the third week, animals who received the mild lesion showed a better improvement reaching an average score of 11; instead, the severe group animals remained at a score of 4. The different recovery rate in the third week after the lesion to the spinal cord is principally correlated to the secondary evolution of the lesion in the experimental animals^{202,222}. In the severe lesion group, the primary lesion extension is bigger compared to the mild lesion group. Hence, the primary lesion conditions the involvement of different tract and nuclei in the spinal cord and the extension during the secondary cascade amplify the damage to the spared tissue surrounding the lesion core^{223,224}. To characterize the gait in the two lesion models completely, we used gait analysis by CatWalk for the classification of the most relevant parameters modified by the lesion. We found that, according to BBB evaluation, the Step Sequence Regularity Index showed a marked difference between the two groups, with the animals in the mild lesion group recovering almost entirely the coordination of the paws. Moreover, animals in the severe group showed a worse performance in most of the spatial, kinetic, and coordination parameters but a similar modification in the comparative parameters. This similarity could be explained with a retained ability to follow the gait cycle in time but the impossibility to perform due to the complete truncation of the corticospinal and rubrospinal tract in the severe group.

Another primary goal of this initial characterization of the SCI model was quantifying the dimension of contusive damage at the chronic stage of the lesion, representing the final phase of the SCI pathophysiological evolution²⁵. The spinal cord tissue analysis at 60 DPL and the quantification of the lesion area revealed a significant difference between the mild and the severe group of SCI. The principal difference was in the rostrocaudal extension of the injury, whereas in the dorsoventral plane, the lesion's dimension is primarily given by the initial damage depth. In the rostrocaudal plane, the lesion spanned from spinal level T7 to lumbar level L2 in the severe lesion group at 60 DPL for a total extension of 5000 μm . In the mild lesion group, the longitudinal extension of the lesion was more contained as expected, starting at the T9 level and reaching the L1 segment of the cord with a maximum length of 4000 μm . The more significant extension of the lesion in the severe group explains the worse functional recovery of the animals in this group. Although there is a complete destruction of the dorsal corticospinal tract in both models of SCI, in the severe model, the extension

of the lesion also invests the lumbar segment containing the motoneurons controlling the hindlimb muscles^{225,226}. The prominent involvement of lumbar segments in the severe lesion model of SCI also causes motoneuron death, compromising the corticospinal pathway of motor information and the effector of transmitting motor information to the muscles and related reflexes. A reduction in the numbers of motoneurons in the lumbar L1 and 2 segments of the spinal cord is directly correlated to a reduction in locomotor ability^{225,226}. Moreover, another minor contribution to the increase of functional deficit in the severe group is the lesion's ventral extension. Although the ventral extension at 60 DPI in both SCI models is very similar, in the initial phase of the lesion, the severe group received a more deep impact, involving 2/3 of the spinal cord. The primary lesion's depth reached the ventral corticospinal tract and the ventral rubrospinal tract in the severe group but not in the mild group. This difference in the primary lesion could also be translated into a worse functional outcome for the severe group lesion.

CONCLUSIONS

Altogether the data obtained from the characterization of our two models of SCI suggest us to use the mild model to study the spontaneous recovery and the effect of novel therapeutic approaches to stimulate endogenous repairs after SCI, principally because the time-window for the functional evaluation is larger compared to the severe group (3 weeks versus 2 weeks respectively). Moreover, the involvement of the ventral horns in the severe lesion directly affects the motoneurons pool in the lumbar segments worsening the functional outcome. Besides, the absence of neurologic bladder in the mild lesion model is more suitable for the 3Rs principles and ameliorates the animals' wellness. In conclusion, from an anatomical perspective, the principal difference between our the severe and the mild lesion in the spinal cord is the primary lesion extension.

4.3. PRV tracing in the CNS: the effect of the virus on mRNA transcription and processing in the infected neurons (*manuscript in preparation*)

Andrea Bighinati¹, Andrea Sartori², Martin Ernst Schwab²

1Department of Veterinary Medical Science, University of Bologna, Italy; 2Intitute of Regenerative Medicine, University of Zurich, Switzerland.

Correspondence:

Martin E. Schwab, MD

University of Zurich and ETH Zurich

Wagistrasse 27, 8952 Schlieren - Switzerland

Email: schwab@irem.uzh.ch

INTRODUCTION

Neuronal tracing with recombinant viral vectors helps understand the circuitries present in the central nervous system (CNS). In particular, the possibility of tracing and reconstructing multiple neurons with multisynaptic viral tracers allows the selective labeling of the cells involved in one particular circuit and controlling a definite function (Saleeba et al., 2019). One of the most critical features of viral tracers is neuronal cells' specificity and their selective directionality in neurons. In particular, the pseudorabies virus (PRV) can label neuronal cells in a retrograde way and of jumping trans-synaptically to the pre-synaptic neurons hierarchically connected to the post-synaptic neuron (Enquist et al., 1998; Aston-Jones and Card, 2000). The utilization of PRVs for neuronal tracing is a common technique in neuroscience laboratories, and this is very useful to study neuronal connections *in vivo* in the whole CNS and peripheral nervous system, being the viral spreading a time-dependent function and the experimenter optimize the time point for the tracing analysis (Card and Enquist, 1999; Aston-Jones and Card, 2000; Jia et al., 2019). The utilization of the attenuated strains identified by Bartha (Bartha, 1961) has been used in the tracing of various circuits in the CNS (Ekstrand et al., 2008). Another optimal PRV characteristic is its ability to jump from muscle tissue in the peripheral nerve and subsequently be transported in the CNS from the peripheral afferent nerves (Card et al., 1990; Enquist et al., 1998; Aston-Jones and Card, 2000). The significant limitation in utilizing transsynaptic viruses as tracers, like the PRVs, is their high toxicity for the host cells and the activation of a robust immune response against the viral particles and infected cells (McCarthy et al., 2009; Saleeba et al., 2019). Moreover, due to the ability of PRV of replicating in pre-synaptic cells, the spreading of the virus is very high and the population of neurons infected undergoes cell death causing a pathological condition in the animal (Brittle et al., 2004; Granstedt et al., 2013). Although this limitation, PRV remains one of the most utilized viral tracers for the identification of neural circuitries in the CNS. The subsequent characterization of the neuronal cells labeled with the viral tracer is fundamental to understand the function of the circuitry in the CNS. One of the most utilized technique is *in-situ* hybridization for the detection of mRNA levels of genes associated with excitatory or inhibitory neurotransmitters receptors/transporters (Grabinski et al., 2015). The coupling of viral tracing with *in-situ* hybridization allows the researchers to univocally label the neurons as activators or inhibitors inside the hierarchically connected neuronal chain. In the present work, we tried to characterize the spinal neurons involved in lower urinary tract (LUT) function by injecting PRV-Bartha.eGFP into the external urethral sphincter (EUS) and perform simultaneous *in-situ* hybridizations for the amount of mRNAs of the excitatory marker vesicular glutamate transporter 2 (VGLUT2), as well as the inhibitory marker glutamate decarboxylase 2 (GAD2). This study aimed to quantify the loss of expression of mRNA in neurons infected by the virus.

MATERIALS AND METHODS

Rats: A total of 11 adult female Lewis rats were investigated in this study [LEW/OrIRj (Lewis); weight, 200-230 g; purchased from Janvier, France]. The rats were housed in groups of 3 per cage, and food (rat chow) and water were provided *ad libitum*. Rats were maintained on a 12:12 h light:dark cycle (light on from 6:00 A.M. until 6:00 P.M.). All experimental procedures were conducted in accordance with ethical guidelines and were approved by the Veterinary Office of the Canton of Zurich, Switzerland (license 136/17).

PRV injections: Animals were initially anesthetized in 5% Isoflurane (Piramal Healthcare, Digwal, Telangana, India) in air, and anesthesia was maintained with an intramuscular injection of a triple-combinatorial preparation of Medetomidine (Dormitor, 0.105mg /kg body weight, Provet AG), Midazolam (Dormicum®, 1.4mg /kg bodyweight, Roche) and Fentanyl (0.007mg /kg bodyweight, KantonsapothekeZürich). The urethra was exposed with a 2cm long incision into the skin above the lower abdomen. Using a 10 μ L microsyringe (Hamilton, VWR International GmbH) attached to a 33G needle (NanoFil, World Precision Instruments), four injections of 1 μ L PRV614 (2.03×10^9 pfu/mL) each were performed on the ventral and lateral sides of the EUS. Animals were then sutured and allowed to recover on a heat blanket for 45min before subcutaneous application of the antidote (Antisedan, 0.75mg /kg bodyweight, Provet AG and Anexate, 1mg /kg body weight, Roche). Analgesics (Rimadyl, 2.5mg /kg bodyweight, Pfizer) and antibiotics (Bactrim, 15mg /kg body weight, Roche) were applied immediately after surgery and daily until the end of the experiment. Two animals did not receive any PRV injections and were used as a reference.

Perfusion and tissue preparation: Three to four days after viral injection, the rats were euthanized with an intraperitoneal overdose of pentobarbital (300 mg/mL, Streuli Pharma, Switzerland). All animals were transcardially perfused with 100 mL Ringer solution containing 1 % Heparin (B.Brown Medical Inc., Switzerland), followed by 350 mL of 4% paraformaldehyde (PFA, Sigma-Aldrich, Switzerland) in phosphate buffer (0.1M, pH 7.4) containing 5 % sucrose. Perfusion fixed spinal cords were dissected and post-fixed for 24 h at 4 °C in 4% paraformaldehyde. Afterward, spinal cords were transferred to a 30% sucrose solution in 0.1M phosphate buffer, pH 7.2, and stored for 3 days for cryoprotection. The lumbosacral cords were resected from the whole central nervous system, embedded in Tissue-Tek OCT compound, frozen in 2-methyl butane (Sigma-Aldrich, Switzerland), cooled to -40°C with liquid nitrogen, and stored at -20°C until further processing. 14 μ m-thick L1-S3 spinal cord cross-sections were cut on a cryostat and collected free-floating in 0.1M phosphate buffer.

Immunofluorescence: Free-floating sections were blocked and permeabilized in TNB blocking solution containing 0.3% Triton-X and 5% normal goat serum for 60 min at room temperature before being incubated with the primary antibody diluted in TNB containing 0.05% Triton-X overnight at 4°C. The sections were then washed three times in 0.1 M PBS for 10 min each, incubated with secondary antibody for 2 hours at room temperature, counterstained with 4',6-Diamidino-2-Phenylindole (DAPI), and ultimately washed three times in 0.1 M PBS and once in 0.05 for 10 min each. The following antibodies were used: mouse anti-NeuN (1:200, Millipore); rabbit anti-Iba1 (1:500, Wako); chicken anti-GFP (1:500, Avés-Labs); mouse anti-rat OX42 (1:500, Biosciences); Goat anti-chicken conjugated to Alexa Fluor 488 (1:500, Abcam); Goat anti-Rabbit conjugated to Alexa Fluor 647 (1:500, Jackson ImmunoResearch Laboratories); Goat anti-Mouse conjugated to Cy3 (1:500, Jackson ImmunoResearch Laboratories). Sections were mounted on-slide, air-dried overnight at 4°C, and ultimately coverslipped with fluorescence mounting medium (Mowiol, Merck). Slides were stored at 4°C until imaging.

***In-situ* hybridization:** Target sequences, preamplifier, amplifier, and label probes are proprietary and commercially available (Advanced Cell Diagnosis). Here, we used probes against rat glutamic acid decarboxylase 2 (GAD2) and vesicular glutamate transporter 2 (vGluT2, Slc17a6). Experimental protocols were conducted according to guidelines from Advanced Cell Diagnosis. Briefly, spinal cord sections were mounted on a slide (Huberlab, Superfrost), let dry in a sterile environment, and subsequently frozen at -20°C for 2 days. Then, the slides were thawed at room temperature for 15 min. Subsequently, slides were treated with hydrogen peroxide (Advanced Cell Diagnosis) for 10 min and washed twice in water for 2 min each, before incubation in target retrieval buffer (Advanced Cell Diagnosis) for 10 min at 98-100°C. Slides were washed first in water and then in 100% EtOH (Reuss Chemie). Then, protease treatment was applied for 30 min at 40°C in a HybEZ oven (Advanced Cell Diagnosis). Subsequently, sections were incubated in a mix containing the two hybridization probes for 2 h at 40°C. After washing the slides twice in washing buffer (Advanced Cell Diagnosis), the two probes were amplified consecutively, with two washing steps in washing buffer (Advanced Cell Diagnosis) in between each amplification step. Further amplification steps were performed with HRP detecting the specific channel of the different probes, always with washing steps with washing buffer (Advanced Cell Diagnosis) in between. The signals were developed with TSA Plus Cyanin3 and TSA Plus Cyanin5 (PerkinElmer, TSA Cy3, Cy5, TMR, Fluorescein Evaluation kit) for the probe targeting GAD2 and vGluT2, respectively. After developing the last probe, sections were washed twice in washing buffer (Advanced Cell Diagnosis) and counterstained with DAPI (Advanced Cell Diagnosis) for 3 min at room temperature. Slides were coverslipped using fluorescence mounting medium (Merck, Mowiol) and let dry overnight in the dark. Afterward, they were stored at 4°C upon imaging.

Immunostaining quantification: 10-12 cross-sections of the spinal cord level between L1 and S2 were randomly picked and imaged with a fluorescent microscope (20x; Zeiss, Axio Scan.Z1). Exposure time was optimized during the first imaging and kept constant across all sections. Mosaic pictures were acquired and merged within the Zeiss software. Maximum intensity projections were created, and pictures were exported in TIFF format for investigation. Further analyses were performed with Fiji. Quantification of total NeuN particles was obtained with Fiji's automatic particle count and segmentation function after regulation of brightness/contrast threshold and binarization of each image. NeuN particles were then automatically grouped based on their area and perimeter in 100 subcategories based on their dimension. Data were represented as the total number of particles for NeuN count and as a percentage of the total number of particles with a specific area or perimeter. Quantification of immunoreactivity for Iba1 and OX42 was obtained by measuring the fluorescence intensity in the lamina X and intermediolateral column (IML) of the lumbosacral spinal cord. Briefly, images were acquired with the same exposure time and brightness/contrast parameter and then binarized for the immunoreactivity analysis. An ROI of 162 x 130 μm was then used to quantify signal in the two areas of interest. Data were expressed as relative intensity on the area of the ROIs. For the analysis of the dendritic length of Iba1 cells, the same ROIs were used. Briefly, ten single cells were selected in the ROIs, automatically skeletonized with Fiji Skeletonize function, and the total dendritic length and number of branches were measured. Quantification of OX42 single positive cell was made by manual counting the cell in the ROI used for the immunoreactivity analysis.

***In-situ* hybridization quantification:** Multiple cross-sections of the spinal levels L6 and S1 were randomly picked and imaged with a fluorescent microscope (20x; Zeiss, Axio Scan.Z1). Exposure time was optimized during the first imaging and kept constant across all sections. Mosaic pictures were acquired and merged within the Zeiss software. Maximum intensity projections were created, and pictures were exported in TIFF format for investigation. Further analyses were performed with Fiji. Briefly, images were acquired with the same parameter of exposure time and brightness/contrast, and representative ROIs of 162 x 130 μm were selected in lamina X of each slide of the spinal cord. Background (total integrate intensity/total area) was then subtracted from the ROIs, and images were thresholded to exclude any unspecific signal, arbitrarily defined as 3 times higher than background intensity. For *in-situ* signal quantification, the automatic analyze particles function of Fiji was used. Data are represented as total intensity/ROI total area.

Statistical analysis: Data are reported as means \pm standard error of the mean (SEM). One-way ANOVA with Tukey's posthoc analysis and Student's t-test was performed for statistical significance. $P < 0.05$ were considered as relevant.

RESULTS

VGlut2 and GAD2 mRNA down-regulation

The intensity of mRNA labeling for both probes was calculated as total intensity per ROI in Area 10 of all the spinal cord segment positive to PRV virus and then normalized to naïve animals' value. *In-situ* hybridization with dual-labeling for vGlut2 and GAD2 in sacral and lumbar spinal cord showed a reduction of positive, infected neurons at the earliest time point of 3 days post-injection (DPI). The reduction was almost 100% for both groups receiving the PRV. GAD2 showed a trend of time-dependent reduction with a further downregulation at 4 DPI. VGlut2 is completely abolished at 3 DPI and then showed a slight increase at 4 DPI (Fig. 1).

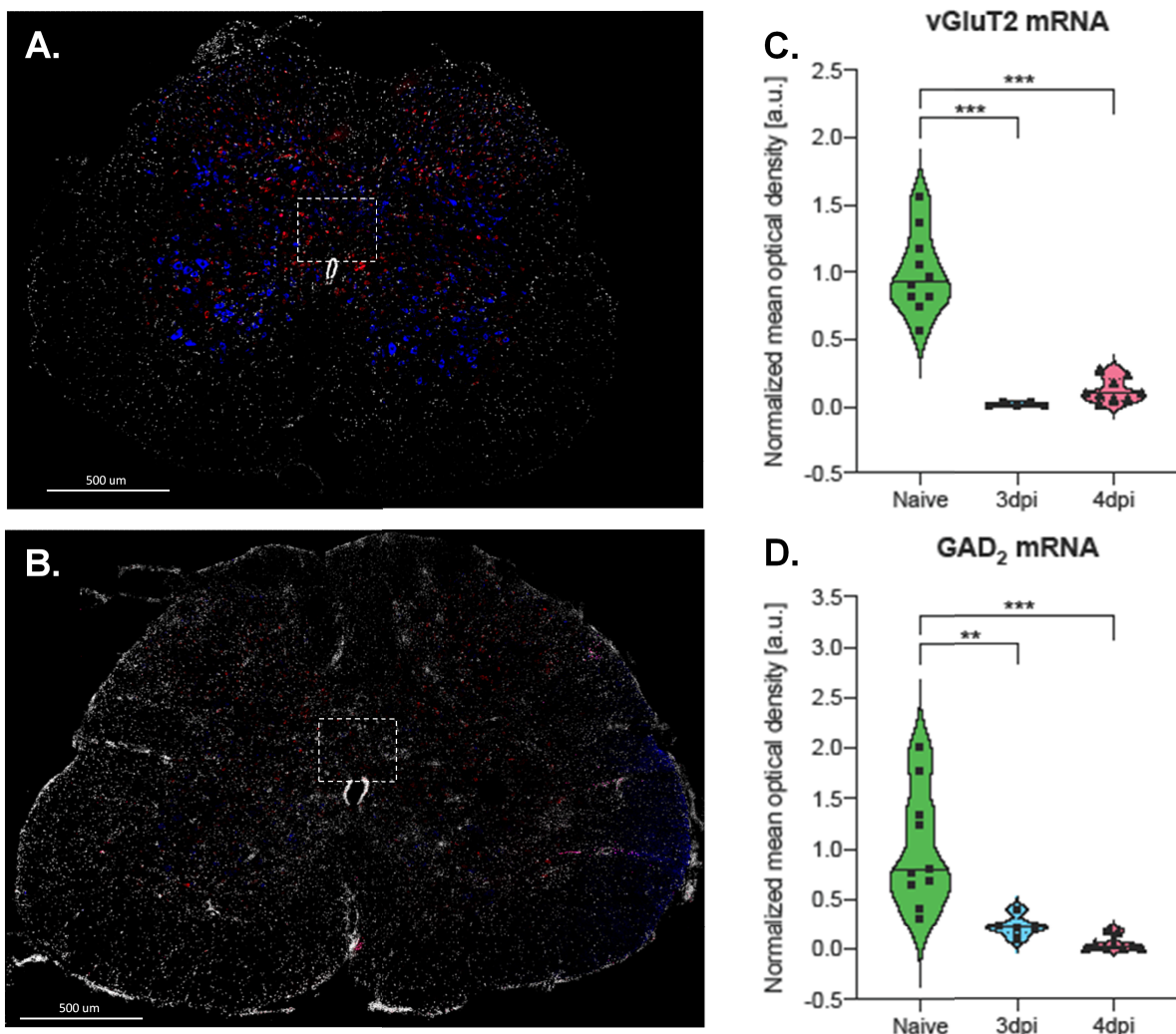


Fig. 1: Panel A and B represent the *in-situ* hybridization for vGlut2 and GAD2 in the spinal cord of naïve and PRV infected animals, respectively. Dotted square reports the Area 10 and the ROIs used for *in-situ* quantification Panel C and D report the normalized optical density of vGlut2 and GAD2 in area 10 of the lumbar and sacral segments. Student's t-test, ** P=0.009, *** P<0.0001.

PRV modifies the expression of proteins in infected neurons

By counting the total number of NeuN positive particles, we observed a reduction in the number of neurons in the infected animals than naïve animals (Fig. 2A). In particular, the reduction of NeuN particle number starts as early as 3 DPI (17% less positive particles), and it is strongly enhanced at 4 DPI (31%). Moreover, the dimension of the NeuN particles in infected animals is generally smaller compared to naïve. The stratification of the particles by dimension (area and perimeter) revealed an increase in the relative number of particles with a surface smaller than $15 \mu\text{m}^2$ starting at 3 DPI (Fig. 2B). This data correlates with the total number of NeuN particles, and at 4 DPI, we observed a further increase in the relative number of small dimension particles.

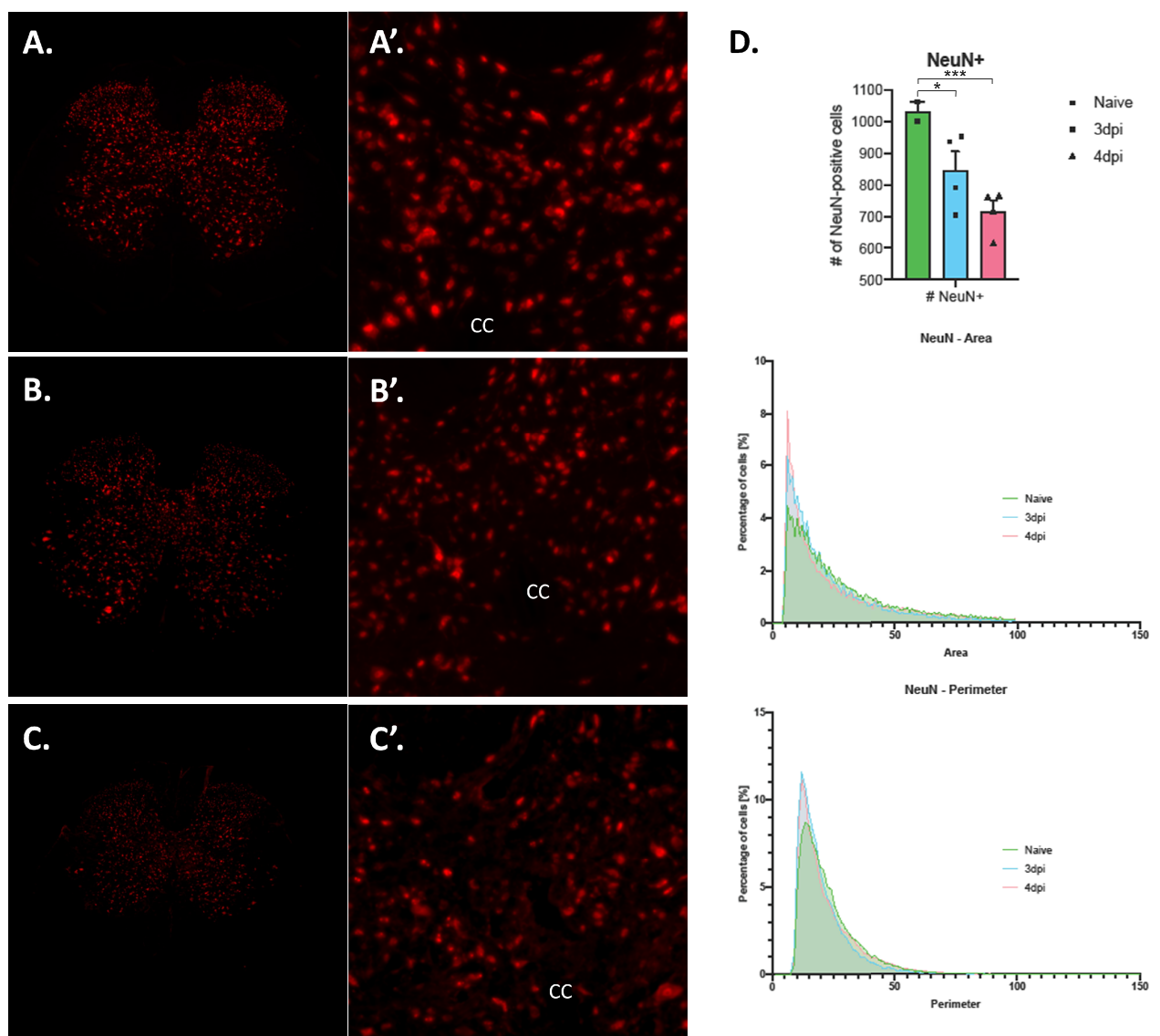


Fig. 2: Panel A, B, and C illustrate the distribution of NeuN in the sacral spinal cord of naïve, 3 DPI, and 4 DPI animals, respectively. Panel A', B', and C' report a magnification of lamina10. Panel D shows the quantification of NeuN particles in all experimental groups and their distribution based on

dimensions. Data are reported as a percentage of the total number of particles. Student's t-test, * P=0.0123; *** P<0.0001.

Immune response stimulation

The activation of inflammatory cells was evaluated with the immunoreactive area for both markers Iba1 and OX42. We found strong activation of microglia/macrophages cells measuring Iba1 intensity (Fig. 3G), starting at 3 DPI in the Lamina X of lumbar spinal levels 2 and 6 (L2, 6), and sacral spinal level 1 (S1) levels but not at the S2 level (Fig. 3C-D). In the IML region at L6 and S1 levels, we observed a weaker positivity for Iba1 than lamina X but the overall activation of microglia/macrophages was also present in the IML area. At 4 DPI, the fluorescence intensity of Iba1 is strongly higher in all the regions compared to the naïve animals (Fig. 3E-F).

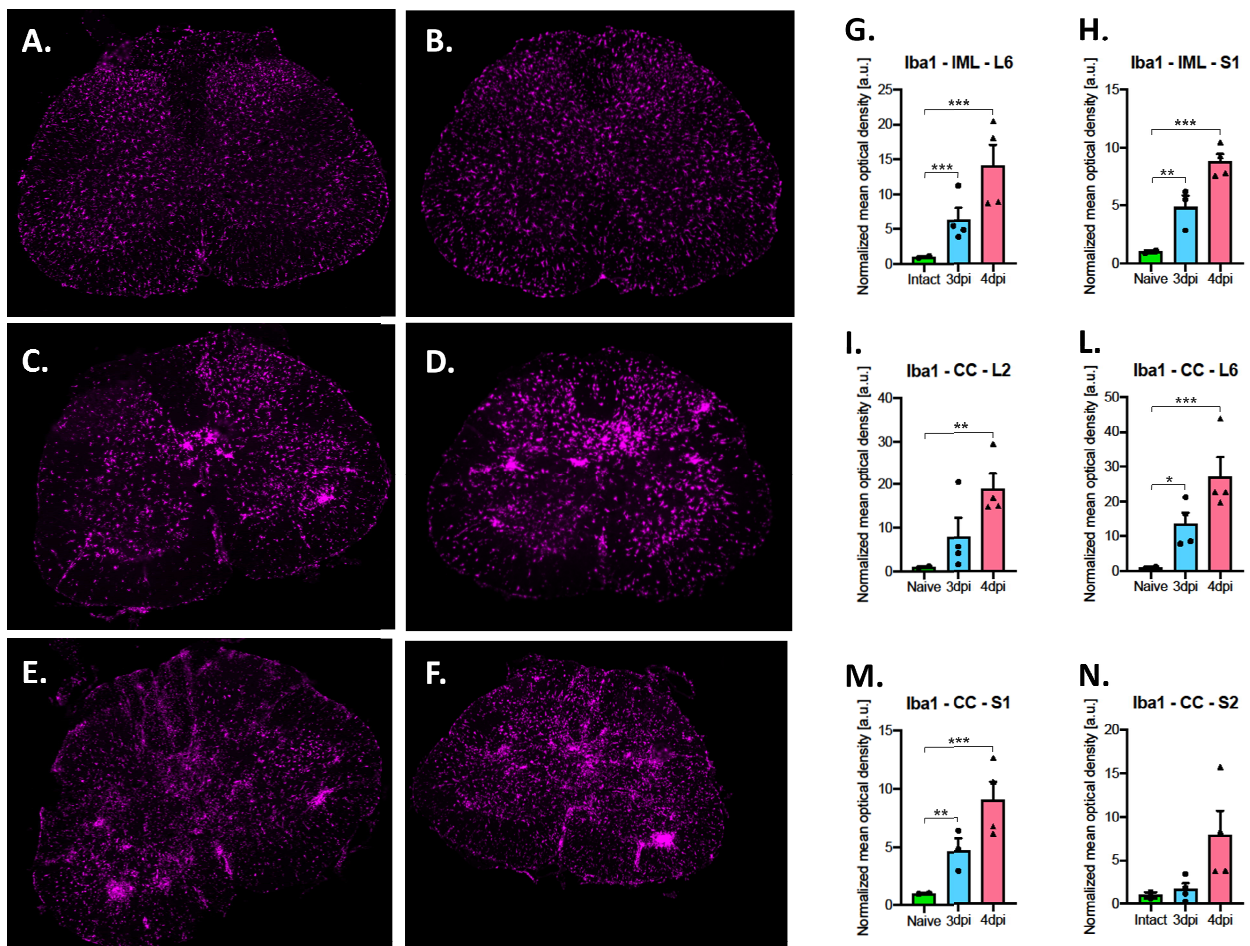


Fig. 3: Panel A, C, and E show the Iba1 labeling in the L6 spinal cord of naïve, 3 DPI, and 4 DPI animals, respectively. Panel B, D, and F report the same labeling in the S1 segment. Quantification of the Iba1 immunoreactivity was reported as the normalized mean of optical density and compared to the naïve animal's levels. Panel G-N reports the levels of Iba1 in the areas of the spinal cord analyzed.

Statistical analysis, Students' t-test (* P<0.05; ** P<0.001; P<0.0001). Abbreviation: CC, central canal; IML, intermediolateral column.

For confirming the activation of microglia cells, we also measured the length of the cellular processes of Iba1 positive cells in the L1 and S1 segments of the spinal cord (Fig. 4). We found a significant reduction in the average length of the cellular process starting at 3 DPI with a marked reduction in the lumbar segment, followed by the sacral segment of infected animals compared to naïve. In particular, L2-6 segments of the cord Iba1 positive cells showed an average dendritic length of 40 µm in naïve animals. After PRV infection, we observed an average length of 18.89 µm and 10.17 µm at 3 and 4 DPI, respectively. In the S1-2 segments of the cord, a similar reduction was observed after PRV injection. The measured average length was 40.7 µm for naïve animals and 26.77 µm at 3 DPI; whereas at 4 DPI, the dendritic length showed a more significant reduction with an average length of 6.94 µm. (Fig.4D) At the latest time point, the shape of the microglial cell is mainly round and indistinguishable from the macrophage.

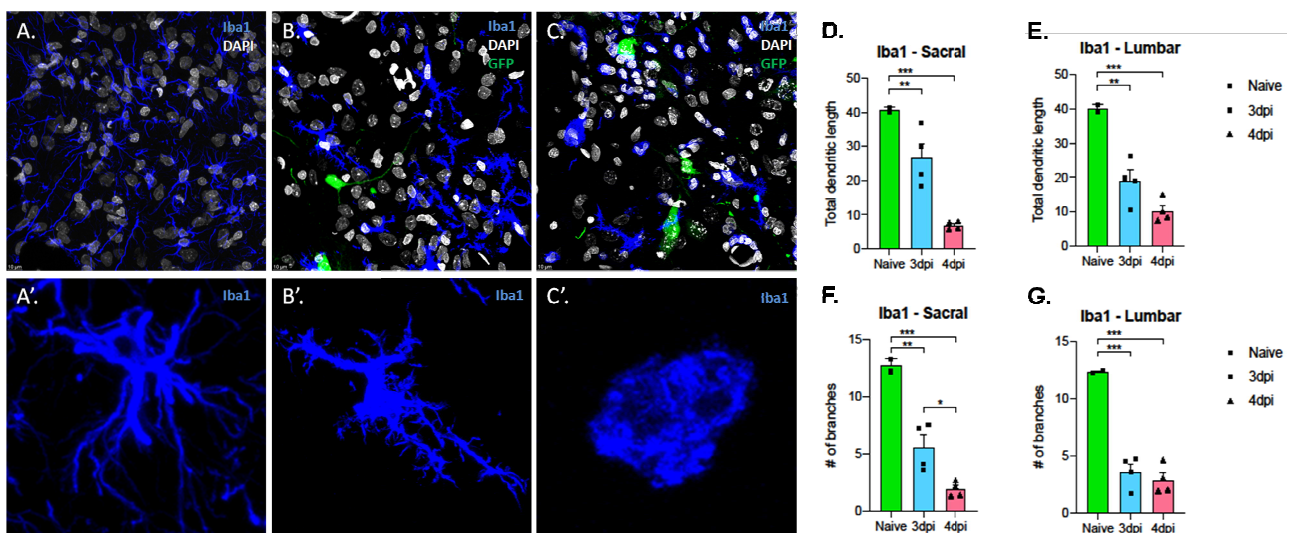


Fig. 4: Panel A, B, and C illustrate the morphological changes of Iba1 positive cells in area 10 of the sacral segment of naïve, 3 DPI, and 4 DPI, respectively. In A', B' and C' are reported the magnification of a single Iba1 cell of the same section. Panel D and E show the quantification of cellular process modification of Iba1 cells as total dendritic length and panel F and G as the number of branches in the lumbosacral spinal cord.

The quantification of OX42 intensity confirms the trend of activation of immune cells reported by Iba1 analysis (Data not shown). We counted the single positive cells to the OX42 marker, representing the infiltrating immune cell from the peripheral tissue (Fig. 5). Since the number of these cells in the infected spinal cord is very low compared to the activated microglia/macrophage

pool, we only divided the spinal cord segments in lumbar and sacral, spanning from L2 to S2, and counted the cells in the lamina X area. We found that the number of OX42 single positive cells increases in all the spinal cord regions analyzed with an average of 4 cells per 21000 μm^2 at 3 DPI for both lumbar and sacral segments. At 4 DPI, the number of single positive OX42 cells increases to 19 per 21000 μm^2 in the lumbar segment and 14 per 21000 μm^2 in the sacral segment.

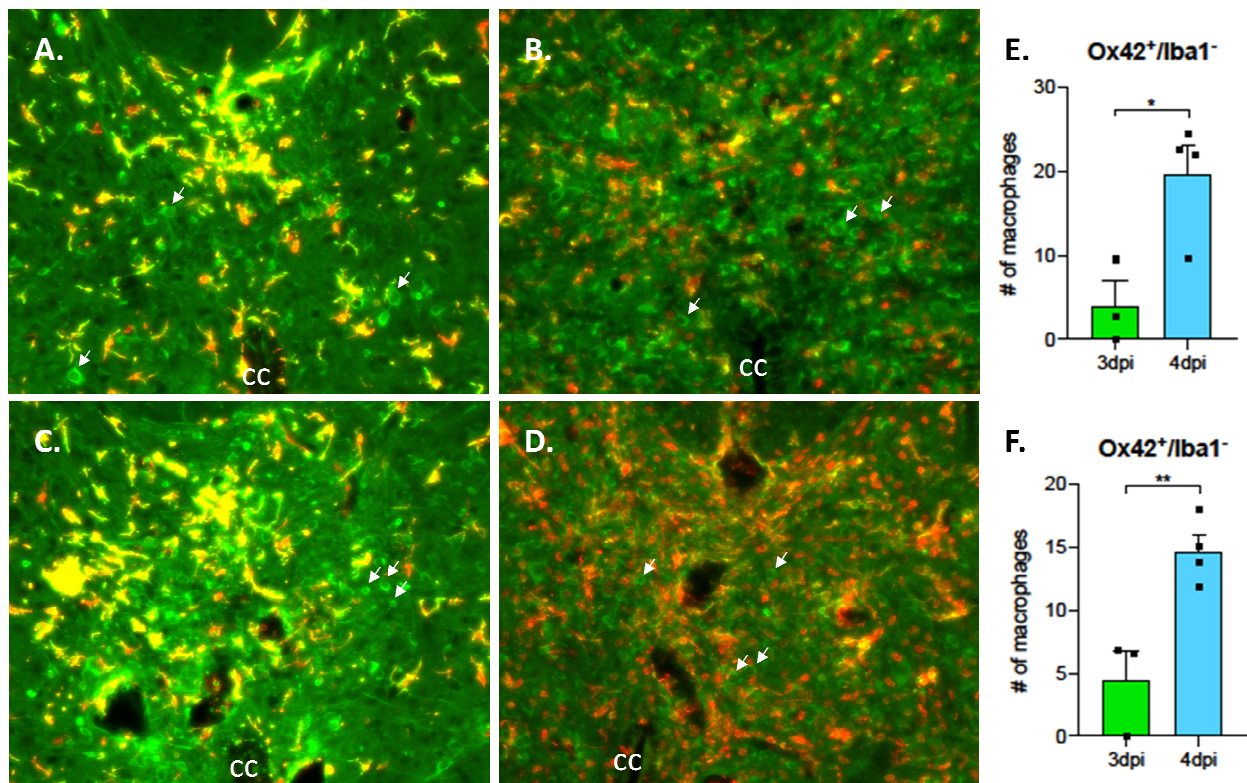


Fig. 5: Panel A and B illustrate the presence of single labeled OX42 cells (white arrows) in the L6 segment of the spinal cord after 3 and 4 days from the infection with PRV. Panel C and D report the presence of the same cells in the S1 segment of the spinal cord. Green is OX42 labeling, and red is Iba1 labeling. Panel E-F shows the quantification as the total number in area 10 of the L6 and S1 segments of the spinal cord. Student's t-test: * $P < 0.05$; ** $P < 0.01$. Abbreviation: CC, central canal.

DISCUSSION

Modification in protein synthesis by PRV

PRV downregulates mRNA expression in infected neurons: The infection with PRV-Bratha of the spinal cord leads to potent inhibition of the mRNA transcription in the cells infected by the virus. This mechanism is known as host shutoff and is typical of *alphaherpesviridae* (Berthomme et al., 1993; Liu et al., 2016). *In-situ* hybridization with dual-labeling for vGlut2 and GAD2 mRNAs in the sacral and lumbar spinal cord reduces positivity for infected neurons at the earliest time point of 3 DPI. Data

obtained from quantification of VGlut2 and GAD2 mRNA levels showed a complete abolishment of the signal in area 10. This reduction is further accentuated at 4 DPI for GAD2 mRNA. Other works have described the reduction of mRNA after infection with PRV, but the overall reduction was reported to be at 50% of the regular expression after 3 DPI for GAD67 and GlyT2 (Stornetta et al., 2004). Our study reported a more marked reduction in mRNA expression for VGlut2 and GAD2, typically expressed in high quantity in the spinal cord of naïve animals. This evidence suggests that cellular modification starts at an earlier time after the infection with PRV, leading to an alteration of RNA and proteins' turnover.

Data obtained from the *in-situ* experiment suggested also controlling the availability of the infected neuronal cells in the spinal cord. It is well known that the ultimate event of tracing with PRV is the death of neuronal cells targeted by the virus. Our data confirm this event in the spinal cord segments where we detected positivity to viral GFP. Moreover, the marker of post-mitotic neurons, NeuN, showed alteration of labeling in the spinal cord segments containing the higher quantity of infected cells by PRV starting at the earliest time point of 3 DPI. In particular, we showed deregulation of NeuN in infected cells. Typically, this protein is present in the nucleus of mature neurons and is a specific marker for neuronal cells (V. V. Gusel'nikova and D. E. Korzhevskiy, 2015). It has been demonstrated that NeuN in neurons acts as a splicing factor, regulating the alternative splicing of neuronal-specific mRNA (Dent et al., 2010). In many pathological conditions, like neurodegenerative diseases, acute trauma, and viral infection, a reduction in NeuN levels is directly linked to neuronal alteration and activation of cell death pathways (Kim et al., 2017). The reduction of NeuN signals in animals infected with PRV-Bartha follows a time course proportional to the spreading of the virus in the tissue. The initial reduction of the NeuN signal is caused by the host shutoff activity of the virus, altering the translation of all mRNAs in infected cells and eliminating the substrate for NeuN activity. This causes the dotted expression of NeuN in the nuclei of infected neurons. After this initial phase, the stress condition and the activation of a robust inflammatory response cause the sufficient cell death of infected neurons, leading to the complete abolishment of NeuN from the nucleus of the cells at later time points. The findings that viral infection alters the expression of structural proteins in the neurons, like NeuN, starting from the early phases of the infection means that the modifications induced by PRV alter dramatically the entire neuronal structure affecting the principal component of the cell (soma, axons, and terminals) compromising the normal neuronal function.

Infection of surrounding cells

We measured the activation of the immune system after viral injection evaluating the expression of Iba1 and OX42 markers in the spinal cord regions mainly infected by the PRV. These regions are the

lamina X from the L2 to the S2 and the IML region in the L6 to S1 levels of the spinal cord. The expression of the GFP marker contained in the PRV virus was not restricted to neuronal cells. We found NeuN negative cells positive to the GFP marker in the area surrounding the primary site of infection. The literature already reported that the spreading of PRV was not confined only to neuronal cells (Card et al., 1993). We found that many Iba1 positive cells also showed labeling for GFP marker. This unselective labeling of immune cells is either caused by active phagocytosis of infected neurons or by an unselective microglial cell infection by PRV.

Moreover, we also identified ependymal cells in the central canal of the spinal cord positive to GFP in the L6-S1 segments. The presence of non-neuronal and non-inflammatory cells positive to GFP confirms the possibility of a non-specific infection of PRV. In addition, the presence of non-neuronal cells infected by PRV underlies the possibility that the infection changes the environment and the functional connectivity in the infected tissue, leading to a malfunction of neurons starting from the very early time points after inoculation.

Inflammatory activation enhances tissue alteration

We showed that at 3 and 4 DPI, the mostly used time-points for neuronal tracing with PRV in the CNS (Card and Enquist, 1999), the response of the immune system after PRV invasion of the CNS is very strong compared to the normal status of microglia/macrophage in the spinal cord of naïve animals. At the earliest time point of 3 DPI, we observed a high level of microglial activation, measured with both intensity of Iba1 and length of the cellular process (Stollg and Jander, 1999; Colton and Wilcock, 2012; Savage et al., 2019). The regions with a high level of microglial activation and GFP expression were the lamina X, IML, and motoneurons pools. Also, microglia showed an active migration from the surrounding areas of the spinal cord toward the site with a higher concentration of GFP-positive cells. A diffuse activation of phagocytosis of infected neurons is already present and detectable in sacral and lumbar segments of the spinal cord, enhancing neuronal death and modification in the CNS connection. The phagocytic mechanism is not restricted to GFP-positive cells, but we also found GFP-negative cells actively phagocytosed by microglia (data not shown). This phenomenon represents a substantial dysregulation of the phagocytic mechanism due to the high inflammatory environment.

We also noted a robust activation of microglia at 4 DPI with the majority of Iba1-positive cells having a round morphology and display a very short cellular process. In literature, it has been reported that activated microglia upregulates the OX42 marker, becoming indistinguishable from the macrophage pool (Savage et al., 2019). We found a complete activation of microglia and the increased expression of the OX42 marker at 4 DPI. At this time point, a higher number of Iba1-negative/OX42-positive cells are present in the spinal cord. These cells probably derive from circulating immune cells migrating

into the spinal cord with an apparent origin from the lymphocytic cell pool. This evidence is supported by the role of Iba1 in actively recruiting and stimulating the proliferation of lymphocytes after viral infections (Zhao et al., 2013; Chinnasamy et al., 2015; Sikora et al., 2020). In the literature, a strong increase in the number of NK lymphocytes has been reported after 3 days from a viral infection (Alsharifi et al., 2006; Poli et al., 2013). This observation is in line with the increase of OX42 single positive cells in the spinal cord of infected animals.

Moreover, the activation of the adaptive immune response and the invasion of T lymphocytes starts at 3 to 4 days post-infection (Griffin et al., 1987; Wilson et al., 2010). The presence of lymphocytes in the spinal cord could derive from leaking of the blood spinal cord barrier (BSCB) or its breakdown due to viral infection. In the infected animals with PRV, the state of the inflammatory process at 3 and 4 DPI is strongly activated, suggesting that the activation of the immune response to infection with PRV begins in the first hours after the injection of the virus. The modification in the microenvironment of the infected spinal cord contribute to the dysfunctional alteration of neuronal cells and amplifies the damage caused by the virus.

CONCLUSION

Neuronal tracing with PRV is a robust and consolidated technique for the identification of neuronal circuits. The issue with working with this type of virus is the complete alteration of gene expression in the early phases of infection, making this neuronal tracing technique unsuitable for neuronal characterization at the mRNA level. Moreover, PRV infection profoundly alters the cytoarchitecture and function of infected cells as early as 3 DPI. These modifications are initiated in the early phases of the infection, leading to a compromise of the structure and functionality of the neuronal cells. The final effect is a profound modification in the expression profile and structural connectivity of neurons underlying the inefficacy of coupling techniques of messenger quantification in the CNS infected with PRV. In addition, the stimulation of a robust immune response enhances cellular death in the infected CNS and shapes the microenvironment enlarging the alteration of functional connectivity. Notably, cell death is not restricted to neurons and affects other cell types, i.e., astrocytes and oligodendrocytes, contributing to the modification of the CNS homeostasis. This effect is further amplified by the ability of PRV to infect non-neuronal cells.

BIBLIOGRAPHY

- Alsharifi M, Lobigs M, Simon MM, Kersten A, Müller K, Koskinen A, Lee E, Müllbacher A (2006) NK cell-mediated immunopathology during an acute viral infection of the CNS. *Eur J Immunol* 36:887–896 Available at: <https://pubmed.ncbi.nlm.nih.gov/16541469/> [Accessed October 29, 2020].
- Aston-Jones G, Card JP (2000) Use of pseudorabies virus to delineate multisynaptic circuits in brain: Opportunities and limitations. *J Neurosci Methods* 103:51–61 Available at: <https://pubmed.ncbi.nlm.nih.gov/11074095/> [Accessed October 25, 2020].
- Bartha A (1961) Experimental reduction of virulence of Aujeszky's disease virus. *Magy Allatorv Lapja* 16:42–45.
- Berthomme H, Jacquemont B, Epstein A (1993) The Pseudorabies Virus Host-Shutoff Homolog Gone: Nucleotide Sequence and Comparison with Alphaherpesvirus Protein Counterparts. *Virology* 193:1028–1032 Available at: <https://pubmed.ncbi.nlm.nih.gov/8384744/> [Accessed October 26, 2020].
- Brittle EE, Reynolds AE, Enquist LW (2004) Two Modes of Pseudorabies Virus Neuroinvasion and Lethality in Mice. *J Virol* 78:12951–12963 Available at: <https://pubmed.ncbi.nlm.nih.gov/15542647/> [Accessed October 25, 2020].
- Card JP, Enquist LW (1999) Transneuronal Circuit Analysis With Pseudorabies Viruses. *Curr Protoc Neurosci* 9:1.5.1-1.5.28 Available at: <https://pubmed.ncbi.nlm.nih.gov/18428451/> [Accessed October 25, 2020].
- Card JP, Rinaman L, Lynn RB, Lee BH, Meade RP, Miselis RR, Enquist LW (1993) Pseudorabies virus infection of the rat central nervous system: Ultrastructural characterization of viral replication, transport, and pathogenesis. *J Neurosci* 13:2515–2539 Available at: <https://pubmed.ncbi.nlm.nih.gov/8388923/> [Accessed December 25, 2020].
- Card JP, Rinaman L, Schwaber JS, Miselis RR, Whealy ME, Robbins AK, Enquist LW (1990) Neurotropic properties of pseudorabies virus: Uptake and transneuronal passage in the rat central nervous system. *J Neurosci* 10:1974–1994 Available at: <https://pubmed.ncbi.nlm.nih.gov/2162388/> [Accessed October 25, 2020].
- Chinnasamy P, Lutz SE, Riascos Bernal DF, Jeganathan V, Casimiro I, Brosnan CF, Sibinga NE (2015) Loss of allograft inflammatory factor-1 ameliorates experimental autoimmune

encephalomyelitis by limiting encephalitogenic CD4 T-cell expansion. *Mol Med* 21:233–241 Available at: <https://molmed.biomedcentral.com/articles/10.2119/molmed.2014.00264> [Accessed October 29, 2020].

Colton CA, Wilcock DM (2012) Assessing Activation States in Microglia. *CNS Neurol Disord - Drug Targets* 9:174–191 Available at: <https://pubmed.ncbi.nlm.nih.gov/20205642/> [Accessed October 26, 2020].

Dent MAR, Segura-Anaya E, Alva-Medina J, Aranda-Anzaldo A (2010) NeuN/Fox-3 is an intrinsic component of the neuronal nuclear matrix. *FEBS Lett* 584:2767–2771 Available at: <https://pubmed.ncbi.nlm.nih.gov/20452351/> [Accessed October 26, 2020].

Ekstrand MI, Enquist LW, Pomeranz LE (2008) The alpha-herpesviruses: molecular pathfinders in nervous system circuits. *Trends Mol Med* 14:134–140 Available at: <https://pubmed.ncbi.nlm.nih.gov/18280208/> [Accessed October 25, 2020].

Enquist LW, Husak PJ, Banfield BW, Smith GA (1998) Infection and spread of alphaherpesviruses in the nervous system. *Adv Virus Res* 51:237–347 Available at: <https://pubmed.ncbi.nlm.nih.gov/9891589/> [Accessed October 25, 2020].

Grabinski TM, Kneynsberg A, Manfredsson FP, Kanaan NM (2015) A method for combining rnascope in situ hybridization with immunohistochemistry in thick free-floating brain sections and primary neuronal cultures. *PLoS One* 10 Available at: <https://pubmed.ncbi.nlm.nih.gov/25794171/> [Accessed December 25, 2020].

Granstedt AE, Bosse JB, Thiberge SY, Enquist LW (2013) In vivo imaging of alphaherpesvirus infection reveals synchronized activity dependent on axonal sorting of viral proteins. *Proc Natl Acad Sci U S A* 110 Available at: <https://pubmed.ncbi.nlm.nih.gov/23980169/> [Accessed October 25, 2020].

Griffin DE, Hess JL, Moench TR (1987) Immune Responses in the Central Nervous System. *Toxicol Pathol* 15:294–302 Available at: <http://journals.sagepub.com/doi/10.1177/019262338701500307> [Accessed December 25, 2020].

Jia F, Lv P, Miao H, Shi X, Mei H, Li L, Xu X, Tao S, Xu F (2019) Optimization of the fluorescent protein expression level based on pseudorabies virus bartha strain for neural circuit tracing. *Front Neuroanat* 13 Available at: <https://pubmed.ncbi.nlm.nih.gov/31281245/> [Accessed October 25, 2020].

- Kim MW, Abid N Bin, Jo MH, Jo MG, Yoon GH, Kim MO (2017) Suppression of adiponectin receptor 1 promotes memory dysfunction and Alzheimer's disease-like pathologies. *Sci Rep* 7 Available at: <https://pubmed.ncbi.nlm.nih.gov/28963462/> [Accessed October 26, 2020].
- Liu YF, Tsai PY, Chulakasian S, Lin FY, Hsu WL (2016) The pseudorabies virus vhs protein cleaves RNA containing an IRES sequence. *FEBS J* 283:899–911 Available at: <https://pubmed.ncbi.nlm.nih.gov/26744129/> [Accessed October 26, 2020].
- McCarthy KM, Tank DW, Enquist LW (2009) Pseudorabies virus infection alters neuronal activity and connectivity in vitro. *PLoS Pathog* 5 Available at: <https://pubmed.ncbi.nlm.nih.gov/19876391/> [Accessed October 25, 2020].
- Poli A, Kmiecik J, Domingues O, Hentges F, Bléry M, Chekenya M, Boucraut J, Zimmer J (2013) NK Cells in Central Nervous System Disorders. *J Immunol* 190:5355–5362 Available at: <http://www.jimmunol.org/content/190/11/5355><http://www.jimmunol.org/content/190/11/5355.full#ref-list-1> [Accessed October 29, 2020].
- Saleeba C, Dempsey B, Le S, Goodchild A, McMullan S (2019) A student's guide to neural circuit tracing. *Front Neurosci* 13 Available at: <https://pubmed.ncbi.nlm.nih.gov/31507369/> [Accessed October 25, 2020].
- Savage JC, Carrier M, Tremblay MÈ (2019) Morphology of Microglia Across Contexts of Health and Disease. In: *Methods in Molecular Biology*, pp 13–26. Humana Press Inc. Available at: <https://pubmed.ncbi.nlm.nih.gov/31392674/> [Accessed October 26, 2020].
- Sikora M, Kopeć B, Piotrowska K, Pawlik A (2020) Role of allograft inflammatory factor-1 in pathogenesis of diseases. *Immunol Lett* 218:1–4.
- Stollg G, Jander S (1999) The role of microglia and macrophages in the pathophysiology of the CNS. *Prog Neurobiol* 58:233–247 Available at: <https://pubmed.ncbi.nlm.nih.gov/10341362/> [Accessed October 26, 2020].
- Stornetta RL, McQuiston TJ, Guyenet PG (2004) GABAergic and glycinergic presympathetic neurons of rat medulla oblongata identified by retrograde transport of pseudorabies virus and in situ hybridization. *J Comp Neurol* 479:257–270 Available at: <https://pubmed.ncbi.nlm.nih.gov/15457502/> [Accessed October 26, 2020].
- V. V. Gusel'nikova, D. E. Korzhevskiy (2015) NeuN as a neuronal nuclear antigen and neuron differentiation marker. *Acta Naturae* 7:42–47 Available at:

</pmc/articles/PMC4463411/?report=abstract> [Accessed October 26, 2020].

Wilson EH, Weninger W, Hunter CA (2010) Trafficking of immune cells in the central nervous system.

J Clin Invest 120:1368–1379 Available at: <http://www.jci.org> [Accessed December 25, 2020].

Zhao YY, Yan DJ, Chen ZW (2013) Role of AIF-1 in the regulation of inflammatory activation and diverse disease processes. Cell Immunol 284:75–83 Available at:

<https://pubmed.ncbi.nlm.nih.gov/23948156/> [Accessed October 29, 2020].

4.4. Time-course changes of extracellular matrix encoding genes in the spinal cord following contusion injury: a data-driven approach

(Int J Mol Sci., 22(4):1744 Feb 9 2021)



Article

Time-Course Changes of Extracellular Matrix Encoding Genes Expression Level in the Spinal Cord Following Contusion Injury—A Data-Driven Approach

Andrea Bighinati ^{1,†} , Zahra Khalajzeyqami ², Vito Antonio Baldassarro ^{3,†} , Luca Lorenzini ¹, Maura Cescatti ², Marzia Moretti ², Luciana Giardino ^{1,2,3} and Laura Calzà ^{3,4,5,*}

- ¹ Department of Veterinary Medical Science, University of Bologna, Ozzano dell'Emilia, 40064 Bologna, Italy; andrea.bighinati@unibo.it (A.B.); luca.lorenzini8@unibo.it (L.L.); luciana.giardino@unibo.it (L.G.)
² Fondazione IRET, Ozzano dell'Emilia, 40064 Bologna, Italy; zahra.khalajzeyqami2@unibo.it (Z.K.); maura.cescatti@unibo.it (M.C.); marzia.moretti3@unibo.it (M.M.)
³ Interdepartmental Center for Industrial Research in Life Sciences and Technologies, University of Bologna, Ozzano dell'Emilia, 40064 Bologna, Italy; vito.baldassarro2@unibo.it
⁴ Department of Pharmacy and Biotechnology, University of Bologna, 40126 Bologna, Italy
⁵ Montecatone Rehabilitation Institute, 40026 Imola (BO), Italy
* Correspondence: laura.calza@unibo.it
† These authors equally contributed to the study.



Citation: Bighinati, A.; Khalajzeyqami, Z.; Baldassarro, V.A.; Lorenzini, L.; Cescatti, M.; Moretti, M.; Giardino, L.; Calzà, L. Time-Course Changes of Extracellular Matrix Encoding Genes Expression Level in the Spinal Cord Following Contusion Injury—A Data-Driven Approach. *Int. J. Mol. Sci.* **2021**, *22*, 1744. <https://doi.org/10.3390/ijms22041744>

Academic Editor: Inbo Han
Received: 14 December 2020
Accepted: 5 February 2021
Published: 9 February 2021

Publisher's Note: MDPI stays neutral with regard to jurisdictional claims in published maps and institutional affiliations.



Copyright: © 2021 by the authors. Licensee MDPI, Basel, Switzerland. This article is an open access article distributed under the terms and conditions of the Creative Commons Attribution (CC BY) license (<https://creativecommons.org/licenses/by/4.0/>).

Abstract: The involvement of the extracellular matrix (ECM) in lesion evolution and functional outcome is well recognized in spinal cord injury. Most attention has been dedicated to the “core” area of the lesion and scar formation, while only scattered reports consider ECM modification based on the temporal evolution and the segments adjacent to the lesion. In this study, we investigated the expression profile of 100 genes encoding for ECM proteins at 1, 8 and 45 days post-injury, in the spinal cord segments rostral and caudal to the lesion and in the scar segment, in a rat model. During both the active lesion phases and the lesion stabilization, we observed an asymmetric gene expression induced by the injury, with a higher regulation in the rostral segment of genes involved in ECM remodeling, adhesion and cell migration. Using bioinformatic approaches, the metalloproteases inhibitor *Timp1* and the hyaluronan receptor *Cd44* emerged as the hub genes at all post-lesion times. Results from the bioinformatic gene expression analysis were then confirmed at protein level by tissue analysis and by cell culture using primary astrocytes. These results indicated that ECM regulation also takes place outside of the lesion area in spinal cord injury.

Keywords: spinal cord injury; extracellular matrix; secondary degeneration; remyelination; timp1; inflammation

1. Introduction

Spinal cord injury (SCI) is a devastating, incurable condition which can severely limit motor abilities but also causes a number of sensory, visceral and systemic symptoms and complications. According to the Global Burden of Diseases, Injuries and Risk Factors Study (GBD) 2019, the age-standardized incidence rate for SCI is 13 per 100,000, while the prevalence is 368 per 100,000 and 90% of cases are due to falls or accidents [1].

When a traumatic injury occurs, a cascade of cellular and molecular events follows the mechanical impact, propagating the primary damage and causing it to spread during a phenomenon known as “secondary degeneration.” Secondary degeneration has been described in both animal models and humans [2] and includes an acute phase beginning immediately after SCI, involving vascular damage, excitotoxicity, free radical formation, inflammation, edema and necrotic cell death. This is followed by the subacute phase, characterized by apoptosis, demyelination, axonal die-back and Wallerian degeneration, matrix remodeling and scar formation. The final component is the chronic phase, involving

the formation of a cystic cavity (syringomyelia, which is present in humans and to a lesser extent in rodents [3], progressive axonal die-back and evolution to a fibrotic scar. The secondary lesion evolves differently rostrally and caudally to the lesion; syringomyelia extension being more severe caudally to the lesion [4], whereas white matter lesion appears to be more severe rostrally to the lesion epicenter [5].

In this complex context, various roles have been attributed to the extracellular matrix (ECM) components over the past decades with regard to the determination of SCI evolution, including free growth factor availability, axonal regeneration, resident and incoming inflammatory cell activation, cell proliferation and migration and attempts at myelin repair. Altered ECM composition after injury is caused by the degradation of certain ECM components and the increased synthesis and activity of others [6]. Different metalloproteases (MMPs), for example, can be released by activated microglia/macrophages, a mechanism triggered by hyaluronan fragments, tenascins and sulfated proteoglycans liberated in the site of injury [7]. The inhibitory role played by the robust up-regulation of chondroitin sulphate proteoglycans on axonal regrowth following injury has been recognized for many years [8]. In the event of injury to the meninges, incoming fibroblasts produce structural components of the ECM, such as fibronectin, collagen and laminin [2]. ECM composition changes are one of the major mechanisms which limit axonal sprouting and regrowth [9] and which alter the process of oligodendrocyte precursor cell (OPC) maturation into newly myelinating oligodendrocytes, responsible for remyelination attempts in the white matter after lesion [10] and regarded as a potential therapeutic target [11].

A clear picture of the cascade of changes in ECM composition and structure at different times after trauma, however, is still elusive, due in part to the complex and evolving nature of this lesion, with no clear distinction between causal and secondary molecular events [12]. Moreover, the succession of partly overlapping pathophysiological events (mechanical trauma, inflammation, excitotoxicity, demyelination and remyelination attempts, neurodegeneration via necrosis, apoptosis, Wallerian and retrograde degeneration, scar formation, etc.) creates a number of confounding interactions. All of these unpredictable variables challenge the classical hypothesis-oriented study design, while the burgeoning availability of “omic” techniques offers a unique opportunity for a target discovery strategy, one which combines a robust experimental design with the bioinformatic analysis of experimental data and confirmatory *in vivo* and *in vitro* experiments.

We therefore designed a study to investigate the ECM protein encoding genes in the spinal cord areas immediately rostral and caudal to the lesion core, using an mRNA array profile and Real Time-Polymerase Chain Reaction (RT-PCR) comprising around 100 genes, with three timepoints corresponding to the inflammatory phase (24 h post-lesion), ongoing secondary degeneration (8 days post-lesion) and the chronic phase (45 days post-lesion), focusing our attention on the segments where most of the ascending and descending tracts were compromised by the lesion. The hypothesis generated from the bioinformatic analysis of the gene expression results was then validated at protein level and by *in vitro* experiments.

2. Results

2.1. Animals and Lesion Characterization

The spinal cord area directly affected by the mechanical lesion is illustrated in a schematic coronal section of the lesion segment of the spinal cord, including the area directly impacted by the punch (Figure 1A, gray area). The general wellness of the animals was monitored by body weight (Figure 1B) and an initial decrease was observed, followed by a recovery starting from 8 Days Post Lesion (DPL). All animals showed a mild to moderate locomotor impairment following SCI, as assessed by the Basso, Beattie, Bresnahan (BBB) locomotor scale and a spontaneous recovery beginning at 7 DPL, which stabilized at 14 DPL (Figure 1C). None of the study rats died.

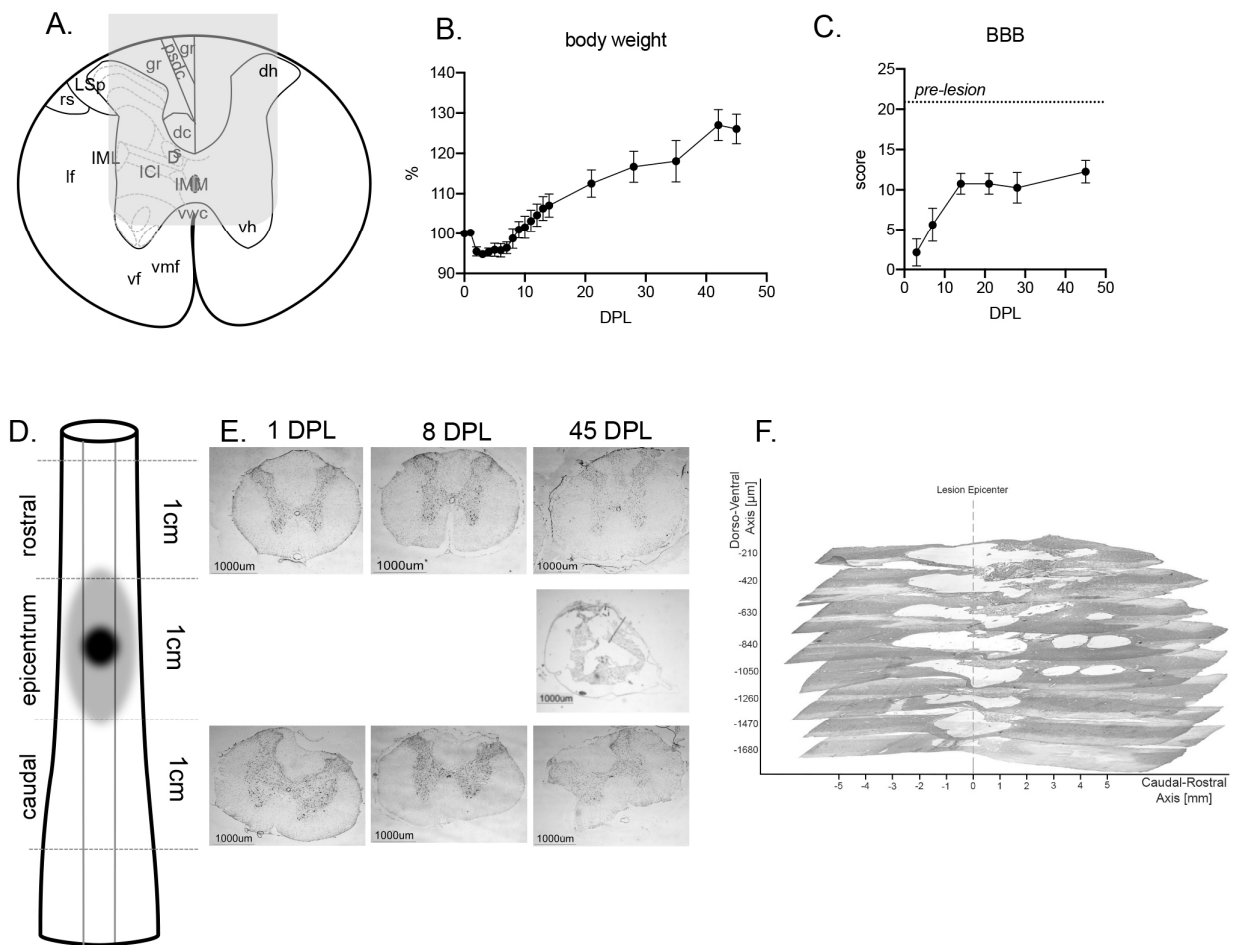


Figure 1. Functional and anatomical characterization of the traumatic spinal cord injury (SCI): (A) Gray area shows the tip of the impactor on the anatomical schema of the spinal cord; (B) Percentage variation of the body weight of lesioned rats over the course of the experiment. Data is expressed as mean \pm SEM; (C) Basso, Beattie, Bresnahan (BBB) score in lesioned animals over the course of the experiment, where 21 is the score of healthy pre-lesion animals. Data is expressed as mean \pm SEM; (D) Schematic diagram of spinal cord sampling; (E) Low-mag micrographs of the coronal section of the spinal cord at the center of the lesion, rostral and caudal levels (Nissl staining) from representative animals sacrificed at 24 h, 8 and 45 days; (F) 3D reconstruction of the spinal cord cavitation at 45 days post lesion (DPL) as derived from low-magnification micrographs of longitudinal sections, showing the rostro-caudal and dorso-ventral extension. Abbreviations: A; dc, dorsal corticospinal tract; dh, dorsal horn; Gr gracile fasciculus; ICI, Intercalated nucleus; IML, intermediolateral column; IMM, intermediomedial column; lf, lateral funiculus; LSp, lateral spinal nucleus; psdc, post synaptic dorsal column; vf, ventral funiculus; vh, ventral horn; vmf, ventral medial fissure; vwc, ventral white commissure.

Lesion extension was analyzed by histology, using both longitudinal and coronal sections. The anatomical schema in Figure 1D shows the general sampling strategy for tissue analysis and includes the area directly affected by the mechanical lesion (center of the lesion) and the rostral and caudal segments affected by secondary degeneration. Panels in Figure 1E show representative micrographs of coronal sections collected at the corresponding rostro-caudal level at 1, 8 and 45 DPL. Sections collected at the center of the lesion at 1 and 8 DPL were almost destroyed and the resulting cavitation is evident at 45 days. Figure 1F shows the rostro-caudal and dorso-ventral extension of the lesion at 45 DPL, as obtained by 3D reconstruction of longitudinal sections from a representative animal. The contusive lesion and secondary degeneration extended to a dorso-ventral depth of approximately 2000 μ m, reaching the ventral horn as expected and 6000 μ m in rostro-caudal direction, from segment T7 to segment T11.

2.2. Gene Expression Profile in the Spinal Cord Segment Rostrally and Caudally to the Lesion Center of the Lesion

The expression of genes encoding for proteins of the ECM was investigated at 1, 8 and 45 DPL following spinal cord lesion, rostrally and caudally to the lesion, therefore in segments which are not directly involved in the mechanical lesion but affected by the secondary degeneration process. This was done by comparing the expression profile of 84 genes to the respective segments of intact animals and the list of the investigated genes is reported in Figure 2. For biological averaging and variance reduction, samples from each group were pooled as for microarray experiments [13–15].

The relative gene expression is shown as a heat map showing correlated gene expression across each group and time point (Figure 2). The relative fold change for each gene is shown in the table next to the clustergram, with red being the maximum and green the minimum difference of expression from the median of each gene analyzed. Due to the low expression in all experimental groups (threshold > 35 Ct), we excluded the *Mmp1* gene from further investigation. The fold of difference normalized on the corresponding spinal cord segment in intact animals is reported in the table, where up-regulated genes are shown in red and down-regulated genes are shown in green.

The main focus of the study was to compare the ECM gene expression in the spinal cord segments rostral and caudal to the lesion. The two hierarchical clusterization analyses obtained using Gene Globe software revealed a similar regulation between the two segments soon after the lesion (1 DPL), characterized mainly by the up-regulation of the genes involved in ECM remodeling (*Timp1*, *Mmps*, *Sell*, *CD44*, *Fn1*). However, the rostral segment showed a higher number of up-regulated genes (rostral, $n = 21$; caudal $n = 6$) and a lower number of down-regulated genes (rostral, $n = 1$; caudal $n = 13$), with *CD44*, *Mmp3*, *Sell*, *Thbs2*, *Timp1* and *Tnc* commonly up-regulated in the two segments. At longer time points from the lesion, the caudal segment showed a similar pattern of gene regulation (8 and 45 DPL), with a slight down-regulation of most analyzed genes. The rostral segments also showed a similar pattern of gene regulation compared to the caudal segments, while the rostral segment clustered alone at 45 DPL, indicating that the overall gene expression regulation differed from the other time points.

At this time point, only the *Timp1* gene was still up-regulated in both segments, while 10 and 5 genes were down-regulated in the rostral and caudal segments respectively, with *Col8a1* the only common down-regulated gene in both segments.

To further investigate the similarities and differences between the rostral and caudal segments in response to spinal cord lesion, we extracted the highly-responsive genes (fold of changes > 4) from the PCR array analysis, grouping them as similar (Figure 3A) or different regulation patterns (Figure 3B) between the two segments. In each graph, the circle represents the rostral and the square the caudal segment, while the dotted horizontal line indicates the intact spinal cord.

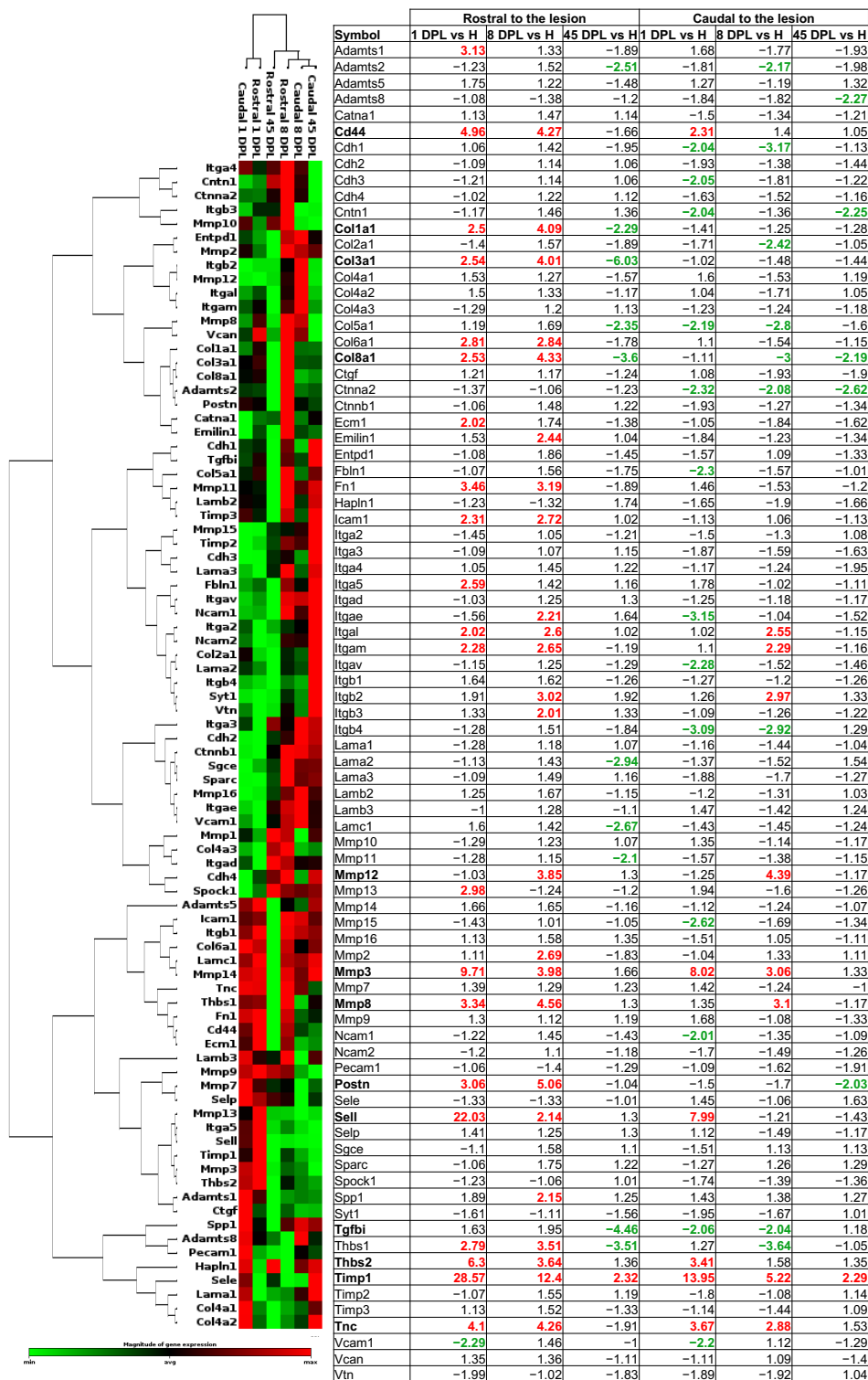


Figure 2. Heat map of the cluster analysis of extracellular matrix (ECM) gene expression regulation. ECM gene mRNA expression in the rostral and caudal segments of the spinal cord at all time points are shown in the table as fold change compared to the pool of intact segments of spinal cord ($n = 5$ per group, pooled). The clustergram shows the co-regulated genes across the group, analyzed with a vertical dendrogram and the clusterization of the segments of spinal cord at each time point illustrated with a horizontal dendrogram. A red color indicates a higher expression with respect to the median of the gene, whereas a green color indicates a lower expression. Gene names in bold indicate the highly regulated genes (fold of change > 4).

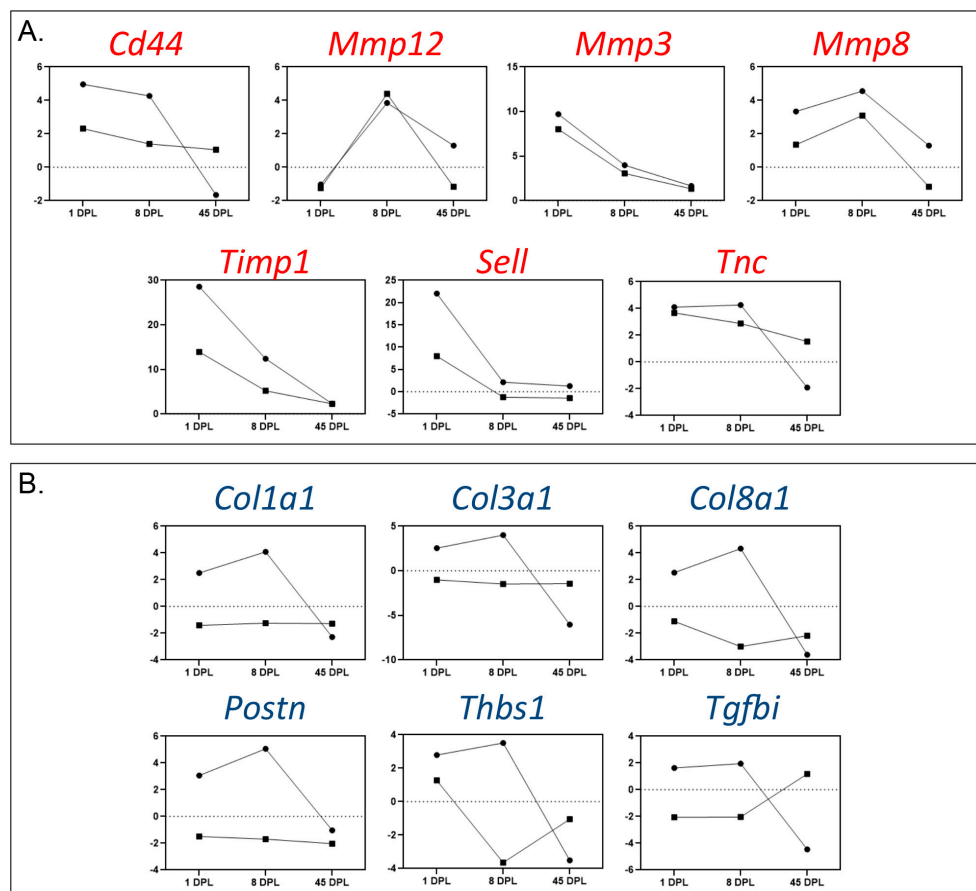


Figure 3. Time-course changes in the mRNA expression level of highly regulated genes. The figure illustrates the data obtained from the Polymerase Chain Reaction (PCR) array of genes regulated more than 4 times in at least one of the two segments and at least one considered time point. Genes are divided into similarly (A) or differently (B) regulated in the rostral and caudal segments. Circles represent the segment rostral while squares the region caudal to the lesion.

The highly responsive genes showing the same regulation pattern between the two segments are mostly involved in ECM reorganization, with a strong representation of Mmps and related proteins (*Mmp3*, *Mmp8*, *Mmp12*, *Timp1*, *CD44*, *Sell* and *Tnc*), while the rostral segment responds to injury with an overexpression of collagen genes (*Col1a1*, *Col3a1* and *Col8a1*) and the related *Postn*, with an up-regulation in early phases (1 and 8 DPL) and a down-regulation at 45 DPL. Moreover, the *Thbs1* gene showed the same temporal pattern, while decreased expression in the caudal segment and the Tgf β induced gene (*Tgfb1*) were strongly down-regulated in the rostral segment at 45 DPL, while being up-regulated in the caudal segment at the same time point.

Since we used a ready-made PCR array profile, we included the mRNA expression analysis of 14 additional genes encoding for proteins of the neural ECM performed by RT-qPCR, also finding different mRNA expression levels between the two segments of spinal cord for these genes over the time points analyzed. We first confirmed the data obtained using PCR arrays for *CD44*, *Fn1*, *Postn*, *Sell* and *Tnc*, showing a strong up-regulation in both segments at 1 and 8 DPL (Supplementary Materials Figure S1). Among the other genes, we found a different regulation in the two segments in 3 genes (*Agrin*, *Bcan* and *Slit2*) in the acute phase (1 DPL) and 1 gene (*Lgals1*) in the sub-acute phase (8 DPL) (Figure 4A). *Agrin* is involved in the regulation of neurite outgrowth and synapse formation; *Bcan* encodes for brevican, a chondroitin sulfate proteoglycan; *Slit2* regulates axonal guidance in the spinal cord, while *Lgals1*, which encodes for Galectin 1, a beta-galactoside binding protein involved in cell-cell and cell-matrix interaction, showed a statistically significant up-regulation in the rostral segment compared to the caudal segment at 8 DPL (2.5 vs.

1.5 Log₂ fold change). No significant variations either in the rostral and caudal segments were observed for *Cspg4*, *Slit1*, *Tnr* or *Ntn1* (Figure 4B).

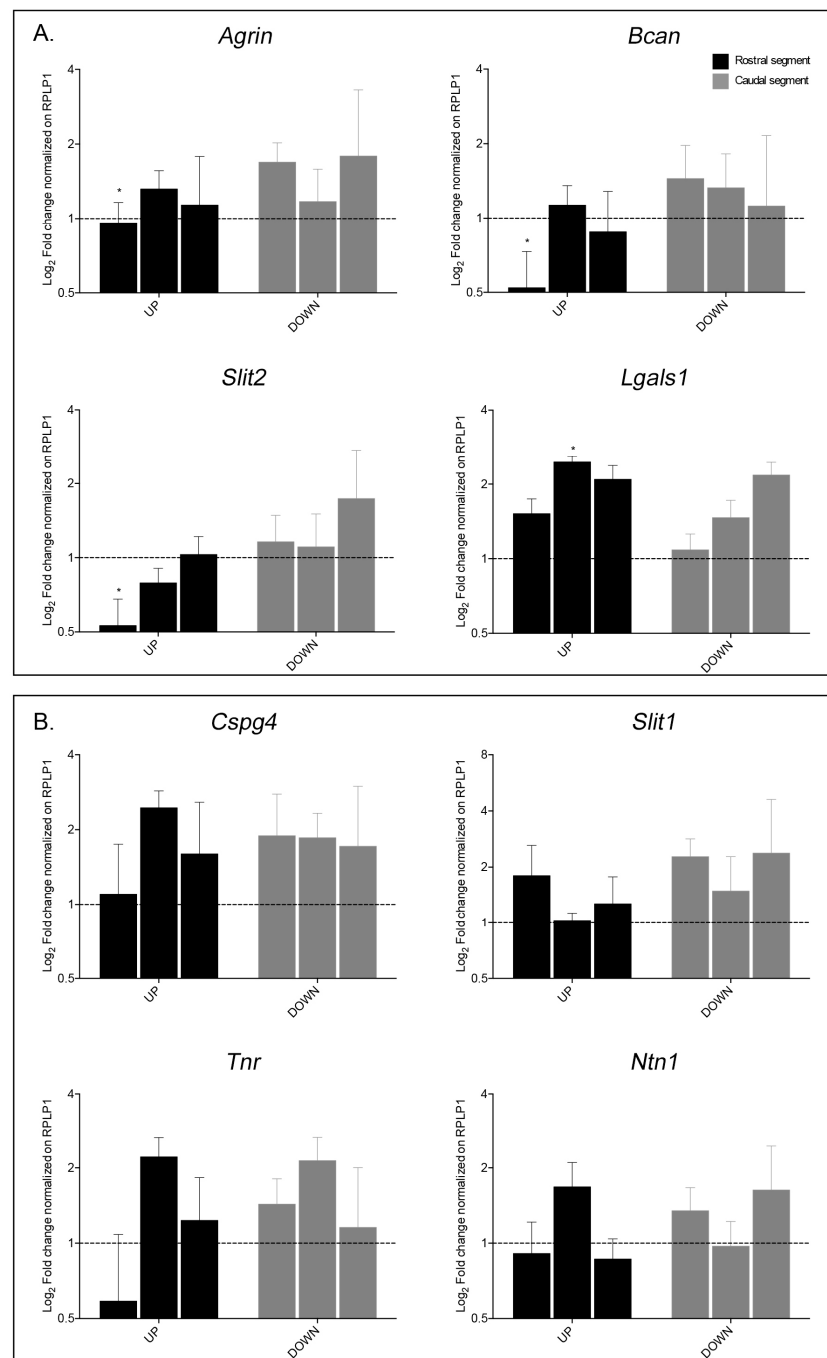


Figure 4. Time-course changes in mRNA expression level for neural extracellular matrix encoding genes: (A) Genes presenting a statistically significant difference in expression level; (B) Genes presenting non-significant variation. Real Time – Polymerase Chain Reaction (RT-PCR) data is represented as Log₂ fold change of gene expression normalized on the respective intact segment of spinal cord, shown by the dotted line ($n = 4$ animals per group per time point). The black bars show the results obtained from the rostral segment, whereas the gray bars show the segment caudal to the lesion. Statistical analysis: one-way ANOVA with Fisher's LSD, *Agrin* $p = 0.041$, $t = 2.146$ (4, 27); *Bcan* $p = 0.0441$, $t = 2.112$ (5, 27); *Slit2* $p = 0.0341$, $t = 2.232$ (5, 27); *Lgals1* $p = 0.035$, $t = 2.22$ (4, 27), * $p < 0.05$.

Moreover, we performed a correlation between the gene expression levels from single animals and the related BBB score, finding no differences for all the analyzed genes (Supplementary Table S1).

2.3. Bioinformatic Analysis and PPI Interaction from Cluster Analysis

We then performed bioinformatic analysis of all genes in the array and RT-PCR single gene analysis. We initially classified the up- and down-regulated genes for each segment and time point using the Panther bioinformatic platform for gene enrichment (Supplementary Materials Figure S2). Gene classification was based on their biological process, as defined by Gene Ontology (GO) analysis. We confirmed the difference observed with the PCR Array clustergram analysis and identified the common biological processes at 1 DPL in both rostral and caudal segments, especially for up-regulated genes. The principal classes of biological process showing different regulation modes between the segments on either side of the lesion epicenter were biological adhesion (GO: 0022610) and cellular process (GO: 0009987) but we also found alterations in immune system process (GO: 0002376), localization (GO: 0051179), biological regulation (GO: 0065007) and developmental process (GO: 0032502).

To identify the major genes involved in ECM remodeling following SCI, the list of genes profiled by the Extracellular Matrix & Adhesion Molecules PCR Array from Qiagen, with the addition of RT-PCR single cell analysis, was analyzed for the protein-protein interaction (PPI) via the String online database and the information used to visualize the ECM cluster on Cytoscape (v3.7.2). Subsequently, the gene expression profiles obtained via PCR array and RT-qPCR for each region and time point were superimposed on to the ECM cluster to include the genes with at least 2-fold change variations. The new sub clusters were filtered by node degree to define a maximum of 10 hub genes for every condition and the results are shown in Figure 5, where the color intensity indicates the folds of gene expression regulation (red, up-regulation; green, down-regulation) and circle size indicates node degree. At 1 DPL, we observed that *Timp1* was the most up-regulated gene in both the rostral and caudal segments, with *Cd44* as the most relevant nodes in both segments, while *Fn1* seemed to be a relevant node in the rostral but not the caudal segment. *Timp1* also maintained a central role at 8 and 45 DPL in both segments, although its expression progressively declined. Notably, *Timp1* was still slightly up-regulated in the stabilized chronic lesion (45 DPL), while all other altered genes (collagens and laminins) were down-regulated.

To validate these bioinformatic results, we performed the *Timp1* protein analysis in the spinal cord tissue (rostral segments) at the same time points and the results are shown in Figure 6A,B, confirming a slight increase and then a progressive *Timp1* content decline over the experimental time frame.

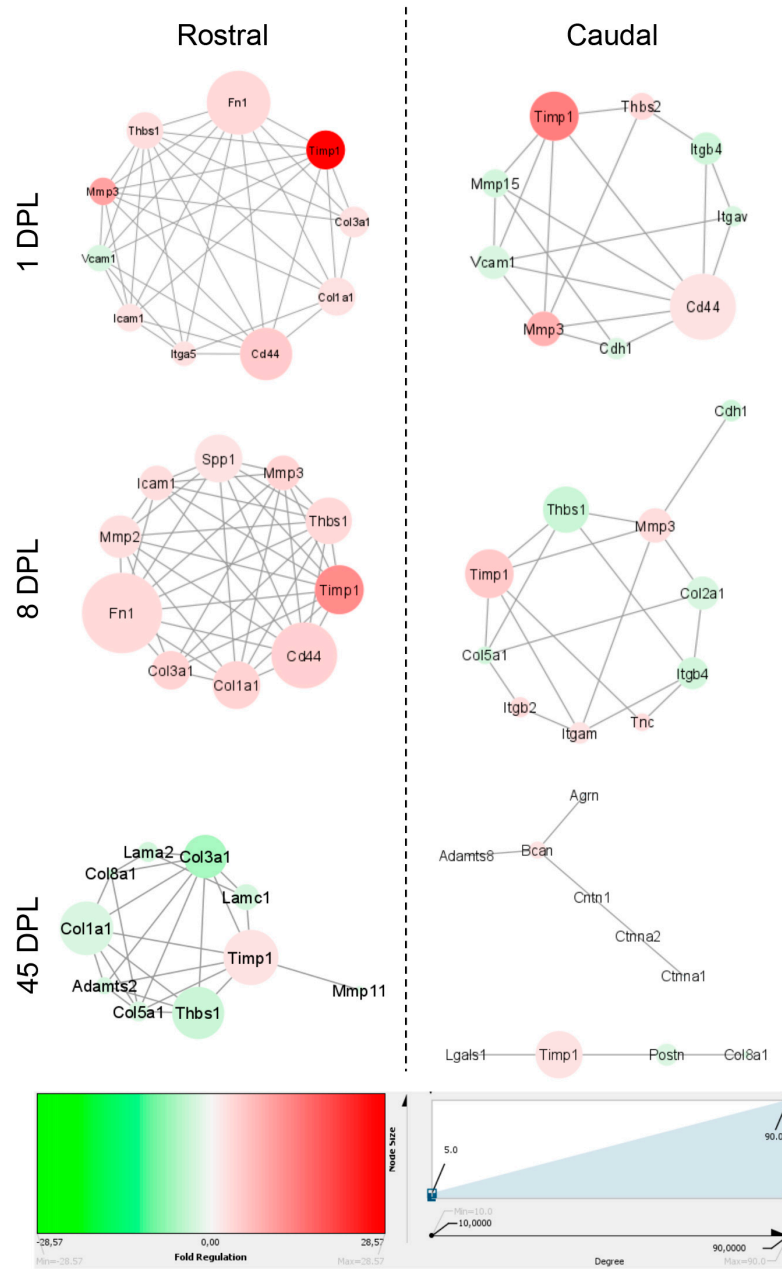


Figure 5. Cluster analysis of the investigated genes. Interaction network resulting from degree and fold change analysis of the general Extracellular Matrix (ECM) network. Colors indicate gene expression as fold regulation, where red indicates up-regulation and green down-regulation. The size of the nodes represents the degree of gene involvement in the ECM network. The edges represent the interactions between each node.

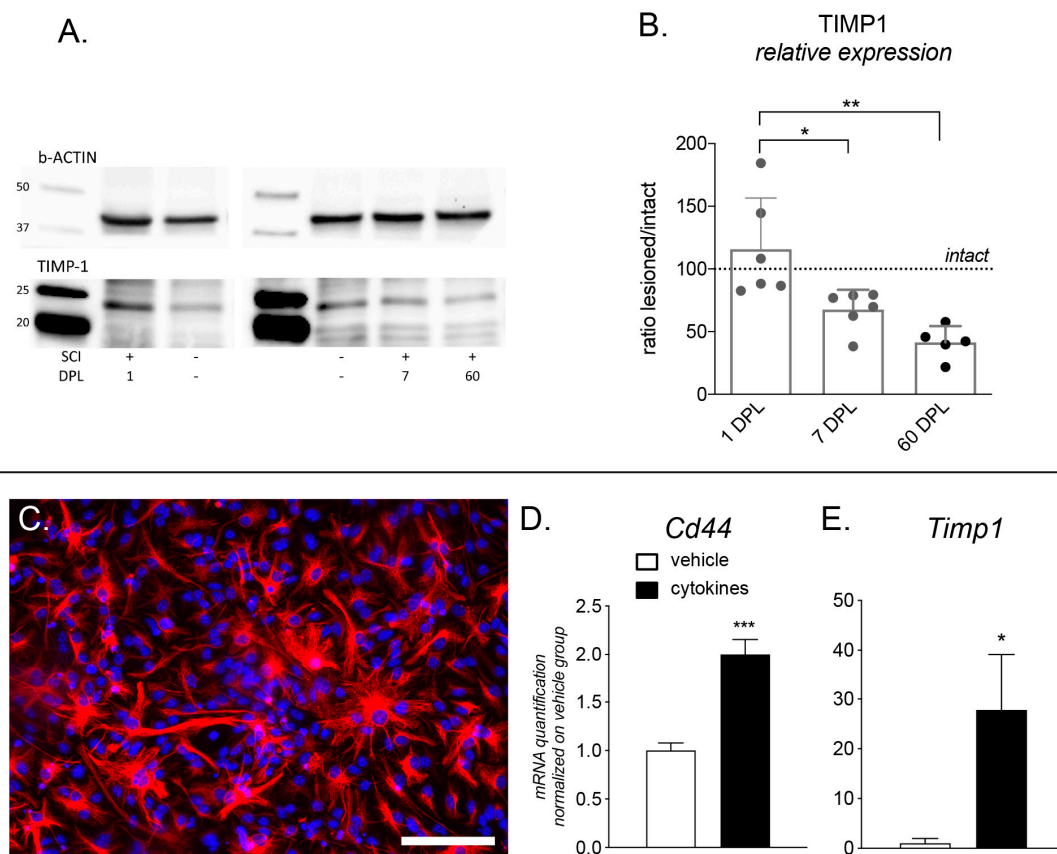


Figure 6. Timp1 protein quantification in the spinal cord and expression of *Cd44* and *Timp1* in primary astrocyte cultures: (A) Two representative gels are shown in the figure. Upper panel shows b-Actin (43 kDa), used as house-keeping protein, lower panel shows Timp1 (23 kDa) in each analyzed group (intact animals: SCI-; lesioned: SCI+ at 1 DPL, 7 DPL and 60 DPL); (B) Graph shows relative *Timp1* expression calculated as signals as measured by densitometry, indicated by relative intensity (lesioned versus controls). Statistical analysis: one-way ANOVA and Tukey post-hoc test, * $p < 0.05$; ** $p < 0.001$; (C) Micrograph illustrates pure astrocyte cultures stained for GFAP marker; (D,E) Graphs show mRNA expression level of *Cd44* (D) and *Timp1* isoform b (E) in cultures exposed to vehicle or cytokine mix for 48 h. Statistical analysis. Student's *t*-test. Asterisk represents difference between vehicle- and cytokine- treated groups (* $p > 0.05$).

2.4. In Vitro Evaluation of the *Cd44* and *Timp1* Response to Inflammation and *Timp1* Protein Quantification in the Spinal Cord

To confirm data from mRNA expression, we quantified Timp1 protein level in the segment rostral to the lesion at 1, 7 and 60 DPL (Figure 6A,B). Quantification results were normalized at each time point on the Timp1 protein level in the same segment of spinal cord from healthy animals, used as control. To minimize inter-gels variability, unlesioned animals were distributed in each gel and inter-gel normalization was made both versus b-actin (housekeeping protein) and lesioned versus unlesioned animals. Timp1 protein at 1 DPL was slightly but not significantly up-regulated in lesioned animals. On the contrary, a significant downregulation of the Timp1 protein level was observed at 7 and 60 days compared to unlesioned animals.

To demonstrate the direct link between inflammation and overexpression of the two genes identified in vivo, we used primary culture of astrocytes (Figure 6C), one of the main responsible for *Cd44* and *Timp1* production, exposed to a cytokine mix containing molecules up-regulated in the CSF 24 h after SCI [16] able to block remyelination [17,18]. Gene expression results are shown in Figure 6D,E. Both *Cd44* and *Timp1* (isoform b) were up-regulated by exposure to the cytokines (Student's *t*-test; *Cd44*, $p = 0.0006$; *Timp1*, $p = 0.0118$). Interestingly, we also analyzed the isoform "a" (precursor) of the *Timp1* gene, which was

not regulated by cytokine exposure (data not shown). Single ΔCt data for each analyzed gene are shown in Supplementary Materials Figure S3.

3. Discussion

Spinal cord trauma is followed by an extremely complex biological syndrome involving different pathophysiological processes (hemorrhage, inflammation, excitotoxicity, demyelination, axonal degeneration, cell death, scar formation, etc.) which evolve over months and even years in humans [2]. Efforts to find a molecular signature which is also able to drive drug discovery is complicated by the impressive regulation of dozens of different cell types and hundreds of molecules which occurs after injury [19] and by the highly personalized nature of each lesion, making each patient's medical history unique.

All components of the neural ECM (interstitial, perineuronal, basement membrane) are recognized as players in SCI evolution, repair attempts and therefore in functional outcome in chronic lesions [12]. Most published reports, however, describe ECM variations at the core of the lesion, focusing on scar formation [20] and to the best of our knowledge, no data is available on the surrounding segments, where the ascending (caudal segment) and descending (rostral segment) nerve pathways reside and where a bridge between the pathological microenvironment of the scar and intact tissue is likely to take place [5,12]. In these areas, active neurons, reactive glia, including astrocytes, microglia and NG2-OPCs are present and play a possible role in ECM modification [21].

To demonstrate the molecular regulation of this microenvironment, spared from mechanical injury and scarring on one hand but hit by a veritable "storm" of pathological changes on the other, in this study we explored the transcriptome profile of the ECM-encoding genes in the spinal cord tissue adjacent to the injury site. Analysis were focused on the protein component of the ECM through gene expression modulation and does not consider the hyaluronan component. We examined both the spatial and temporal changes, examining the spinal cord segments adjacent to the lesion center of the lesion, in both rostral and caudal directions and analyzing three time points after lesion corresponding to the direct effects of the mechanical impact (24 h post-lesion; 1 DPL), secondary degeneration (8 DPL) and the chronic, stabilized phase (45 DPL).

First of all, we carefully characterized the lesion extension at the investigated times. The areas directly affected by the Impactor tip included the gray matter (dorsal and part of the ventral horn) and the white matter with regard to the dorsal funiculus, which includes the ascending fasciculus gracilis and the descending corticospinal tracts. Following contusion injury, the lesion developed a cystic cavity at the center of the lesion, which spread coronally and longitudinally in both rostral and caudal directions from the 1.5 mm wide impact, extending for more than 4.0 mm across the center of the lesion at 3 DPL, then expanding further, surrounded by scar tissue, an evolution which corresponds to the literature in the field [4,22–24]. Quantitative MRI indicated that most of the axons directly affected by the impact degenerated rostrally to the injury site, while minor damage was observed caudally [25]. Axonal damage and myelin pathology in the descending corticospinal tract were also clear, both caudally and rostrally to the injury, due to axonal retraction (rostral) and axonal dieback (caudal), expanding for up to 8 weeks even at a long distance from the injury site.

Overall, we observed an unexpected asymmetry in ECM gene expression regulation in the rostral compared to the caudal segment. Grouping the results of the gene array analysis in "active lesion phases" including 1 and 8 DPL and considering ≥ 2 folds regulation as significant, we observed that 28 out of 80 genes were up-regulated in the rostral segment, while only 10 were up-regulated in the caudal segment. On the contrary, 20 genes were down-regulated in the caudal segment, while none were down-regulated in the rostral segment. It should also be noted that the more strongly up-regulated genes, such as *CD44*, *Mmp3*, *Sell*, *Timp1*, *Tnc*, were regulated in both segments. At lesion stabilization (45 DPL), 10 genes were down-regulated and only one up-regulated (*Timp1*) in the rostral segment, while 3 were down-regulated and one up-regulated (*Timp1*) in the caudal segment.

Notably, it has been described that other proteins not related to the ECM are differentially regulated at the center of the lesion and in the rostral and caudal segments [26–28], thus confirming the asymmetric profile of molecular regulation around the injury site. Since the meninges were undamaged in the contusive model, these molecular changes do not involve peripheral cells such as fibroblasts but are described as mainly due to astrocytes, pericytes and other glial cell types [29].

Even if it has been described that Mmp1 protein is strongly activated after SCI in both humans and animals [30,31], this protein activation is not confirmed at gene expression level in our model. However, Mmp1 is normally in an inactive state as a pro-proteinase requiring the proteolysis from other metalloproteinases, like Mmp3, for its activation [32] (<https://reactome.org/content/detail/R-RNO-1592297>). In fact, we found a strong upregulation of Mmp3 at 1 DPL which is sustained also at 8 DPL. Thus, we hypothesized that the absence of Mmp1 expression is not correlated to the absence of this proteinase in the lesioned spinal cord but rather to the activation of Mmp1 at protein level.

With regard to highly regulated genes ($\times 4$ fold change), different collagen and collagen-related genes (*Col1a1*, *Col3a1*, *Col8a1*, *Postn*) were strongly responsive in the rostral but not in the caudal segment. Type 1 collagen has already been described as up-regulated in SCI models in the segment rostral to the lesion [33] but a difference between the rostral and caudal segments has never been described. In the healthy CNS, fibril-forming collagens are present in the vessel structure and in meningeal membranes, while non-fibril-forming collagen proteins are widely distributed throughout the CNS, where they play a major role in CNS wiring and repair [34,35]. Although collagen IV is the most widely studied component of the fibrous scar tissue which develops after CNS injury [36], an up-regulation of collagen 1 is also seen as an activator of astrocytes, driving them to a scar-forming phenotype [37]. Interestingly, *Col1a1*-positive cells have recently been identified as perivascular stromal cells activated following brain and spinal cord injuries, participating in fibrosis scar formation and secreting retinoic acid and other fundamental signaling molecules [38]. The *Thbs1* gene, which encodes for thrombospondin 1, is a key astrocyte-derived factor regulating synaptogenesis in the developing brain [39], and is reactivated in case of injuries and inflammation [40,41]. *Thbs1* has been also described as a synaptogenic molecule expressed by astrocytes in the perineuronal process and involved in the recovery of excitatory synapses on axotomized motor neurons in the CNS [42]. Moreover, together with $Tgf\beta$, thrombospondin 1 levels rapidly increase at the injury site and both proteins are implicated in angiogenesis, scar deposition and inflammation, as well as affecting astrocyte mobility [43]. Finally, *Tgfbi*, a collagen-related protein, seems to be involved in both axonal regeneration [44] and scar formation [45] in the spinal cord following injury. These collagen-related genes are not regulated in the caudal segment.

Several genes were also equally regulated in the rostral and caudal segments in the acute phase of the lesion (1 DPL) and most were then down-regulated at 45 DPL. The mostly up-regulated genes included *Cd44*, *Mmp12*, *Mmp3*, *Mmp8*, *Timp1*, *Sell* and *Tnc*, indicating the Mmps-related mechanisms as those most affected by injury. Using a bioinformatic approach, we identified *Timp1* and *Cd44* as the hub genes, which emerged as the most strongly up-regulated gene and most connected gene, respectively, at all post-lesion times. *Timp1* is an inhibitory molecule which regulates matrix metalloproteinases (MMPs), a disintegrin and metalloproteases (ADAMs) and ADAMs with thrombospondin motifs (ADAMTSs) [46]. In the context of a traumatic lesion of the CNS, MMPs including *Timp1* are critical for synaptic recovery following axonal injury, mediating secondary degeneration and regulating angiogenesis and glial scar formation [47]. *Timp1* also has pro-oligodendroglial properties in different in vitro contexts which promote OPC maturation [48] and in vivo inhibition of *Timp1* activity completely abolishes spontaneous remyelination [49]. This protein is also associated with various integrins, including *ItgaV*, *Itgb1* and *Itgb3*, which are involved in OPC differentiation into myelinating oligodendrocytes [50]. Our data shows that there is a strong increase in the translation of mRNA of *Timp1* especially in the segment rostral to the center of the lesion. Moreover, the western

blot analysis of the same region of the spinal cord showed a marked decrease in Timp1 protein level in the cell, this could be coupled to the higher release of Timp1 in the extracellular environment, confirming an increased activation of this protein after SCI [51]. This protein, in fact, is a fundamental inducer for OPCs cell division and axonal regeneration after injury [52].

CD44, a non-kinase transmembrane glycoprotein, belongs to a family of cell surface glycoprotein receptors which are widely expressed in normal adult tissues, serving as adhesion molecules and mediating various biological processes, including wound repair and leucocyte trafficking [53]. CD44 is also required for migration of the myelin-repairing cells known as OPCs to focal inflammatory demyelinating lesions in the spinal cord [54]. Even if in the present study we focused only on the protein component of the ECM, Cd44 is a hyaluronic acid receptor and the hyaluronan component of the ECM is affected by the SCI, being also directly involved in the induction of astrocytes proliferation [55]. Thus, the regulation of *Cd44* expression by SCI suggests an involvement of the hyaluronan component remodeling.

Using a bioinformatic approach, we analyzed the differentially regulated genes in correlation with their role in the ECM protein-protein interaction net, finding a central role of *Timp1* and *Cd44*. The need of an informatic-based approach was also highlighted by lack of correlation between the single gene expression analysis and the motor-functional BBB score. The bioinformatic resources is able to expand the obtained results through algorithms involving protein-protein interactions from validated literature databases adding also different molecular players outside the analyzed genes net.

The bioinformatic prediction was then experimentally confirmed by the protein analysis of Timp1 in spinal cord tissue and by in vitro experiments using primary astrocytes, mainly involving Cd44 [56] and TIMP1- producing cells [57]; indeed when cultures of primary astrocytes are exposed to inflammatory stimuli, a strong activation in the expression level of both proteins is observed.

In conclusion, in this study, we demonstrated that a complex regulation of ECM composition, one which is both anatomically and temporally specific, takes place in the spinal cord segments outside the lesioned area following injury. This indicates that not only the ECM related to the scar formation but also the ECM adjacent to the lesion areas (interstitial, perineuronal, basement membrane), are profoundly altered in SCI. The temporal and anatomical profile of such regulation mechanisms should also be considered for regenerative medicine purposes, including the use of “smart” biomaterials.

4. Materials and Methods

4.1. Animals and Surgery

All animal protocols described herein were carried out according to European Community Council Directive 2010/63/EU and Italian legislation (Legislative Decree 26/2014) and in compliance with the ARRIVE (Animal Research Reporting of In Vivo Experiments) guidelines and NIH Guide for the Care and Use of Laboratory Animals. The project has been reviewed by the Animal Welfare Body of IRET Foundation and approved by the Italian Ministry of Health (authorization no. 574/2015-PR of 22/06/2015).

Female CD-Sprague Dawley rats (200–250 g) were used in this study (Charles River Laboratories, Lecco, Italy). All animals were housed in pairs and had food and water ad libitum. On the day of surgery, the rats were pre-medicated with enrofloxacin and tramadol (5 mg/kg, s.c.), then anesthetized with isoflurane (1–3%) in O₂, before undergoing a contusive spinal cord lesion at thoracic level T9. Briefly, the rats were immobilized on the stereotaxic table and a 4 cm longitudinal, median dorsal incision made from T8 to T10. The soft tissues were dissected layer by layer to fully expose the processus spinosus of T8 to T11 and the T9 processus spinosus and lamina were removed by clamp to expose the spinal canal and spinal dura. Spinal cord injury was performed using Impact One Impactor (Leica Biosystems, Wetzlar, Germany) at T9 level using a 1.5 mm tip with a force of 1 N (0.75 m/s) and 0 s of stance time and the depth of impact was 1.5 mm in order to reach the ventral

horns of the gray matter. The back muscles were sutured and the skin incision closed with wound clips. The rats were treated with antibiotics and painkillers (enrofloxacin 5 mg/kg and tramadol 5 mg/kg s.c.) for 3 days post lesion and unlesioned animals were used as a control group.

The wellness of the rats was assessed by body weight monitoring and clinical score recording, evaluated daily for the first two weeks, then once a week until the day of sacrifice. Hind limb functional locomotor loss was evaluated using the BBB score [58] prior to the lesion, three days post-lesion, then once a week after surgery. Lesioned animals receiving a score greater than 10 at 3 DPL were excluded from the study.

On the day of sacrifice at 1, 8 or 45 DPL, the rats were euthanized with chloral hydrate (37%). The tissues of interest were dissected, immediately snap frozen and stored at -80°C until use (gene expression study) or perfused with 4% paraformaldehyde and 14% picric acid in 0.2 M Sorensen buffer (pH 6.9) (histology study). The number of animals included in each experiment is indicated in the results section and in the legend to the figures.

4.2. Molecular Biology Analysis

For mRNA pathway array analysis, spinal cord segments of 1 cm length rostral and caudal to the lesion were collected, snap frozen and stored at -80°C . The total RNA was extracted from the homogenized tissues using RNeasy Plus Universal Mini Kit (Qiagen, Hilden, Germany) according to manufacturer's instructions. For cDNA synthesis, 5 μg of pooled RNAs were used from each experimental group. The cDNA was synthesized using the RT2 first strand kit (Qiagen). Eighty-four genes involved in the extracellular matrix were analyzed using the RT2 Profiler Extracellular Matrix and Adhesion Molecules PCR Array (Qiagen, PARN-013ZD). According to the manufacturer's protocol, real-time PCR was performed using the RT2 SYBR Green qPCR Mastermix (Qiagen) with the CFX96 Touch Real Time PCR Detection System (Biorad, CA, USA).

For RT-qPCR analysis, cDNA synthesis of 1 μg of single sample RNA was performed using the iScriptg DNA Clear cDNA Synthesis Kit (Biorad), according to the manufacturer's protocol. A total of 10 ng per sample of cDNA was used for each RT-qPCR for single gene analysis (see Table 1 for primer list). Amplification was performed using the SsoAdvanced Universal SYBR Green Supermix (Biorad) and CFX96 Touch Real Time PCR Detection System (Biorad). Relative quantification of mRNA was calculated using the comparative cycle threshold method. Ct values were collected for each gene analyzed, standardized on the *Rplp1* house-keeping gene and normalized on the respective intact segment of spinal cord. Gene expression fold change was then calculated as $2^{(-\Delta\Delta\text{Ct})}$.

Table 1. Sequences and genetic loci of primers used for RT-qPCR analysis.

Gene	Specificity	Genetic Locus	Forward Sequence (5'–3')	Reverse Sequence (5'–3')
<i>Acan</i>	rat	NM_022190.1	GTGAGATCGACCAGGAGCCA	TCGGGAAAGTGGCGATAACA
<i>Agrin</i>	rat	NM_175754.1	CCTGCAACATCTGCTTGATCC	GGATTCCAGGTTTGTAGTTGCTG
<i>Bcan</i>	rat	NM_001033665.1	GGACCTCACAAGTTCTTCCAAGT	CTTTCAGGTCATCAGCGAGGG
<i>Cd44</i>	rat	NM_012924.2	AACTACAGCCTTGATGACTACCC	ATGACTCTTGGACTCTGATGGTT
<i>Cd44</i>	mouse	NM_009851.2	AGAAGAGCACCCCAGAAAGC	CTTGCAATGGTGGCCAAGG
<i>Cspg4</i>	rat	NM_031022.1	AACAGGAAAAAGCACCCCCA	ACCTGTCTTGTGCGTTTGC
<i>Fn1</i>	rat	NM_019143.2	AAGACAGATGAGCTTCCCCAA	TGAACTGTGGAGGGAACATCC
<i>Gapdh</i>	rat/mouse	NM_001113417.1	GGCAAGTTCAATGGCACAGTCAAG	CATACTCAGCACCAGCATCAC
<i>Lgals1</i>	rat	NM_019904.1	TTCAATCATGGCCTGTGGTCT	CTCTCCCCGAACCTTTGAGACA
<i>Ntn1</i>	rat	NM_053731.2	AGGACTATGCTGTCCAGATCCA	TACGACTTGTGCCCTGCTTG

Table 1. Cont.

Gene	Specificity	Genetic Locus	Forward Sequence (5'–3')	Reverse Sequence (5'–3')
<i>Postn</i>	rat	NM_001108550.1	TGCAAAAAGACACACCTGCAAA	GGCCTTCTCTTGATCGCCTT
<i>Rplp1</i>	rat	NM_001007604.2	GGCAGTCTACAGCATGGCTT	GTTGACATTGGCCAGAGCCT
<i>Sell</i>	rat	NM_019177.3	ATCGCAGGAAAGGATGGATGAT	GGTTTTTGGTGGCGGTTGTT
<i>Slit1</i>	rat	NM_022953.2	CGCAAGGGCGCATCGT	GGGGCTATCTCCAGGTGCTAT
<i>Slit2</i>	rat	NM_022632.2	GGGGCCATAATGTAGCAGAGG	GACTGGTGACCTTCTTCCTCA
<i>Tnc</i>	rat	NM_053861.1	ATTGTCTACCTCTCTGGAATTGCTC	TTCCGGTTCAGCTTCTGTGG
<i>Tnr</i>	rat	NM_013045.1	CCTCAATGGGGAGTTAAGCCA	CTGAAAACAATCCAGCCGC
<i>Timp1-a</i>	mouse	NM_011593.2	TGGGTGGATGAGTAATGCGTC	GGCCATCATGGTATCTCTGGT
<i>Timp1-b</i>	mouse	NM_001294280.2	CAACTCGGACCTGGATGCTAA	ACTCTTCACTGCGGTTCTGG

4.3. Bioinformatic Data Analysis

The data obtained from the PCR array was analyzed using the GeneGlobe platform (Qiagen) All PCR arrays were normalized on the same house-keeping gene (*Rplp1*) as suggested by the software and cut-off for Ct was set at 35. Gene expression variation was expressed as fold change with the Δ Ct method, with respect to each segment from the intact animal group. To visualize the distribution of gene expression across the group and their clusterization, gene expression was plotted on a clustergram using the Cts values for each gene in the array and relative gene expression shown using heat maps of the PCR array. Genes with a fold change of ± 2 or more were used for bioinformatic analysis. Panther software was used for clustering genes according to the biological function [59].

The Search Tool for the Retrieval of Interacting Genes (STRING v11) online database (<http://string-db.org/>) gives a critical assessment as well as the integration of PPIs, including experimental and predicted associations [60]. The Qiagen RT2 PCR array gene list was elaborated by the STRING software to outline protein-protein interactions (PPIs) of the ECM. Cytoscape v3.7.2 [61] is a widely used opensource software tool for the visualization of complex networks, with the ability to integrate all types of attribute data. Cytoscape was used to identify the hub genes, using a gene expression profile superimposed over the ECM network to eliminate nodes with fold regulation $> \pm 2$. This generated a specific network for each sample and the networks were continuously filtered based on degree parameter to give a maximum of 10 nodes. These genes were then used for further investigations.

4.4. Histology

After perfusion, the spinal cord tissue was dissected, post-fixed for 24 h, then washed in 5% sucrose in 0.2 M Sorensen buffer (pH 7.4). The spinal cords were collected and divided into 1 cm segments rostral and caudal to the lesion. Coronal ($n = 3$) and longitudinal ($n = 3$) cryostat sections (CM1950, Leica Biosystems) with a thickness of 14 μ m were collected and processed for hematoxylin/eosin (H/E) and Nissl staining, to characterize the lesion extension at all time points. To define the lesion area, sections were captured using a Nikon Microphot—FXA equipped with a Nikon DXM1200F CCD camera (Nikon) at 4 \times magnification and reconstructed using Photoshop's photomerge function (Adobe). The lesion area was then determined for each reconstructed section using ImageJ software (NIH) by calculating the number of pixels occupying the lesion site and different levels of the same spinal cord were aligned to give a 3D reconstruction (sampling step 210 μ m).

4.5. Western Blot

Western blot analysis was performed to quantify Timp1 protein expression in the spinal cord at 1, 7 and 60 DPL. The rostral segments of spinal cord were homogenized according to RNeasy Mini Kit (Qiagen) protocol (with a ratio of mg of tissue to ml of lysis buffer, provided by the kit, equivalent to 1:10 weight/volume). Protein isolation was

performed from the first flow-through of the spin column, by precipitation in acetone. Briefly, four volumes of ice-cold acetone were added to the flow-through from the RNeasy spin column, then incubated for 30 min at $-20\text{ }^{\circ}\text{C}$. After spinning at $15,300\times g$ for 10 min and removing the supernatant, the pellet was allowed to dry, then resuspended in RIPA buffer and protease inhibitor ($1\times$ Cocktail Sigma, 1 nM of PMSEF, 10 nM of sodium fluoride, 1 nM of sodium orthovanadate).

Total protein concentration was estimated using a standard colorimetric method based on the Lowry assay (DC Protein Assay, Bio-Rad). For each sample, 40 μg of proteins and the marker protein (Precision Plus Protein Standards, Bio-Rad), diluted at a ratio of 1:100, was added to a solution of Laemmle/ β -mercaptoethanol and after heating treatment ($100\text{ }^{\circ}\text{C}$, 5 min), the proteins were resolved in 4–20% Mini-PROTEAN TGX Stain-Free Gels (Bio-Rad). Nitrocellulose Membrane (Bio-Rad AmershamProtran 0.45 μm) has been used for protein transfer. A solution of 2.5% BSA in TBST (Tris Buffer Saline solution containing 1% Tween20) has been used for blocking. Incubation with the primary antibody (rabbit Timp1 Abcam ab61224, 1:500; mouse β -actin, Santa Cruz Biotechnology -Dallas, Texas, 1:200) has been performed overnight at $4\text{ }^{\circ}\text{C}$, whereas the incubation with HRP-conjugated secondary antibodies (swine anti-rabbit, Dako, 1:5000; swine anti-mouse, Dako, 1:5000) and HRP-conjugated protein for marker visualization (Precision Protein StrepTactin HRP-conjugate, Bio-Rad, 1:20,000) for 1 h at RT. Three washes with TBST was performed after incubation with antibodies, either the primary both the secondary. Clarity Western ECL Substrate (Bio-Rad –5 min incubation at RT in darkness) and the BioRadChemi DOC MP imaging system was used to detect immunoreactive signal.

The Fiji (ImageJ v2.1.0) software was used to measure densitometry. TIMP1 signal was normalized first on β -actin and then the ratio of lesioned (SCI+) to intact (SCI-) was calculated with samples present in the same gel.

4.6. Cell Cultures, Gene Expression Analysis and Immunocytochemistry

Primary astrocytes were isolated from 7-day-old mice using a standard protocol [62] and cultured in Dulbecco's Modified Eagle's Medium (DMEM) containing 15% fetal bovine serum (FBS), non-essential amino acid mixture (Sigma-Aldrich, St Louis, MO, USA) pen/strep (Invitrogen, Carlsbad, CA, USA) and 2 mM Glutamine (Invitrogen). Cultures were seeded in T25 flasks ($125,000\text{ cells}/\text{cm}^2$) and maintained at $37\text{ }^{\circ}\text{C}$ 5% CO_2 , detached with trypsin (10 min, $37\text{ }^{\circ}\text{C}$) and split twice before use.

When astrocytes shown 70% confluence the cytokine mix (TGF- β 1, TNF- α , IL-1 β , IL-6, IL-17 and IFN- γ ; 20 ng/mL each; (Thermo Fisher Scientific, Waltham, MA, USA) or vehicle (0.04% of the cytokine solvent: 10% glycerol/100 nM glycine/25 nM Tris, pH 7.3) was added in the culture medium for 48 h. Cells were then lysed and the total RNA extracted using the RNeasy micro kit (Qiagen) following the manufacturer's instructions and total RNA quantified by Nanodrop 2000 spectrophotometer. First strand cDNA was obtained using iScriptTM cDNA Synthesis Kit (Bio-Rad) following the manufacturer's instructions and using a No-RT sample to check for genomic DNA contamination.

Semi-quantitative real-time PCR was performed using the CFX96 real-time PCR system (Bio-Rad) with 20 μL total volume, containing $1\times$ SYBR Green qPCR master mix (Bio-Rad), 0.4 μM forward and reverse primers and 10 ng cDNA. The PCR reaction thermal profile consisted of 40 cycles of amplification ($95\text{ }^{\circ}\text{C}$ for 15 s and $60\text{ }^{\circ}\text{C}$ for 60 s) after an initial denaturation step ($95\text{ }^{\circ}\text{C}$, 2 min). Melting curves of the amplified products were obtained according to the following temperature/time scheme. The $2^{-(\Delta\Delta\text{Ct})}$ method was used for the calculation of the relative gene expression, using *Gapdh* as house-keeping gene and the two isoforms of *Timp1* (a and b) and *Cd44* as investigated genes.

To check the quality of the cultures, a number of astrocytes were seeded on coverslips, fixed and stained for GFAP expression. In particular, the cells were fixed with ice-cold 4% paraformaldehyde for 20 min at RT. After two washes in PBS, the cells were incubated for 1 h with 1% BSA/1% donkey serum in PBS-0.3% Triton-X 100, then incubated overnight with primary antibody anti-GFAP (rabbit, Dako, 1:1000) diluted in PBS-0.3% Triton-X 100.

The cells were then washed with PBS and incubated with secondary antibody goat Alexa 568-conjugated anti-rabbit (Invitrogen) for 30 min at 37 °C. After immunofluorescence staining, cells were incubated with the nuclear dye Hoechst 33,258 (1 µg/mL in PBS, 0.3% Triton-X 100) for 20 min at RT. As a final step, the cells were washed in PBS and coverslipped in glycerol and PBS (3:1, *v/v*) as mounting medium containing 0.1% paraphenylenediamine. A Nikon Eclipse E600 microscope (Nikon Instruments Europe BV, Amsterdam, Netherland) equipped with a QImaging Retiga 20002V digital CCD camera (QImaging, Surrey, BC, Canada) was used for the acquisition of representative images.

4.7. Statistical Analysis

All statistical analyses were performed using GraphPad Prism v8.0 (GraphPad Software, San Diego, CA, USA). BBB scoring and animal weight were represented as mean ± SEM. For PCR array analysis, the data was reported as relative fold change expression. For the mRNA expression analysis obtained with qPCR, the data was reported as the Log₂ of fold change and *p* values were calculated using one-way ANOVA on the $\Delta\Delta C_t$ s from each single animal, normalized on the mean of the ΔC_t of the respective group of intact spinal cord segment. Uncorrected Fisher's LSD post hoc analysis was used to compare the relative expression of each time point in the spinal cord segments rostral and caudal to the lesion and Dunnett's post hoc analysis was used to compare the relative expression of lesioned animals compared to intact. *p* values inferior to 0.05 were considered significant.

Supplementary Materials: The following are available online at <https://www.mdpi.com/1422-0067/22/4/1744/s1>.

Author Contributions: Conceptualization, L.G. and L.C.; methodology, A.B., Z.K., V.A.B., L.L., M.C. and M.M.; software, A.B., Z.K. and V.A.B.; validation, L.G. and L.C.; formal analysis, L.C.; investigation, L.C.; resources, L.G. and L.C.; data curation, A.B., V.A.B. and L.C.; writing—original draft preparation, A.B. and L.C.; writing—review and editing, V.A.B. and L.C.; visualization, L.G.; supervision, L.L., L.G. and L.C.; project administration, L.G. and L.C.; funding acquisition, L.G. and L.C. All authors have read and agreed to the published version of the manuscript.

Funding: This research was funded by POR-FESR Emilia Romagna 2014–2020 (Step-by-Step project, L.C. and Mat2Rep project, L.C. and L.G.) and the MIUR IRMI project (CTN01_00177_888744, L.C.).

Institutional Review Board Statement: The study was conducted according to the European Community Council Directives (86/609/EEC), complied with the guidelines published in the *NIH Guide for the Care and Use of Laboratory*, and approved by the Italian Ministry of Health (Authorization n. 574/2015-PR issued the 31th March 2015)

Informed Consent Statement: Not applicable.

Data Availability Statement: The data presented in this study are available on request from the corresponding author.

Conflicts of Interest: The authors declare no conflict of interest. The funders had no role in the design of the study; in the collection, analyses or interpretation of data; in the writing of the manuscript or in the decision to publish the results.

Abbreviations

DPL	Days post-lesion
ECM	Extracellular matrix
MMPs	Metalloproteases
OPC	Oligodendrocyte precursor cell
SCI	Spinal cord injury

References

1. James, S.L.; Theadom, A.; Ellenbogen, R.G.; Bannick, M.S.; Montjoy-Venning, W.; Lucchesi, L.R.; Abbasi, N.; Abdulkader, R.; Abraha, H.N.; Adsuar, J.C.; et al. Global, regional, and national burden of traumatic brain injury and spinal cord injury, 1990–2016: A systematic analysis for the Global Burden of Disease Study. *Lancet Neurol.* **2019**, *18*, 56–87. [[CrossRef](#)]
2. Alizadeh, A.; Dyck, S.M.; Karimi-Abdolrezaee, S. Traumatic spinal cord injury: An overview of pathophysiology, models and acute injury mechanisms. *Front. Neurol.* **2019**, *10*, 282. [[CrossRef](#)] [[PubMed](#)]
3. Sroga, J.M.; Jones, T.B.; Kigerl, K.A.; McGaughy, V.M.; Popovich, P.G. Rats and mice exhibit distinct inflammatory reactions after spinal cord injury. *J. Comp. Neurol.* **2003**, *462*, 223–240. [[CrossRef](#)] [[PubMed](#)]
4. Liao, S.-H.; Ni, S.; Cao, Y.; Yin, X.; Wu, T.; Lu, H.; Hu, J.; Wu, H.; Lang, Y. The 3D characteristics of post-traumatic syringomyelia in a rat model: A propagation-based synchrotron radiation microtomography study. *J. Synchrotron Radiat.* **2017**, *24*, 1218–1225. [[CrossRef](#)] [[PubMed](#)]
5. Ward, R.; Huang, W.; Kostusiak, M.; Pallier, P.; Michael-Titus, A.; Priestley, J. A characterization of white matter pathology following spinal cord compression injury in the rat. *Neuroscience* **2014**, *260*, 227–239. [[CrossRef](#)] [[PubMed](#)]
6. Abou-El-Hassan, H.; Bsar, S.; Sukhon, F.; Assaf, E.J.; Mondello, S.; Kobeissy, F.; Wang, K.K.W.; Weiner, H.L.; Omeis, I.A. Protein degradome of spinal cord injury: Biomarkers and potential therapeutic targets. *Mol. Neurobiol.* **2020**, *57*, 2702–2726. [[CrossRef](#)] [[PubMed](#)]
7. Gaudet, A.D.; Popovich, P.G. Extracellular matrix regulation of inflammation in the healthy and injured spinal cord. *Exp. Neurol.* **2014**, *258*, 24–34. [[CrossRef](#)]
8. Dou, C.; Levine, J. Inhibition of neurite growth by the NG2 chondroitin sulfate proteoglycan. *J. Neurosci.* **1994**, *14*, 7616–7628. [[CrossRef](#)]
9. Jones, L.L.; Sajed, D.; Tuszynski, M.H. Axonal regeneration through regions of chondroitin sulfate proteoglycan deposition after spinal cord injury: A balance of permissiveness and inhibition. *J. Neurosci.* **2003**, *23*, 9276–9288. [[CrossRef](#)] [[PubMed](#)]
10. Pukos, N.; Goodus, M.T.; Sahinkaya, F.R.; McTigue, D.M. Myelin status and oligodendrocyte lineage cells over time after spinal cord injury: What do we know and what still needs to be unwrapped? *Glia* **2019**, *67*, 2178–2202. [[CrossRef](#)]
11. Haggerty, A.; Marlow, M.M.; Oudega, M. Extracellular matrix components as therapeutics for spinal cord injury. *Neurosci. Lett.* **2017**, *652*, 50–55. [[CrossRef](#)]
12. Quraishe, S.; Forbes, L.H.; Andrews, M.R. The extracellular environment of the CNS: Influence on plasticity, sprouting, and axonal regeneration after spinal cord injury. *Neural Plast.* **2018**, *2018*, 1–18. [[CrossRef](#)]
13. Kendzierski, C.M.; Newton, M.A.; Lan, H.; Gould, M.N. On parametric empirical Bayes methods for comparing multiple groups using replicated gene expression profiles. *Stat. Med.* **2003**, *22*, 3899–3914. [[CrossRef](#)]
14. Kendzierski, C.; Zhang, Y.; Lan, H.; Attie, A.D. The efficiency of pooling mRNA in microarray experiments. *Biostatistics* **2003**, *4*, 465–477. [[CrossRef](#)]
15. Borjini, N.; Fernández, M.; Giardino, L.; Calzà, L. Cytokine and chemokine alterations in tissue, CSF, and plasma in early presymptomatic phase of experimental allergic encephalomyelitis (EAE), in a rat model of multiple sclerosis. *J. Neuroinflamm.* **2016**, *13*, 1–16. [[CrossRef](#)] [[PubMed](#)]
16. Fernández, M.; Baldassarro, V.A.; Capirossi, R.; Montevecchi, R.; Bonavita, J.; Cescatti, M.; Giovannini, T.; Giovannini, G.; Uneddu, M.; Giovanni, G.; et al. Possible strategies to optimize a biomarker discovery approach to correlate with neurological outcome in patients with spinal cord injury: A pilot study. *J. Neurotrauma* **2020**, *37*, 431–440. [[CrossRef](#)]
17. Fernández, M.; Baldassarro, V.A.; Sivilia, S.; Giardino, L.; Calzà, L. Inflammation severely alters thyroid hormone signaling in the central nervous system during experimental allergic encephalomyelitis in rat: Direct impact on OPCs differentiation failure. *Glia* **2016**, *64*, 1573–1589. [[CrossRef](#)] [[PubMed](#)]
18. Baldassarro, V.A.; Krężel, W.; Fernández, M.; Schuhbaur, B.; Giardino, L.; Calzà, L. The role of nuclear receptors in the differentiation of oligodendrocyte precursor cells derived from fetal and adult neural stem cells. *Stem Cell Res.* **2019**, *37*, 101443. [[CrossRef](#)]
19. Wang, S.; Smith, G.M.; Selzer, M.E.; Li, S. Emerging molecular therapeutic targets for spinal cord injury. *Expert Opin. Targets* **2019**, *23*, 787–803. [[CrossRef](#)] [[PubMed](#)]
20. Kjell, J.; Götz, M. Filling the gaps—a call for comprehensive analysis of extracellular matrix of the glial scar in region- and injury-specific contexts. *Front. Cell. Neurosci.* **2020**, *14*. [[CrossRef](#)]
21. O’Shea, T.M.; Burda, J.E.; Sofroniew, M.V. Cell biology of spinal cord injury and repair. *J. Clin. Investig.* **2017**, *127*, 3259–3270. [[CrossRef](#)]
22. Liu, X.Z.; Xu, X.M.; Hu, R.; Du, C.; Zhang, S.X.; McDonald, J.W.; Dong, H.X.; Wu, Y.J.; Fan, G.S.; Jacquin, M.F.; et al. Neuronal and glial apoptosis after traumatic spinal cord injury. *J. Neurosci.* **1997**, *17*, 5395–5406. [[CrossRef](#)]
23. Tomko, P.; Farkaš, D.; Cizkova, D.; Vanický, I. Longitudinal enlargement of the lesion after spinal cord injury in the rat: A consequence of malignant edema? *Spinal Cord* **2016**, *55*, 255–263. [[CrossRef](#)]
24. Bighinati, A.; Focarete, M.L.; Gualandi, C.; Pannella, M.; Giuliani, A.; Beggiano, S.; Ferraro, L.; Lorenzini, L.; Giardino, L.; Calzà, L.; et al. Improved functional recovery in rat spinal cord injury induced by a drug combination administered with an implantable polymeric delivery system. *J. Neurotrauma* **2020**, *37*, 1708–1719. [[CrossRef](#)]
25. Kozłowski, P.; Raj, D.; Liu, J.; Lam, C.; Yung, A.C.; Tetzlaff, W. Characterizing white matter damage in rat spinal cord with quantitative MRI and histology. *J. Neurotrauma* **2008**, *25*, 653–676. [[CrossRef](#)] [[PubMed](#)]

26. Burnside, E.R.; Bradbury, E.J. Review: Manipulating the extracellular matrix and its role in brain and spinal cord plasticity and repair. *Neuropathol. Appl. Neurobiol.* **2014**, *40*, 26–59. [[CrossRef](#)] [[PubMed](#)]
27. Moghieb, A.; Bramlett, H.M.; Das, J.H.; Yang, Z.; Selig, T.; Yost, R.A.; Wang, M.S.; Dietrich, W.D.; Wang, K.K.W. Differential neuroproteomic and systems biology analysis of spinal cord injury. *Mol. Cell. Proteom.* **2016**, *15*, 2379–2395. [[CrossRef](#)]
28. Devaux, S.; Cizkova, D.; Quanico, J.; Franck, J.; Nataf, S.; Pays, L.; Hauberg-Lotte, L.; Maass, P.; Kobarg, J.H.; Kobeissy, F.; et al. Proteomic analysis of the spatio-temporal based molecular kinetics of acute spinal cord injury identifies a time- and segment-specific window for effective tissue repair. *Mol. Cell. Proteom.* **2016**, *15*, 2641–2670. [[CrossRef](#)]
29. Bradbury, E.J.; Burnside, E.R. Moving beyond the glial scar for spinal cord repair. *Nat. Commun.* **2019**, *10*, 1–15. [[CrossRef](#)] [[PubMed](#)]
30. Buss, A.; Pech, K.; Kakulas, B.A.; Martin, D.; Schoenen, J.; Noth, J.; Brook, G.A. Matrix metalloproteinases and their inhibitors in human traumatic spinal cord injury. *BMC Neurol.* **2007**, *7*. [[CrossRef](#)] [[PubMed](#)]
31. Zhou, Y.; Cui, Z.; Xia, X.; Liu, C.; Zhu, X.; Cao, J.; Wu, Y.; Zhou, L.; Ben, Z.; Song, Y.; et al. Matrix metalloproteinase-1 (MMP-1) expression in rat spinal cord injury model. *Cell. Mol. Neurobiol.* **2014**, *34*, 1151–1163. [[CrossRef](#)] [[PubMed](#)]
32. Nagase, H.; Suzuki, K.; Morodomi, T.; Enghild, J.J.; Salvesen, G. Activation mechanisms of the precursors of matrix metalloproteinases 1, 2 and 3. *Matrix* **1992**, *1*, 237–244. [[PubMed](#)]
33. Okada, M.; Miyamoto, O.; Shibuya, S.; Zhang, X.; Yamamoto, T.; Itano, T. Expression and role of type I collagen in a rat spinal cord contusion injury model. *Neurosci. Res.* **2007**, *58*, 371–377. [[CrossRef](#)]
34. Fox, M.A. Novel roles for collagens in wiring the vertebrate nervous system. *Curr. Opin. Cell Biol.* **2008**, *20*, 508–513. [[CrossRef](#)] [[PubMed](#)]
35. Hubert, T.; Grimal, S.; Carroll, P.; Fichard-Carroll, A. Collagens in the developing and diseased nervous system. *Cell. Mol. Life Sci.* **2009**, *66*, 1223–1238. [[CrossRef](#)] [[PubMed](#)]
36. Klapka, N.; Müller, H.W. Collagen matrix in spinal cord injury. *J. Neurotrauma* **2006**, *23*, 422–436. [[CrossRef](#)]
37. Tang, B.L.; Neo, S.H. Collagen 1 signaling at the central nervous system injury site and astrogliosis. *Neural Regen. Res.* **2017**, *12*, 1600–1601. [[CrossRef](#)]
38. Kelly, K.K.; MacPherson, A.M.; Grewal, H.; Strnad, F.; Jones, J.W.; Yu, J.; Pierzchalski, K.; Kane, M.A.; Herson, P.S.; Siegenthaler, J.A.; et al. Col1a1+ perivascular cells in the brain are a source of retinoic acid following stroke. *BMC Neurosci.* **2016**, *17*. [[CrossRef](#)]
39. Lu, Z.; Kipnis, J. Thrombospondin 1—a key astrocyte-derived neurogenic factor. *FASEB J.* **2010**, *24*, 1925–1934. [[CrossRef](#)]
40. Pu, Y.; Meng, K.; Gu, C.; Wang, L.; Zhang, X. Thrombospondin-1 modified bone marrow mesenchymal stem cells (BMSCs) promote neurite outgrowth and functional recovery in rats with spinal cord injury. *Oncotarget* **2017**, *8*, 96276–96289. [[CrossRef](#)]
41. Hennekinne, L.; Colasse, S.; Triller, A.; Renner, M. Differential control of thrombospondin over synaptic glycine and AMPA receptors in spinal cord neurons. *J. Neurosci.* **2013**, *33*, 11432–11439. [[CrossRef](#)]
42. Tyzack, G.E.; Sitnikov, S.; Barson, D.; Adams-Carr, K.L.; Lau, N.K.; Kwok, J.C.; Zhao, C.; Franklin, R.J.M.; Karadottir, R.T.; Fawcett, J.W.; et al. Astrocyte response to motor neuron injury promotes structural synaptic plasticity via STAT3-regulated TSP-1 expression. *Nat. Commun.* **2014**, *5*, 4294. [[CrossRef](#)]
43. Wang, X.-J.; Maier, K.; Fuse, S.; Willis, A.I.; Olson, E.; Nesselroth, S.; Sumpio, B.E.; Gahtan, V. Thrombospondin-1-induced migration is functionally dependent upon focal adhesion kinase. *Vasc. Endovasc. Surg.* **2008**, *42*, 256–262. [[CrossRef](#)] [[PubMed](#)]
44. Shih, C.-H.; Lacagnina, M.; Leuer-Biscioti, K.; Pröschel, C. Astroglial-derived periostin promotes axonal regeneration after spinal cord injury. *J. Neurosci.* **2014**, *34*, 2438–2443. [[CrossRef](#)] [[PubMed](#)]
45. Yokota, K.; Kobayakawa, K.; Saito, T.; Hara, M.; Kijima, K.; Ohkawa, Y.; Harada, A.; Okazaki, K.; Ishihara, K.; Yoshida, S.; et al. Periostin promotes scar formation through the interaction between pericytes and infiltrating monocytes/macrophages after spinal cord injury. *Am. J. Pathol.* **2017**, *187*, 639–653. [[CrossRef](#)]
46. Arpino, V.; Brock, M.; Gill, S.E. The role of TIMPs in regulation of extracellular matrix proteolysis. *Matrix Biol.* **2015**, *44*, 247–254. [[CrossRef](#)] [[PubMed](#)]
47. Trivedi, A.; Noble-Haesslein, L.J.; Levine, J.M.; Santucci, A.D.; Reeves, T.M.; Phillips, L.L. Matrix metalloproteinase signals following neurotrauma are right on cue. *Cell. Mol. Life Sci.* **2019**, *76*, 3141–3156. [[CrossRef](#)] [[PubMed](#)]
48. Nicaise, A.M.; Johnson, K.M.; Willis, C.M.; Guzzo, R.M.; Crocker, S.J. TIMP-1 Promotes oligodendrocyte differentiation through receptor-mediated signaling. *Mol. Neurobiol.* **2019**, *56*, 3380–3392. [[CrossRef](#)]
49. Houben, E.; Janssens, K.; Hermans, D.; Vandooren, J.; Haute, C.V.D.; Schepers, M.; Vanmierlo, T.; Lambrechts, I.; Van Horsen, J.; Baekelandt, V.; et al. Oncostatin M-induced astrocytic tissue inhibitor of metalloproteinases-1 drives remyelination. *Proc. Natl. Acad. Sci. USA* **2020**, *117*, 5028–5038. [[CrossRef](#)]
50. Baron, W.; Colognato, H.; Ffrench-Constant, C. Integrin-growth factor interactions as regulators of oligodendroglial development and function. *Glia* **2005**, *49*, 467–479. [[CrossRef](#)]
51. Shilts, J.; Broadie, K. Secreted tissue inhibitor of matrix metalloproteinase restricts trans-synaptic signaling to coordinate synaptogenesis. *J. Cell Sci.* **2017**, *130*, 2344–2358. [[CrossRef](#)]
52. Liu, H.; Angert, M.; Nishihara, T.; Shubayev, I.; Dolkas, J.; Shubayev, V.I. Spinal glia division contributes to conditioning lesion-induced axon regeneration into the injured spinal cord. *J. Neuropathol. Exp. Neurol.* **2015**, *74*, 500–511. [[CrossRef](#)] [[PubMed](#)]
53. Stephenson, E.L.; Yong, V.W. Pro-inflammatory roles of chondroitin sulfate proteoglycans in disorders of the central nervous system. *Matrix Biol.* **2018**, *71*, 432–442. [[CrossRef](#)]

54. Piao, J.-H.; Wang, Y.; Duncan, I. CD44 is required for the migration of transplanted oligodendrocyte progenitor cells to focal inflammatory demyelinating lesions in the spinal cord. *Glia* **2012**, *61*, 361–367. [[CrossRef](#)]
55. Struve, J.; Maher, P.C.; Li, Y.-Q.; Kinney, S.; Fehlings, M.G.; Kuntz, C.; Sherman, L.S. Disruption of the hyaluronan-based extracellular matrix in spinal cord promotes astrocyte proliferation. *Glia* **2005**, *52*, 16–24. [[CrossRef](#)]
56. Moon, C.; Heo, S.; Sim, K.-B.; Shin, T. Upregulation of CD44 expression in the spinal cords of rats with clip compression injury. *Neurosci. Lett.* **2004**, *367*, 133–136. [[CrossRef](#)] [[PubMed](#)]
57. Gardner, J.; Ghorpade, A. Tissue inhibitor of metalloproteinase (TIMP)-1: The TIMPed balance of matrix metalloproteinases in the central nervous system. *J. Neurosci. Res.* **2003**, *74*, 801–806. [[CrossRef](#)] [[PubMed](#)]
58. Basso, D.M.; Beattie, M.S.; Bresnahan, J.C. A sensitive and reliable locomotor rating scale for open field testing in rats. *J. Neurotrauma* **1995**, *12*, 1–21. [[CrossRef](#)] [[PubMed](#)]
59. Mi, H.; Muruganujan, A.; Huang, X.; Ebert, D.; Mills, C.; Guo, X.; Thomas, P.D. Protocol update for large-scale genome and gene function analysis with the PANTHER classification system (v.14.0). *Nat. Protoc.* **2019**, *14*, 703–721. [[CrossRef](#)]
60. Szklarczyk, D.; Gable, A.L.; Lyon, D.; Junge, A.; Wyder, S.; Huerta-Cepas, J.; Simonovic, M.; Doncheva, N.T.; Morris, J.H.; Bork, P.; et al. STRING v11: Protein–protein association networks with increased coverage, supporting functional discovery in genome-wide experimental datasets. *Nucleic Acids Res.* **2019**, *47*, D607–D613. [[CrossRef](#)]
61. Shannon, P.; Markiel, A.; Ozier, O.; Baliga, N.S.; Wang, J.T.; Ramage, D.; Amin, N.; Schwikowski, B.; Ideker, T. Cytoscape: A software environment for integrated models of biomolecular interaction networks. *Genome Res.* **2003**, *13*, 2498–2504. [[CrossRef](#)] [[PubMed](#)]
62. Baldassarro, V.A.; Marchesini, A.; Giardino, L.; Calzà, L. Vulnerability of primary neurons derived from Tg2576 Alzheimer mice to oxygen and glucose deprivation: Role of intraneuronal amyloid- β accumulation and astrocytes. *Dis. Model. Mech.* **2017**, *10*, 671–678. [[CrossRef](#)] [[PubMed](#)]

4.5. A time-course study of the expression levels of synaptic plasticity-associated genes in a rat model of spinal cord injury: focus on unlesioned brain and spinal cord areas (*manuscript in preparation*)

¹Bighinati A., ¹Giuliani A., ^{2,3}Baldassarro V.A., ²Gusciglio M., ^{1,2,3}Giardino L., ^{3,4,5}Calzà L.

¹DIMEVET, University of Bologna, Bologna, Italy; ²IRET Foundation, Ozzano Emilia, Italy; ³Health Sciences and Technologies – Interdepartmental Center for Industrial Research, University of Bologna; ⁴Fabit, University of Bologna, Bologna, Italy; ⁵Montecatone Rehabilitation Institute, Imola, Italy.

Running time: Synaptic plasticity genes in spinal cord injury

Keywords: spinal cord injury, rat, synaptic plasticity, gene expression regulation

ABSTRACT

“Neuroplasticity “ is often evoked to explain adaptation and compensation after acute lesions of the Central Nervous System (CNS). Neuroplasticity is supported by functional and structural changes, also including long-lasting gene expression changes. In this study, we investigated the modification of 80 genes involved in synaptic plasticity at different times (1, 8, and 45 days) from the traumatic spinal cord injury. mRNA expression levels were analyzed in the motor cortex, basal ganglia, cerebellum, cervical, thoracic, and lumbar spinal cord. The main results of the study can be summarized as follow: (i) few gene, all related to inflammation, are upregulated in the spinal cord caudally to the lesion at all investigated times; (ii) Fos and Jun, and NGF are upregulated in the spinal cord segment rostral to the lesion at 1 DPL; (iii) several genes are also transiently down-regulated in the motor cortex at 24 hours after lesion, including glutamate receptors, second messengers, transcription factors encoding genes; (iv) synaptic plasticity in motor cortex with the upregulation of Cnr1 is counteracted by a consistent downregulation of Igf1 at all time points. These data suggest that (i) in the spinal cord, the modification in synaptic plasticity involves the rostral segment from the lesion with an upregulation in the acute phase of early genes and neurotrophic factor NGF; (ii) in the cerebral cortex, the long time modulation of neuroplasticity induced by the expression of Cnr1 and Gria1 is strongly inhibited by the downregulation of neurotrophins and growth factors; (iii) an anatomical mapping of synaptic plasticity encoding genes could be a useful tool to investigate the brain and spinal cord functional reorganization after spinal cord injury.

INTRODUCTION

An acute lesion of the central nervous system (CNS) is followed by an ensemble of reactive phenomena, embracing the molecular, structural, electrophysiological, and functional levels, which involve not only the lesion site but all CNS areas directly or indirectly connected to the lesion site. The anatomical and functional changes occurring in the spinal cord multisynaptic pathways after a lesion extend over a long time-span, from the trauma to the consolidated outcome, and might be responsible for partial or complete functional recovery, but also aberrant phenomena, like abnormal motor pattern supporting spasticity and sensory pattern supporting chronic neuropathic pain¹. For example, electrophysiological studies have suggested that neuronal circuits below the spinal cord level of injury, thus deprived of supra-spinal inputs, undergo progressive and long-lasting remodeling², being this a possible source of dysfunctions in spontaneous motoneuron firing³.

On the other hand, while anatomical and functional restoration at the lesion side is strongly limited by the poor repair capability of the CNS and by the anatomical disruption that follows traumatic lesions, the overall recovery of a complex function, like locomotion, might involve the recruitment of alternative or dormant pathways and re-learning processes. For example, an alteration of the resting-state of the sensorimotor network and increased connectivity between motor components has been demonstrated in patients with spinal cord injury (SCI) in several task-evoked functional magnetic resonance imaging (fMRI) studies⁴.

These phenomena are often grouped under the term “neuroplasticity”, including in this term, both systems/circuitry and cellular/molecular levels⁵. The underlying molecular net includes Immediate-Early-Late Response Genes, Long Term Potentiation (LTP) and Depression- (LTD) related genes, Cell Adhesion and Extracellular Matrix (ECM) Molecules, CREB Cofactors, Neuronal Receptors, and Postsynaptic Density (PSD) proteins. Although neuroplasticity is regarded as the biological substrate of rehabilitative motor training, one of the most widely used approaches to promote moderate recovery following injuries of the CNS, very few preclinical data useful for translational purposes are available to support and provide experimental evidence on undergoing molecular and structural events⁶. The study of the regional and temporal pattern of expression of plasticity associated genes in experimental animals might help understanding of these phenomena from a translational perspective, also because of the recent progress in rehabilitation technologies applied to animal models of contusion lesion of the spinal cord^{7,8}.

In order to highlight a still poorly investigate aspect in a rat model for SCI, i.e., gene expression regulation in unlesioned areas, in this study, we investigated changes in the expression level of 84 genes associated with synaptic plasticity at 1, 8, and 45 days after contusive SCI in rats, in the motor

cortex, basal ganglia, cerebellum, and un-injured spinal cord, e.g., the segments rostral and caudal the lesion level and the cervical tract. The molecular study has been performed in animals fully characterized in terms of clinical state, locomotor behavior, and anatomy of the lesion. The investigated genes include Immediate-Early (IEGs) and Late Response Genes, Long Term Potentiation (LTP) and Long Term Depression (LTD) associated genes, genes encoding for Cell Adhesion Molecules, Extracellular Matrix (ECM) Molecules, CREB Cofactors, Neuronal Receptors, Postsynaptic Density Proteins (PSD).

MATERIALS AND METHODS

Animals and surgery

All animal protocols described herein were carried out according to European Community Council Directives 2010/63/EU, and approved by the Italian Ministry of Health (Legislative Decree 26/2014, authorization no. 574/2015-PR), and in compliance with the ARRIVE (Animal Research: Reporting of In Vivo Experiments) guidelines and the NIH Guide for the Care and Use of Laboratory Animals.

Female CD-Sprague Dawley rats (200-250 g) n=18 total animals, were used in this study, housed in pairs, and had food and water ad libitum. SCI was performed at the T9 vertebral level with the Impact One Impactor (Leica Biosystems, Wetzlar, Germany) using a 1.5 mm tip with a force of 1 N (0.75 m/s) and 0 s of stance time. Animals received antibiotic and painkiller medication the day of the surgery and the following 5 days (enrofloxacin and tramadol, 5 mg/kg, s.c). Age and weight-matched unlesioned animals were used as a control group.

Animals were evaluated daily in the first two weeks for clinical wellness, then once a week weighted as a general indicator of health. Lesion functional deficit was evaluated with BBB scale⁹ before the lesion, then at 3 and 7 DPL and once weekly from the second week. Animals with a score in the BBB greater than 10 at 3 DPL were discharged from further analysis.

Animals were sacrificed at different time points. For gene expression analysis, animals were euthanized with chloral hydrate (37%) at 1, 8, and 45 DPL, then spinal cord and brain tissues were dissected and immediately snap-frozen in liquid nitrogen. For histological analysis, animals were perfused with 4% paraformaldehyde and 14% picric acid in 0.2 M Sorensen buffer (pH 6.9) at 45 DPL. Coronal sectioning of the spinal cord was perfumed at 14 μ m with CM1950 cryostat (Leica Biosystem) with a sampling step of 210 μ m. Sections were then stained with Toluidine blue. For the lesion extension determination, the distance was measured from the first to the last coronal section with cavitation sign in the tissue. The number of animals included in each experiment is indicated in the results section and the legend to the figures.

Molecular biology analysis

According to the manufacturer's instructions, tissues dissected from the spinal cord and the brain were then homogenized and the RNA extracted using RNeasy Plus Universal Mini Kit (Qiagen, Hilden, Germany). The retrotranscription of the RNA was performed using 5 µg of pooled RNAs of each experimental group with the RT² first strand kit (Qiagen). Eighty-four genes involved in the synaptic plasticity were analyzed using the RT² PCR Array (Qiagen, PARN-126ZD). Amplification of the cDNAs was performed with CFX96 Touch Real-Time PCR Detection System (Biorad, California, USA) using RT² SYBR Green qPCR Mastermix (Qiagen) accordingly to the manufacturer's protocol.

For the evaluation of gene expression, C_t values were standardized on the Rplp1 house-keeping gene and then normalized on the expression levels of the correspondent area in the healthy control group. Gene expression fold change was then calculated as $2^{(-\Delta\Delta C_t)}$, and genes with a fold change greater than ± 2 were considered significant. Data of gene expression were represented as 2D clustergram for each gene C_t variation with the GeneGlobe software (Qiagen). Genes considered statistically significant were also represented as line graphs for each area of the CNS analyzed with the distinction between the upregulated and the downregulated genes.

Statistical analysis

All statistical analyses were performed using GraphPad Prism (v 8.0) software (GraphPad Software). BBB scoring, animal weight, and lesion extension were represented as mean \pm SEM. For the lesion extension, statistical analysis was made with Students't-test between the rostral and the caudal extension of the lesion in injured animals. P values inferior to 0.05 were considered significant. For PCR array analysis, the data was reported as relative fold change expression, and genes with a fold change variation greater than ± 2 were considered significant.

RESULTS.

Anatomical and functional lesion characterization

The spinal cord's coronal reconstruction in fig. 1 A shows the rostrocaudal extension of the lesion in the cord at 45 DPL. The maximum extension observed is 6000 µm in the rostrocaudal plane, reaching the T8 segment in the rostralmost extension and L2 in the caudal most extension of the spinal cord. Dorsoventrally the lesion extends for approximately 2000 µm reaching the ventral horns and the ventral corticospinal tract. The secondary lesion extension resulted in a dishomogeneous between the two directions of spreading (Fig. 1 B). The secondary degeneration showed a spreading of around

4000 μm in the cord's caudal segments from the lesion epicenter, whereas it showed a more contained expansion of 1500 μm in the rostral segment.

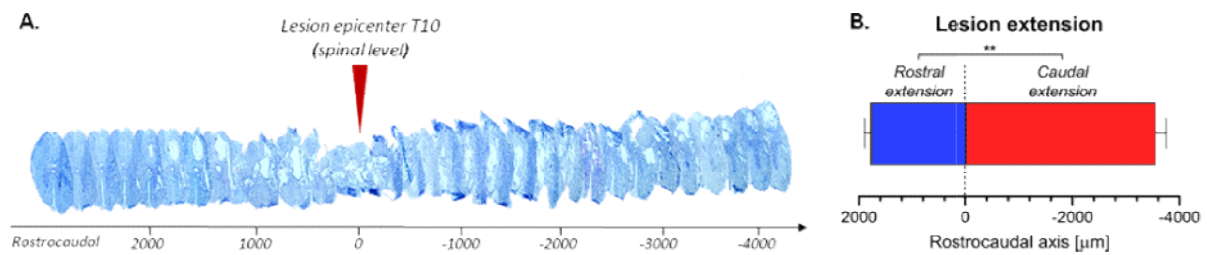


Fig. 2: The image represents the extension of the spinal cord lesion at 45 DPL. In panel A is reported a 3D reconstruction of the coronal section of the spinal cord, including the lesion epicenter and the degenerated tissue in the caudal and rostral segment from the epicenter. In panel B, the extension in μm of the secondary degeneration in the rostral (blue) and caudal segment of the spinal cord (red) is reported. Statistical analysis: t-test, $P=0.0015$, $n=3$ animals.

Animals were monitored daily for the first two weeks post-lesion for their clinical scoring and weight evaluation. All animals showed an initial phase of worsening of clinical condition in the first week after SCI followed by a recovery in their condition as showed by the rapid increase in their body weight starting from the second week (Fig. 2 A). The deficit in locomotion was followed by spontaneous recovery in hind limb functionality in the first two weeks from the lesion, as represented by the BBB score (Fig. 2 B).

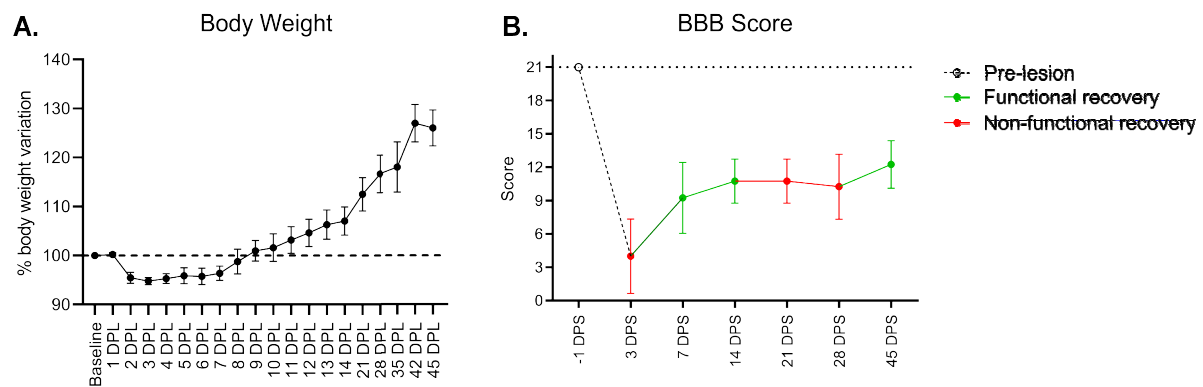


Fig. 3: In panel A are reported the variation expressed as a percentage of the body weight after the surgical procedure and the spinal lesion. Panel B represents the functional evaluation of the animal's locomotor function with the BBB scale. The empty circle is the score pre lesion, in red are represented the non-recovery phase in the longitudinal observation, and in green the recovery of locomotor function ($n=5$ animals).

mRNA expression level of synaptic plasticity associated genes.

For biological averaging and variance reduction, samples from each group were pooled for microarray experiments; in fact, for minimal designs, pooling improves accuracy dramatically¹⁰⁻¹². Five animals for each time-point and 5 control, unlesioned rats were included in the study. We analyzed supraspinal areas involved in controlling motor function and the tract of the spinal cord at

each different subdivision, cervical (from C3 to C7), thoracic (from T9 to T6), and lumbar (from T12 to L3). In fig. 3, results are presented as clustegram analysis of differentially regulated genes compared to the control group. Criteria for significance are established as 2-fold change with respect to the control group, and significant variations are indicated in tables 1 and 2 for spinal and supraspinal regions, respectively. Red numbers indicate upregulated genes, and green numbers indicate down-regulated genes at the three investigated times.

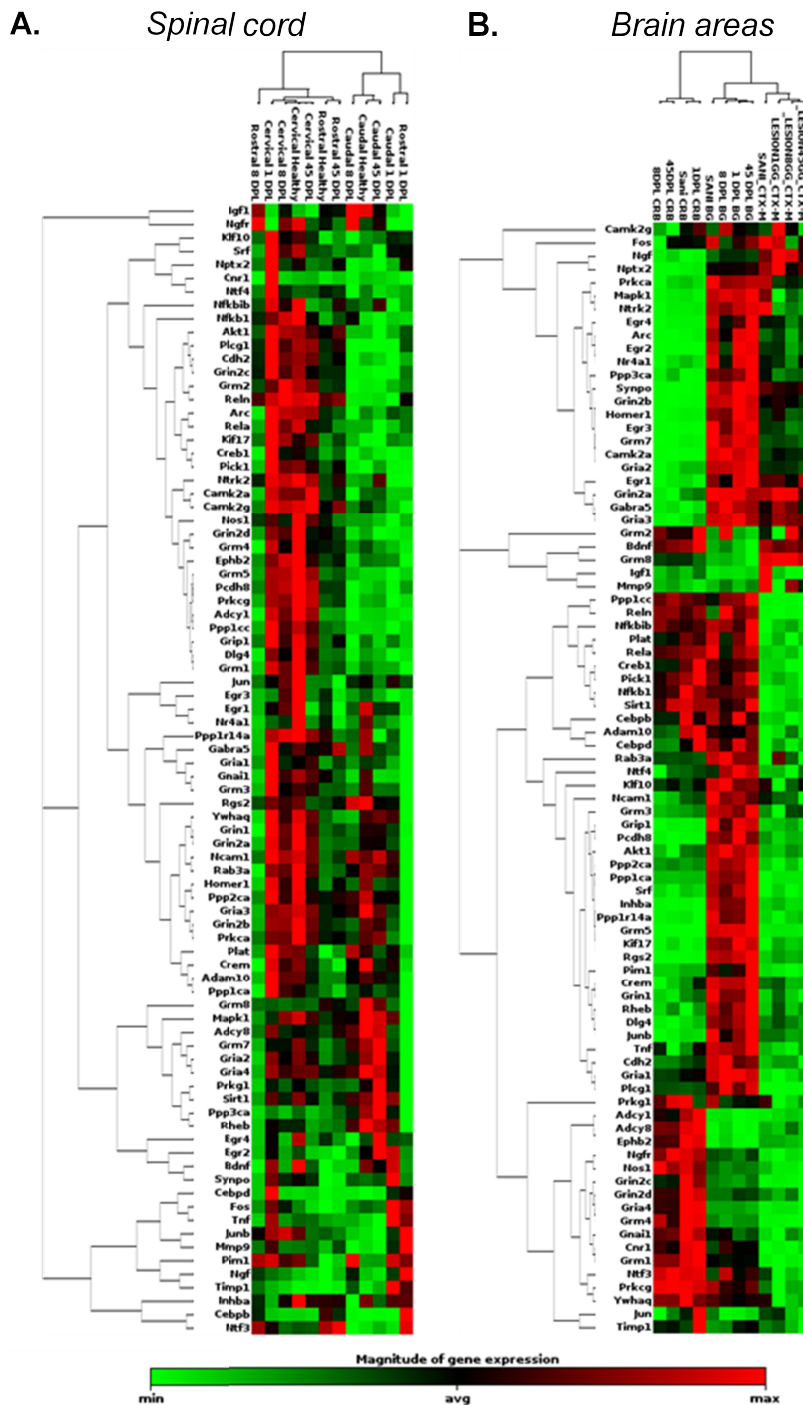


Fig. 3: The picture represents the 2D clustergram of the PCR array gene expression Ct. In panel A are reported data from the three spinal areas analyzed, whereas, in panel B, data from the three cerebral areas involved in motor function control are reported. In red are labeled genes with Ct higher than the average Ct for all groups, and in green, genes with Ct lower than the average.

We observed a different regulation pattern in supraspinal and spinal areas after spinal cord lesion (Fig. 3), while the supraspinal motor areas cerebellum and basal ganglia showed fewer genes undergoing regulation after SCI compared to spinal cord areas. On the contrary, remarkable gene expression regulations are observed in the motor cortex.

In the spinal cord's cervical cord, we found a remarkable transient downregulation of *Ngfr* and *Bdnf* at 1 DPL and 8 DPL, while *Erg* genes (1-4) showed both transiently and consistently downregulation at 1, 8, and 45 DPL. *Nr4a1* was the only gene downregulated at all the investigated time points. The upregulated genes in the cervical segment were *Cebpd* and *Cnr1* at 1 DPL and *Timp1* at all time points (Fig. 4).

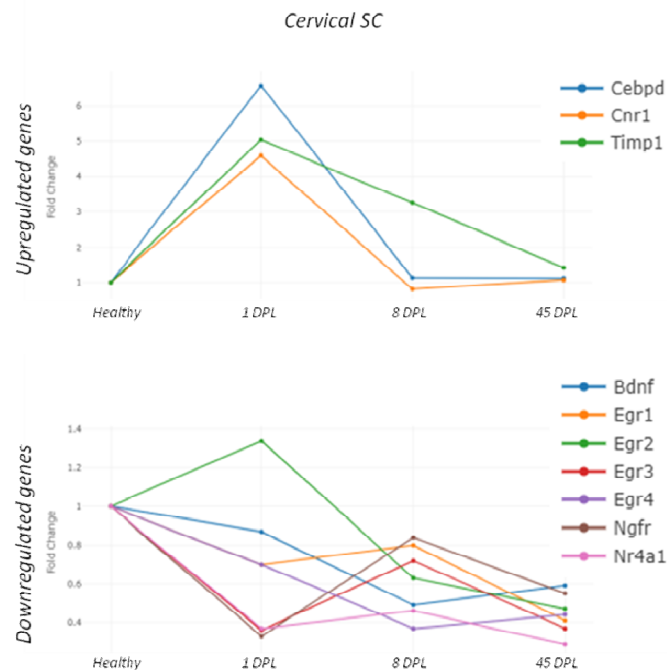


Fig. 4: The picture illustrates the upregulated and downregulated genes in the cervical segment of the spinal cord after the SCI. Gene expression is represented as fold change variation and normalized on the healthy control group.

The thoracic and the lumbar segments surrounding the lesion epicenter showed a similar number of genes up and down-regulated. In the thoracic segment, almost all downregulated genes at 1 and 8 DPL (*Arc*, *Camk2g*, *Gnai1*, *Grm3*, *Grm8*, *Igf1*) recover to basal expression at 45 DPL. The only genes with a consistent downregulation at 45 DPL were *Erg3* and *Nr4a1*. In this segment, *Cebpd*, *Fos*, *Junb*, *Mmp9*, and *Ngf* were upregulated at 1 DPL, *Ngf* showed an upregulation also at 8 DPL. *Timp1* was consistently upregulated at all time points (Fig. 5).

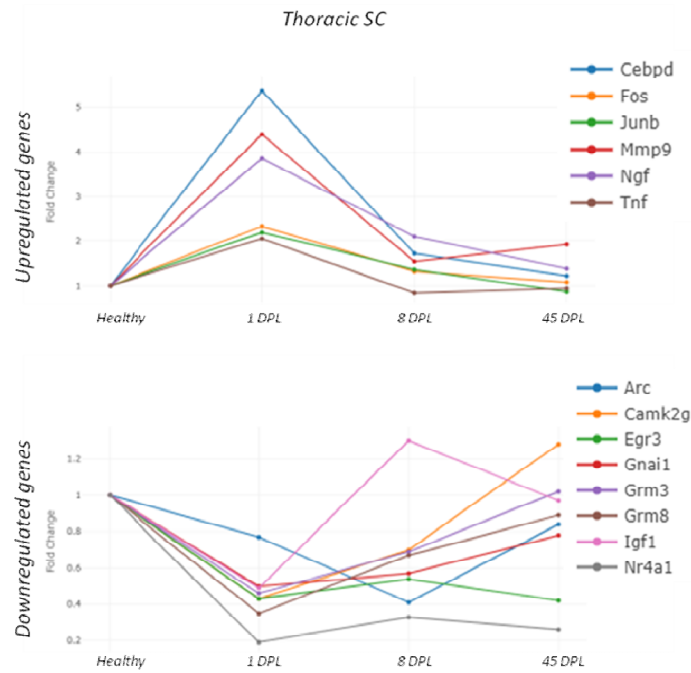


Fig. 5: The picture illustrates the upregulated and downregulated genes in the thoracic segment (rostral from the lesion) of the spinal cord after the SCI. Gene expression is represented as fold change variation and normalized on the healthy control group. Expression of Timp1 is not reported because of its high level of upregulation compared to the other genes.

In the lumbar spinal cord, we observed that at 1 DPL, the downregulated gene are principally neurotransmitter receptors or early phase genes like Erg3, Grm8, Igf1, and Nr4a1. As for the other spinal cord segments, we found a constant downregulation of Nr4a1 at all time points. The transiently upregulated genes at 1 DPL are the same genes found upregulated in the thoracic segment except for Ngf and Fos, which are not modified in the segment caudal to the lesion. Timp was the only gene upregulated at all time points (Fig. 6).

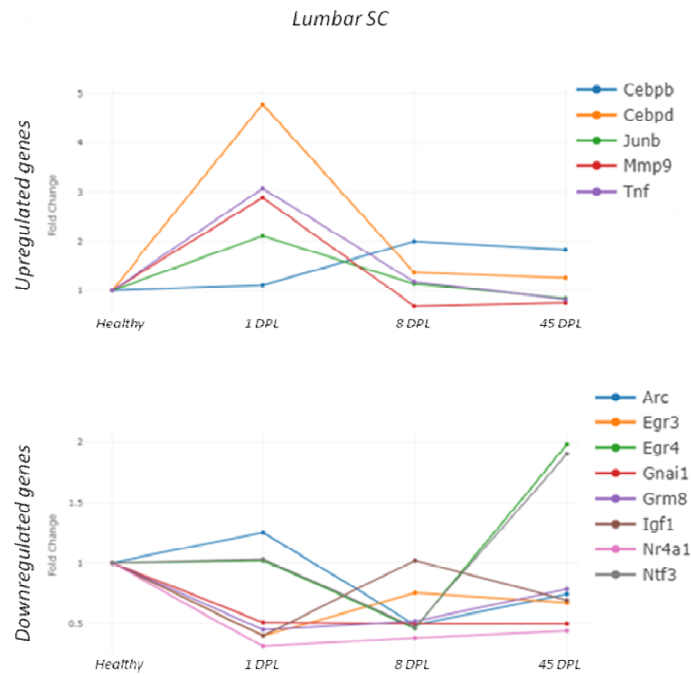


Fig. 6: The picture illustrates the upregulated and downregulated genes in the lumbar segment (caudal from the lesion) of the spinal cord after the SCI. Gene expression is represented as fold change variation and normalized on the healthy control group. Expression of Timp1 is not reported because of its high level of upregulation compared to the other genes.

Basal ganglia and cerebellum showed a poor regulation in gene expression after SCI, but again a strong upregulation of Ngf and Reln remains in both areas at 45 DPL. All the other genes in these areas were only transiently modified by the lesion and then returned to their basal expression levels. The motor cortex showed significant changes in gene expression after the lesion (Fig. 7).

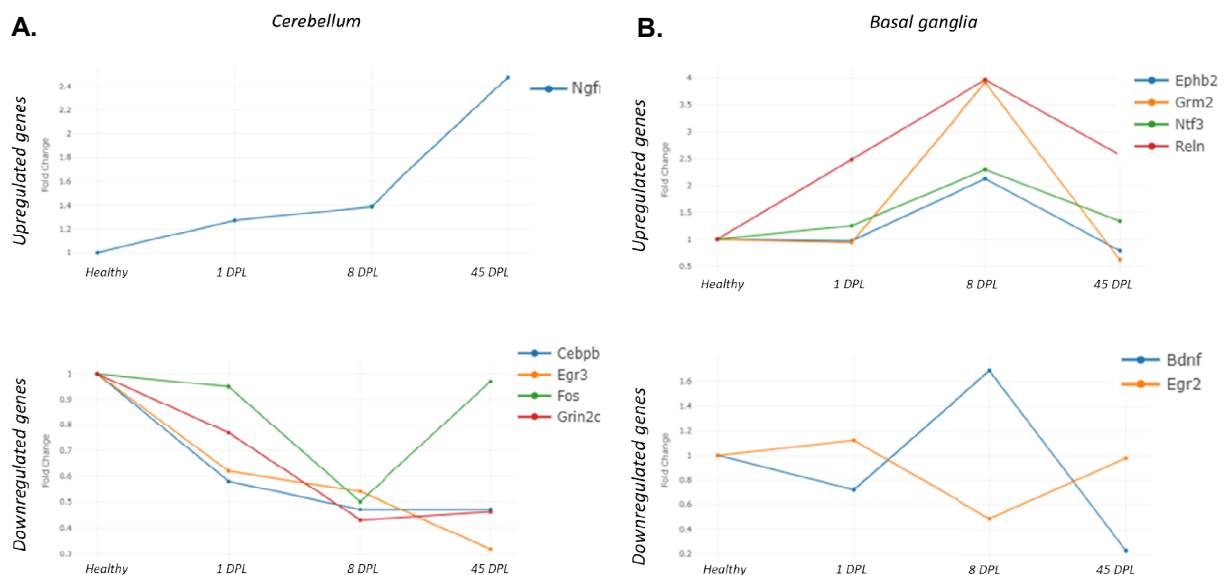


Fig. 7: The picture illustrates the upregulated and downregulated genes in the cerebellum (panel A) and the basal ganglia (panel B). Gene expression is represented as fold change variation and normalized on the healthy control group.

We found that the modification in gene expression in the motor cortex was long-lasting and remained for all the time points investigated. We identified 4 classes of differentially expressed genes in the motor cortex, based on their alteration of expression in the different phases of the SCI. The first class is the upregulated genes (Fig. 8 A) and comprises *Cebpd*, *Cnr1*, *Gria1*, and *Kif17*; these genes are upregulated at 1 DPL (*Cebpd* and *Kif17*) and 45 DPL (*Cebpd*, *Cnr1*, and *Gria1*). The second class of genes is the early downregulated genes (Fig. 8 B) and is formed by *Igf1*, *Mapk1*, *Nos1*, *Ntf3*, *Ntrk2*, *Prkg1*, and *Ywhaq*. Some of these genes are transiently downregulated at 1 DPL only or 1 and 8 DPL (*Mapk1*, *Pcdh8*, and *Prkg1*). The others are consistently downregulated at all time points. The third class of genes identified showed an initial decrease in expression levels after SCI and a recovery in the later time points (Fig. 8 C). This group mainly presents genes for receptors and early phase genes like *Grm2*, *Grm3*, *Klf10*, *Mmp9*, *Ngfr*, *Pcdh8*, and *Prkcg*. The last defined group comprises genes with a late downregulation after SCI (Fig. 8 D), including *Cebpb*, *Egr2*, and *Fos*.

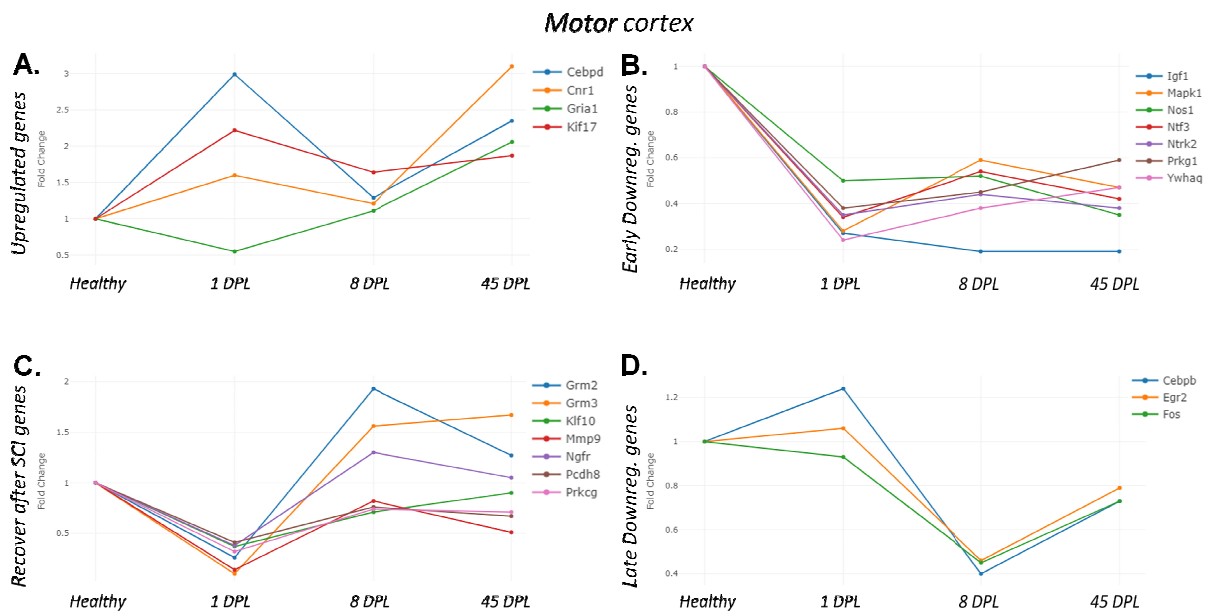


Fig. 8: The picture illustrates the modulation of genes in the motor cortex after SCI. In panel A are represented the upregulated genes. In panel B and D are reported the early and late downregulated genes, respectively. In panel C are reported genes with a recovery in their expression levels in the acute and chronic phase of SCI. Gene expression is represented as fold change variation and normalized on the healthy control group.

DISCUSSION

Lesion characterization

Data obtained from the lesion extension analysis in the spinal cord at 45 DPL showed a marked asymmetry in the lesion propagation from the lesion epicenter, with the caudal segment more involved in the secondary degeneration cascade compared to the rostral segments.

Since the lesion model used in this study, we can assume that the spinal cord segments caudal to the lesion are poorly connected to the descending tracts, resulting in a “deafferentation”. This lack of connections might impair the translocation of molecules possibly involved in gene expression regulation in the descending pathways, being the estimated anterograde and retrograde axonal transport speed as 1 m/sec for the synaptophysin containing vesicles¹³. Moreover, the evaluation of spontaneous motor recovery after SCI with the BBB scoring highlighted the presence of time-defined windows for functional amelioration. We observed the greater window of locomotion recovery in the first two weeks after SCI, then a less relevant amelioration at the latest time point of 45 DPL. Interestingly, the major gene regulation involves the spinal cord in the first week after injury, whereas, at 45 DPL the areas with the greater gene response to the lesion are the supraspinal areas, in particular the motor cortex.

Synaptic plasticity: gene expression analysis

Neuroplasticity is regarded as a possible resource to compensate, at least partially, functional and structural deficits after acute lesions of the Central Nervous System. In spinal cord injury, the lesion progression’s pathophysiology offers additional possibilities for therapeutic approaches based on neuroplasticity, like training-dependent rehabilitation¹⁴. In fact, while the contusion injury determines immediate mechanical damage of the spinal cord, secondary degeneration takes place over a defined and relative long time-window (from a few minutes to a few weeks/months after the injury), enlarging the original lesion area and determining the final anatomical and functional outcome of the patient (chronic phase, some months to years after the injury)^{15,16}.

Molecular neuroplasticity aspects include membrane signaling (i.e., fast, calcium-dependent) and intracellular events via second messengers and gene expression regulation¹⁷. Few research papers have attempted to provide preclinical evidence on cellular and molecular events linked to “neuroplasticity” after spinal cord lesion, and, at best of our knowledge, these studies were focused on the areas directly impacted by the lesion (e.g., lesion epicenter) also using the Gene Expression Omnibus (GEO) database¹⁸⁻²¹. On the contrary, in this study, we investigated the regulation of mRNA expression level of neural plasticity associated genes in brain and spinal cord areas outside the

lesioned segment, i.e., in the motor cortex, basal ganglia, cerebellum, and spinal cord segments rostral (T6-T9) and caudal (T12-L3) to the lesion (spinal T10), and cervical (C3-C8) and at different times points (24 hours, 8 and 45 days), thus covering the acute phase, the secondary neurodegeneration and chronic phase. Because gene expression regulation is a crucial step in neural plasticity, in particular concerning long-lasting changes, we used a pathway array approach, including in the analysis Immediate-Early (IEGs) and Late Response Genes, Long Term Potentiation (LTP) and Long Term Depression (LTD) associated genes, genes encoding for Cell Adhesion Molecules, Extracellular Matrix (ECM) Molecules, CREB Cofactors, Neuronal Receptors, Postsynaptic Density Proteins (PSD). The observed results can be ascribed to different cell types: neurons, astrocytes, oligodendrocytes, oligodendrocyte precursor cells, microglia.

A relevant result from this study is the substantial different pattern of gene expression regulation observed in cells located in the spinal cord and the brain, respectively. In fact, while the expression level of few genes is regulated in the brain, more genes are modulated by the injury in the spinal cord segments adjacent to the lesion. A notable exception is the motor cortex, where we found the higher gene modification at long term (45 DPL) when the lesion is stabilized from an anatomical point of view and spontaneous functional recovery completed. Notably, the upregulated genes in the spinal cord segments caudal to the lesion are all related to inflammation: *Cebpd* participates in the regulating proinflammatory gene expression in glial activation²² also in traumatic brain injury²³; *Mmp9* is a metalloprotease involved in several neuroinflammatory diseases²⁴ such as their tissue inhibitor *Timp1*²⁵; *Tnf* is a well-known mediator of neuroinflammation^{26,27} also in spinal cord injury²⁸. Thus, it is possible that the changes, most of them observed at 24 hours after lesion, only derive from a microenvironmental alteration in the proximity of the lesion that includes calcium homeostasis²⁹ and macrophages³⁰. The alteration of the expression level of mRNA encoding for inflammation-related proteins was also described in the lumbar spinal cord after traumatic injury at the thoracic level³¹.

In the spinal cord segments rostral to the lesion, we found the upregulation of *Fos* and *Ngf* at the earliest time points. Being the expression of genes related to synaptic plasticity very much “activity-dependent”, we can assume that the abrupt interruption of synaptic activity³² can trigger rapid and long-lasting nuclear changes in the neurons originating axons of the descending spinal tracts³³. This is also suggested by the upregulation of *Fos* and *Jun* early genes, which are considered markers for neural activation^{34,35}.

Most of the transiently down-regulated genes at 8 days encode for neurotransmitter receptors, including ionotropic and metabotropic glutamatergic, GABAergic, cannabinoid receptors, and second

messengers proteins, including adenylate cyclase, protein kinases, G-proteins, and protein phosphatase regulators. In the cervical segment of the spinal cord, we found a similar downregulation pattern of genes as in the other spinal cord segments, but the upregulated genes are not related to the inflammatory pathways, except for Timp1. Cebpd is commonly upregulated in all the spinal segments; this gene encodes for a bZIP transcription factor which can bind as a homodimer to CCAAT regulatory regions in the DNA. The encoded protein is essential in regulating genes involved in immune and inflammatory responses and may involve the regulation of genes associated with activation and/or differentiation of macrophages. In the context of the traumatic lesion to the CNS, there has been a transient elevation of this gene at 24 hours from the initial damage²².

Finally, several genes are modulated in the motor cortex after lesion, including glutamate receptors, NGF receptor, second messengers, transcription factors encoding genes. This result is not surprising in light of the human studies describing motor cortical maps reorganization after spinal cord injury³⁶⁻³⁸. These studies have also provided the background and the appropriate end-point to evaluate the efficacy of neuro-rehabilitation and neurostimulation protocols³⁹, that evoke “neuroplasticity” as a possible mechanism⁵, also because of abnormal neuronal engagement⁴. The gene expression regulation that we observed in our experiment possibly reflects the profound reorganization of motor pathways that starts immediately after injury^{40,41}. Recent studies using a transcranial optogenetic mapping of the motor cortex indicate an initial loss of motor map and subsequent partial recovery^{42,43}. Also, in the motor cortex, we observed an upregulation of the Cebpd gene in the first 24 hours post-injury. Surprisingly, this gene remains upregulated in the long term in this region even if it is far from the lesion site and the gene expression is not stimulated by inflammation in the motor cortex, as confirmed by the absence of modification in other genes related to the inflammation (e.g., Timp1). The presence of Cebpd and the other member of the C/EBP family in the CNS has also been associated with axonal elongation and neurite extension of deafferented neurons²². In the motor cortex, we also found a stable upregulation of Cnr1 in SCI’s chronic phase. The upregulation of the cannabinoid receptor after spinal cord lesions might be associated with the anti-nociceptive effects of these receptors in many different areas of the CNS⁴⁴. It is also known that Cnr1 is associated with synaptic plasticity and expressed in the presynaptic neurons involved in motor control in brain motor areas (basal ganglia, motor cortex, and cerebellum) and the spinal cord⁴⁵. The long-lasting increased levels of Cnr1 in the motor cortex could be related to the mechanism of the plasticity of the locomotor control.

On the other hand, the failure to recreate functional connections between supraspinal and spinal motoneurons causes the complete deafferentation of the latter cells. This phenomenon is

transduced in the downregulation of many genes in the motor cortex involved in synaptic plasticity. Among these genes, the most downregulated gene in the motor cortex at all time points was IGF1, which encodes for the insulin-like growth factor 1, involved in many different functions in the CNS. The abolishment of a standard motor function caused by the SCI and the subsequent hind limb immobility causes the potent downregulation of this gene⁴⁶.

Overall, our data suggest that a molecular mapping could be a useful tool to investigate the brain and spinal cord reorganization after spinal cord injury, also because of the need to identify reliable and straightforward tools to evaluate the efficacy of potential therapeutic approaches in preclinical models of spinal cord injury^{7,8}.

ACKNOWLEDGMENTS

This work has been supported by the POR-FESR 2014-18, project “Step-by-Step” and Mat2Rep, Emilia Romagna Region (LC) and by the Cluster Tecnologici Nazionali, project IRMI, MIUR (LC). The contribution of “Fondazione Montecatone”, Imola, Italy, and the technical assistance of Michele Sannia is also gratefully acknowledged.

AUTHOR DISCLOSURE STATEMENT

No competing financial interests exist.

Table 1: The table reports the fold changes of each gene modified by the lesion at all the time points examined for the spinal segments surrounding the lesion epicenter (thoracic and lumbar) and the distal cervical segment.

1 DPL	Cervical SC	Thoracic SC	Lumbar SC	8 DPL	Cervical SC	Thoracic SC	Lumbar SC	45 DPL	Cervical SC	Thoracic SC	Lumbar SC
Camk2g	-2.30	-2.30	-2.30	Arc	-2.04	-2.45	-2.02	Egr1	-2.46	-2.40	-2.01
Cebpd	6.58	5.38	4.78	Bdnf	-2.04	-2.45	-2.02	Egr2	-2.13	-3.80	-2.28
Cnr1	4.59			Cebpb	-2.68	2.10	2.00	Egr3	-2.73	-2.35	
Egr3	-2.76	-2.34	-2.50	Egr4	-2.16	2.10	-2.16	Egr4	-2.28		
Fos	2.33			Ngf	-2.16	-3.05	-2.60	Gnai1	-3.48	-3.80	-2.01
Gnai1	-2.01	-2.01		Nr4a1	-2.16	-3.05	-2.60	Nr4a1	-3.48	-3.80	-2.28
Grm3	-2.18	-2.18		Timpt1	3.26	12.28	6.22	Timpt1		2.40	2.98
Grm8	-2.85	-2.85	-2.21								
Igf1	-2.04	-2.04	-2.50								
Junb	2.19	2.19	2.11								
Mmp9	4.40	4.40	2.89								
Ngf	3.86	3.86									
Ngfr	-3.00	-3.00									
Nr4a1	-2.73	-3.05	-2.28								
Timpt1	5.03	27.25	17.80								

Table 2: The table reports the fold changes of each gene modified by the lesion at all the time points examined for the supraspinal areas.

1 DPL	Basal ganglia	Motor cortex	8 DPL	Cerebellum	Basal ganglia	Motor cortex	45 DPL	Cerebellum	Basal ganglia	Motor cortex
Cebpd		2.99	Cebpb	-2.13		-2.53	Bdnf		-4.38	
Grm2		-3.84	Egr2		-2.04	-2.19	Cebpb	-2.11		
Grm3		-9.99	Ephb2		2.13		Cebpd			2.35
Igf1		-3.66	Fos	-2.01		-2.22	Cnr1			3.10
Klf10		-2.71	Grin2c	-2.31			Egr3	-3.12		
Mapk1		-3.61	Grm2		3.92		Gria1			2.06
Mmp9		-6.96	Igf1			-5.21	Grin2c	-2.16		
Ngfr		-2.64	Ntf3		2.30		Igf1			-5.35
Nos1		-2.01	Ntrk2			-2.28	Mapk1			-2.14
Ntf3		-2.95	Prkg1			-2.22	Ngf	2.48		
Ntrk2		-2.85	Reln		3.97		Nos1			-2.85
Pcdh8		-2.46	Ywhaq			-2.60	Ntf3			-2.39
Prkg		-3.14					Ntrk2			-2.64
Prkg1		-2.60					Reln		2.57	
Reln	2.48						Ywhaq			-2.14
Klf17		2.22								
Ywhaq		-4.08								

REFERENCES

1. Beuparlant, J. *et al.* Undirected compensatory plasticity contributes to neuronal dysfunction after severe spinal cord injury. *Brain* **136**, 3347–3361 (2013).
2. Dietz, V. Behavior of spinal neurons deprived of supraspinal input. *Nat. Rev. Neurol.* **6**, 167–174 (2010).
3. Dietz, V. Degradation of neuronal function following a spinal cord injury: mechanisms and countermeasures. *Brain* **127**, 2221–2231 (2004).
4. Min, Y.-S. *et al.* Alteration of Resting-State Brain Sensorimotor Connectivity following Spinal Cord Injury: A Resting-State Functional Magnetic Resonance Imaging Study. *J. Neurotrauma* **32**, 1422–1427 (2015).
5. Krucoff, M. O. *et al.* Toward Functional Restoration of the Central Nervous System: A Review of Translational Neuroscience Principles. *Neurosurgery* (2018). doi:10.1093/neuros/nyy128
6. Torres-Espín, A. *et al.* Eliciting inflammation enables successful rehabilitative training in chronic spinal cord injury. *Brain* **141**, 1946–1962 (2018).
7. Van Den Brand, R. *et al.* Restoring voluntary control of locomotion after paralyzing spinal cord injury. *Science (80-.)*. **336**, 1182–1185 (2012).
8. Kadoya, K. *et al.* Spinal cord reconstitution with homologous neural grafts enables robust corticospinal regeneration. *Nat. Med.* **22**, 479–487 (2016).
9. Basso, D. M., Beattie, M. S. & Bresnahan, J. C. A sensitive and reliable locomotor rating scale for open field testing in rats. *J. Neurotrauma* **12**, 1–21 (1995).
10. Chabas, D. *et al.* The Influence of the Proinflammatory Cytokine, Osteopontin, on Autoimmune Demyelinating Disease. *Science (80-.)*. **294**, 1731–1735 (2001).
11. Kendzierski, C., Irizarry, R. A., Chen, K.-S., Haag, J. D. & Gould, M. N. On the utility of pooling biological samples in microarray experiments. *Proc. Natl. Acad. Sci.* **102**, 4252–4257 (2005).
12. Kendzierski, C. M., Newton, M. A., Lan, H. & Gould, M. N. On parametric empirical Bayes methods for comparing multiple groups using replicated gene expression profiles. *Stat. Med. Stat. Med* **22**, 3899–3914 (2003).
13. Mar, F. M. *et al.* CNS Axons Globally Increase Axonal Transport after Peripheral Conditioning. *J. Neurosci.* **34**, 5965–5970 (2014).
14. Caeyenberghs, K. *et al.* Evidence for Training-Dependent Structural Neuroplasticity in Brain-Injured Patients: A Critical Review. *Neurorehabilitation and Neural Repair* **32**, 99–114 (2018).
15. Kjell, J. & Olson, L. Rat models of spinal cord injury: from pathology to potential therapies. *Dis. Model. Mech.* **9**, 1125–1137 (2016).
16. Tran, A. P., Warren, P. M. & Silver, J. The Biology of Regeneration Failure and Success After Spinal Cord Injury. *Physiol. Rev.* **98**, 881–917 (2018).
17. Sweatt, J. D. Neural plasticity and behavior – sixty years of conceptual advances. *J. Neurochem.* **139**, 179–199 (2016).
18. Chen, X. J., Mou, X. Q., Zou, Y., Peng, Z. Y. & Yang, J. X. Screening of key genes associated with contused rat spinal cord with DNA microarray. *Eur. Rev. Med. Pharmacol. Sci.* **17**, 2949–2955 (2013).
19. Lai, J. *et al.* Gene expression signature analysis and Protein-Protein interaction network construction of Spinal

- Cord Injury. *Eur. Rev. Med. Pharmacol. Sci.* **17**, 2941–8 (2013).
20. Liu, Y. *et al.* DNA Microarray Analysis in Screening Features of Genes Involved in Spinal Cord Injury. *Med Sci Monit* **22**, 1571–1581 (2016).
 21. Zhu, Z., Shen, Q., Zhu, L. & Wei, X. Identification of pivotal genes and pathways for spinal cord injury via bioinformatics analysis. *Mol. Med. Rep.* **16**, 3929–3937 (2017).
 22. Ko, C. Y., Chang, W. C. & Wang, J. M. Biological roles of CCAAT/enhancer-binding protein delta during inflammation. *J. Biomed. Sci.* **22**, (2015).
 23. von Gertten, C., Morales, A. F., Holmin, S., Mathiesen, T. & Nordqvist, A. C. S. Genomic responses in rat cerebral cortex after traumatic brain injury. *BMC Neurosci.* **6**, 69 (2005).
 24. Vafadari, B., Salamian, A. & Kaczmarek, L. MMP-9 in translation: from molecule to brain physiology, pathology, and therapy. *J. Neurochem.* **139**, 91–114 (2016).
 25. Petković, F. *et al.* Activity, but not mRNA expression of gelatinases correlates with susceptibility to experimental autoimmune encephalomyelitis. *Neuroscience* **292**, 1–12 (2015).
 26. Borjini, N., Fernández, M., Giardino, L. & Calzà, L. Cytokine and chemokine alterations in tissue, CSF, and plasma in early presymptomatic phase of experimental allergic encephalomyelitis (EAE), in a rat model of multiple sclerosis. *J. Neuroinflammation* **13**, (2016).
 27. Fernández, M., Baldassarro, V. A., Sivilia, S., Giardino, L. & Calzà, L. Inflammation severely alters thyroid hormone signaling in the central nervous system during experimental allergic encephalomyelitis in rat: Direct impact on OPCs differentiation failure. *Glia* **64**, 1573–1589 (2016).
 28. Rowe, R. K. *et al.* Novel TNF receptor-1 inhibitors identified as potential therapeutic candidates for traumatic brain injury. *J. Neuroinflammation* **15**, 154 (2018).
 29. Khariv, V. & Elkabes, S. Contribution of Plasma Membrane Calcium ATPases to neuronal maladaptive responses: Focus on spinal nociceptive mechanisms and neurodegeneration. *Neurosci. Lett.* **663**, 60–65 (2018).
 30. Norden, D. M. *et al.* Bone Marrow-derived Monocytes Drive the Inflammatory Microenvironment in Local and Remote Regions after Thoracic SCI. *J. Neurotrauma* neu.2018.5806 (2018). doi:10.1089/neu.2018.5806
 31. Shin, H. Y. *et al.* Molecular and cellular changes in the lumbar spinal cord following thoracic injury: Regulation by treadmill locomotor training. *PLoS One* **9**, e88215 (2014).
 32. Jacobi, A., Schmalz, A. & Bareyre, F. M. Abundant expression of guidance and synaptogenic molecules in the injured spinal cord. *PLoS One* **9**, (2014).
 33. Lim, A. F. Y., Lim, W. L. & Ch'ng, T. H. Activity-dependent synapse to nucleus signaling. *Neurobiol. Learn. Mem.* **138**, 78–84 (2017).
 34. Bullitt, E. Expression of c-fos-like protein as a marker for neuronal activity following noxious stimulation in the rat. *J. Comp. Neurol.* **296**, 517–530 (1990).
 35. Hughes, P. E. *et al.* Activity and injury-dependent expression of inducible transcription factors, growth factors and apoptosis-related genes within the central nervous system. *Prog. Neurobiol.* **57**, 421–450 (1999).
 36. Henderson, L. A., Gustin, S. M., Macey, P. M., Wrigley, P. J. & Siddall, P. J. Functional Reorganization of the Brain in Humans Following Spinal Cord Injury: Evidence for Underlying Changes in Cortical Anatomy. *J.*

- Neurosci.* **31**, 2630–2637 (2011).
37. Freund, P. *et al.* MRI investigation of the sensorimotor cortex and the corticospinal tract after acute spinal cord injury: A prospective longitudinal study. *Lancet Neurol.* **12**, 873–881 (2013).
 38. Serradj, N., Agger, S. F. & Hollis, E. R. Corticospinal circuit plasticity in motor rehabilitation from spinal cord injury. *Neurosci. Lett.* **652**, 94–104 (2017).
 39. Christiansen, L. & Perez, M. A. Targeted-Plasticity in the Corticospinal Tract After Human Spinal Cord Injury. *Neurotherapeutics* **15**, 618–627 (2018).
 40. Bazley, F. A. *et al.* Electrophysiological evaluation of sensory and motor pathways after incomplete unilateral spinal cord contusion. *J. Neurosurg. Spine* **16**, 414–423 (2012).
 41. Vipin, A. *et al.* Natural Progression of Spinal Cord Transection Injury and Reorganization of Neural Pathways. *J. Neurotrauma* **33**, 2191–2201 (2016).
 42. Hilton, B. J. *et al.* Re-Establishment of Cortical Motor Output Maps and Spontaneous Functional Recovery via Spared Dorsolaterally Projecting Corticospinal Neurons after Dorsal Column Spinal Cord Injury in Adult Mice. *J. Neurosci.* **36**, 4080–4092 (2016).
 43. Qian, J. *et al.* Longitudinal optogenetic motor mapping revealed structural and functional impairments and enhanced corticorubral projection following contusive spinal cord injury in mice. *J. Neurotrauma* neu.2018.5713 (2018). doi:10.1089/neu.2018.5713
 44. Knerlich-Lukoschus, F. *et al.* Spinal cord injuries induce changes in CB1 cannabinoid receptor and C-C chemokine expression in brain areas underlying circuitry of chronic pain conditions. *J. Neurotrauma* **28**, 619–634 (2011).
 45. Herkenham, M. *et al.* Characterization and localization of cannabinoid receptors in rat brain: A quantitative in vitro autoradiographic study. *J. Neurosci.* **11**, 563–583 (1991).
 46. Mysoet, J. *et al.* Reorganization of motor cortex and impairment of motor performance induced by hindlimb unloading are partially reversed by cortical IGF-1 administration. *Behav. Brain Res.* **317**, 434–443 (2017).

4.6. Improved Functional Recovery in Rat Spinal Cord Injury Induced by a Drug Combination Administered with an Implantable Polymeric Delivery System (*J Neurotrauma*, 37:1708–1719, August 1, 2020)

Improved Functional Recovery in Rat Spinal Cord Injury Induced by a Drug Combination Administered with an Implantable Polymeric Delivery System

Andrea Bighinati,¹ Maria Letizia Focarete,^{2,3} Chiara Gualandi,³ Micaela Pannella,⁵ Alessandro Giuliani,¹ Sarah Beggiato,⁴ Luca Ferraro,^{4,5} Luca Lorenzini,¹ Luciana Giardino,^{1,2,5} and Laura Calzà^{2,5,6}

Abstract

Spinal cord injury (SCI) is an incurable condition, in which a cascade of cellular and molecular events triggered by inflammation and excitotoxicity impairs endogenous regeneration, namely remyelination and axonal outgrowth. We designed a treatment solution based on an implantable biomaterial (electrospun poly (L-lactic acid) [PLLA]) loaded with ibuprofen and triiodothyronine (T3) to counteract inflammation, thus improving endogenous regeneration. *In vivo* efficacy was tested by implanting the drug-loaded PLLA in the rat model of T8 contusion SCI. We observed the expected recovery of locomotion beginning on day 7. In PLLA-implanted rats (i.e., controls), the recovery stabilized at 21 days post-lesion (DPL), after which no further improvement was observed. On the contrary, in PLLA + ibuprofen (Ibu) + T3 (PLLA-Ibu-T3) rats a further recovery and a significant treatment effect were observed, also confirmed by the gait analysis on 49 DPL. Glutamate release at 24 h and 8 DPL was reduced in PLLA-Ibu-T3– compared to PLLA-implanted rats, such as the estimated lesion volume at 60 DPL. The myelin- and 200-neurofilament–positive area fraction was higher in PLLA-Ibu-T3–implanted rats, where the percentage of astrocytes was significantly reduced. The implant of a PLLA electrospun scaffold loaded with Ibu and T3 significantly improves the endogenous regeneration, leading to an improvement of functional locomotion outcome in the SCI.

Keywords: glutamate; ibuprofen; myelination; secondary neurodegeneration; thyroid hormone

Introduction

SPINAL CORD INJURY (SCI) causes disability and death and represents a severe medical, social, and economic burden at global level.¹ Incidence varies from 15 to 45 cases per million, a figure which translates to 2.5 million people are living with SCI, with >130,000 new injuries reported annually. In spite of the impressive advancements in the medical and surgical treatments of these critical patients, and although a large body of pre-clinical evidence has been accumulated on cellular and molecular mechanisms occurring during the very early phase of the lesion, SCI is still considered an incurable condition. Routine protocols for the acute phase are presently aimed at reducing edema. Although some drugs, approved for other neurological diseases, are currently being tested (e.g., riluzole, Nogo-A targeting drugs, Rho inhibitor, cethrin, and minocycline), none currently appear to be effective in rescuing the sensory and motor functions.

The pathophysiology of SCI includes different phases following a defined time frame.² The primary phase develops within minutes and continues for 8–12 h.³ The ischemic damage, reflecting the trauma suffered (contusion, compression, and shear injury), is characterized by elevation of excitatory amino-acid extracellular levels and tissue inflammation, including infiltration of neutrophils and macrophages; these cells promote a series of self-propagating events determining the secondary phase (or secondary injury), which is a predictor of long-term SCI morbidity and mortality. It is sustained by the inflammatory cell cascade, involves astrocytes and microglial cells, and is characterized by demyelination progression, scar formation, neurodegeneration, and central cavitation.⁴ This well-established phenomenon in experimental SCI is now recognized and described in humans by magnetic resonance imaging, including its self-propagation.^{5,6}

Given that the inflammatory response characterizing the acute phase is a recognized primary therapeutic target in SCI, the use of

¹Department of Veterinary Medical Sciences, ²Health Sciences and Technologies (HST) CIRI-SDV, ³Department of Chemistry “Giacomo Ciamician” and National Consortium of Materials Science and Technology (INSTM, Bologna RU), ⁶Pharmacy and Biotechnology, Alma Mater Studiorum–University of Bologna, Bologna, Italy.

⁴Department of Life Sciences and Biotechnology, Section of Medicinal and Health Products, University of Ferrara, Ferrara, Italy.

⁵Iret Foundation, Ozzano Emilia, Emilia, Italy.

anti-inflammatory drugs has been extensively proposed. However, steroid administration is still disputed because of the small benefit/risk ratio of these drugs. Actually, this approach is being abandoned and considered a “harmful standard of care” in many trauma centers.^{7,8} The systemic administration of various nonsteroidal anti-inflammatory drugs (NSAIDs) is not associated with a significant improvement in locomotor function, and, similarly, no effective therapies for reducing secondary neurodegeneration are available.^{4,9} We envisaged that a main reason underlying the current failure in SCI pharmacological treatment could be the monotherapy approach, which seems inadequate to break the vicious cycle between excitotoxicity, increased inflammation, impaired remyelination, and neurodegeneration. Along these lines, we hypothesized that an approach based on the combination of an anti-inflammatory drug plus a remyelinating agent could act on two key points of the complex SCI pathological cascade. Thus, we selected ibuprofen (Ibu), whose systemic administration has been widely tested for acute SCI in pre-clinical studies, as an anti-inflammatory drug.

In fact, besides to inhibit cyclooxygenase activity, Ibu decreases the activation of RhoA, a key enzyme impeding axonal sprouting after axonal damage.¹⁰ This dual activity is potentially unique in the context of the double-edged-sword role of inflammation in SCI and has formed the rational basis for a clinical study aimed at repurposing Ibu in the treatment of SCI.¹¹ As a promyelinating agent, we selected the active form of thyroid hormone (TH), triiodothyronine (T3). T3 is a key component of the molecular machinery permitting the maturation of non-myelinating oligodendrocyte precursor cells (OPCs) into myelinating oligodendrocytes (OLs), maturation which is blocked during inflammation.^{12–14} After that, our laboratory proposed TH systemic administration to improve remyelination in inflammatory-demyelinating diseases; different and independent rodent and non-human-primate studies have confirmed that exogenous TH administration is effective in overcoming the OPC differentiation blockade, in protecting myelin and axons, finally ameliorating the clinical outcome in a different experimental model.^{15–17}

A pharmacological strategy based on the combination of Ibu and T3 to target two main pathogenic events in acute SCI (i.e., inflammation and demyelination) faces, however, major obstacles in the necessity of drug systemic administration. For instance, it seems probable that high Ibu doses are necessary to inhibit central nervous system (CNS) RhoA activity, thus rendering this approach likely burdened with severe side effects.¹⁸ Similarly, prolonged systemic administration of T3 exposes the patient to the risk of hyperthyroidism. To overcome these issues, we designed a polymeric delivery system based on a polylactic acid-based biodegradable scaffold (poly [L-lactic acid]; PLLA) loaded with the two drugs, to be implanted at the lesion site immediately after the lesion occurrence and ensuring a controlled and prolonged drug release rate.

In this study, we demonstrated that an Ibu- and T3-loaded electrospun scaffold, when implanted *in vivo* in the contusion SCI rat model, reduces glutamate release, tissue inflammation, and astroglial reaction at 24 h and 8 days post-lesion (DPL); over the long term, it reduces lesion volume and improves the morphological indices of myelination and axonal injury (55 DPL), finally improving long-term locomotor outcome.

Methods

See also the Supplementary Materials and Methods.

Animals and study design

CD/Sprague-Dawley female rats ($N=86$; 200–250 g; Charles River, Calco, Italy) were used. All animal protocols described here were carried out according to European Community Council Directives 2010/63/UE, approved by the Italian Ministry of Health (D.Lgs 26/2014, authorization no. 574/2015-PR). Moreover, animal protocols were carried out in compliance with the ARRIVE (Animal Research: Reporting of In Vivo Experiments) guidelines and the NIH Guide for the Care and Use of Laboratory Animals. Animals underwent a contusive spinal cord lesion at the thoracic level, T9. Rats were pre-medicated with enrofloxacin and tramadol (5 mg/kg, subcutaneously [s.c.]) and then anesthetized with isoflurane (1–3%) in O₂. The contusive lesion of the spinal cord was obtained using an Impact One impactor (Leica Microsystems GmbH, Wetzlar, Germany), using a 1.5-mm-diameter cylindrical tip with a force of 1 N and 0 sec of stance time; the depth of impact was 1.5 mm. After performing the spinal cord lesion, PLLA scaffolds, either conjugated or unconjugated with drugs, were locally implanted and coated with surgical adhesive (BioGlue; CryoLife, Kennesaw, GA).

This proof-of-concept study was aimed at reducing secondary injury in SCI, by the controlled, local delivery of two drugs achieved by implanting a drugs-loaded biomaterial at the spinal cord lesion site (Fig. 1A). The expected therapeutic effect on locomotion recovery of the drugs-loaded PLLA, also considering efficacy parameters of other pre-clinical studies aimed to limit secondary degeneration, was established as $\geq 20\%$ compared to drugs-unloaded PLLA. On this basis, and also considering the most used locomotion readout in published data, the power analysis for the sample-size calculation was performed by considering the improvement of the Basso, Beattie, and Bresnahan (BBB) scale as the primary end point.¹⁹ For $\alpha=0.05$, power (1- β)=0.80, and an effect size (d)=1.12, 14 animals per group were required (G* Power 3.1.9.2 software). A randomized surgery list was generated, to assign the rats to the two cohorts (i.e., PLLA and PLLA-Ibu-T3), and a further randomization in each cohort was performed at the euthanization, assigning the animals to the different exploratory end-point experiments (flow cytometry, molecular biology, histology, and immunohistochemistry; Fig. 1B,D). We also pre-determined inclusion/exclusion criteria for lesion efficacy. According to the BBB scale guidelines, in order to obtain a moderate-severity lesion in all animals, rats with a BBB score ≥ 15 at day 3 after lesion were excluded. On this basis, 1 rat from the PLLA group was excluded from the study.

To test the hypothesis supporting the new drug formulation, we euthanized animals at three time points. To verify whether the PLLA-Ibu-T3 scaffold counteracts glutamate excitotoxicity and inflammation, we euthanized two groups of animals at 24 h and 8 DPL, respectively, to analyze glutamate release from synaptosomal preparations and inflammatory cellular infiltrate at the lesion site. To verify whether the PLLA-Ibu-T3 scaffold applied in the acute post-trauma phase ameliorates anatomical and functional outcome, we performed the last locomotion tests (BBB score and gait analysis), histological measurement of the lesion volume, plus immunohistochemistry (IHC) analysis of microglia and astrocyte reaction, myelin, and axon damage at long-term post-lesion.

Scaffolds preparation

Scaffolds of PLLA were produced by co-electrospinning two different solutions and collecting the corresponding fibers evenly distributed on a rotating collector. The delivery system containing T3 and Ibu was produced by co-electrospinning two different PLLA solutions, one containing a suitable amount of Ibu to give a 5-wt percentage of drug in the final fibers and the other one containing a suitable amount of T3 to give a 0.6-wt percentage of drug in the final fibers. An electrospun control sample was produced by

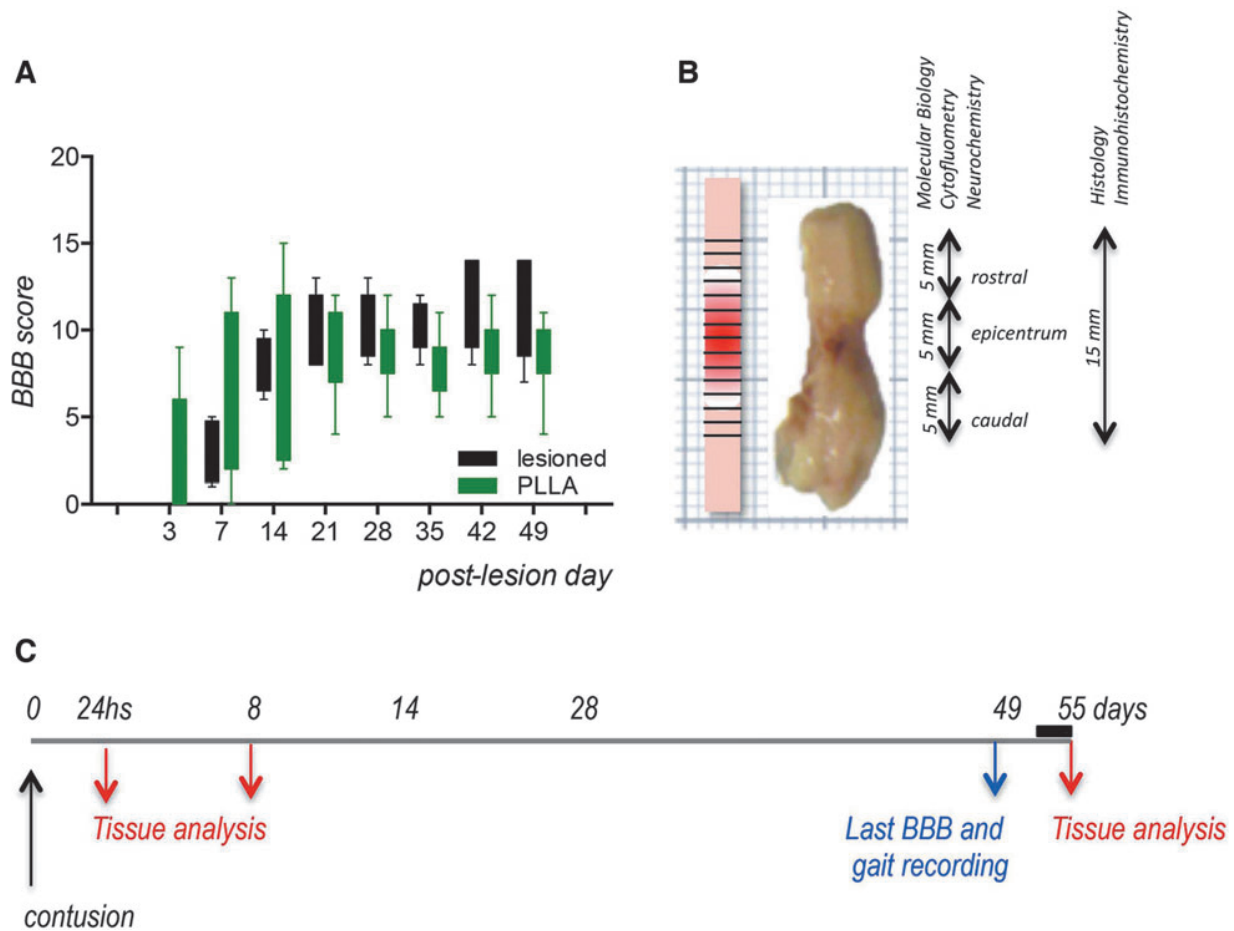


FIG. 1. Study design and pilot experiment. **(A)** Results from the pilot study to establish the most appropriate control group, showing the BBB score in lesioned (black) and lesioned rats implanted with PLLA, alone (green). **(B)** Sampling schema for tissue processing. **(C)** Experimental schedule pointing on the timing for tissue and biological fluids analysis (red arrows) and last locomotion testing (blue arrow). BBB, Basso, Beattie, Bresnahan Locomotor Rating Scale; Ibu, ibuprofen; PLLA, poly (L-lactic acid); T3, triiodothyronine.

co-electrospinning the aforementioned described polymeric solutions not loaded with drugs. Scaffolds were sterilized using gamma rays (25 KGy) before implantation.

Drug analytical procedure

Drug release from the PLLA was measured *in vitro* as described in the Supplementary Materials. Briefly, rectangular electrospun samples were immersed in phosphate-buffered saline (PBS; 0.1 M, pH=7.4) and incubated in a shaking water bath at 37°C for a maximum period of 15 days. At regular intervals, PBS was completely removed and replaced with fresh buffer. Aliquots were analyzed by means of high-performance liquid chromatography/ultraviolet and mass spectrometry to determine Ibu and T3 release, respectively. The results are reported as cumulative release.

Locomotion analysis

To evaluate loss of hindlimb function, 15 animals per group were used at the time point of 60 DPL. The BBB score was evaluated before spinal cord lesion, 3 DPL, and then once per week until animal euthanization. One animal retained normal locomotion after spinal cord lesion and failed to show gait deficit and was excluded from the study.

Gait analysis was performed using the CatWalk (Noldus, Wageningen, The Netherlands) automatized system. Animals were

trained to walk repeatedly along the platform before surgery, then tested 2 days before spinal cord lesion and at 14, 28, and 49 DPL. Gait analysis was evaluated using the following parameters: print area, maximum contact area (spatial parameters), stride length, step cycle (comparative parameters), stand time, swing time, swing speed, single stance (kinetic parameters), duty cycle, step sequence regularity index, and cadence (coordination parameters).

Histology and immunohistochemistry

Tissue analysis was carried out in paraffin or cryostat sections, using EE and toluidine blue staining, and IHC.

Flow cytometry

A 10-mm spinal cord segment enclosing the injury site was processed for flow cytometry. Briefly, animals were euthanized and perfused with 100 mL of Dulbecco's modified PBS (DPBS; Lonza, Basel, Switzerland) in order to remove circulating inflammatory cells. Cells were isolated with the Adult Brain Dissociation Kit solutions and GentleMACS Octo Dissociator (Miltenyi Biotec, Bergisch Gladbach, Germany). At least 2×10^5 cells were suspended in DPBS. Cell populations were marked respectively with CD11b-PE-Vio770 (1:10), CD45-APC-Vio770 (1:10), GLAST-PE (1:10), CD32-APC (1:10), and CD86-VioBright-FITC (1:10) for the identification of macrophagic ($CD11^+CD45^+$), microglial

(CD11⁺CD45⁻), lymphocytic (CD11⁻CD45⁺), astrocytic (GLAST⁺), and M2 lineages (CD32⁻/CD86⁻; Miltenyi Biotec). In order to distinguish live cells, 4',6-diamidino-2-phenylindole staining solution (0.1 µg/mL) was used. Immunolabeled cell-count analysis was made by MACSQuant Analyzers and FlowLogic software (Miltenyi Biotec).

Synaptosome preparation, glutamate, and gamma aminobutyric acid assay

See the Supplementary Material.

RNA isolation, reverse transcription real-time polymerase chain reaction, and real-time polymerase chain reaction

Total RNA isolation was performed by using the RNeasy Micro kit (Qiagen, Milan, Italy), following the manufacturer's instructions. First-strand complementary DNAs (cDNAs) were obtained using the iScript[™]cDNA Synthesis Kit (Bio-Rad Laboratories, Hercules, CA). An RNA sample with no reverse-transcriptase enzyme in the reaction mix was processed as a no-reverse transcription control sample. Semiquantitative real-time polymerase chain reaction (PCR) was performed using the CFX96 real-time PCR system (Bio-Rad).

Statistical analysis

Results were expressed as mean ± standard error (SEM) and plotted on graphs. Statistical analyses were performed using Prism software (GraphPad v7; GraphPad Software Inc., La Jolla, CA). Student's *t*-test was used for comparison of two groups and ordinary one-way analysis of variance (ANOVA) and post-hoc test for comparison of more than two groups. BBB score and gait analysis data have been analyzed using the two-way ANOVA test. Results were considered significant when the probability of their occurrence as a result of chance alone was <5% ($p < 0.05$).

Data and materials availability

All raw data, materials, images, videos, and analysis generated for this study are available on request.

Results

Poly (L-lactic acid) electrospun nanofibers guaranteed the expected ibuprofen and triiodothyronine release profile over time

To realize the dual-drug delivery system in a translational perspective, we used two marketed drugs together with biodegradable polymers already approved by the U.S. Food and Drug Administration (FDA) for derma filling and endovascular scaffolds that have been manufactured as electrospun fibers. Polymeric electrospun scaffolds were designed and manufactured in order to guarantee a release rate of Ibu and T3, starting within the first 24 h after injury and continuing for at least 8–10 DPL, to prevent/limit secondary neurodegeneration. To prepare a dual-drug delivery electrospun system, Ibu and T3 were individually encapsulated by "direct blending" in different polymeric solutions, which were simultaneously coelectrospun on the same collector to give a fibrous scaffold consisting of differently loaded fibers. Drug release was measured as indicated in the Methods (see also Supplementary Materials). This scaffold released 48 µg/mL of Ibu over 14 days, with an estimated daily release of 3.4 µg/mL, and 50 ng/mL of T3, with an estimated daily release of 3.5 ng/mL.

The poly (L-lactic acid)/ibuprofen/triiodothyronine scaffold counteracted molecular and cellular events elicited in the acute spinal cord injury (24 h and 8 days post-lesion)

The contusion model of SCI in rats was used to test efficacy. According to the ARRIVE guidelines, a pilot study ($N=9$ animals per group) was performed to determine the most appropriate control group, by comparing lesioned animals to lesioned animals implanted with PLLA without drugs, expecting PLLA to be an inactive component of the proposed therapeutic solution. The BBB score, established as the primary end point of the efficacy study, was subsequently used for this pilot study also. Given that no differences were observed in the BBB score during the observational time (two-way ANOVA, treatment effect, $F_{(1, 127)}=1.171$; $p=0.2813$; 49 DPL; Fig. 1A), the control, sham-operated group consisted of rats lesioned and implanted with drug-unloaded PLLA.

For the analysis of the main molecular and cellular mechanisms responsible for secondary degeneration onset, PLLA- and PLLA-Ibu-T3-implanted animals were euthanized at 24 h or 8 DPL (Fig. 1C). Figure 1B shows tissue collection details. First, glutamate release was measured from lesioned spinal cord synaptosomes ($N=5$ animals per group). In the PLLA group, similar basal glutamate release was observed in synaptosomes from tissues dissected 24 h or 8 days after SCI (6.63 ± 1.35 and 6.87 ± 2.23 pmol/5 min/mg of protein, respectively; Fig. 2A). Basal glutamate release in synaptosomes from tissue dissected from the PLLA-Ibu-T3 group 24 h after SCI was significantly lower (3.72 ± 0.66 pmol/5 min/mg of protein) than that measured in the respective control group (PLLA group, 24 h; Fig. 2A). A tendency toward a similar effect was also observed in the PLLA-Ibu-T3 synaptosomes from tissue dissected 8 days after the lesion. In the PLLA group, K⁺-evoked glutamate release was similar in rat spinal cord synaptosomes from tissue dissected 24 h and 8 days after the lesion ($202 \pm 23\%$ and $205 \pm 21\%$ of basal values, respectively). K⁺-evoked glutamate release in synaptosomes from tissue dissected from the PLLA-Ibu-T3 group 8 days after SCI was significantly lower ($153 \pm 4\%$ of basal values) than that measured in the respective control group (PLLA group, 8 days; Fig. 2A).

Contrarily, K⁺-evoked glutamate release in PLLA-Ibu-T3 synaptosomes from tissue dissected 24 h after the lesion ($179 \pm 13\%$ of basal values) was comparable to that observed in the respective PLLA group (Fig. 2A). To verify whether the effect of PLLA-Ibu-T3 is specific for glutamate, we also analyzed synaptosomal gamma aminobutyric acid (GABA) release. In the PLLA group, similar basal GABA release was observed in synaptosomes from tissues dissected 24 h or 8 days after SCI (1.91 ± 0.60 and 2.31 ± 0.61 pmol/5 min/mg of protein, respectively; Fig. 2B). Comparable values were observed in synaptosomes from tissues dissected from the PLLA-Ibu-T3 group 24 h and 8 days after SCI (2.07 ± 0.4 and 3.04 ± 0.9 pmol/5 min/mg of protein, respectively; Fig. 2B). In the PLLA group, K⁺-evoked GABA release was comparable in rat spinal cord synaptosomes from tissue dissected 24 h and 8 days after the lesion ($166 \pm 8\%$ and $203 \pm 21\%$ of basal values, respectively). K⁺-evoked GABA release in synaptosomes from tissue dissected from the PLLA-Ibu-T3 group 24 h and 8 days after SCI ($193 \pm 6\%$ and $172 \pm 10\%$ of basal values, respectively) was similar to that observed in the PLLA group (Fig. 2B).

To verify whether the PLLA-Ibu-T3 scaffold regulates inflammatory cellular responses in the spinal cord, we analyzed cells expressing inflammation-related membrane markers by flow cytometry analysis ($N=4$ animals per group). Results are presented in

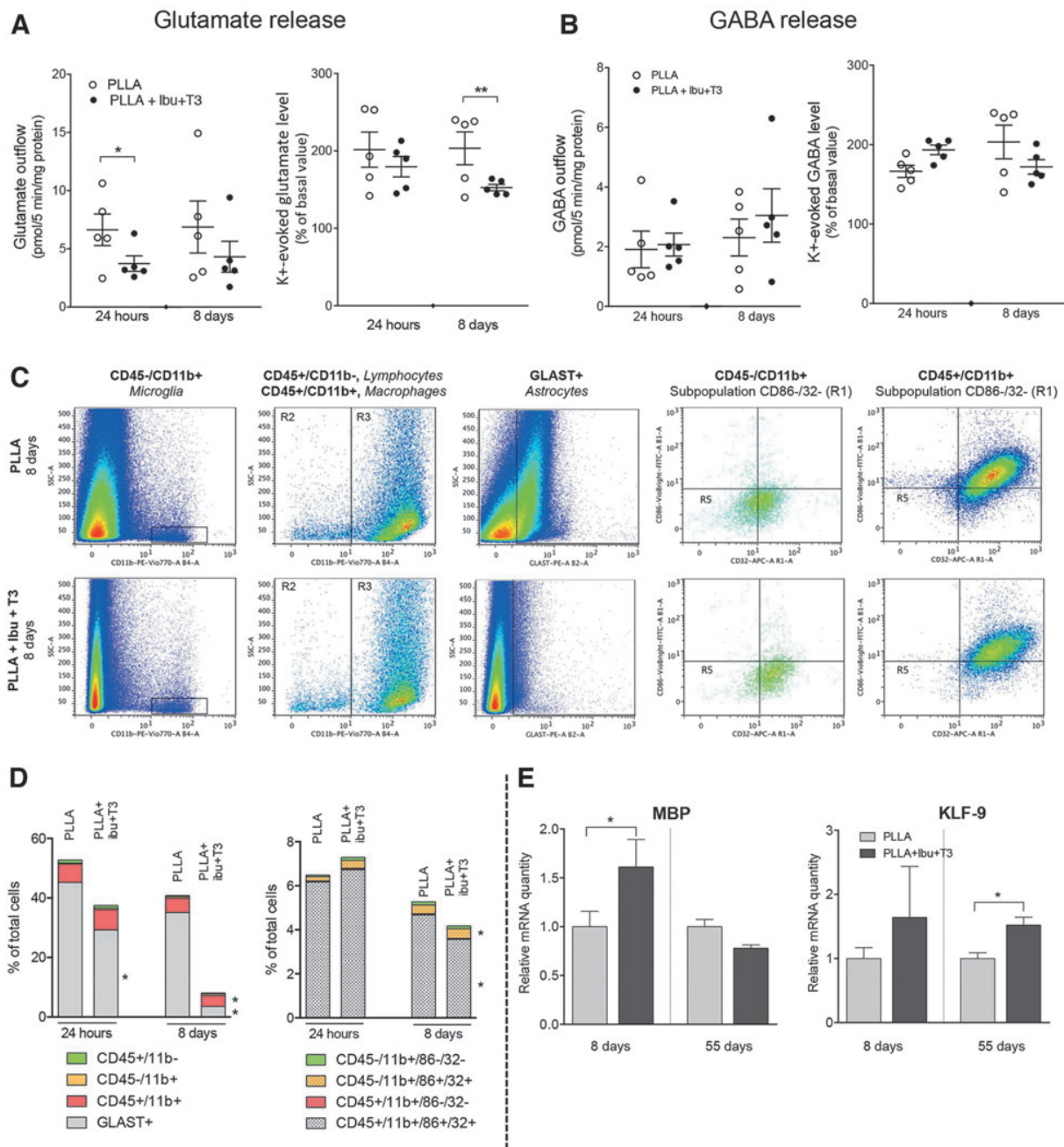


FIG. 2. PLLA-Ibu-T3 scaffolds reduce glutamate level and inflammatory cellular infiltrate at short term after lesion. (A,B) Spontaneous and K^+ -evoked glutamate (A) and GABA (B) release from synaptosomal preparation in the spinal cord at 24 h and 8 days after contusion. (C) Representative plots of the analyzed cell population by flow cytometry from PLLA and PLLA-Ibu-T3 groups at 8 days. (D) Results from the flow cytometry analysis at 24 h and 8 days, expressed as percent value of total counted cells. (E) mRNA expression level of MBP and KLF-9 in the injured spinal cord, at 8 and 55 days after lesion. Statistical analysis: one-way ANOVA and post-hoc test, $*p \leq 0.05$, $**p \leq 0.01$ for three groups comparison; Student's *t*-test, $*p \leq 0.05$, $***p \leq 0.001$ for two groups comparison. ANOVA, analysis of variance; GABA, gamma aminobutyric acid; GLAST, glutamate aspartate transporter; Ibu, ibuprofen; KLF-9, Kruppel-like factor 9; MBP, myelin basic protein; mRNA, messenger RNA; PLLA, poly (L-lactic acid); T3, triiodothyronine.

Figure 2C,D, where a representative plot for each treatment (Fig. 2C) and means variations of the respective markers (Fig. 2D) are shown. At 8 DPL, the number and proportion of $CD45^+CD11b^+$, identified as macrophages and microglia-activated cells, were significantly reduced by the treatment (PLLA, $4.83 \pm 0.85\%$; PLLA-Ibu-T3, $3.60 \pm 0.47\%$; $p < 0.05$). Inactive microglia, marked

with $CD45^{low}CD11b^+$, showed a non-significant reduction at 8 DPL in PLLA-Ibu-T3-implanted rats. Also, $CD45^+CD11b^-$ cells, which identify lymphocyte lineage, showed a non-significant trend toward reduction, and treatment-related differences were found in $CD45^+CD11b^+$ cells (microglial markers). We also investigated M1/M2 macrophage transition, using CD86 and CD32 as M1 markers

with respect to CD45⁺CD11b⁺ and CD45⁻CD11b⁺ cells. Flow cytometry data did not reveal any differences in CD86 and 32 positive cells in either group, but confirmed that the subpopulation of CD45⁺CD11b⁺ cells is reduced in PLLA-Ibu-T3-implanted rats. Finally, we also analyzed glutamate/aspartate transporter (GLAST)-positive cells, which are considered as cells belonging to the astrocytic lineage, which significantly decreased in rats treated with PLLA-Ibu-T3 (PLLA = 36.43 ± 3.57%; PLLA-Ibu-T3 = 3.60 ± 1.26%; $p < 0.0001$).

As a fast readout to test the impact of reduced inflammation on remyelination, we investigated messenger RNAs (mRNA) expression level for myelin basic protein (MBP), the most abundant myelin protein, and for KLF-9 (Kruppel-like factor 9), a T3-responsive gene implicated in OPC terminal differentiation. Both markers were upregulated in PLLA-Ibu-T3- compared to PLLA-implanted rats (Fig. 2E).^{20–22}

The poly (L-lactic acid)/ibuprofen/triiodothyronine scaffold improved functional recovery and mitigated spinal cord degeneration

Functional recovery in contused rats was monitored using the 21-point BBB scale (primary end point) and gait analysis. In the mild contusion model we used, bladder function was preserved.²³ BBB scale results are presented in Figure 3A as an interquartile range. According to the inclusion criteria of the study design, the PLLA groups included 14 rats, whereas the PLLA-Ibu-T3 group included 15 rats. Two-way ANOVA revealed a time-dependent recovery ($F_{(7,216)} = 16.57$; $p < 0.0001$), starting at day 7. In PLLA-implanted rats, the recovery stabilized at 21 DPL, after which no further improvement was observed. A significant treatment effect was observed ($F_{(7,216)} = 13.22$; $p = 0.0003$), at the analyzed time points (interaction, $F_{(7,216)} = 13.22$; $p = 0.003$). Notably, at the final observational time point (49 DPL), only 20% of PLLA-implanted rats achieved a BBB score ≥ 10 , whereas 60% of PLLA-Ibu-T3 rats achieved a score of 10 and a further 27% achieved a score ≥ 15 (Fig. 3B). At 49 DPL, the BBB recovery rate was 54.2% in PLLA-Ibu-T3 compared to 37% in PLLA implanted rats.

Recovery of locomotion was also monitored by the gait analysis (automatic trace analysis), which allows the quantification of the spatial, kinetic, comparative, and coordinator parameters of both front and hind paws. Figure 3C shows representative traces and color-coded footprints from both groups, where warm colors correspond to higher pressure. The results of the quantitative gait analysis are shown in Figure 3D, where the main spatial, comparative, kinetic, and coordination parameters are illustrated. Statistical analysis was performed by the two-tailed non-parametric Mann-Whitney U test (95% confidence level). Many parameters were different in the two groups, with higher performance, such as print/contact area for both front and hind paws and stand time of hind paws, observed in the PLLA-Ibu-T3- compared to the PLLA-implanted rats. In particular, gait coordination strongly improved in PLLA-Ibu-T3-implanted compared to control rats, as indicated by the cadence and step regularity index.

We then analyzed the anatomical outcome of the treatment, by estimating lesion volume at euthanization ($N = 10$ rats per group). The spinal cord was coronally ($N = 5$ rats per group; Fig. 4B) and longitudinally ($N = 5$ rats per group; Fig. 4D) sectioned all over the rostrocaudal and dorsoventral extension of the lesion, respectively, and the area of lesion was measured at 15 levels and expressed as a percentage area. The lesion extension covered 10 mm in a rostrocaudal direction (Fig. 4A) and 2.5 mm in depth (Fig. 4C) in both groups. However, the estimated lesion volume in PLLA-Ibu-T3-implanted rats was significantly lower compared to PLLA rats (two-way ANOVA, treatment effect, rostrocaudal, $F_{(1,105)} = 6.854$, $p = 0.0101$; dorsoventral, $F_{(1,116)} = 8.553$, $p = 0.0041$). In particular, the treatment limited the severity of lesion extension caudal to the lesion *epicentrum* and also limited its ventral progression.

We then analyzed several parameters for long-lasting tissue inflammation, demyelination, astrocyte reaction, and neuroprotection, in the spinal cord rostrally (5.6–4.8 mm) and caudally (5.6–4.8 mm) to the lesion *epicentrum*, by IHC and image analysis ($N = 5$ rats/group animals). OX42-IR, which recognizes the CR3 complement receptor (CD11b/CD18) in microglia and macrophages, was used to analyze the persistent inflammatory tissue reaction in the white (dorsal *funiculus*) and gray (dorsal horn) matter (Fig. 5A–D). In both areas, both rostrally and caudally to the lesion, OX42-IR was lower in PLLA-Ibu-T3- compared to PLLA-implanted rats (Fig. 5E,F). The drug-loaded scaffold also reduced long-lasting astroglial reaction in the gray matter (ventral horn) in particular (Fig. 5G,H), as also shown in the high-mag micrographs illustrating the ventral horn (Fig. 5I,J) and image analysis performed in the white (dorsal *funiculus*) and gray matter (dorsal and ventral horn; Fig. 5K–M). Myelin distribution was analyzed using the lipophilic stain, FluoroMyelin™, that at low magnification illustrated the more uniform myelin distribution in PLLA-Ibu-T3 compared to PLLA (Fig. 5N,O, respectively), in particular in the lateral and ventral *funiculus*. The high-power micrographs (Fig. 5P,Q, respectively) illustrated the myelin sheath rarefaction, more evident in the inserts (p,q) obtained by applying a deconvolution procedure to the original image. The FluoroMyelin-positive area fraction measured in the dorsal, lateral, and ventral *funiculus* is presented in Fig. 5R–T. Finally, we investigated the potential axonal protection in the dorsal *funiculus* (see Fig. 5X for the sampled area), which is the spinal cord area more directly involved in the contusion lesion, by analyzing the NF200-IR (Fig. 5U,V). Residual F200-IR was much higher in PLLA-Ibu-T3- compared to PLLA-implanted rats (Fig. 5W).

Discussion

Functional outcome after a spinal cord trauma is determined by the physical characteristics of the impact and by the so-called secondary degeneration, which induces and supports the progressive and long-lasting degeneration of myelin and neurons, as well as tissue cavitation. The acute phase of the lesion is therefore a recognized target for limiting the functional deficit after SCI. The

FIG. 3. PLLA-Ibu-T3 scaffolds ameliorate the locomotor recovery. (A) BBB score in rat implanted with PLLA and PLLA-Ibu-T3. Statistical analysis: two-way ANOVA; the value indicates the treatment effect. (B) Percentage of rats showing a score higher than 10 and 15, respectively, at 49 days after the contusion injury. (C) Gait trace and footprints of representative rats from the two experimental groups. The code of the respective animal is indicated (#). (D) Spatial, comparative, kinetics, and coordination parameters of the gait analysis at 49 days after the injury. All data are expressed as mean ± SEM, whereas cadence and step regularity index are reported as single rat value. Statistical analysis: Student's *t*-test, * $p < 0.05$; ** $p < 0.001$. ANOVA, analysis of variance; BBB, Basso, Beattie, Bresnahan Locomotor Rating Scale; Ibu, ibuprofen; PLD, post-lesion days; PLLA, poly (L-lactic acid); SEM, standard error of the mean; T3, triiodothyronine.

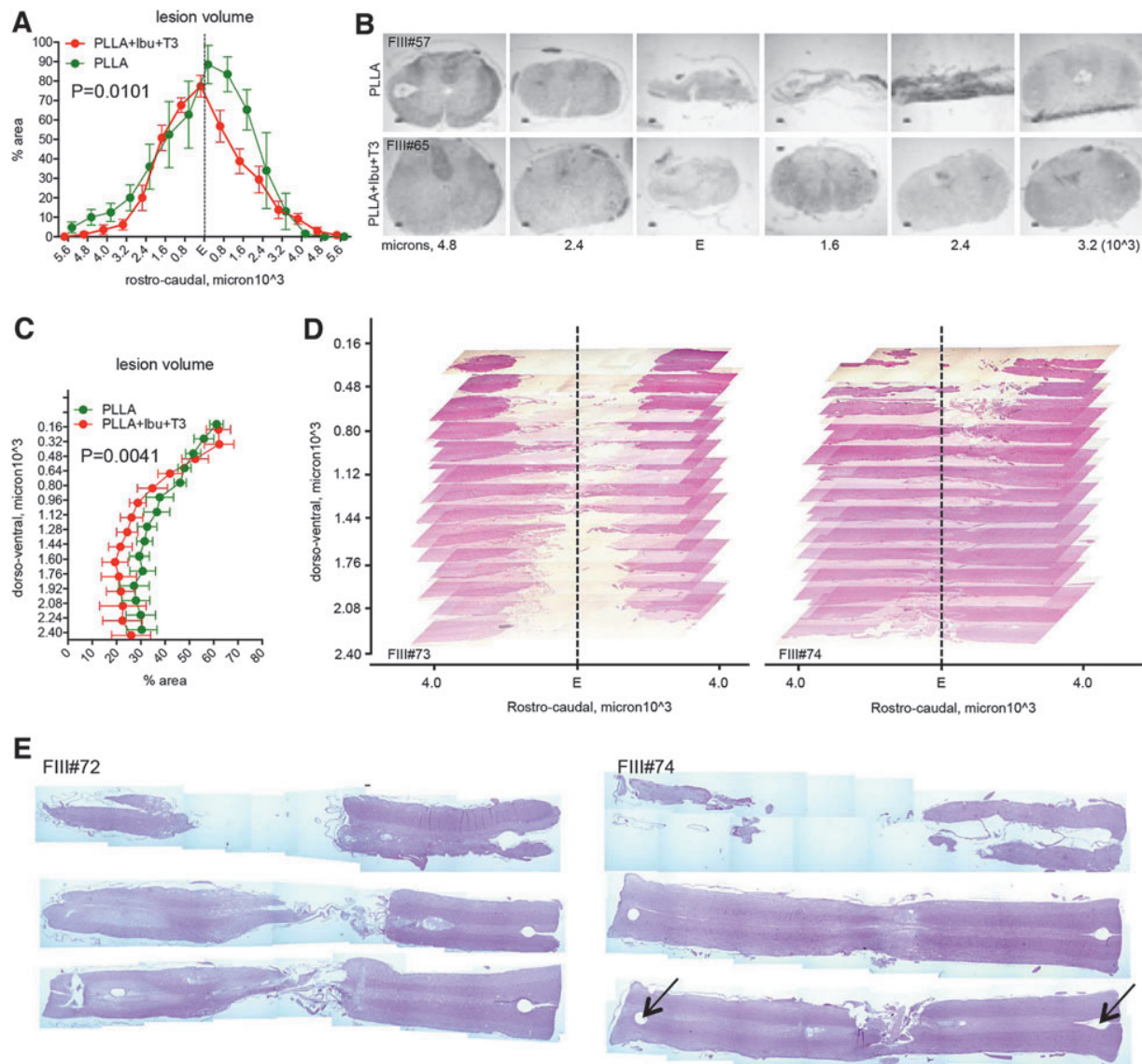


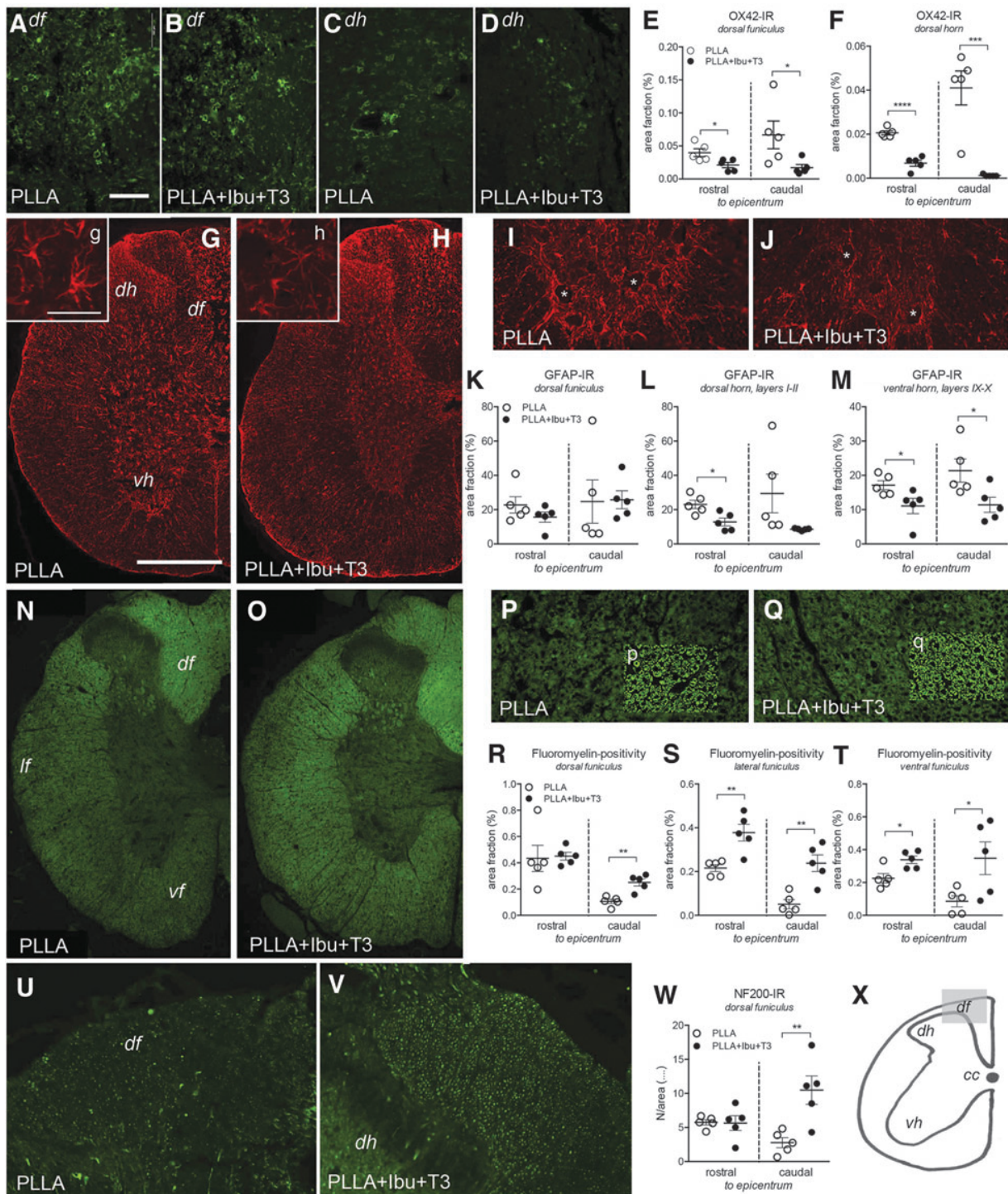
FIG. 4. PLLA-Ibu-T3 scaffolds reduces the spinal cord lesion extension. (A) Lesion extension calculated as lesioned area (%) in coronal section, over 11.2mm, rostrally and caudally to the lesion *epicentrum*. (B) Micrographs of toluidine blue stained coronal section at different rostrocaudal levels from representative rats in the two treatment groups. The animal code is indicated. (C) Lesion extension calculated as lesioned area (%) in longitudinal section (D), over the entire dorsoventral extension. (D) 3D reconstruction of the lesion by micrographs of EE-stained longitudinal section at different dorsoventral analyzed levels from representative rats in the two treatment groups. The animal code is indicated. (E) Power micrographs of EE representative stained longitudinal section at different dorsoventral levels from representative rats in the two treatment groups. The animal code is indicated. Statistical analysis: two-way ANOVA, the number refers to the treatment effect. 3D, three-dimensional; ANOVA, analysis of variance; Ibu, ibuprofen; PLLA, poly (L-lactic acid); T3, triiodothyronine.

complex molecular pathology and the limited CNS drug targeting make systemic monotherapy often inadequate for limiting secondary neurodegeneration. In this proof-of-concept study, we provide evidence that a drug combination composed by Ibu and T3 locally delivered by electrospun PLLA scaffold implanted in the spinal cord immediately after the lesion, and providing a long-lasting drug release, improves locomotion and gait coordination, resulting in a recovery rate of 46% higher compared to control, at the late observational time (49 DPL). Moreover, we demonstrated that the PLLA-Ibu-T3 scaffold improves remyelination, as indicated by the increased MBP mRNA expression level, and over-

comes the OPC differentiation block, as indicated by the KLF-9 upregulation.

The two marketed drugs, Ibu as anti-inflammatory drug, T3 as promyelinating and neuroprotective agent, and an FDA-approved biomaterial for implant in humans (PLLA), were chosen given that the study was designed to exploit drugs repositioning, combinatory therapy, and the translational potential.

NSAIDs, and in particular Ibu, has attracted great interest for the treatment of neurological diseases, currently being tested in several clinical trials. In the context of human SCI, Ibu has been indicated as a plausible strategy for the pharmacological augmentation of



neurorehabilitation and has been included in the phase I SCISSOR clinical trial (NCT02096913).^{11,24} Pre-clinical studies in which Ibu was systemically administered have provided contrasting results. In particular, in one study, long-term administration of Ibu (60 mg/kg/d, twice per day, over 42 days), reduced microglial reactivity early on, but failed to improve functional recovery, and no histological sign of neuroprotection was observed.²⁵ In another study, long-term s.c. Ibu delivery by an osmotic minipump (filled with 500 mg of Ibu, 2.5 μ L/h for 28 days, releasing 70 mg/kg/d) led to a 28% improvement of the BBB scale.²⁶

Other studies in which Ibu was orally administered showed no effect on histological or functional outcome, even in combinatory therapies.²⁷ These contrasting results have been, at least partially, explained by the limited Ibu CNS targeting; despite the fact that free Ibu rapidly crosses the blood–brain barrier, plasma protein binding limits the vascular-corrected brain concentration to 1–2% by reducing the free fraction in the bloodstream.^{18,28} Moreover, severe side effects are observed in the case of overdose by Ibu systemic administration, including CNS effects ranging from drowsiness to coma.²⁹ Notably, when Ibu was locally applied in the contused spinal cord with a poly(trimethylene carbonate-co- ϵ -caprolactone) patch, which produces a 100% drug release over 24 h, RhoA-GTP activity was decreased, demonstrating the local pharmacological activity of the drug.³⁰

In order to expand the therapeutic efficacy of Ibu in SCI, we combined it with a promyelinating agent. In fact, white matter injury is generally recognized as a major determinant in outcome after CNS traumatic and vascular lesions, impacting on axons integrity and function, and retrograde neuronal degeneration. Accordingly, remyelination, and specifically the OPCs, became a target for pharmacological as well as cell- and biomaterial-based therapeutic approaches.³¹ OPC is, in fact, the cell responsible for myelin repair, and T3 is a key component of the molecular machinery driving cell-cycle exit and terminal differentiation into myelinating oligodendrocyte.^{12,32} This process, and subsequently remyelination, is impaired during pathological conditions characterized by severe inflammation, mainly because of the OPC differentiation block, which is sustained by the inflammation-induced rise in cytokine, including tumor necrosis factor alpha, and by alteration of intracellular T3 availability in OPC.^{14,33–35}

Different and independent pre-clinical studies in rodents and non-human primates have demonstrated that exogenous TH administration is effective in overcoming the OPCs differentiation block during inflammatory/demyelinating diseases, protecting myelin and axons, and ameliorating the clinical outcome in experimental models of inflammatory/demyelinating diseases.^{16,17} However, although T3 crosses the blood–brain barrier by diffusion of by selective transporters, its systemic administration exposes one to the risk of hyperthyroidism and thyroid function suppression.

The designed electrospun scaffold guarantees a local release of the drugs compatible with available data of Ibu and T3 CNS concentration. In fact, CNS tissue concentration of Ibu after systemic administration of 60 mg/kg in constant infusion was $\sim 0.7 \mu\text{g/g}$ in the rat; the cerebrospinal fluid concentration in humans was $\sim 0.5 \mu\text{g/mL}$ after a single 800-mg oral administration.^{18,36} The physiological T3 concentration in the CNS is $\sim 15 \text{ ng} \times \text{g}^{-1}$ of CNS tissue.^{16,17} Moreover, it has been demonstrated that electrospun nanofibrous scaffold of PLLA was not completely degraded up to 12 weeks of implantation s.c. in the rat.³⁷

The proposed dual-drug delivery system is intended to be used in acute SCI, to limit secondary neurodegeneration onset and progression by controlling the injured spinal cord microenvironment,

thus affecting in cascade glial scar formation, axonal remyelination failure, and, ultimately, functional outcome. To test this hypothesis, we have included several molecular and histological exploratory end points in the study design, starting from glutamate release and macrophage infiltration in spinal cord tissue. It has been reported that after a damaging insult, several mechanisms (e.g., intracellular changes, reversal of glutamate transport, and metabolic alterations) contribute to the massive spontaneous glutamate leakage from nerve terminals.^{38–40} On the contrary, K^+ -evoked glutamate efflux is mainly associated with the neurosecretory coupling mechanisms leading to the release of the neurotransmitter from the synaptic vesicles. We proved that early (i.e., 24 h after the lesion) spontaneous glutamate release is strongly and specifically reduced in PLLA-Ibu-T3-implanted rats, an effect that appears to be reduced in synaptosomes from tissue dissected 8 days after the lesion. On the contrary, K^+ -evoked glutamate efflux is reduced in synaptosomes from tissue dissected from the PLLA-Ibu-T3 group 8 days, but not 24 h, after SCI.

Although other hypotheses cannot be ruled out, it could be speculated that excessive glutamate efflux is mainly attributed to increased glutamate leakage during the primary phase of SCI pathophysiology, while also an increase in neurosecretory coupling mechanisms seems to sustain increased glutamate release during the secondary phase. Interestingly, we proved that both early- and secondary-associated events are reduced in PLLA-Ibu-T3-implanted rats. These effects are considered beneficial in reducing not only neuronal cell death, but particularly in reducing the delayed post-traumatic white matter degeneration in the spinal cord.⁴¹

We also obtained a partial control of inflammatory infiltrate at the lesion side, and particularly macrophage tissue infiltration and microglia activation, as indicated by the reduction of CD45/CD11b-positive cells. Notably, drug-loaded PLLA also reduces astrogliosis, as measured by flow cytometry of GLAST⁺ cells at 24 h and 8 days.

This locally delivered drug combination ameliorates the primary end point (BBB score and gait parameters) of efficacy studies. Locomotion parameters in rats implanted with PLLA-Ibu-T3 scaffold are 46% higher than in control rats implanted with drug-unloaded PLLA. This therapeutic efficacy is comparable to even greater than those described in pre-clinical studies supporting ongoing clinical trials.^{42,43} In fact, and considering only positive pre-clinical data of drugs in a comparable experimental setting (i.e., in acute SCI) and the same readout (i.e., BBB score at 6–7 weeks), the BBB score amelioration in treated versus control rats was: 33% by methylprednisolone; 23% by ganglioside GM1; 35% by nimodipine; 29% by minocycline; 19% by riluzole; 30% by Rho-kinase inhibitors; 57% by granulocyte colony-stimulating factor; and 17% by anti-Nogo-A antibody.^{44–51}

In terms of long-term histopathological outcome, lesion volume was reduced in PLLA-Ibu-T3- compared to PLLA-implanted rats. Several histopathological components are potentially involved in this effect. First of all, the limitation of astroglial reaction also reduces glial fibrillary acidic protein-positive cell density at long term. The multiple roles of astrocytes in brain and spinal cord trauma are known. In the context of SCI, astrocytes are considered a major component of the glial scar, starting activation immediately after SCI and eventually leading to cyst and cavity formation.⁵² Myelin, too, is positively affected, in both ascending and descending pathways, indicating that this drug combination and its local concentration protects OPCs, also favoring the full differentiation into myelinating OL. Although there is conflicting evidence in experimental SCI as to whether chronic demyelination is a component of

long-term SCI pathophysiology and functional outcome, extensive literature indicates that oligodendrogenesis and early remyelination exert an important role in protecting axons from long-term degeneration (Preferred Reporting Items for Systematic Reviews and Meta-Analyses [PRISMA] meta-analysis).^{53,54}

Overall, this proof-of-concept study leads us to conclude that 1) locally delivered drug combinations should be investigated for their ability to target complex conditions, such as the early phase of the SCI. Notably, when Ibu or T3 are locally delivered as monotherapy in SCI, no long-term functional recovery was observed^{55,56}; 2) biomaterial-assisted delivery systems might help to overcome the severe brain diffusion problems, which limits pharmacological interventions; 3) Ibu + T3 delivered locally are able to limit secondary degeneration, leading to a substantial improvement of the functional locomotor outcome; 4) given that these results are obtained by already-marketed drugs and an FDA-approved polymer for tissue implantation, this therapeutic solution could have a shorter regulatory path; and 5) there is also ample room for improvement of this mixed device toward possible clinical application, as different fabrication solution such as micro- and nanoparticles resulting in an injectable solution that could be used in closed spinal cord lesions and in other brain lesions characterized by inflammation and extensive demyelination.

Acknowledgments

Prof. Nadia Passerini (FaBit, University of Bologna) and Prof. Giampiero Pagliuca (DIMEVET, University of Bologna) are gratefully acknowledged for Ibu and T3 assay, respectively. Prof. Maria Laura Bolognesi (FaBit, University of Bologna) is gratefully acknowledged for useful discussion in drug-delivery solution. We thank the patients of the Montecatone Rehabilitation Institute, Montecatone, Imola, Italy, for the continuous stimulus “from the bedside.” A special thanks to R.V.

Author Contributions

A.B., A.G., and L.L. performed animal surgery and care, locomotion testing; M.L.F., C.G. performed material design and preparation; M.P. performed Immunohistochemistry and image analysis; A.B. and M.P. performed flow cytometry experiments; S.B. and L.F. performed GABA and glutamate dosage; L.G. contributed to the study design and data analysis; L.C. ideated and designed the study, performed statistical analysis, interpreted the data, and wrote the manuscript.

Funding Information

This work has been supported by the POR-FESR 2014-18, project “Step-by-Step”, Emilia Romagna Region (to L.C.). The contribution of “Fondazione Montecatone”, Imola, Italy, and Cluster Tecnologici Nazionali, project IRMI (CTN01_00177_888744), MIUR (to L.C.) are also acknowledged. A special acknowledgment to the GLP-certified CRO TransMed Research srl, who provided the GLP studies for free, in the frame of the “Step-by-Step” project.

Author Disclosure Statement

An international patent application from the University of Bologna is pending (PCT/IT2018/000084) (inventors: L.C., L.G., M.L.F., C.G.; no competing financial interests exist for A.B., L.L., A.G., M.P., S.B., L.F.).

References

- van den Berg, M.E., Castellote, J.M., Mahillo-Fernandez, I., and de Pedro-Cuesta, J. (2010). Incidence of spinal cord injury worldwide: a systematic review. *Neuroepidemiology* 34, 184–192.
- Saghazadeh, A., and Rezaei, N. (2017). The role of timing in the treatment of spinal cord injury. *Biomed. Pharmacother.* 92, 128–139.
- Rossignol, S., Schwab, M., Schwartz, M., and Fehlings, M.G. (2007). Spinal cord injury: time to move? *J. Neurosci.* 27, 11782–11792.
- Hayta, E., Elden, H. (2018). Acute spinal cord injury: a review of pathophysiology and potential of non-steroidal anti-inflammatory drugs for pharmacological intervention. *J. Chem. Neuroanat.* 87, 25–31.
- Scholtes, F., Adriaensens, P., Storme, L., Buss, A., Kakulas, A.B., Gelan, J., Beuls, E., Schoenen, J., Brook, G.A., and Martin, D. (2006). Correlation of postmortem 9.4 tesla magnetic resonance imaging and immunohistopathology of the human thoracic spinal cord 7 months after traumatic cervical spine injury. *Neurosurgery* 59, 671–678.
- Aarabi, B., Simard, J.M., Kufera, J.A., Alexander, M., Zacherl, K.M., Mirvis, S.E., Shanmuganathan, K., Schwartzbauer, G., Maulucci, C.M., Slavin, J., Ali, K., Massetti, J., and Eisenberg, H.M. (2012). Intramedullary lesion expansion on magnetic resonance imaging in patients with motor complete cervical spinal cord injury. *J. Neurosurg. Spine* 17, 243–250.
- Evaniew, N., Belley-Côté, E.P., Fallah, N., Noonan, V.K., Rivers, C.S., and Dvorak, M.F. (2016). Methylprednisolone for the treatment of patients with acute spinal cord injuries: a systematic review and meta-analysis. *J. Neurotrauma* 33, 468–481.
- Stahel, P.F., VanderHeiden, T., and Finn, M.A. (2012). Management strategies for acute spinal cord injury: current options and future perspectives. *Curr. Opin. Crit. Care* 18, 651–660.
- Shank, C.D., Walters, B.C., and Hadley, M.N., (2017). Management of acute traumatic spinal cord injuries. *Handb. Clin. Neurol.* 140, 275–298.
- Wang, X., Budel, S., Baughman, K., Gould, G., Song, K.H., and Strittmatter, S.M. (2009). Ibuprofen enhances recovery from spinal cord injury by limiting tissue loss and stimulating axonal growth. *J. Neurotrauma* 26, 81–95.
- Kopp, M.A., Liebscher, T., Watzlawick, R., Martus, P., Laufer, S., Blex, C., Schindler, R., Jungehulsing, G.J., Knüppel, S., Kreuzträger, M., Ekkernkamp, A., Dirnagl, U., Strittmatter S.M., Niedeggen, A., and Schwab, J.M. (2016). SCISSOR-Spinal Cord Injury Study on Small molecule-derived Rho inhibition: a clinical study protocol. *BMJ Open* 6, e010651.
- Billon, N., Jolicœur, C., Tokumoto, Y., Vennström, B., and Raff, M. (2002). Normal timing of oligodendrocyte development depends on thyroid hormone receptor alpha 1 (TRalpha1). *EMBO J.* 21, 6452–6460.
- Kuhlmann, T., Miron, V., Cui, Q., Wegner, C., Antel, J., and Brück, W. (2008). Differentiation block of oligodendroglial progenitor cells as a cause for remyelination failure in chronic multiple sclerosis. *Brain* 131, 1749–1758.
- Fernández, M., Baldassarro, V.A., Sivilia, S., Giardino, L., and Calzà, L. (2016). Inflammation severely alters thyroid hormone signaling in the central nervous system during experimental allergic encephalomyelitis in rat: direct impact on OPCs differentiation failure. *Glia* 64, 1573–1589.
- Calzà, L., Fernández, M., Giuliani, A., Aloe, L., and Giardino, L. (2002). Thyroid hormone activates oligodendrocyte precursors and increases a myelin-forming protein and NGF content in the spinal cord during experimental allergic encephalomyelitis. *Proc. Natl. Acad. Sci. U. S. A.* 99, 3258–3263.
- Calzà, L., Fernández, M., and Giardino, L. (2015). Role of the thyroid system in myelination and neural connectivity. *Compr. Physiol.* 5, 1405–1421.
- Calzà, L., Baldassarro, V.A., Fernández, M., Giuliani, A., Lorenzini, L., and Giardino, L. (2018). Thyroid hormone and the white matter of the central nervous system: from development to repair. *Vitam. Horm.* 106, 253–281.
- Mannila, A., Rautio, J., Lehtonen, M., Järvinen, T., and Savolainen, J. (2005). Inefficient central nervous system delivery limits the use of ibuprofen in neurodegenerative diseases. *Eur. J. Pharm. Sci.* 24, 101–105.
- Basso, D.B., Beattie M.S., and Bresnahan, J.C. (1995). A sensitive and reliable locomotor rating scale for open field testing in rats. *J. Neurotrauma* 12, 1–21.
- Baldassarro, V.A., Krężel, W., Fernández, M., Schuhbauer, B., Giardino, L., and Calzà, L. (2019). The role of nuclear receptors in the

- differentiation of oligodendrocyte precursor cells derived from fetal and adult neural stem cells. *Stem Cell Res.* 37, 101443.
21. Ozgen, H., Baron, W., Hoekstra, D., and Kahya N. (2016). Oligodendroglial membrane dynamics in relation to myelin biogenesis. *Cell. Mol. Life Sci.* 73, 3291–3310.
 22. Dugas, J.C., Ibrahim, A., and Barres, B.A. (2012). The T3-induced gene KLF9 regulates oligodendrocyte differentiation and myelin regeneration. *Mol. Cell. Neurosci.* 50, 45–57.
 23. Pikov, V., and Wrathall, J.R. (2001). Coordination of the bladder detrusor and the external urethral sphincter in a rat model of spinal cord injury: effect of injury severity. *J. Neurosci.* 21, 559–569.
 24. Watzlawick, R., Sena, E.S., Dirnagl, U., Brommer, B., Kopp, M.A., Macleod, M.R., Howells, D.W., and Schwab, J.M. (2014). Effect and reporting bias of RhoA/ROCK-blockade intervention on locomotor recovery after spinal cord injury: a systematic review and meta-analysis. *JAMA Neurol.* 71, 91–99.
 25. Redondo-Castro, E., and Navarro, X. (2014). Chronic ibuprofen administration reduces neuropathic pain but does not exert neuroprotection after spinal cord injury in adult rats. *Exp. Neurol.* 252, 95–103.
 26. Sharp, K.G., Yee, K.M., Stiles, T.L., Aguilar, R.M., and Steward, O. (2013). A re-assessment of the effects of treatment with a non-steroidal anti-inflammatory (ibuprofen) on promoting axon regeneration via RhoA inhibition after spinal cord injury. *Exp. Neurol.* 248, 321–337.
 27. Streijger, F., Lee, J.H., Duncan, G.J., Ng, M.T., Assinck, P., Bhatnagar, T., Plunet, W.T., Tetzlaff, W., and Kwon, B.K. (2014). Combinatorial treatment of acute spinal cord injury with ghrelin, ibuprofen, C16, and ketogenic diet does not result in improved histologic or functional outcome. *J. Neurosci. Res.* 92, 870–883.
 28. Parepally, J.M., Mandula, H., and Smith, Q.R. (2006). Brain uptake of nonsteroidal anti-inflammatory drugs: ibuprofen, flurbiprofen, and indomethacin. *Pharm. Res.* 23, 873–881.
 29. Auriel, E., Regev, K., and Korczyn, A.D. (2014). Nonsteroidal anti-inflammatory drugs exposure and the central nervous system. *Handb. Clin. Neurol.* 119, 577–584.
 30. Pires, L.R., Lopes, C.D.F., Salvador, D., Rocha, D.N., and Pêgo, A.P. (2017). Ibuprofen-loaded fibrous patches-taming inhibition at the spinal cord injury site. *J. Mater. Sci. Mater. Med.* 28, 157.
 31. Chew, L.J., and DeBoy, C.A. (2016). Pharmacological approaches to intervention in hypomyelinating and demyelinating white matter pathology. *Neuropharmacology* 110, 605–625.
 32. Lee, J.Y., and Petratos, S. (2016). Thyroid hormone signaling in oligodendrocytes: from extracellular transport to intracellular signal. *Mol. Neurobiol.* 53, 6568–6583.
 33. Hassannejad, Z., Shakouri-Motlagh, A., Mokhtab, M., Zadeegan, S.A., Sharif-Alhoseini, M., Shokraneh, F., and Rahimi-Movaghar, V. (2019). Oligodendroglialogenesis and axon remyelination after traumatic spinal cord injuries in animal studies: a systematic review. *Neuroscience* 402, 37–50.
 34. Billiards, S.S., Haynes, R.L., Folkert, R.D., Borenstein, N.S., Trachtenberg, F.L., Rowitch, D.H., Ligon, K.L., Volpe, J.J., and Kinney, H.C. (2008). Myelin abnormalities without oligodendrocyte loss in periventricular leukomalacia. *Brain Pathol.* 18, 153–163.
 35. Valentin-Torres, A., Savarin, C., Barnett, J., and Bergmann, C.C. (2018). Blockade of sustained tumor necrosis factor in a transgenic model of progressive autoimmune encephalomyelitis limits oligodendrocyte apoptosis and promotes oligodendrocyte maturation. *J. Neuroinflammation* 15, 121.
 36. Bannwarth, B., Lopicque, F., Pehourcq, F., Gillet, P., Schaefferbeke, T., Laborde, C., Dehais, J., Gaucher, A., and Netter, P. (1995). Stereoselective disposition of ibuprofen enantiomers in human cerebrospinal fluid. *Br. J. Clin. Pharmacol.* 40, 266–269.
 37. Ishii, D., Ying, T.H., Mahara, A., Murakami, S., Yamaoka, T., Lee, W.K., and Iwata, T. (2009). In vivo tissue response and degradation behavior of PLLA and stereocomplexed PLA nanofibers. *Biomacromolecules* 10, 237–242.
 38. Phillis, J.W., and O'Regan, M.H. (1996). Mechanisms of glutamate and aspartate release in the ischemic rat cerebral cortex. *Brain Res.* 730, 150–164.
 39. Li, S., Mealing, G.A., Morley, P., and Stys, P.K. (1999). Novel injury mechanism in anoxia and trauma of spinal cord white matter: glutamate release via reverse Na⁺-dependent glutamate transport. *J. Neurosci.* 19, RC16.
 40. Sheldon, A.L., and Robinson, M.B. (2007). The role of glutamate transporters in neurodegenerative diseases and potential opportunities for intervention. *Neurochem. Int.* 51, 333–355.
 41. Park, E., Velumian, A.A., and Fehlings, M.G. (2004). The role of excitotoxicity in secondary mechanisms of spinal cord injury: a review with an emphasis on the implications for white matter degeneration. *J. Neurotrauma* 21, 754–774.
 42. Badhiwala, J.H., Ahuja, C.S., and Fehlings, M.G. (2018). Time is spine: a review of translational advances in spinal cord injury. *J. Neurosurg. Spine* 30, 1–18.
 43. Gomes-Osman, J., Cortes, M., Guest, J., and Pascual-Leone, A. (2019). Systematic review of experimental strategies aimed at improving motor function after acute and chronic spinal cord injury. *J. Neurotrauma* 33, 425–438.
 44. Liu, D., Shan, Y., Valluru, L., and Bao, F. (2013). Mn (III) tetrakis (4-benzoic acid) porphyrin scavenges reactive species, reduces oxidative stress, and improves functional recovery after experimental spinal cord injury in rats: comparison with methylprednisolone. *BMC Neurosci.* 14, 23.
 45. Marcon, R.M., Cristante, A.F., de Barros Filho, T.E., de Oliveira, R.P., and dos Santos, G.B. (2010). Potentializing the effects of GM1 by hyperbaric oxygen therapy in acute experimental spinal cord lesion in rats. *Spinal Cord* 48, 808–813.
 46. Jia, Y.F., Gao, H.L., Ma, L.J., and Li, J. (2015). Effect of nimodipine on rat spinal cord injury. *Genet. Mol. Res.* 14, 1269–1276.
 47. Ahmad, M., Zakaria, A., and Almutairi, K.M. (2016). Effectiveness of minocycline and FK506 alone and in combination on enhanced behavioral and biochemical recovery from spinal cord injury in rats. *Pharmacol. Biochem. Behav.* 145, 45–54.
 48. Mu, X., Azbill, R.D., and Springer, J.E. (2000). Riluzole and methylprednisolone combined treatment improves functional recovery in traumatic spinal cord injury. *J. Neurotrauma* 17, 773–780.
 49. Dergham, P., Ellezam, B., Essagian, C., Avedissian, H., Lubell, W.D., and McKerracher, L. (2002). Rho signalling pathway targeted to promote spinal cord repair. *J. Neurosci.* 22, 6570–6577.
 50. Chen, W.F., Chen, C.H., Chen, N.F., Sung, C.S., and Wen, Z.H. (2015). Neuroprotective effects of direct intrathecal administration of granulocyte colony-stimulating factor in rats with spinal cord injury. *CNS Neurosci. Ther.* 21, 698–707.
 51. Liebscher, T., Schnell, L., Schnell, D., Scholl, J., Schneider, R., Gullo, M., Fouad, K., Mir, A., Rausch, M., Kindler, D., Hamers, F.P., and Schwab, M.E. (2005). Nogo-A antibody improves regeneration and locomotion of spinal cord-injured rats. *Ann. Neurol.* 58, 706–719.
 52. Okada, S., Hara, M., Kobayakawa, K., Matsumoto, Y., and Nakashima, Y. (2018). Astrocyte reactivity and astrogliosis after spinal cord injury. *Neurosci. Res.* 126, 39–43.
 53. Duncan, G.J., Manesh, S.B., Hilton, B.J., Assinck, P., Liu, J., Moulson, A., Plemel, J.R., and Tetzlaff, W. (2018). Locomotor recovery following contusive spinal cord injury does not require oligodendrocyte remyelination. *Nat. Commun.* 9, 3066.
 54. Hassannejad, Z., Shakouri-Motlagh, A., Mokhtab, M., Zadeegan, S.A., Sharif-Alhoseini, M., Shokraneh, F., and Rahimi-Movaghar, V. (2019). Oligodendroglialogenesis and axon remyelination after traumatic spinal cord injuries in animal studies: a systematic review. *Neuroscience* 402, 37–50.
 55. Qi, L., Jiang, H., Cui, X., Liang, G., Gao, M., Huang, Z., and Xi, Q. (2017). Synthesis of methylprednisolone loaded ibuprofen modified dextran based nanoparticles and their application for drug delivery in acute spinal cord injury. *Oncotarget* 8, 99666–99680.
 56. Shultz, R.B., Wang, Z., Nong, J., Zhang, Z., and Zhong, Y. (2017). Local delivery of thyroid hormone enhances oligodendrogenesis and myelination after spinal cord injury. *J. Neural Eng.* 14, 036014.

Address correspondence to:

Laura Calzà, MD
CIRI-SDV and FaBit
University of Bologna
Via Tolara di Sopra 41/E
40064 Ozzano Emilia, Bologna
Italy

E-mail: laura.calza@unibo.it

4.7. White Matter and Neuroprotection in Alzheimer's Dementia

(Molecules, 25:503-517, 2020)

Review

White Matter and Neuroprotection in Alzheimer's Dementia

Luca Lorenzini ^{1,2}, Mercedes Fernandez ¹, Vito Antonio Baldassarro ^{3,4} , Andrea Bighinati ¹ , Alessandro Giuliani ¹ , Laura Calza ^{2,3} and Luciana Giardino ^{1,2,*}

¹ Department of Veterinary Medical Sciences, University of Bologna, Ozzano Emilia, 40064 Bologna, Italy; luca.lorenzini8@unibo.it (L.L.); mercedes.fernandez@unibo.it (M.F.); andrea.bighinati@unibo.it (A.B.); a.giuliani@unibo.it (A.G.)

² Interdepartmental Center for Industrial Research in Life Sciences and Technologies, University of Bologna, Ozzano Emilia, 40064 Bologna, Italy; laura.calza@unibo.it

³ Department of Pharmacy and Biotechnology, University of Bologna, 40126 Bologna, Italy; vito.baldassarro2@unibo.it

⁴ Fondazione IRET, Ozzano Emilia, 40064 Bologna, Italy

* Correspondence: luciana.giardino@unibo.it

Received: 27 December 2019; Accepted: 21 January 2020; Published: 23 January 2020



Abstract: Myelin is the main component of the white matter of the central nervous system (CNS), allowing the proper electrical function of the neurons by ensheathing and insulating the axons. The extensive use of magnetic resonance imaging has highlighted the white matter alterations in Alzheimer's dementia (AD) and other neurodegenerative diseases, alterations which are early, extended, and regionally selective. Given that the white matter turnover is considerable in the adulthood, and that myelin repair is currently recognized as being the only true reparative capability of the mature CNS, oligodendrocyte precursor cells (OPCs), the cells that differentiate in oligodendrocyte, responsible for myelin formation and repair, are regarded as a potential target for neuroprotection. In this review, several aspects of the OPC biology are reviewed. The histology and functional role of OPCs in the neurovascular-neuroglial unit as described in preclinical and clinical studies on AD is discussed, such as the OPC vulnerability to hypoxia-ischemia, neuroinflammation, and amyloid deposition. Finally, the position of OPCs in drug discovery strategies for dementia is discussed.

Keywords: amyloid; oligodendrocyte precursor cells; oxygen-glucose deprivation; drug screening

1. Introduction

“White matter” (WM) in the central nervous system (CNS) represents approximately 50% of brain mass [1]. WM mainly contains axons ensheathed by repeated windings of oligodendrocyte (OL) cytoplasm, providing a “myelin enriched” sheath which insulates the axons to permit proper electrical functioning of the neurons [2]. In fact, OLs are the cells responsible for myelin production in the CNS and contribute to providing metabolic support for the neurons.

The WM compartment is highly dynamic, due to the biochemical turnover of the main constitutive proteins (proteolipid protein (PLP) and myelin basic protein (MBP)) and lipids (cholesterol and the galactolipids galactosylceramide and sulfatide), but also to the phenomena known as “WM plasticity” or “myelin plasticity”. These terms refer to the de novo myelination of previously unmyelinated axons, to myelin sheaths replacement, or to the myelin remodeling which occurs during a person's lifetime, as a consequence of multiple environmental factors such as voluntary physical exercise, social enrichment, motor learning, and cognitive training [3–5].

This plasticity, together with the increasing knowledge of the cell types responsible for myelin dynamics, i.e., the oligodendrocyte precursor cell (OPC), has raised a number of questions regarding

the possible role of myelin and/or myelin-forming cells in neuropathology, not only in multiple sclerosis (MS), where the myelin is the target of the autoimmune attack, but also in a variety of other neurodegenerative diseases.

In this review we will discuss data regarding the possible role of WM pathology in the onset/progression of Alzheimer's dementia (AD), focusing on OPCs as potential therapeutic target.

2. White Matter Plasticity in the Adult Brain, Ageing, Cognitive Decline, and Alzheimer's Dementia: Focus on Oligodendrocyte Precursor Cells (OPC)

An important observation highlighting WM contribution to the human brain function is that WM has expanded more than the grey matter throughout human evolution, suggesting that human cognition depends on brain connectivity [6,7]. The persistence of an appropriate myelin plasticity over the lifespan, moreover, means that axon wrapping by the OLs is modified depending on functional demand [8]: indeed the wrapping of OL cytoplasm around the axons determines the thickness of the myelin sheath and the internode length [9]. Moreover, OLs are metabolically active and functionally connected to the axon via cytoplasm-rich "myelinic channels", through which the OL takes up blood-derived glucose and delivers glycolysis products (pyruvate/lactate) to myelinated axons via monocarboxylate transporters (MCT1 and MCT2) [10,11]. WM plasticity is influenced by a variety of regulators, including daylight rhythm, gender and pregnancy, voluntary physical exercise, environmental and social environment, motor learning, and cognitive training [3].

The cellular compartments most probably responsible for correlating complex behaviors to the myelin structure is the OL-axon unit. OLs derive from OPCs generated during development, which fully differentiate into myelinating OLs throughout birth and in the postnatal period. However, a significant population of OPCs persists in the adult CNS, as identified by the expression of the Neuron-glia antigen 2, a chondroitin sulfate proteoglycan referred as NG2 (CSPG4) and of platelet-derived growth factor alpha receptor (PDGF α R). Under appropriate conditions, resident and newly generated OPCs from neural stem cells (NSCs) of the subventricular zone (SVZ) actively proliferate, migrate to the nude axons, and differentiate into mature OLs [12,13]. NG2-positive OPCs are responsible for the generation of OLs across the lifespan to replace lost myelin, provide new OLs to myelinate new connections formed in response to increased neural activity, and repair the myelin in the event of injury or disease [14,15]. This process is finely and temporally regulated by a complex interplay between intrinsic and extrinsic factors.

OPCs also play an active role in activity-dependent neuronal plasticity, forming synaptic-like structures with presynaptic elements in several brain regions which contribute to activity-dependent neural plasticity [16,17], whereas presynaptic neurotransmitters bind to OPC receptors regulating OPC proliferation and differentiation [18,19]. Via this mechanism, therefore, which involves several molecules (ATP, LIF, adenosine, etc), receptors (NMDAR), and vesicular and non-vesicular release, neuronal inputs regulate OPC proliferation and differentiation [5]. Increasing recent evidence shows that neuronal activity induced by learning and by behavioral experiences such as locomotor activity promote myelination *in vivo*, whereas reduced social interaction decreases myelin-related gene products and myelin thickness [5]. This evidence obtained in laboratory animals is also supported by MRI studies in humans [20], proving the dynamic nature of myelin in adulthood and its close relation to neuronal activity.

Age-related structural and functional brain changes are well documented in humans as well as in laboratory animals, and include smaller global brain volumes, reduced cortical thickness, and expansion of the ventricular system, leading to the view that the decline in motor, sensory, and cognitive abilities in aging might be also associated with these structural changes [21]. The extensive use of MRI has shown that WM alterations in aging are numerous and extensive and different studies have identified WM atrophy [22], WM tract disruption [23], and loss of myelination [24]. Histopathological findings in human samples and aged experimental animals also reveal that the integrity of paranodes, which anchor the myelin sheath to the axon membrane, may be altered in aging, possibly due to the

age-related alteration of MBP 21.5 kDa isoform, or the dysregulation of the enzyme cyclic nucleotide phosphodiesterase (CNPase). OL generation slows with ageing, due to the OPCs spending more time in the early G1 phase, resulting in a longer cell cycle [3]. OPCs in older mice also differentiate much more slowly than in younger mice, possibly because of epigenetic changes, i.e., histone deacetylase recruitment [25].

The contribution of WM alteration to the disturbance of cognitive function is documented by clinical neurology and MRI and Diffusion Tensor Imaging (DTI), techniques which allow researchers to visualize the WM tract [7]. WM hyperintensities (WMHs) are related to cognitive dysfunction in the general population, and a significant WM loss manifesting both microstructurally and macrostructurally has been described in AD patients. These alterations are evident in several fiber pathways, while a reduction in fiber density and cross-section in mild cognitive impairment patients have been described in the posterior cingulum only. Notably, these degenerative changes have not been associated with a high amyloid plaque burden [26,27], while other studies correlates WM pathology in preclinical AD with biomarkers in the cerebrospinal fluid [28].

3. OPCs and Mature Oligodendrocytes in Alzheimer's Disease and Animal Models

AD has classically been associated with a pathological Grey Matter (GM) process, where extracellular neuritic plaques of amyloid-beta ($A\beta$) and intraneuronal aggregates of neurofibrillary tangles made of phosphorylated tau protein are considered the main cause of neurodegeneration. In spite of the fact that, in the last years, many studies have demonstrated the involvement of WM in AD pathogenesis, the mechanism underlying these alterations, as also investigated in AD animal models, are not clear [29,30].

In particular, the timing of OPC and WM abnormalities with regard to the early onset of cognitive impairment has not been clarified. Actually, AD clinical signs appear after a presymptomatic preclinical phase lasting decades, which is also resumed by available animal models, and it is generally believed that this phase must be regarded with particular attention to find the appropriate time window for therapeutic approaches. We have extensively studied the histopathology and neurochemistry of the preclinical phase of AD in the mouse model Tg2576, carrying the APP KM670/671NL (Swedish) modification, showing that (1) intraneuronal and intraglial $A\beta$ accumulation precedes amyloid plaque deposition [31,32]; (2) intraneuronal $A\beta$ accumulation increases neuronal vulnerability to oxygen-glucose deprivation (OGD) [33]; (3) a molecular dysfunction involving HIF signaling in the cerebral cortex, also regarding the vascular endothelial growth factor receptor, is already present in 3-month-old animals, while plaque deposition starts at 8 months [32]; and that neurotransmitters (acetylcholine, GABA and glutamate) are also altered prior to plaque deposition [34,35]. We then investigated molecular markers for OPC and myelin formation at different ages (1, 3, 5, 10–14, 27–30 months) in the Tg2576 model, compared to an age-matched wild-type (Wt, for materials and methods see Appendix A). We have analyzed *PDGFaR*, as a marker of OPC/pre-OL stage, and *MBP* as marker for mature myelinating OLs (Figure 1). In our animal model, the mRNA expression of *PDGFaR* peaks at 5 months in both genotypes (around 6-fold in Wt and 2.5-fold in Tg2576), mRNA levels being significantly lower in the Tg2576 compared to Wt at this time point. The expression of *PDGFaR* is then down-regulated at 10–14 months and at the last group of age studied, 27–30 months, the last age group studied (Figure 1A). Overall, and according to the two-way ANOVA analysis, the expression level of *PDGFaR* is different in the two genotypes. *MBP* mRNA slightly higher in the Wt group of animals at 3 months, whereas in Tg2576 animals it decreases (around 0.5-fold), but peaks afterwards at 5 months in both genotypes (around 4-fold in Wt and 2-fold in Tg2576). It subsequently decreases at 10–14 months, finally increasing to achieve the same level of expression at the oldest age investigated (Figure 1B).

We then studied the expression of the transcription factors involved in OPC differentiation into mature myelinating OLs, i.e., *Olig-1* and *Olig-2*, whose expression spans from the neuroprecursor cell stage to mature myelinating OLs, and *Klf-9* (*Kruppel-like factor 9*), which is up-regulated as soon as

the OPCs exit the cell cycle in the presence of T3, to fully differentiate (Figure 2). Considering the age of 1 month as the 100%, the expression of *Olig-1* increases at 3 months of age in the Wt group of animals (at around 107%), peaks at 5 months (at around 128%), then decreases at the 10–14 and 27–30 time points (to around 117% and 121%, respectively). In the Tg2576 group of animals, *Olig-1* expression decreases at 3 months (to around 94%), increases at 5 months to the higher mRNA level (to around 117%), then decreases again at 10–14 months, finally increasing at 20–27 months, the last time point studied (at around 118%) (Figure 2A). The changes in the mRNA levels of *Olig-2* in both the Wt and Tg2576 animals are lower than the changes in *Olig-1* mRNA. In the Wt animals it reaches the highest level from between 5 and 10–14 months (at around 107%), then decreasing to 104% (Figure 2B). The *Olig-2* expression profile in the Tg2576 group of animals is the opposite of the Wt group, significantly decreasing to around 94% at 3 months, before returning to 100% at the last time points. Overall, and according to the two-way ANOVA analysis, the expression level of both *Olig-1* and *Olig-2* is different in the two genotypes. The age-related changes in *Klf-9* mRNA is the same in both Wt and Tg2576 (Figure 2C), decreasing at 3 months (to around 90%), then peaking at 5 months (to around 130%). It decreases again at 10–14 months (to around 110%) and finally it increases (to around 125%).

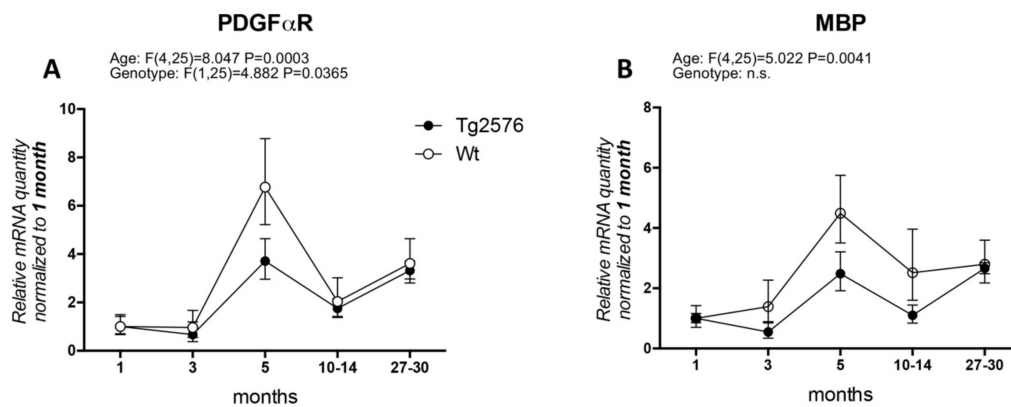


Figure 1. Age-related variation of oligodendrocyte lineage markers. (A) platelet-derived growth factor alpha receptor (*PDGF α R*) gene expression in Wt and Tg2576 at different age timepoints; (B) myelin basic protein (*MBP*) gene expression in Wt and Tg2576 at different age time points. Relative expression has been normalized to 1 month matched for each genotype. Statistical analysis has been performed through 2-way ANOVA, considering age (months) and genotype (Wt and Tg2576) as variables; $n = 3-5$. Results are significant when $p < 0.05$.

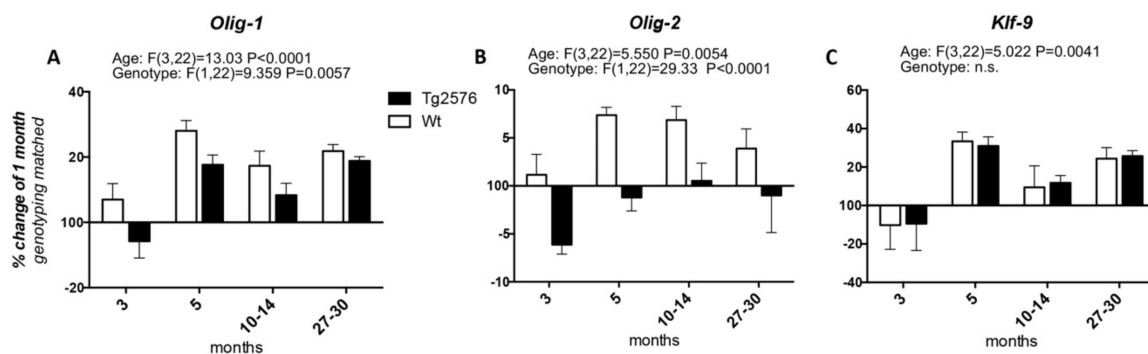


Figure 2. Age-related variation of oligodendrocyte precursor cells to oligodendrocyte transcription factors. The graphs show the expression profile of *Olig-1* (A), *Olig-2* (B), and *Klf-9* (C) transcription factors. Relative expression has been normalized to 1-month for each genotype and given the value of 100%. Results are expressed as the % of variation compared to the 1-month genotype-matched, Wt and Tg2576, groups of animals. Statistical analysis has been performed through 2-way ANOVA, considering age (months) and genotype (Wt and Tg2576) as variables; $n = 3-5$. Results are significant when $p < 0.05$.

To the best of our knowledge, the literature regarding the study of OPCs/OLs in AD and related animal models is scarce. Studies in APP-PS1 mice have demonstrated an increase in OPCs at 6–8 months of age [36], as observed in our Tg2576 mice where the expression level of the OPC marker *PDGF α R* gene is significantly higher at 5 months. Similarly, studies performed in postmortem human AD have revealed an increase in the number of PDGF α R positive cells in WM lesions [37], while a decrease in Olig-2 positive cells has been described [36]. We also observed a decrease in *Olig2* expression level at all ages in Tg2576 compared to Wt, suggesting a defect in the key molecular signaling involved in OPC differentiation in AD mice, indeed the expression of the *MBP*, the main myelin protein, is lower in the Tg2576 group than the Wt group at most ages. This hypothesis is also confirmed by the decreased number of mature non-myelinating OLs at 6 months of age in 3 × Tg-AD [38].

MBP is one of the main myelin-related protein and it is found to be associated with amyloid plaques [39]. However, different myelin proteins (i.e., MBP, MAG, MOG, and PLP) are proposed as target for early biomarkers for memory loss in AD, since the antibodies titers in sera of AD patients significantly increases in early stages of the disease [40].

4. OPC Vulnerability in Neurodegenerative Diseases

The contribution of OPC/OL injury to certain demyelinating diseases, such as MS, is clear and proven as the major cause of the neuronal degeneration. However, the damage of myelin and myelin-forming cells contribute to a wide range of neurodegenerative diseases and CNS injuries, a predictable finding given the complex role exerted by these cells in neuronal functions, not only in providing physical and anatomical support, but also as a functional player in neuronal processes, from metabolism to signaling regulation [41,42]. Cells belonging to the OL lineage are as vulnerable as neurons to noxious stimuli, enough to be considered as the most vulnerable cells of the CNS [43–45] highlighting their implication in the onset and progression of neurodegenerative diseases. A comparative analysis of cell death in neuronal pure and neurons-astrocytes mixed culture, in OPC at different differentiation stages (NG2-positivity for OPC, CNPase-positivity for mature OLs and MBP-positivity for myelinating OLs), and astrocytes after exposure to OGD is presented in Figure 3.

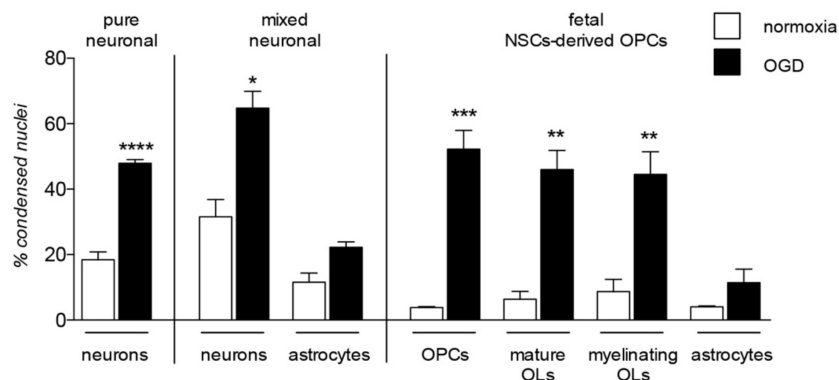


Figure 3. Lineage specific vulnerability to oxygen-glucose deprivation in in vitro models. The graph shows vulnerability to the in vitro model of hypoxia/ischemia, the oxygen-glucose deprivation (OGD), analyzed in three different in vitro models: pure neuronal, mixed neuronal/astroglial and neural stem cells (NSCs)-derived OPCs cultures. This is a summary chart of already published data [45,46], measured by cell-based high content screening and represented as percentage of condensed nuclei. Statistical analysis has been performed by Student's t-test and asterisks represent the differences between normoxia and OGD exposed cells of the same lineage (* $p < 0.05$, ** $p < 0.01$, *** $p = 0.001$).

The most significant and well-described pathological mechanism affecting the cell survival and differentiation processes of the OL lineage is the establishment of an inflammatory microenvironment. It was proven that acute inflammation increases the OPCs proliferation, migration and differentiation

thorough immune cells [47] and specific cytokines [48,49] as a response to demyelination insults. However, in the complex pathological environment of MS, the remyelination process progressively fails, in parallel to the establishment of the inflammation environment [50]. This is probably mediated by cytokines secreted by immune system cells as proven by the OPC differentiation block mediated by lymphocytes isolated from MS patients [51]. This leads to two main pathological outcomes: cell death of mature OLs, and OPC differentiation block, resulting in enhanced demyelination and remyelination impairment [52], which seems to be mediated by the alteration of the local content of triiodothyronine (T3) [53]. An appropriate intracellular T3 concentration is mandatory for cell cycle exit and terminal differentiation [54]. This pathological process has been widely investigated, since inflammation-mediated OPC differentiation block is considered responsible for remyelination failure in MS and other demyelinating diseases. However, the damage of myelin and myelin-forming cells is a major pathological event not only in inflammatory diseases, but also in vascular and traumatic lesions of the CNS, and a major cause of consequent neurodegeneration and chronic disabilities in both infants and adults [55]. These injuries impact on axonal integrity and function [56], making WM pathology a recognized target for pharmacological strategies [57]. Oligodendroglial lineage includes cells which are differentiating and maturing, from precursors through preOLs to myelinating OLs, showing huge differences in their biology throughout the entire differentiation process and leading to different responses to adverse stimuli [58].

The first link between the neurodegeneration described in AD and myelin cell vulnerability is the accumulation of A β peptide, which induces OL dysfunction and death both *in vivo* and *in vitro* [59,60]. The mechanism underlying the A β toxicity in OPCs and OLs is still unclear, but a number of studies seem to describe a complex multifactorial process involving different pathways: nSMase-ceramide cascade, TNF α , p75NTR, Fas, mitochondrial dysfunction, and oxidative stress, in which mature OLs seem to be more vulnerable than precursors [61]. However, a positive effect of acute exposure to A β oligomeric forms has also been described, increasing MBP translation in OLs, and promoting differentiation as well as cell survival in cultured OLs. The mechanism involves Itgb1 signaling, Fyn kinase and intracellular Ca²⁺ level modification. A β oligomers also seem to contribute to OL differentiation in cultured cerebellar slices, and to enhance remyelination following lysolecithin-induced demyelination [62]. This contrasting evidence highlights the complexity of the A β functions in physiological and pathological conditions, corroborating the hypothesis that OL toxicity induced by A β accumulation is a multifactorial process. This is also proven by the accumulation of A β in a mouse model of familial AD lacking the PS1 gene, showing WM dysfunctions linked to glutamate and calcium signaling dysregulation [63].

Tauopathy is the second AD hallmark, directly connected to A β toxicity. AD shows predominantly neuronal tau pathology in the form of neurofibrillary tangles, in contrast to other tauopathies characterized by the presence of glial tau pathologies. In OLs, this leads to myelin fragmentation and atrophy, exacerbating axonal instability. Moreover, pathological tau accumulation reduces the capability of astrocytes to uptake glutamate, leading to excitotoxicity mechanisms, an important player in both OL and neuronal vulnerability [64]. In this context, however, tau also seems to have a positive side function, in that axonal injury seems to promote the differentiation of OPCs during the remyelination process, thanks to the expression of a pathological form of tau [65].

Closely related to inflammatory pathological processes and A β toxicity, both OPCs and OLs are highly vulnerable to hypoxia/ischemia (HI) a common event in most neurodegenerative diseases and CNS injuries [66]. In fact, beyond the pathological mechanisms directly correlated to hypoxia and metabolic stress, HI also induces an inflammatory response [67]. Moreover, HI-induced cell death in neurons is exacerbated by A β accumulation [33], demonstrating how all these pathological mechanisms are interconnected. Notably, the severity and the pattern of the injury mediated by HI is strictly dependent on the developmental [68] and maturation [69] stages involved. OPCs/OLs are more vulnerable during developmental myelination, and precursors are more susceptible than mature OLs. This has been proven by the comparison between OPCs derived from fetal and from adult neural

stem cells (NSCs) exposed to OGD, the *in vitro* model of HI. These experiments lead show that only fetal cells are vulnerable to OGD-mediated cell toxicity [45] while, notably, both fetal and adult OPCs respond in the same way to inflammation-induced differentiation block. The differing responses of fetal and adult OPCs in the HI context is not surprising, since the two cell types, even with the same derivation (i.e., the NSC) show differences in their biology and differentiation processes [70].

The onset of a hypoxic/ischemic microenvironment also leads to other noxious consequences, all of which undermine the cell viability and functions of both neurons and glial cells: Indeed HI affects DNA stability, induces oxidative stress, and increases iron levels [29]. An emerging hypothesis suggests myelin degradation in sporadic AD as being the one of the earliest structural changes, independent of amyloid plaque formation and linked to DNA damage [71]. Oxidative stress is also directly linked to A β oligomers accumulation and cell death induction [61]. In particular, OLs show a low content of glutathione and low antioxidant defenses, coupled with a high consumption of oxygen and ATP, making these cells highly vulnerable to ROS production, inducing lipid peroxidation, impairing protein and nucleic acid production and promoting membrane disruption [42,72]. Notably, this mechanism of OL degeneration seems to form the basis of the secondary degeneration in neurotrauma [73].

As mentioned above, glutamate excitotoxicity is strictly linked to A β toxicity, and glutamate receptor overactivation is the main player in HI-induced cell death. Glutamate exerts a physiological role in OPC differentiation and OL signaling [74], but AMPA/kainite receptors also mediate glutamate excitotoxicity in glial cells [75], and in the preOLs in particular [76]. Mature OLs especially undergo HI-induced cell death due to an early excitotoxic-oxidative cascade, caused by the reduction of the high-energy phosphate metabolism. This leads to an increase in lactic acid, and to a failure in ion transport across the cell membrane, which combined with the destruction of the cytoskeleton, causes depolarization and excessive glutamate release. This condition is also worsened by the depleted glutamate reuptake caused by the reduced availability of glucose [67]. However, due to the significant differences in response to noxious events based on the variations in their differentiation and developmental stages, glutamate receptor inhibition is unable to protect fetal NSC-derived OPCs from HI-induced cell death. In this spontaneous astrocyte/OPCs co-cultures, the glucose deprivation acts as the major trigger for HI-mediated injury. The high heterogeneity between juvenile and adult OPCs and OLs populations was also confirmed by single cell RNAseq analysis [77]. Moreover, in the adult brain transcriptome analysis revealed that OLs are not included in a single family, can be split in six different classes based on their RNA expression profile [78].

5. OPCs as Target for Neuroprotection

As a complex and multifactorial disease, an effective neuroprotective strategy for AD should target multiple biological processes, and myelin and OPCs should be taken into account, given their fundamental role in neuronal and axonal function, and the evidences of their involvement in the disease onset and progression. Cells along the oligodendroglial lineage show remarkable differences (i.e., OPCs maturation) of physiological characteristics and vulnerability to noxious stimuli. Thus, neuroprotective strategies aimed to protect myelin and myelin forming cells should pursue two main objectives: (i) Protection of mature OLs and resident OPCs from cell death and (ii) enhancement of remyelination through proper OPCs differentiation. As described above, pathological AD mechanisms affect both of these aspects and the entire oligodendroglial lineage (Figure 4).

The importance of myelin-forming cells in the context of neurodegeneration and neuroprotection is dramatically illustrated by demyelinating diseases such as MS. Remyelination is the most efficient regenerative process in the adult CNS, the only one that can bring about a complete anatomical and functional recovery [79] and is not performed by preexisting OLs but by resident and NSC-derived OPCs. Thus, a number of neuroprotective strategies based on OPCs protection have been suggested for MS, including restoration of proper T3 signaling impaired by inflammation [53]. It is now clear that the remyelination failure occurring in MS is a complex event involving different mechanisms, a process in which OPC differentiation failure plays a central role [80]. Strategies may directly target pathways

or receptors involved in this process. and a variety of receptor tyrosine kinases and their growth factor ligands (PDGF, HGF, EGF, NGF, BDNF, and FGF), G protein-coupled receptors (histamine, muscarinic cholinergic, dopamine, and serotonin receptors) as well as other receptors [81–83]. The deep investigation of these physiological players in OPCs differentiation and remyelination process paves the way to a number of pharmacological trials acting on them [81]. It is also foreseeable that nuclear receptors involved in the T3 signaling may be putative targets. This is the case of RXR γ , described as one of the main partners in the thyroid hormone receptors heterodimers leading to OPCs differentiation and implied in remyelination process [84] and now clearly essential for the T3-mediated differentiation induction [70].

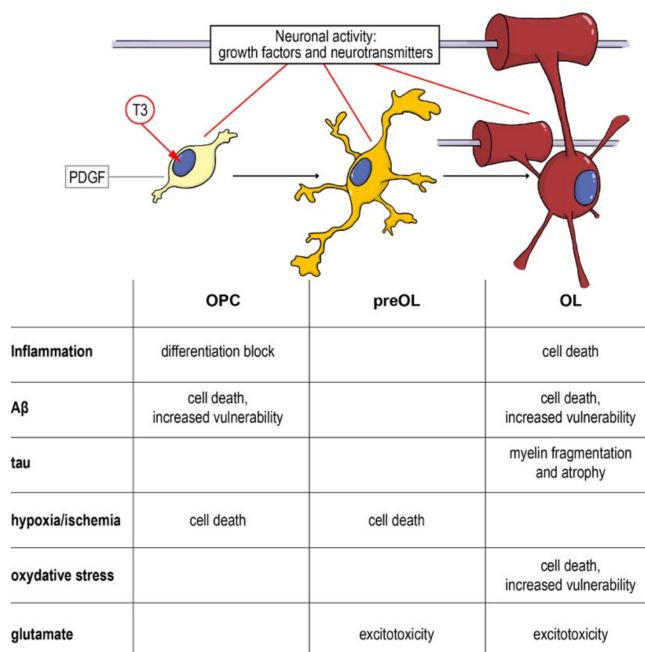


Figure 4. From the precursor to the mature oligodendrocyte: impact of noxious stimuli on differentiation and viability. Schematic representation of the physiological differentiation from the oligodendrocyte precursor cell (OPC) to myelinating OL. T3, the active form of the thyroid hormone, is the trigger of the process, driving the cell out of the cell cycle and starting the differentiation machinery. Neurotransmitters (such as GABA, glutamate and NO) directly contribute to regulating the process and the interaction between the axon and its activity and the OPCs/OLs. In the table are summarized the different component of neurodegenerative and demyelinating diseases affecting the different differentiation stages. Abbreviations: A β , amyloid beta; OL, oligodendrocyte; OPC, oligodendrocyte precursor cell; PDGF, platelet derived growth factor; T3, triiodothyronine.

Screening for targets of remyelination, and molecules acting on these processes, seems to be the most widely used drug discovery strategy, based on isolated primary OPCs, embryonic/ neural stem cell-derived OPCs, or induced pluripotent cell-differentiated OPCs, all cell systems which allow a molecular analysis of the physiological OPC differentiation process [85,86]. As we are learning from MS, however, pathological conditions interfere greatly with physiological mechanisms and the microenvironment where OPCs undergo differentiation/maturation processes, highlighting the need to develop new strategies based on pathological in vitro and in vivo models [53]: One such example emerged from a pharmacological strategy developed to save neurons from cell death, based on the inhibition of the poly(ADP-ribose) polymerase (PARP). Drugs inhibiting PARP activity show promising neuroprotective action in both fetal CNS injury, such as neonatal HI, and in adult diseases, such as MS. In MS animal models, pharmacological inhibition of PARP also exerts a protective action on mature OLs [87]. However, when tested for neonatal HI, a special consideration should be given to OPCs due to of the key time window (perinatal/early postnatal) for the developmental myelination. While PARP

inhibition shows no effect on adult NSCs-derived OPCs, its effects are highly toxic when performed on fetal-derived OPCs [88], again highlighting the importance of taking into account not only OPCs in neuroprotective strategies development, but also their high variability in terms of maturation and developmental stage.

Even if the fact that myelin and myelin forming cells damages may play an important role in the onset and/or progression of AD is clear, none of the AD treatment is directly targeting them. However, some treatments may indirectly target OPCs and OLs, acting on immune system and inflammation. This is the case of the above mentioned CHF5074 molecule, which is acting not only on amyloid production, but also modulating the microglia activation [89] as also proven in a phase II clinical trial [90].

6. Conclusions

The multifactorial nature of AD pathology, the multiple roles of myelin and myelin forming cells, and the accumulating evidences about WM abnormalities not only in late AD, but also in MCI, support the view that effective neuroprotective strategies should consider multiple cellular and molecular targets and specific time-windows. In this context, the capability of endogenous regeneration of myelin thanks to the presence of OPCs, offers an opportunity still to be explored.

Author Contributions: Conceptualization, L.G. and L.C.; investigation, A.B., A.G.; data curation, M.F.; writing—original draft preparation L.L., V.A.B., M.F.; writing—review and editing, L.C. and L.G.; funding acquisition, L.G. All authors have read and agreed to the published version of the manuscript.

Funding: This research was funded by Amici di Casa Insieme, non-profit association, Mercato Saraceno, FC, Italy.

Conflicts of Interest: The authors declare no conflict of interest. The funders had no role in the design of the study; in the collection, analyses, or interpretation of data; in the writing of the manuscript, or in the decision to publish the results.

Appendix A

Material and Methods for RT-PCR original data reported in the manuscript.

Appendix A.1 Materials and Methods

In this study Tg2576 transgenic mice (mice carrying a transgene coding for the 695-amino acid isoform of human APP derived from a large Swedish family with early-onset AD, as described by Hsiao et al. [91] and non-transgenic littermates (001349-W, WT) were used. Animals have been purchased from Taconic Europe (Lille Skensved, Denmark).

Wild-type and Tg2576 animals at 1, 3, 5, 14, and 27-old months of age were included in the study. The number of animals for each experimental group was 3–5. Tg2576 mice were tested for the retinal degeneration Pde6b (rd1) (rd) mutation, resulting as negative.

All animal protocols described here were carried out according to the European Community Council Directives 86/609/EEC, approved by Italian Ministry of Health (D.Lgs 116/92) as well as the European Community Council Directives 2010/63/UE. Animal protocols were carried out in compliance with the guidelines published in the NIH Guide for the Care and Use of the precursor protein gene used for the experiments.

The cerebral cortex of the Wt and Tg2576 mice were processed for the isolation of total RNA using the RNeasy Minikit (Qiagen, Milan, Italy). Isolated RNA was quantified using the Nanodrop 2000 Spectrophotometer (Thermo Scientific) and then subjected to retrotranscription using the iScript cDNA Synthesis Kit (BioRad, Hercules, CA) according to manufacturer's instructions. To assess any possible genomic DNA contamination, no reverse transcription sample was processed in parallel as a control sample.

Semiquantitative QPCR was performed by using the SsoAdvanced™ Universal SYBR Green Supermix (BioRad). An amount of 10 ng of cDNA per sample was used for all the primer-specific QPCR reactions performed. The final volume of reactions was 20 µL in which 0.4 µM of forward and

reverse primer mix was used. The control sample was also processed by QPCR for each specific primer mix used. Reactions were performed using the CFX96 QPCR instrument (BioRad) according to the following temperature/time profile: 95 °C/2 min, for polymerase activation and DNA denaturation, followed by 40 cycles of amplification (95 °C/15 s, denaturation, 60 °C/60 s, annealing/extension). Melt curve analysis of the amplified products was performed by heating from 65 °C to 95 °C with an increase of 0.5 °C/s. The specificity of the PCR reactions was revealed by the single peak obtained following melt analysis. The $2^{(-\Delta\Delta Ct)}$ method was used for the analysis of the relative gene expression, given that the efficiency of all the primers used herein was between 95 and 102%.

The sequence of specific primers used is described in the Table A1. The *GAPDH* was used as housekeeping gene (Cq WT vs Tg, Student's t-test, $p = 0.279$; Cq Wt age-matched vs Tg2576 age-matched, 1-way ANOVA, $p = 0.272$).

Table A1. Primers sequences.

Gene	NCBI Acc. N.	Primer Sequences
<i>GAPDH</i>	NM_17701	F: 5'-ggcaagttcaatggcacagtcaag-3' R: 5'-acatactcagcaccagcatcacc-3'
<i>Klf-9</i>	NM_010638.4	F: 5'-agtggcttcgaaggggaaac-3' R: 5'-tccgagcgcgagaactttt-3'
<i>MBP</i>	NM_001025251	F: 5'-gcctgtccctcagcagattt-3' R: 5'-gtcgtaggccccctgaatc-3'
<i>Olig-1</i>	NM_016968	F: 5'-ccgcccagatgtactatgc-3' R: 5'-aaccaccagctcatcacgc-3'
<i>Olig-2</i>	NM_016967.2	F: 5'-gcttagatcatccctggggc-3' R: 5'-agatcatcggttctgggga-3'
<i>PDGFαR</i>	NM_001083316.2	F: 5'-cggaacctcagagagaatcg-3' R: 5'-tcccatagctctgagacc-3'

Information about gene name, NCBI (National Center for Biotechnology Information) genbank accession number, forward (F) and reverse (R) sequences description has been included. *Klf-9*, *Krüppel-like factor 9*; *GAPDH*, *Glyceraldehyde-3-phosphate dehydrogenase*; *Olig-1*, *Oligodendrocyte transcription factor 1*; *Olig-2*, *Oligodendrocyte transcription factor 2*; *MBP*, myelin basic protein; *PDGF α R*, platelet derived growth factor receptor α .

References

- Lüders, E.; Steinmetz, H.; Jäncke, L. Brain size and grey matter volume in the healthy human brain. *Neuroreport* **2002**, *13*, 2371–2374. [\[CrossRef\]](#)
- Ozgen, H.; Baron, W.; Hoekstra, D.; Kahya, N. Oligodendroglial membrane dynamics in relation to myelin biogenesis. *Cell. Mol. Life Sci.* **2016**, *73*, 3291–3310. [\[CrossRef\]](#)
- Wang, S.; Young, K.M. White matter plasticity in adulthood. *Neuroscience* **2014**, *276*, 148–160. [\[CrossRef\]](#)
- Swire, M.; Ffrench-Constant, C. Seeing Is Believing: Myelin Dynamics in the Adult CNS. *Neuron* **2018**, *98*, 684–686. [\[CrossRef\]](#)
- Kato, D.; Wake, H. Activity-Dependent Myelination. *Adv. Exp. Med. Biol.* **2019**, *1190*, 43–51. [\[PubMed\]](#)
- Zhang, K.; Sejnowski, T.J. A universal scaling law between gray matter and white matter of cerebral cortex. *Proc. Natl. Acad. Sci. USA* **2000**, *97*, 5621–5626. [\[CrossRef\]](#) [\[PubMed\]](#)
- Filley, C.M.; Fields, R.D. White matter and cognition: Making the connection. *J. Neurophysiol.* **2016**, *116*, 2093–2104. [\[CrossRef\]](#) [\[PubMed\]](#)
- Saab, A.S.; Nave, K.-A. Myelin dynamics: protecting and shaping neuronal functions. *Curr. Opin. Neurobiol.* **2017**, *47*, 104–112. [\[CrossRef\]](#)
- Stassart, R.M.; Möbius, W.; Nave, K.-A.; Edgar, J.M. The Axon-Myelin Unit in Development and Degenerative Disease. *Front. Neurosci.* **2018**, *12*, 467. [\[CrossRef\]](#)
- Simons, M.; Nave, K.A. Oligodendrocytes: Myelination and axonal support. *Cold Spring Harb. Perspect. Biol.* **2015**, *8*, a020479. [\[CrossRef\]](#)

11. Stadelmann, C.; Timmler, S.; Barrantes-Freer, A.; Simons, M. Myelin in the central nervous system: Structure, function, and pathology. *Physiol. Rev.* **2019**, *99*, 1381–1431. [[CrossRef](#)] [[PubMed](#)]
12. Crawford, A.H.; Chambers, C.; Franklin, R.J.M. Remyelination: The true regeneration of the central nervous system. *J. Comp. Pathol.* **2013**, *149*, 242–254. [[CrossRef](#)] [[PubMed](#)]
13. Trotter, J.; Karram, K.; Nishiyama, A. NG2 cells: Properties, progeny and origin. *Brain Res. Rev.* **2010**, *63*, 72–82. [[CrossRef](#)] [[PubMed](#)]
14. Hughes, E.G.; Kang, S.H.; Fukaya, M.; Bergles, D.E. Oligodendrocyte progenitors balance growth with self-repulsion to achieve homeostasis in the adult brain. *Nat. Neurosci.* **2013**, *16*, 668–676. [[CrossRef](#)] [[PubMed](#)]
15. Butt, A.M.; Papanikolaou, M.; Rivera, A. Physiology of Oligodendroglia. In *Neuroglia in Neurodegenerative Diseases*; Verkhratsky, A., Ho, M., Zorec, R., Parpura, V., Eds.; Springer: Singapore, Singapore, 2019; pp. 117–128.
16. Barres, B.A.; Raff, M.C. Proliferation of oligodendrocyte precursor cells depends on electrical activity in axons. *Nature* **1993**, *361*, 258–260. [[CrossRef](#)]
17. Bergles, D.E.; Roberts, J.D.B.; Somogyi, P.; Jahr, C.E. Glutamatergic synapses on oligodendrocyte precursor cells in the hippocampus. *Nature* **2000**, *405*, 187–191. [[CrossRef](#)]
18. Gallo, V.; Armstrong, R.C. Myelin repair strategies: A cellular view. *Curr. Opin. Neurol.* **2008**, *21*, 278–283. [[CrossRef](#)]
19. Hill, R.A.; Nishiyama, A. NG2 cells (polydendrocytes): Listeners to the neural network with diverse properties. *Glia* **2014**, *62*, 1195–1210. [[CrossRef](#)]
20. Fields, R.D. Imaging learning: The search for a memory trace. *Neuroscientist* **2011**, *17*, 185–196. [[CrossRef](#)]
21. Liu, H.; Yang, Y.; Xia, Y.; Zhu, W.; Leak, R.K.; Wei, Z.; Wang, J.; Hu, X. Aging of cerebral white matter. *Ageing Res. Rev.* **2017**, *34*, 64–76. [[CrossRef](#)]
22. Lemaître, H.; Crivello, F.; Grassiot, B.; Alperovitch, A.; Tzourio, C.; Mazoyer, B. Age- and sex-related effects on the neuroanatomy of healthy elderly. *Neuroimage* **2005**, *26*, 900–911. [[CrossRef](#)] [[PubMed](#)]
23. Shenkin, S.D.; Bastin, M.E.; MacGillivray, T.J.; Deary, I.J.; Starr, J.M.; Rivers, C.S.; Wardlaw, J.M. Cognitive Correlates of Cerebral White Matter Lesions and Water Diffusion Tensor Parameters in Community-Dwelling Older People. *Cerebrovasc. Dis.* **2005**, *20*, 310–318. [[CrossRef](#)] [[PubMed](#)]
24. Marner, L.; Nyengaard, J.R.; Tang, Y.; Pakkenberg, B. Marked loss of myelinated nerve fibers in the human brain with age. *J. Comp. Neurol.* **2003**, *462*, 144–152. [[CrossRef](#)] [[PubMed](#)]
25. Liu, J.; Casaccia, P. Epigenetic regulation of oligodendrocyte identity. *Trends Neurosci.* **2010**, *33*, 193–201. [[CrossRef](#)]
26. Mito, R.; Raffelt, D.; Dhollander, T.; Vaughan, D.N.; Tournier, J.D.; Salvado, O.; Brodtmann, A.; Rowe, C.C.; Villemagne, V.L.; Connelly, A. Fibre-specific white matter reductions in Alzheimer’s disease and mild cognitive impairment. *Brain* **2018**, *141*, 888–902. [[CrossRef](#)] [[PubMed](#)]
27. Van den Berg, E.; Geerlings, M.I.; Biessels, G.J.; Nederkoorn, P.J.; Kloppenborg, R.P. White Matter Hyperintensities and Cognition in Mild Cognitive Impairment and Alzheimer’s Disease: A Domain-Specific Meta-Analysis. *J. Alzheimers Dis.* **2018**, *63*, 515–527. [[CrossRef](#)]
28. Dean, D.C.; Hurley, S.A.; Kecskemeti, S.R.; O’Grady, J.P.; Canda, C.; Davenport-Sis, N.J.; Carlsson, C.M.; Zetterberg, H.; Blennow, K.; Asthana, S.; et al. Association of Amyloid Pathology With Myelin Alteration in Preclinical Alzheimer Disease. *JAMA Neurol.* **2017**, *74*, 41–49. [[CrossRef](#)]
29. Nasrabady, S.E.; Rizvi, B.; Goldman, J.E.; Brickman, A.M. White matter changes in Alzheimer’s disease: a focus on myelin and oligodendrocytes. *Acta Neuropathol. Commun.* **2018**, *6*, 22. [[CrossRef](#)]
30. Baldassarro, V.A.; Bighinati, A.; Sannia, M.; Giardino, L.; Calzà, L. Brain susceptibility to hypoxia/hypoxemia and metabolic dysfunction in Alzheimer’s disease: Insights from animal and in vitro models. In *The Neuroscience of Dementia: Genetics, Neurology, Behavior and Diet*; Preedy, V.R., Martin, C.R., Eds.; Elsevier Inc.: Amsterdam, The Netherlands, 2020.
31. Balducci, C.; Mehdaawy, B.; Mare, L.; Giuliani, A.; Lorenzini, L.; Sivilia, S.; Giardino, L.; Calzà, L.; Lanzillotta, A.; Sarnico, I.; et al. The γ -secretase modulator CHF5074 restores memory and hippocampal synaptic plasticity in plaque-free Tg2576 mice. *J. Alzheimer’s Dis.* **2011**, *24*, 799–816. [[CrossRef](#)]
32. Giuliani, A.; Sivilia, S.; Baldassarro, V.A.; Gusciglio, M.; Lorenzini, L.; Sannia, M.; Calza, L.; Giardino, L. Age-related changes of the neurovascular unit in the cerebral cortex of Alzheimer disease mouse models: A neuroanatomical and molecular study. *J. Neuropathol. Exp. Neurol.* **2019**, *78*, 101–112. [[CrossRef](#)]

33. Baldassarro, V.A.; Marchesini, A.; Giardino, L.; Calza, L. Vulnerability of primary neurons derived from Tg2576 Alzheimer mice to oxygen and glucose deprivation: Role of intraneuronal amyloid- β accumulation and astrocytes. *DMM Dis. Model. Mech.* **2017**, *10*, 671–678. [[CrossRef](#)] [[PubMed](#)]
34. Giuliani, A.; Beggiato, S.; Baldassarro, V.A.; Mangano, C.; Giardino, L.; Imbimbo, B.P.; Antonelli, T.; Calzà, L.; Ferraro, L. CHF5074 restores visual memory ability and pre-synaptic cortical acetylcholine release in pre-plaque Tg2576 mice. *J. Neurochem.* **2013**, *124*, 613–620. [[CrossRef](#)] [[PubMed](#)]
35. Beggiato, S.; Giuliani, A.; Sivilia, S.; Lorenzini, L.; Antonelli, T.; Imbimbo, B.P.; Giardino, L.; Calzà, L.; Ferraro, L. CHF5074 and LY450139 sub-acute treatments differently affect cortical extracellular glutamate levels in pre-plaque Tg2576 mice. *Neuroscience* **2014**, *266*, 13–22. [[CrossRef](#)] [[PubMed](#)]
36. Behrendt, G.; Baer, K.; Buffo, A.; Curtis, M.A.; Faull, R.L.; Rees, M.I.; Götz, M.; Dimou, L. Dynamic changes in myelin aberrations and oligodendrocyte generation in chronic amyloidosis in mice and men. *Glia* **2013**, *61*, 273–286. [[CrossRef](#)]
37. Simpson, J.E.; Fernando, M.S.; Clark, L.; Ince, P.G.; Matthews, F.; Forster, G.; O'Brien, J.T.; Barber, R.; Kalaria, R.N.; Brayne, C.; et al. White matter lesions in an unselected cohort of the elderly: Astrocytic, microglial and oligodendrocyte precursor cell responses. *Neuropathol. Appl. Neurobiol.* **2007**, *33*, 410–419. [[CrossRef](#)]
38. Desai, M.K.; Mastrangelo, M.A.; Ryan, D.A.; Sudol, K.L.; Narrow, W.C.; Bowers, W.J. Early oligodendrocyte/myelin pathology in Alzheimer's disease mice constitutes a novel therapeutic target. *Am. J. Pathol.* **2010**, *177*, 1422–1435. [[CrossRef](#)]
39. Zhan, X.; Jickling, G.C.; Ander, B.P.; Stamova, B.; Liu, D.; Kao, P.F.; Zelin, M.A.; Jin, L.W.; Decarli, C.; Sharp, F.R. Myelin basic protein associates with A β PP, A β 1-42, and Amyloid plaques in cortex of Alzheimer's disease brain. *J. Alzheimers Dis.* **2015**, *44*, 1213–1229. [[CrossRef](#)]
40. Papuč, E.; Kurys-Denis, E.; Krupski, W.; Tatar, M.; Rejdak, K. Can antibodies against glial derived antigens be early biomarkers of hippocampal demyelination and memory loss in Alzheimer's disease? *J. Alzheimers Dis.* **2015**, *48*, 115–121. [[CrossRef](#)]
41. Tognatta, R.; Miller, R.H. Contribution of the oligodendrocyte lineage to CNS repair and neurodegenerative pathologies. *Neuropharmacology* **2016**, *110*, 539–547. [[CrossRef](#)]
42. Barateiro, A.; Brites, D.; Fernandes, A. Oligodendrocyte Development and Myelination in Neurodevelopment: Molecular Mechanisms in Health and Disease. *Curr. Pharm. Des.* **2016**, *22*, 656–679. [[CrossRef](#)]
43. Bradl, M.; Lassmann, H. Oligodendrocytes: Biology and pathology. *Acta Neuropathol.* **2010**, *119*, 37–53. [[CrossRef](#)] [[PubMed](#)]
44. Lee, Y.; Morrison, B.M.; Li, Y.; Lengacher, S.; Farah, M.H.; Hoffman, P.N.; Liu, Y.; Tsingalia, A.; Jin, L.; Zhang, P.W.; et al. Oligodendroglia metabolically support axons and contribute to neurodegeneration. *Nature* **2012**, *487*, 443–448. [[CrossRef](#)] [[PubMed](#)]
45. Baldassarro, V.A.; Marchesini, A.; Giardino, L.; Calzà, L. Differential effects of glucose deprivation on the survival of fetal versus adult neural stem cells-derived oligodendrocyte precursor cells. *Glia* **2019**. [[CrossRef](#)] [[PubMed](#)]
46. Baldassarro, V.A.; Marchesini, A.; Facchinetti, F.; Villetti, G.; Calzà, L.; Giardino, L. Cell death in pure-neuronal and neuron-astrocyte mixed primary culture subjected to oxygen-glucose deprivation: The contribution of poly(ADP-ribose) polymerases and caspases. *Microchem. J.* **2018**, *136*, 215–222. [[CrossRef](#)]
47. Dombrowski, Y.; O'Hagan, T.; Dittmer, M.; Penalva, R.; Mayoral, S.R.; Bankhead, P.; Fleville, S.; Eleftheriadis, G.; Zhao, C.; Naughton, M.; et al. Regulatory T cells promote myelin regeneration in the central nervous system. *Nat. Neurosci.* **2017**, *20*, 674–680. [[CrossRef](#)] [[PubMed](#)]
48. Miron, V.E.; Boyd, A.; Zhao, J.W.; Yuen, T.J.; Ruckh, J.M.; Shadrach, J.L.; Van Wijngaarden, P.; Wagers, A.J.; Williams, A.; Franklin, R.J.M.; et al. M2 microglia and macrophages drive oligodendrocyte differentiation during CNS remyelination. *Nat. Neurosci.* **2013**, *16*, 1211–1218. [[CrossRef](#)] [[PubMed](#)]
49. Setzu, A.; Lathia, J.D.; Zhao, C.; Wells, K.; Rao, M.S.; Ffrench-Constant, C.; Franklin, R.J.M. Inflammation stimulates myelination by transplanted oligodendrocyte precursor cells. *Glia* **2006**, *54*, 297–303. [[CrossRef](#)]
50. Schaeffer, J.; Cossetti, C.; Mallucci, G.; Pluchino, S. Multiple Sclerosis. In *Neurobiology of Brain Disorders: Biological Basis of Neurological and Psychiatric Disorders*; Elsevier Inc.: Amsterdam, The Netherlands, 2015; pp. 497–520.

51. El Behi, M.; Sanson, C.; Bachelin, C.; Guillot-Noël, L.; Fransson, J.; Stankoff, B.; Maillart, E.; Sarrazin, N.; Guillemot, V.; Abdi, H.; et al. Adaptive human immunity drives remyelination in a mouse model of demyelination. *Brain* **2017**, *140*, 967–980. [[CrossRef](#)]
52. Matthews, P.M. Chronic inflammation in multiple sclerosis—Seeing what was always there. *Nat. Rev. Neurol.* **2019**, *15*, 582–593. [[CrossRef](#)]
53. Fernández, M.; Baldassarro, V.A.; Sivilia, S.; Giardino, L.; Calzà, L. Inflammation severely alters thyroid hormone signaling in the central nervous system during experimental allergic encephalomyelitis in rat: Direct impact on OPCs differentiation failure. *Glia* **2016**, *64*, 1573–1589. [[CrossRef](#)]
54. Lee, J.Y.; Petratos, S. Thyroid Hormone Signaling in Oligodendrocytes: From Extracellular Transport to Intracellular Signal. *Mol. Neurobiol.* **2016**, *53*, 6568–6583. [[CrossRef](#)] [[PubMed](#)]
55. Verden, D.; Macklin, W.B. Neuroprotection by central nervous system remyelination: Molecular, cellular, and functional considerations. *J. Neurosci. Res.* **2016**, *94*, 1411–1420. [[CrossRef](#)] [[PubMed](#)]
56. Fern, R.F.; Matute, C.; Stys, P.K. White matter injury: Ischemic and nonischemic. *Glia* **2014**, *62*, 1780–1789. [[CrossRef](#)] [[PubMed](#)]
57. Chew, L.-J.; DeBoy, C.A. Pharmacological approaches to intervention in hypomyelinating and demyelinating white matter pathology. *Neuropharmacology* **2016**, *110*, 605–625. [[CrossRef](#)]
58. Amaral, A.I.; Hadera, M.G.; Tavares, J.M.; Kotter, M.R.N.; Sonnewald, U. Characterization of glucose-related metabolic pathways in differentiated rat oligodendrocyte lineage cells. *Glia* **2016**, *64*, 21–34. [[CrossRef](#)]
59. Lee, J.T.; Xu, J.; Lee, J.M.; Ku, G.; Han, X.; Yang, D.I.; Chen, S.; Hsu, C.Y. Amyloid- β peptide induces oligodendrocyte death by activating the neutral sphingomyelinase-ceramide pathway. *J. Cell Biol.* **2004**, *164*, 123–131. [[CrossRef](#)]
60. Zhang, M.; Zhang, J.; Zhang, W.; Yao, Z. Demyelination Takes Place Prior To Neuronal Damage Following Intracerebroventricular Injection of Amyloid-Beta Oligomer. *Neuropsychiatry* **2018**, *8*, 1770–1785.
61. Roth, A.D.; Ramírez, G.; Alarcón, R.; Von Bernhardi, R. Oligodendrocytes damage in Alzheimer’s disease: Beta amyloid toxicity and inflammation. *Biol. Res.* **2005**, *38*, 381–387. [[CrossRef](#)]
62. Quintela-López, T.; Ortiz-Sanz, C.; Serrano-Regal, M.P.; Gaminde-Blasco, A.; Valero, J.; Baleriola, J.; Sánchez-Gómez, M.V.; Matute, C.; Alberdi, E. A β oligomers promote oligodendrocyte differentiation and maturation via integrin β 1 and Fyn kinase signaling. *Cell Death Dis.* **2019**, *10*, 445. [[CrossRef](#)]
63. Pak, K.; Chan, S.L.; Mattson, M.P. Presenilin-1 mutation sensitizes oligodendrocytes to glutamate and amyloid toxicities, and exacerbates white matter damage and memory impairment in mice. *NeuroMolecular Med.* **2003**, *3*, 53–64. [[CrossRef](#)]
64. Kahlon, M.A.; Colodner, K.J. Glial tau pathology in tauopathies: Functional consequences. *J. Exp. Neurosci.* **2015**, *9* (Suppl. S2), 43–50. [[CrossRef](#)]
65. Ossola, B.; Zhao, C.; Compston, A.; Pluchino, S.; Franklin, R.J.M.; Spillantini, M.G. Neuronal expression of pathological tau accelerates oligodendrocyte progenitor cell differentiation. *Glia* **2016**, *64*, 457–471. [[CrossRef](#)] [[PubMed](#)]
66. Nalivaeva, N.N.; Rybnikova, E.A. Editorial: Brain Hypoxia and Ischemia: New Insights Into Neurodegeneration and Neuroprotection. *Front. Neurosci.* **2019**, *13*, 770. [[CrossRef](#)]
67. Rocha-Ferreira, E.; Hristova, M. Plasticity in the Neonatal Brain following Hypoxic-Ischaemic Injury. *Neural Plast.* **2016**, *2016*, 1–16. [[CrossRef](#)] [[PubMed](#)]
68. Jablonska, B.; Scafidi, J.; Aguirre, A.; Vaccarino, F.; Nguyen, V.; Borok, E.; Horvath, T.L.; Rowitch, D.H.; Gallo, V. Oligodendrocyte Regeneration after Neonatal Hypoxia Requires FoxO1-Mediated p27Kip1 Expression. *J. Neurosci.* **2012**, *32*, 14775–14793. [[CrossRef](#)] [[PubMed](#)]
69. Back, S.A.; Han, B.H.; Luo, N.L.; Chricton, C.A.; Xanthoudakis, S.; Tam, J.; Arvin, K.L.; Holtzman, D.M. Selective Vulnerability of Late Oligodendrocyte Progenitors to Hypoxia-Ischemia. *J. Neurosci.* **2002**, *22*, 455–463. [[CrossRef](#)] [[PubMed](#)]
70. Baldassarro, V.A.; Krężel, W.; Fernández, M.; Schuhbaur, B.; Giardino, L.; Calzà, L. The role of nuclear receptors in the differentiation of oligodendrocyte precursor cells derived from fetal and adult neural stem cells. *Stem Cell Res.* **2019**, *37*, 101443. [[CrossRef](#)] [[PubMed](#)]
71. Tse, K.H.; Cheng, A.; Ma, F.; Herrup, K. DNA damage-associated oligodendrocyte degeneration precedes amyloid pathology and contributes to Alzheimer’s disease and dementia. *Alzheimers Dement.* **2018**, *14*, 664–679. [[CrossRef](#)]

72. Dewar, D.; Underhill, S.M.; Goldberg, M.P. Oligodendrocytes and Ischemic Brain Injury. *J. Cereb. Blood Flow Metab.* **2003**, *23*, 263–274. [[CrossRef](#)]
73. Giacci, M.K.; Bartlett, C.A.; Smith, N.M.; Iyer, K.S.; Toomey, L.M.; Jiang, H.; Guagliardo, P.; Kilburn, M.R.; Fitzgerald, M. Oligodendroglia are particularly vulnerable to oxidative damage after neurotrauma in vivo. *J. Neurosci.* **2018**, *38*, 6491–6504. [[CrossRef](#)]
74. Kolodziejczyk, K.; Saab, A.S.; Nave, K.A.; Attwell, D. Why do oligodendrocyte lineage cells express glutamate receptors? *F1000 Biol. Rep.* **2010**, *2*, 57. [[PubMed](#)]
75. Tekkök, S.B.; Goldberg, M.P. Ampa/kainate receptor activation mediates hypoxic oligodendrocyte death and axonal injury in cerebral white matter. *J. Neurosci.* **2001**, *21*, 4237–4248. [[CrossRef](#)] [[PubMed](#)]
76. Deng, W.; Yue, Q.; Rosenberg, P.A.; Volpe, J.J.; Jensen, F.E. Oligodendrocyte excitotoxicity determined by local glutamate accumulation and mitochondrial function. *J. Neurochem.* **2006**, *98*, 213–222. [[CrossRef](#)] [[PubMed](#)]
77. Marques, S.; Zeisel, A.; Codeluppi, S.; Van Bruggen, D.; Falcão, A.M.; Xiao, L.; Li, H.; Häring, M.; Hochgerner, H.; Romanov, R.A.; et al. Oligodendrocyte heterogeneity in the mouse juvenile and adult central nervous system. *Science* **2016**, *352*, 1326–1329. [[CrossRef](#)]
78. Zeisel, A.; Moz-Manchado, A.B.; Codeluppi, S.; Lönnerberg, P.; Manno, G.L.; Juréus, A.; Marques, S.; Munguba, H.; He, L.; Betsholtz, C.; et al. Cell types in the mouse cortex and hippocampus revealed by single-cell RNA-seq. *Science* **2015**, *347*, 1138–1142. [[CrossRef](#)]
79. Franklin, R.J.M.; Ffrench-Constant, C.; Edgar, J.M.; Smith, K.J. Neuroprotection and repair in multiple sclerosis. *Nat. Rev. Neurol.* **2012**, *8*, 624–634. [[CrossRef](#)]
80. Gruchot, J.; Weyers, V.; Göttle, P.; Förster, M.; Hartung, H.-P.; Küry, P.; Kremer, D. The Molecular Basis for Remyelination Failure in Multiple Sclerosis. *Cells* **2019**, *8*, 825. [[CrossRef](#)]
81. Bothwell, M. Mechanisms and Medicines for Remyelination. *Annu. Rev. Med.* **2017**, *68*, 431–443. [[CrossRef](#)]
82. Cole, K.L.H.; Early, J.J.; Lyons, D.A. Drug discovery for remyelination and treatment of MS. *Glia* **2017**, *65*, 1565–1589. [[CrossRef](#)]
83. Skaper, S.D. Oligodendrocyte precursor cells as a therapeutic target for demyelinating diseases. In *Progress in Brain Research*; Elsevier B.V.: Amsterdam, The Netherlands, 2019.
84. Huang, J.K.; Jarjour, A.A.; Oumesmar, B.N.; Kerninon, C.; Williams, A.; Krezel, W.; Kagechika, H.; Bauer, J.; Zhao, C.; Evercooren, A.B.V.; et al. Retinoid X receptor gamma signaling accelerates CNS remyelination. *Nat. Neurosci.* **2011**, *14*, 45–55. [[CrossRef](#)]
85. Lariosa-Willingham, K.D.; Rosler, E.S.; Tung, J.S.; Dugas, J.C.; Collins, T.L.; Leonoudakis, D. A high throughput drug screening assay to identify compounds that promote oligodendrocyte differentiation using acutely dissociated and purified oligodendrocyte precursor cells. *BMC Res. Notes* **2016**, *9*, 419. [[CrossRef](#)] [[PubMed](#)]
86. Bove, R.M.; Green, A.J. Remyelinating Pharmacotherapies in Multiple Sclerosis. *Neurotherapeutics* **2017**, *14*, 894–904. [[CrossRef](#)] [[PubMed](#)]
87. Veto, S.; Acs, P.; Bauer, J.; Lassmann, H.; Berente, Z.; Setalo, G.; Borgulya, G.; Sumegi, B.; Komoly, S.; Gallyas, F.; et al. Inhibiting poly(ADP-ribose) polymerase: A potential therapy against oligodendrocyte death. *Brain* **2010**, *133*, 822–834. [[CrossRef](#)] [[PubMed](#)]
88. Baldassarro, V.A.; Marchesini, A.; Giardino, L.; Calzà, L. PARP activity and inhibition in fetal and adult oligodendrocyte precursor cells: Effect on cell survival and differentiation. *Stem Cell Res.* **2017**, *22*, 54–60. [[CrossRef](#)] [[PubMed](#)]
89. Porrini, V.; Lanzillotta, A.; Branca, C.; Benarese, M.; Parrella, E.; Lorenzini, L.; Calzà, L.; Flaibani, R.; Spano, P.F.; Imbimbo, B.P.; et al. CHF5074 (CSP-1103) induces microglia alternative activation in plaque-free Tg2576 mice and primary glial cultures exposed to beta-amyloid. *Neuroscience* **2015**, *302*, 112–120. [[CrossRef](#)] [[PubMed](#)]
90. Ross, J.; Sharma, S.; Winston, J.; Nunez, M.; Bottini, G.; Franceschi, M.; Scarpini, E.; Frigerio, E.; Fiorentini, F.; Fernandez, M.; et al. CHF5074 Reduces Biomarkers of Neuroinflammation in Patients with Mild Cognitive Impairment: A 12-Week, Double-Blind, Placebo- Controlled Study. *Curr. Alzheimer Res.* **2013**, *10*, 742–753. [[CrossRef](#)]
91. Hsiao, K.; Chapman, P.; Nilsen, S.; Eckman, C.; Harigaya, Y.; Younkin, S.; Yang, F.; Cole, G. Correlative memory deficits, A β elevation, and amyloid plaques in transgenic mice. *Science* **1996**, *274*, 99–102. [[CrossRef](#)]



4.8. NGF and endogenous regeneration: from embryology toward therapies (*paper under review, Advances in Experimental Medicine and Biology*)

Baldassarro Vito Antonio¹, Lorenzini Luca^{1,2}, Bighinati Andrea², Giuliani Alessandro², Alastra Giuseppe¹, Pannella Micaela³, Fernandez Mercedes², Giardino Luciana^{1,2,3}, Calzà Laura^{1,4,5}.

¹ Health Science and Technologies Interdepartmental Center for Industrial Research (HST-ICIR), University of Bologna, Ozzano Emilia, Bologna, Italy

² Department of Veterinary Medical Sciences, University of Bologna, Ozzano Emilia, Bologna, Italy

³ IRET Foundation, Ozzano Emilia, Bologna, Italy

⁴ Department of Pharmacy and Biotechnology, University of Bologna, Bologna, Italy

⁵ Montecatone Rehabilitation Institute, Montecatone, Bologna, Italy

Corresponding author:

Laura Calzà, MD

CIRI-SDV, University of Bologna,

Via Tolara di Sopra 41/E

40064 Ozzano Emilia (Bologna)

Email: laura.calza@unibo.it

ABSTRACT

The self-repair ability of tissues and organs in case of injury and disease is a fundamental biological mechanism and an important therapeutic target. The tissue plasticity and the presence of adult stem cell niches open a new path in pharmacological and non-pharmacological treatments development finalized to improve the intrinsic regeneration.

In this context, Nerve Growth Factor (NGF) is widely studied for its capability of driving endogenous regeneration of ectoderm-derived tissues, directly acting on the cell targets and through the regulation of the stem cell niches. In fact, this growth factor is very promising for its key role in development and the multiplicity of the cellular targets.

In this chapter we have travelled across the recent history of NGF pleiotropic role in ectodermal tissues generation and repairment, from embryonic development to skin wound healing, axonal regrowth and remyelination.

The better understanding of both the biological mechanisms underlying regeneration and the physiological role of NGF in development and injury response will open new therapeutic strategies, driven by the potential applications of this growth factor as an agent for improving endogenous regeneration processes.

Keywords:

Nerve growth factor, embryogenesis, embryonic stem cells, skin, axons regeneration, remyelination. This field

1. Introduction

“Endogenous regeneration” refers to the ability of tissues and organs to self-repair in the event of injury or disease. This capability varies significantly between the different animal species and districts of the body; tailed amphibians, for example, can completely regenerate parts of the body, such as limbs, tails, jaws, eyes, and a variety of internal structures. In mammals, tissues with a high cell turnover such as the skin may effectively regenerate in the event of extensive lesions, while other tissue, such as that of the central nervous system, has a very limited regenerative capability, confined to the myelin sheath. In both cases, this capability may be severely impaired by disease or excessive lesion area.

Since the discovery of stem cell niches in most adult mammal tissues and organs, which contribute to the respective and tissue-specific cell turnover rate (Bagnara 2020), the self-repair capability of adult tissue has been the focus of increasing interest. In some tissues, such as the skin, the proliferation rate of niche stem and precursor cells increases in the event of injury, while asymmetric division provides precursors, thus increasing cell turnover in affected tissue, and ultimately leading to tissue repair. In other tissues, such as that of the central nervous system (CNS), stem cells in the neurogenic niches react weakly to injuries, an activation which has no substantial effects on lesion or pathology evolution (Sun 2016). On the contrary, oligodendrocyte precursor cells disseminated throughout the white and gray matter, or newly generated from the glycolytic niches, may efficiently repair the myelin, restoring appropriate axonal function (Bruce et al. 2010).

The subsequent hypothesis was that organ and tissue plasticity, and endogenous regeneration as a result, could be improved by pharmacological and non-pharmacological treatments able to direct the stem cell niches (Wells and Watt 2018). This area is also defined “in vivo regenerative medicine” or “autotherapies” (Lumelsky et al. 2018).

The role of growth and neurotrophic factors during development makes these biomolecules natural candidates for improving endogenous regeneration. NGF in particular is very attractive from this point of view, being a pleiotropic molecule acting on many different cell types, both during development and in adulthood (Aloe and Calzà 2004). In this short review, we will focus on data supporting the potential applications of NGF as an agent for improving endogenous regeneration of ectoderm-derived tissues, summarizing the basic and translation findings supporting the development of NGF as a drug.

2. NGF and embryonic development

NGF and its receptors appear very early during development (reviewed by (Bracci-Laudiero and De Stefano 2016)). NGF mRNA is found in oocytes at different maturation stages and is involved in follicle and oocyte maturation. p75^{NTR} and TrkA appear in mouse embryos at the blastocyst stage, being confined to the inner cell mass and absent in the trophoblast. NGF receptor expression then differentiates into specific areas during gastrulation and neurulation, suggesting that NGF plays a role in germinal layer differentiation and early body shape specification. NGF neutralization experiments in chickens indicate that NGF absence alters body axis rotation and notochord and somite formation and evolution.

During neurulation, p75^{NTR} expression in neural crest cells correlates with the beginning of cell migration (Wislet et al. 2018). The different isoforms of Trk receptors then appear during neural crest cell migration and differentiation (Martin-Zanca et al. 1990).

Both mouse (Moscatelli et al. 2009) and human embryonic stem cells (Pyle et al. 2006) express NGF receptors, and differentiation studies of 3D embryonic stem cell cultures indicate that exposure to NGF *plus* retinoic acid (RA) favors the ectodermal and mesodermal lineages (Inanç et al. 2008).

We studied the expression of NGF and its receptors in embryonic stem cells derived from rat blastocytes (RESCs), using a cell line isolated in our laboratory (Fernández et al. 2011) (Fig. 1). These cells can be maintained: 1) as clusters (CL), growing in the presence of LF and bFGF in ultra-low attachment plates; 2) as a mixed population of single cells (SC) and clusters (CL), growing in the presence of LIF and bFGF, in attaching and floating conditions, respectively; or 3) as embryoid bodies (EB), whose formation can be induced by growing the cells obtained from cluster splitting (RESC-CL) in ultra-low attachment plates without LIF but in the presence of bFGF (Pannella et al. 2018). These EBs recapitulate the first steps toward differentiation, gradually losing their pluripotency to become specific germinative layer committed cells.

The mRNA expression profile of NGF, trkA and p75^{NTR} under these different *in vitro* conditions are presented in Fig 1. We observed that all mRNAs are expressed in the aforementioned culture conditions, with a significant increase of p75^{NTR} expression level in EBs, around 10 times higher than in clusters (** p=0.0077) and all the other studied conditions (SC, CL mixed population, ** p=0.0093, p=0.0091). Interestingly, the trkA expression was significantly lower (around 0.5-fold) in single cells only compared to the reference group (** p=0.0084).

NGF also regulates organogenesis and tissue maturation in several districts, acting through both sensory innervation and angiogenesis (Kim et al. 2013), as in the case of endochondral bone, but also acts directly on non-neural cells, such as during odontogenesis (Mitsiadis and Pagella 2016).

Finally, classical neutralization experiments have indicated that several neural populations and pathways in the peripheral nervous system (PNS), including the sensory and sympathetic neurons, and selective neural populations in the CNS, such as the cholinergic neurons of the basal forebrain, require NGF for appropriate axonal growth, cell differentiation, cell migration, and promotion and control of nerve regeneration (Levi-Montalcini 1997). The sympathetic neurons of the superior cervical ganglion are the best-studied example of the role of NGF in controlling pro-survival vs pro-apoptotic pathways during development: these cells require NGF at the time of target innervation, and *in vitro* experiments indicate that NGF withdrawal activates the mitochondrial (intrinsic) pathway of apoptosis involving caspases, Bcl-2 (B-cell CLL/lymphoma 2) family proteins and XIAP (X-linked inhibitor of apoptosis protein) (Kristiansen and Ham 2014).

However, the role of NGF in mature neural phenotype maintenance in the adult nervous system, in cell reaction to lesion either as survival or repair, and as a pro-apoptotic factor, is still disputed, being dependent on: i) the involved receptor subtype, ii) the synthesis pathway from the pro-NGF, and iii) the target cell type.

3. NGF and epithelial wound healing

The skin is the largest organ in the body, covering its entire external surface, and forms the physical barrier between the host and the external environment. The skin protects the entire body against numerous insults, prevents excessive body water loss, and plays a role in immune surveillance and sensory detection.

The epithelial component of the skin derives from the embryonic surface ectoderm, whereas the underlying derma derives from the mesoderm. During development, NGF plays a major role in the development of selective skin components: in particular, the development of thinly myelinated A δ or unmyelinated C-fibers that innervate the skin (dermis and epidermis) is NGF-dependent (Indo 2012), and half of the nociceptive sensory neurons innervating the mature skin are dependent upon an appropriate NGF supply (Snider and McMahon 1998). Neurotrophins, including NGF, play a complex role in the hair follicle cycle (Botchkarev et al. 2004), and the low-affinity neurotrophin receptor is a key regulator of the melanocytic cell lineage (Kasemeier-Kulesa and Kulesa 2018). During development, cell types other than keratinocytes – for example melanocytes – also require NGF, which derives from the neural crest: p75^{NTR} is in fact a marker for neural crest cells, and is also used for cell sorting experiments. Recently, p75^{NTR} - (CD271) positivity has been associated with an aggressive clinical subtype of melanoma which metastasizes to the brain, being indicated as a mediator of phenotype switching which suppresses melanoma cell proliferation, while concomitantly promoting metastasis formation *in vivo* (Kasemeier-Kulesa and Kulesa 2018).

The breakdown of skin integrity, when it is incorrectly and rapidly repaired, results in a substantial physiological imbalance and renders a patient vulnerable to a number of pathological conditions, such as infection, fluid loss, and electrolyte imbalance (Reinke and Sorg 2012), underlining the critical importance of a complete and efficient healing of cutaneous wounds. The wound healing process is characterized by four sequential and overlapping phases: hemostasis and early inflammation (0–several hours after injury), inflammation (1–3 days), proliferation (4–21days) and maturation and remodeling (21 days–1 year) (Reinke and Sorg 2012). Deregulation of any of these steps results in impaired healing, potentially leading to chronic ulcers (Sen et al., 2009).

Several *in vitro* and *in vivo* studies have shown that NGF affects several cell types involved in skin wound healing. TrkA and/or p75^{NTR} expression is not limited to sensory nerve endings, but also includes inflammatory cells (neutrophils, macrophages, mast cells and lymphocytes), keratinocytes, fibroblasts and endothelial cells. NGF is also secreted by fibroblasts (Matsuda et al., 1991), keratinocytes (Tron et al. 1990), mast cells (Leon et al. 1994) and T cells (Ehrhard et al. 1993), and has angiogenic properties, *via* nitric oxide synthase (NOS) and vascular endothelial growth factor (VEGF) (Calzà et al. 2001).

We recently demonstrated that human fibroblasts (BJ cells) and keratinocytes (HEK cells), as well as human endothelial cells (HUVECs), express both high- (TrkA) and low-affinity (p75^{NTR}) receptors for NGF, and key physiological properties of these cells, such as proliferation, migration, and angio-tube formation, are affected by NGF exposure in both physiological and pathological (hyperglycemia) conditions (Gostynska et al. 2019).

The underlying molecular mechanism, activated by TrkA, includes the PI3K/Akt and ERK/MAPK signaling pathways and the downstream mTOR. Notably, several NGF-mediated effects during development, such as endothelial cell invasion and cord formation (Park et al. 2007), angiogenesis in bone (Yu et al. 2019), as well as neuroprotection (Elsherbiny et al. 2019), activate these pathways. Moreover, an impairment of the AKT-mTOR pathway has been indicated as a possible cause of wound healing impairment in diabetic mice (Jere et al. 2019).

A role of endogenous NGF in wound healing has been suggested by several studies in animal models, human pathologies and *in vitro* models. In particular, diabetic skin is characterized by a reduced epidermal innervation, considered to be a main cause of diabetic “small-fiber neuropathy” (Ebenezer and Polydefkis 2014), leading to chronic ulcers (Laverdet et al. 2015). Notably, a reduction in neurotrophic support to PNS neurons has been indicated as responsible for peripheral neuropathy (Sima 2003).

Topical application of NGF has therefore been considered as a possible therapy for skin wound healing in chronic ulcers (Tuveri et al. 2000; Generini et al. 2004), and several *in vivo* studies report the positive effect on fibroblast migration, re-epithelialization and capillary lumen formation, and an increase in wound contraction in the full-thickness excision model. One limiting side-effect of the therapeutic use of NGF is local hyperalgesia to mechanical and electrical stimuli lasting for weeks, due to nociceptor sensitization of both sensory and axonal components (Obreja et al. 2018).

Use of NGF as therapeutic agent has been approved for lesions of the corneal epithelium (Sacchetti et al. 2020), and recombinant human NGF has been an approved drug (Oxervate®) since 2017 as eye drops for neurotrophic keratitis.

4. NGF and axonal regrowth

NGF exerts multiple effects on NGF-sensitive neural pathway formation, including axonal elongation and guidance (Guthrie 2007). Moreover, NGF binding at TrkA or p75^{NTR} receptors activates either prosurvival or proapoptotic pathways. During development, nervous system post-synaptic cells are responsible for the majority of NGF release, thus directing the appropriate target innervation. The binding of NGF to TrkA on sympathetic and sensory neurite terminals, for example, leads to receptor dimerization and internalization in the soma of the neurite, then the complex NGF/TrkA is retrogradely transported to the neuronal cell body, where it activates molecular pathways for neuronal survival and differentiation (Johnson et al. 1980). Neuronal cell survival is mediated by the phosphorylation and activation of phosphatidylinositol 3-kinase (PI-3K) and MAPK which leads to Akt activation, the final result of which is the inhibition of pro-apoptotic genes (Bim and FasL) in the developing neuron (Reichardt 2006).

The role of p75^{NTR} in nervous system development is complex, promoting either survival and growth or apoptosis and degeneration, depending on the expression of its coreceptors and ligands. p75^{NTR}-TrkA complexes elicit pro-survival and axonal growth signaling in response to NGF, while neurotrophin binding to p75^{NTR} alone, or the binding of proNGF, can trigger cell death and axonal degeneration. Moreover, p75^{NTR} intracellular trafficking is not yet fully understood (Edward Hickman et al. 2018).

In addition to the neurotrophic effect mediated by the action on pro-survival genes, NGF promotes neurite and axonal elongation, the biological effect from which this neurotrophin take its name, as derived from the historical experiments by Levi-Montalcini and Hamburger. The original experiments described the sympathetic innervation of solid tumors secreting this molecule, when ectopically implanted in chick embryos (Levi-Montalcini and Hamburger 1951). In this system, NGF acts as chemoattractant for axons and neurites, and it has been demonstrated that the elongation of neuron processes mediated by NGF depends on neurite arborization rather than retrograde axonal transport for its action. In fact, as demonstrated in an *in vitro* model of sympathetic neuron cultures, NGF application to the cell body compartment does not

promote neurite extension retrogradely or anterogradely, while NGF application to the neurite compartment promotes neurite elongation, depending on concentration gradient (Campenot 1994).

At molecular level, TrkA activation in neuronal cells leads to an increase in β -actin concentration and its polymerization in the growth cones, ultimately resulting in axonal elongation via PI-3K and PLC- γ activation and subsequent stabilization by de-phosphorylation of the actin-stabilizing complex ADF/Cofilin (Meberg et al. 1998). The activation of p75^{NTR} in the developing nervous system also leads to growth cone stabilization and axon elongation through inactivation of RhoA, which normally phosphorylates and destabilizes ADF/Cofilin via the ROCK cascade (Yamashita et al. 1999).

The role of NGF on the target neural population in the mature nervous system is much more disputed, and differs in the central and peripheral nervous systems. It is noteworthy that p75^{NTR} levels are reduced in neuronal cells during adulthood, and activation of this receptor by NGF has been shown to cause neuronal death in motor neurons, in particular through activation of the JNK and NF- κ B pathway (Wiese et al. 1999), suggesting a switch between pro- and anti-neurotrophic NGF signaling via p75^{NTR} in adulthood. In addition, NGF levels are reduced in adult neurons once nervous system development is complete (Terenghi 1999).

The PNS and the CNS differ substantially in their ability to respond and regenerate axons after damage. In both districts, the “sprouting” of a stump occurs following axon transection, but this sprouting is followed by axonal elongation in the PNS only, while this attempt aborts in the CNS (Cafferty et al. 2010). The main reason for this different behavior, as proven by Aguayo and collaborators’ pioneering work in bridging spinal cord lesions with peripheral nerve grafts, seems to be the non-permissive microenvironment of the CNS compared to the PNS (Richardson et al. 1980; David and Aguayo 1981; Benfey and Aguayo 1982; Richardson and Riopelle 1984). This microenvironment is determined by several factors, including inflammatory stimuli (glial activation and scarring in the CNS versus Wallerian degeneration in the PNS), myelin and cellular debris from the core of the injury, extracellular matrix composition, availability of growth-promoting proteins, and different remyelinating cells (oligodendrocytes and astrocytes in the CNS versus Schwann cells and macrophages in the PNS) (Mietto et al. 2015).

In the CNS, maintenance of the basal cholinergic system phenotype is NGF-dependent, but spontaneous axonal regrowth does not occur even in the event of extreme axonal degeneration, as in the case of experimental lesions or in Alzheimer’s disease (Mesulam et al. 2019). In the PNS, damage to the adult nerves induces a rapid and robust increase in the synthesis of neurotrophins by the surrounding milieu near the lesion. NGF synthesis, for example, increases in the sensory neurons in the dorsal root ganglia (DRG), thus reactivating the cellular mechanisms active during development, and switching their phenotype from “transmitting mode” to “regenerating/regrowth mode” (Richner et al. 2014).

Due to the pleiotropic nature of this molecule, however, NGF synthesis also increases in non-neuronal cells, such as the Schwann cells and perineural fibroblasts surrounding the stumps following axon lesion (Matsuoka et al. 1991), and acts on axons of the afferent sensory neurons in the proximal stump via TrkA. NGF is retrogradely transported to the cell body, where it mediates a trophic effect, enhancing the levels of the pro survival gene GAP-43 (Melville et al. 1989; Wiese et al. 1992; Verge 1996). NGF also stimulates Schwann cell migration and recruitment in the distal stump of the transected nerve (Taniuchi et al. 1988).

On the contrary, deafferentation of adult sympathetic neurons does not modify the expression level of NGF or TrkA (DeCouto et al. 2003), while axotomy of the cervical vagus nerve results in increased expression of mRNAs for NGF in non-neuronal cells at both the proximal and distal segments of the transected nerve segment (Lee et al. 2001).

The indirect effects of NGF on axonal regrowth support the pharmacological use of this neurotrophin in non-NGF-dependent pathways, including the use of innovative approaches based on biomaterials. Taking results obtained from conventional grafts loaded with NGF, such as nerve bridges (Derby et al. 1993), or vein grafts (Gravvanis et al. 2004) as a starting point, more recent approaches have extended the potential use of NGF to treating spinal cord injury. For example, the incorporation of NGF into an electrospun scaffold (Colello et al. 2016) or nanoparticles (Xu et al. 2019) have led to improved axonal regrowth in spinal cord injury, possibly regulating the inflammation and angiogenesis associated with contusion damage.

5. NGF and remyelination

Myelination is the process whereby the axons are wrapped in a multilayer lipid-enriched membrane known as myelin sheath, the thickness of which depends upon axon diameter, to guarantee the appropriate axonal potential conduction. Myelination occurs during development in both the central (CNS) and peripheral (PNS) nervous systems during late gestation and the early post-natal period, and is carried out by two distinct cell types, oligodendrocyte precursor cells (OPCs) and Schwann cells precursors (SCP).

In the CNS, three different sequential waves (E12.5, E15.5, E18.5; in mice) generate the OPCs, which spread throughout all brain and spinal cord regions, with a single mature oligodendrocyte (OL) wrapping multiple axons, in a process which reaches its peak at 2-4 weeks postnatal age in mice. During development of the PNS, SCPs are generated from the neural crest, which then migrate along with growing axons to the peripheral nerves, where the whole cell body wraps around the nude axon. In addition, the transcriptional networks that drive OPC and SCP differentiation, such as central and peripheral myelination and remyelination, are substantially different (Sock and Wegner 2019).

Since neurotrophins play important roles in the development of both the CNS and the PNS, exerting their activities through Trks and $p75^{NTR}$ receptors, a role of these molecules in regulating myelination has been suggested and demonstrated by a number of studies. In fact, it has been suggested that NGF acts as a potent regulator of the axonal signals that control the myelination of TrkA-expressing DRGs. Unexpectedly, these NGF-regulated axonal signals have opposite effects on the myelination of the peripheral and central branch of the pseudounipolar neuron in DRGs, promoting peripheral myelination by Schwann cells (SCs) but reducing central myelination by OLs (Chan et al. 2004).

This discrepant effect is still a topic of debate, since little is known about the role of NGF and other neurotrophins in the regulation of CNS myelination, with most of the data deriving from *in vitro* models (Xiao et al. 2009). Whereas NGF is ineffective in promoting myelination in axon-oligodendrocyte DRG co-cultures, while promoting myelination in axon-Schwann cell DRG (Chan et al. 2004), this neurotrophin increases the expression of genes encoding for myelin-related proteins in oligodendrocytes by acting on both $p75^{NTR}$ and TrkA receptors (Du et al. 2003; Du et al. 2006). Moreover, since NGF is also able to interact directly with the myelin oligodendrocyte glycoprotein (MOG), modulating axon growth and survival, this novel mechanism may mediate communication between growing axons and myelination (von Büdingen et al. 2015).

In the PNS, converging results indicate that NGF regulates both the migration and differentiation of SCPs. The study of *Ntrk1* (the gene encoding for TrkA) expression in the sciatic nerve during development shows its high expression at E17, before decreasing at E19 and disappearing postnatally. $p75^{NTR}$ also increases at E19 and decreases at the postnatal stages (Piirsoo et al. 2010). This dynamic expression is also involved in SCP/SC differentiation and myelination, supporting the bi-directional signaling occurring between developing axons and SCs. *In vitro* data also supports the role of NGF in SC differentiation, the *Ngf* gene being constantly over-expressed at all stages compared to differentiated cells. *Ntrk1* expression is also higher than during proliferation and the growth-arrest state, and $p75^{NTR}$ expression is induced by differentiation (Bentley and Lee 2000).

In both the CNS and the PNS, the complex machinery of myelin repair in adulthood is orchestrated by numerous cell characteristics and signaling molecules deriving from the demyelination process, or from glial and neuronal cell signals. In the CNS, a significant number of the OPCs generated during development do not differentiate but remain quiescent, producing the pool of adult precursors identified by the expression of specific markers (e.g. NG2 and PDGFR α). Resident and newly formed OPCs, derived from neural stem cells (NSCs), are activated by demyelinating insults, and by signals produced by demyelinated axons, resident astrocytes and microglia, and may efficiently repair the myelin, thus restoring saltatory conduction: indeed, remyelination offers a unique example of endogenous regeneration in a system with

poor regeneration capabilities, such as the CNS (Crawford et al. 2013). This remyelination process shares some aspects and mechanisms with developmental myelination, as supported by the recapitulation hypothesis (Fancy et al. 2011). However, it is now clear that developmental myelination and remyelination present important differences (Miron et al. 2011; Baldassarro et al. 2019b; Baldassarro et al. 2019a); there are also important regional differences in the remyelination capabilities of the adult CNS (Horiuchi et al. 2017; Kuhn et al. 2019). A large body of data on the possible role of NGF in myelin protection and/or repair in the CNS comes from animal models of inflammatory/demyelinating diseases. In experimental allergic encephalomyelitis, the most widely used animal model for multiple sclerosis (MS), an increase in tissue NGF concentration has been described (Calzà et al. 1997; Micera et al. 1998; Acosta et al. 2013), such as an increase of p75^{NTR} positive cells in the SVZ (Calzà et al. 1997). These cells, recognized as OPCs (Oderfeld-Nowak et al. 2009), migrate to the corpus callosum (Calzà et al. 1998), p75^{NTR} being a main regulator of the migration process during remyelination also (Anton et al. 1994; Bentley and Lee 2000). In addition, OLs expressing p75^{NTR} have been also found in MS patients (Chang et al. 2000). The importance of the NGF low-affinity receptor in OPC biology is also confirmed by the exacerbation of symptoms in MS animal models lacking p75^{NTR} (Coprav et al. 2004), in which an altered composition of the inflammatory cellular infiltrates is described (Küst et al. 2006). On the other hand, a protective effect on OLs has been shown by a synthetic ligand for TrkA in the cuprizone demyelination model (Bonetto et al. 2017).

The general view of the possible role of NGF in OPC/OL cell fate, as derived from *in vitro* experiments, has been proposed by Casaccia-Bonelli and Chao (Casaccia-Bonelli et al. 2000). In brief, the binding of neurotrophins to Trk receptor tyrosine kinases initiates signaling cascades which promote cell survival and differentiation. In contrast, p75^{NTR} modulates the susceptibility to death of fully differentiated, but not oligodendrocyte progenitor cells, in specific conditions. NGF has no toxic effects on trkA or p75^{NTR} pig-derived OPCs (Althaus and Klöppner 2006), such as oligodendroglia isolated from the rat cerebrum and expressing p75^{NTR} (Starkey et al. 2001), in fact NGF overexpression in human NSCs increases OL differentiation (Marei et al. 2013). Lastly, NGF exposure protects OLs from TNF α -induced toxicity, not only in resident precursors, but also in OPCs generated in the SVZ (Takano et al. 2000; Petratos et al. 2004). Overall, the final picture of p75^{NTR} and Trks expression throughout OPC differentiation is still disputed, depending on the animal species, cell system and animal model used for *in vitro* and *in vivo* experiments (Althaus et al., 2008b, Guo et al., 2013).

SCs, like OLs, are postmitotic and fully differentiated cells. Peripheral demyelination, however, leads to a rapid response of these cells, which de-differentiate, re-enter the cell cycle, and activate the repair process (Jessen et al. 2015). In addition, SC lineage is characterized by differences throughout the different phases of development and differentiation, but heterogeneity is lower compared to OLs (Jessen et al. 2015).

There is much evidence to suggest that NGF and other neurotrophins play different roles in these complex contexts (Althaus et al. 2008a; Webber and Zochodne 2010). p75^{NTR} plays a role in the regulation of SCP migration to the PNS (Anton et al. 1994). Throughout p75^{NTR} activation, NGF treatment following peripheral nerve lesions promotes SC autophagy, enhancing the clearance of myelin debris and accelerating recovery from the injury (Li et al. 2020). NGF also acts as chemo-attractant and chemo-kinetic cue for both SCs and SCPs (Maniwa et al. 2003; Cornejo et al. 2010).

Data briefly summarized shows a clear portrait of the pro-myelinating role of NGF in PNS, while the effect on OPCs/OLs, and therefore on central myelination, is still uncertain. In both districts, moreover, it is still unclear whether NGF acts directly on myelinating cells, or indirectly through axons or the satellite cells (fibroblasts, inflammatory cells, glial cells other than myelinating, etc.).

REFERENCES

- Acosta CMR, Cortes C, MacPhee H, Namaka MP (2013) Exploring the role of nerve growth factor in multiple sclerosis: implications in myelin repair. *CNS Neurol Disord Drug Targets* 12:1242–56
- Aloe L, Calzà L (2004) NGF and related molecules in health and disease: Preface. In: *Progress in Brain Research*. p 544
- Althaus HH, Klöppner S (2006) Mature pig oligodendrocytes rapidly process human recombinant pro-nerve growth factor and do not undergo cell death. *J Neurochem* 98:506–17 .
<https://doi.org/10.1111/j.1471-4159.2006.03891.x>
- Althaus HH, Klöppner S, Klopffleisch S, Schmitz M (2008a) Oligodendroglial cells and neurotrophins: A polyphonic cantata in major and minor. *J. Mol. Neurosci.* 35:65–79
- Althaus HH, Klöppner S, Klopffleisch S, Schmitz M (2008b) Oligodendroglial cells and neurotrophins: a polyphonic cantata in major and minor. *J Mol Neurosci* 35:65–79 . <https://doi.org/10.1007/s12031-008-9053-y>
- Anton ES, Weskamp G, Reichardt LF, Matthew WD (1994) Nerve growth factor and its low-affinity receptor promote Schwann cell migration. *Proc Natl Acad Sci U S A* 91:2795–2799 .
<https://doi.org/10.1073/pnas.91.7.2795>
- Bagnara GP (2020) STEM CELLS. SOCIETA EDITRICE ESCULAPI
- Baldassarro VA, Krężel W, Fernández M, Schuhbauer B, Giardino L, Calzà L (2019a) The role of nuclear receptors in the differentiation of oligodendrocyte precursor cells derived from fetal and adult neural stem cells. *Stem Cell Res* 37:101443 . <https://doi.org/10.1016/j.scr.2019.101443>
- Baldassarro VA, Marchesini A, Giardino L, Calzà L (2019b) Differential effects of glucose deprivation on the survival of fetal versus adult neural stem cells-derived oligodendrocyte precursor cells. *Glia* 101:23750 . <https://doi.org/10.1002/glia.23750>
- Benfey M, Aguayo AJ (1982) Extensive elongation of axons from rat brain into peripheral nerve grafts. *Nature* 296:150–2 . <https://doi.org/10.1038/296150a0>
- Bentley CA, Lee KF (2000) p75 Is important for axon growth and Schwann cell migration during development. *J Neurosci* 20:7706–7715 . <https://doi.org/10.1523/jneurosci.20-20-07706.2000>
- Bonetto G, Charalampopoulos I, Gravanis A, Karagogeos D (2017) The novel synthetic microneurotrophin BNN27 protects mature oligodendrocytes against cuprizone-induced death, through the NGF receptor

TrkA. *Glia* 65:1376–1394 . <https://doi.org/10.1002/glia.23170>

Botchkarev VA, Botchkareva N V., Peters EMJ, Paus R (2004) Epithelial growth control by neurotrophins: Leads and lessons from the hair follicle. In: *Progress in Brain Research*. Elsevier, pp 493–513

Bracci-Laudiero L, De Stefano ME (2016) NGF in early embryogenesis, differentiation, and pathology in the nervous and immune systems. In: *Current Topics in Behavioral Neurosciences*. Springer Verlag, pp 125–152

Bruce CC, Zhao C, Franklin RJM (2010) Remyelination - An effective means of neuroprotection. *Horm Behav* 57:56–62 . <https://doi.org/10.1016/j.yhbeh.2009.06.004>

Cafferty WBJ, Duffy P, Huebner E, Strittmatter SM (2010) MAG and OMgp synergize with Nogo-A to restrict axonal growth and neurological recovery after spinal cord trauma. *J Neurosci* 30:6825–37 . <https://doi.org/10.1523/JNEUROSCI.6239-09.2010>

Calzà L, Giardino L, Giuliani A, Aloe L, Levi-Montalcini R (2001) Nerve growth factor control of neuronal expression of angiogenetic and vasoactive factors. *Proc Natl Acad Sci U S A* 98:4160–4165 . <https://doi.org/10.1073/pnas.051626998>

Calzà L, Giardino L, Pozza M, Bettelli C, Micera A, Aloe L (1998) Proliferation and phenotype regulation in the subventricular zone during experimental allergic encephalomyelitis: in vivo evidence of a role for nerve growth factor. *Proc Natl Acad Sci U S A* 95:3209–14 . <https://doi.org/10.1073/pnas.95.6.3209>

Calzà L, Giardino L, Pozza M, Micera A, Aloe L (1997) Time-course changes of nerve growth factor, corticotropin-releasing hormone, and nitric oxide synthase isoforms and their possible role in the development of inflammatory response in experimental allergic encephalomyelitis. *Proc Natl Acad Sci U S A* 94:3368–3373 . <https://doi.org/10.1073/pnas.94.7.3368>

Campenot RB (1994) NGF and the local control of nerve terminal growth. *J Neurobiol* 25:599–611 . <https://doi.org/10.1002/neu.480250603>

Casaccia-Bonofil P, Gu C, Chao M V. (2000) Neurotrophins in cell survival/death decisions. *Adv Exp Med Biol* 468:275–282 . https://doi.org/10.1007/978-1-4615-4685-6_22

Chan JR, Watkins TA, Cosgaya JM, Zhang C, Chen L, Reichardt LF, Shooter EM, Barres BA (2004) NGF controls axonal receptivity to myelination by Schwann cells or oligodendrocytes. *Neuron* 43:183–191 . <https://doi.org/10.1016/j.neuron.2004.06.024>

Chang A, Nishiyama A, Peterson J, Prineas J, Trapp BD (2000) NG2-positive oligodendrocyte progenitor cells

in adult human brain and multiple sclerosis lesions. *J Neurosci* 20:6404–6412 .

<https://doi.org/10.1523/jneurosci.20-17-06404.2000>

Colello RJ, Chow WN, Bigbee JW, Lin C, Dalton D, Brown D, Jha BS, Mathern BE, Lee KD, Simpson DG (2016)

The incorporation of growth factor and chondroitinase ABC into an electrospun scaffold to promote axon regrowth following spinal cord injury. *J Tissue Eng Regen Med* 10:656–668 .

<https://doi.org/10.1002/term.1805>

Coprav S, Küst B, Emmer B, Lin MY, Liem R, Amor S, De Vries H, Floris S, Boddeke E (2004) Deficient p75

low-affinity neurotrophin receptor expression exacerbates experimental allergic encephalomyelitis in C57/BL6 mice. *J Neuroimmunol* 148:41–53 . <https://doi.org/10.1016/j.jneuroim.2003.11.008>

Cornejo M, Nambi D, Walheim C, Somerville M, Walker J, Kim L, Ollison L, Diamante G, Vyawahare S, De

Bellard ME (2010) Effect of NRG1, GDNF, EGF and NGF in the migration of a Schwann cell precursor line. *Neurochem Res* 35:1643–1651 . <https://doi.org/10.1007/s11064-010-0225-0>

Crawford AH, Chambers C, Franklin RJM (2013) Remyelination: The True Regeneration of the Central

Nervous System. *J Comp Pathol* 149:242–254 . <https://doi.org/10.1016/j.jcpa.2013.05.004>

David S, Aguayo A (1981) Axonal elongation into peripheral nervous system “bridges” after central nervous

system injury in adult rats. *Science* (80-) 214:931–933 . <https://doi.org/10.1126/science.6171034>

DeCouto SA, Jones EE, Kudwa AE, Shoemaker SE, Shafer AJ, Brieschke MA, James PF, Vaughn JC, Isaacson

LG (2003) The effects of deafferentation and exogenous NGF on neurotrophins and neurotrophin receptor mRNA expression in the adult superior cervical ganglion. *Brain Res Mol Brain Res* 119:73–82 .

<https://doi.org/10.1016/j.molbrainres.2003.08.015>

Derby A, Engleman VW, Friedrich GE, Neises G, Rapp SR, Roufa DG (1993) Nerve growth factor facilitates

regeneration across nerve gaps: morphological and behavioral studies in rat sciatic nerve. *Exp Neurol* 119:176–91 . <https://doi.org/10.1006/exnr.1993.1019>

Du Y, Fischer TZ, Clinton-Luke P, Lercher LD, Dreyfus CF (2006) Distinct effects of p75 in mediating actions of

neurotrophins on basal forebrain oligodendrocytes. *Mol Cell Neurosci* 31:366–375 .

<https://doi.org/10.1016/j.mcn.2005.11.001>

Du Y, Fischer TZ, Lee LN, Lercher LD, Dreyfus CF (2003) Regionally Specific Effects of BDNF on

Oligodendrocytes. *Dev Neurosci* 25:116–126 . <https://doi.org/10.1159/000072261>

Ebenezer G, Polydefkis M (2014) Epidermal innervation in diabetes. In: *Handbook of Clinical Neurology*.

Elsevier B.V., pp 261–274

- Edward Hickman F, Stanley EM, Carter BD (2018) Neurotrophin responsiveness of sympathetic neurons is regulated by rapid mobilization of the p75 receptor to the cell surface through trka activation of arf6. *J Neurosci* 38:5606–5619 . <https://doi.org/10.1523/JNEUROSCI.0788-16.2018>
- Ehrhard PB, Erb P, Graumann U, Otten U (1993) Expression of nerve growth factor and nerve growth factor receptor tyrosine kinase Trk in activated CD4-positive T-cell clones. *Proc Natl Acad Sci U S A* 90:10984–10988 . <https://doi.org/10.1073/pnas.90.23.10984>
- Elsherbiny NM, Abdel-Mottaleb Y, Elkazaz AY, Atef H, Lashine RM, Youssef AM, Ezzat W, El-Ghaiesh SH, Elshaer RE, El-Shafey M, Zaitone SA (2019) Carbamazepine Alleviates Retinal and Optic Nerve Neural Degeneration in Diabetic Mice via Nerve Growth Factor-Induced PI3K/Akt/mTOR Activation. *Front Neurosci* 13: . <https://doi.org/10.3389/fnins.2019.01089>
- Fancy SPJ, Chan JR, Baranzini SE, Franklin RJM, Rowitch DH (2011) Myelin Regeneration: A Recapitulation of Development? *Annu Rev Neurosci* 34:21–43 . <https://doi.org/10.1146/annurev-neuro-061010-113629>
- Fernández M, Pironi S, Chen BL, Del Vecchio G, Alessandri M, Farnedi A, Pession A, Feki A, Jaconi MEE, Calzà L (2011) Isolation of rat embryonic stem-like cells: A tool for stem cell research and drug discovery. *Dev Dyn* 240:2482–2494 . <https://doi.org/10.1002/dvdy.22761>
- Generini S, Tuveri MA, Matucci Cerinic M, Mastinu F, Manni L, Aloe L (2004) Topical application of nerve growth factor in human diabetic foot ulcers. A study of three cases. *Exp Clin Endocrinol Diabetes* 112:542–544 . <https://doi.org/10.1055/s-2004-821313>
- Gostynska N, Pannella M, Rocco ML, Giardino L, Aloe L, Calzà L (2019) The pleiotropic molecule NGF regulates the in vitro properties of fibroblasts, keratinocytes and endothelial cells: implications for wound healing. *Am J Physiol Physiol* ajpcell.00180.2019 . <https://doi.org/10.1152/ajpcell.00180.2019>
- Gravvanis AI, Tsoutsos DA, Tagaris GA, Papalois AE, Patralexis CG, Iconomou TG, Panayotou PN, Ioannovich JD (2004) Beneficial effect of nerve growth factor-7S on peripheral nerve regeneration through inside-out vein grafts: An experimental study. *Microsurgery* 24:408–415 . <https://doi.org/10.1002/micr.20055>
- Guthrie S (2007) Neurotrophic factors: Are they axon guidance molecules? *Adv. Exp. Med. Biol.* 621:81–94
- Horiuchi M, Suzuki-Horiuchi Y, Akiyama T, Itoh A, Pleasure D, Carstens E, Itoh T (2017) Differing intrinsic biological properties between forebrain and spinal oligodendroglial lineage cells. *J Neurochem* 142:378–391 . <https://doi.org/10.1111/jnc.14074>
- Inanç B, Elçin AE, Elçin YM (2008) Human Embryonic Stem Cell Differentiation on Tissue Engineering

Scaffolds: Effects of NGF and Retinoic Acid Induction. *Tissue Eng Part A* 0:080422095744451 .
<https://doi.org/10.1089/tea.2007.0213>

Indo Y (2012) Nerve growth factor and the physiology of pain: Lessons from congenital insensitivity to pain with anhidrosis. *Clin. Genet.* 82:341–350

Jere SW, Houreld NN, Abrahamse H (2019) Role of the PI3K/AKT (mTOR and GSK3 β) signalling pathway and photobiomodulation in diabetic wound healing. *Cytokine Growth Factor Rev.* 50:52–59

Jessen KR, Mirsky R, Lloyd AC (2015) Schwann cells: Development and role in nerve repair. *Cold Spring Harb Perspect Biol* 7:1–15 . <https://doi.org/10.1101/cshperspect.a020487>

Johnson EM, Gorin PD, Brandeis LD, Pearson J (1980) Dorsal root ganglion neurons are destroyed by exposure in utero to maternal antibody to nerve growth factor. *Science* 210:916–8 .
<https://doi.org/10.1126/science.7192014>

Kasemeier-Kulesa JC, Kulesa PM (2018) The convergent roles of CD271/p75 in neural crest-derived melanoma plasticity. *Dev Biol* 444:S352–S355 . <https://doi.org/10.1016/j.ydbio.2018.04.008>

Kim YS, Jo DH, Lee H, Kim JH, Kim KW, Kim JH (2013) Nerve growth factor-mediated vascular endothelial growth factor expression of astrocyte in retinal vascular development. *Biochem Biophys Res Commun* 431:740–745 . <https://doi.org/10.1016/j.bbrc.2013.01.045>

Kristiansen M, Ham J (2014) Programmed cell death during neuronal development: The sympathetic neuron model. *Cell Death Differ.* 21:1025–1035

Kuhn S, Gritti L, Crooks D, Dombrowski Y (2019) Oligodendrocytes in Development, Myelin Generation and Beyond. *Cells* 8:1424 . <https://doi.org/10.3390/cells8111424>

Küst B, Mantingh-Otter I, Boddeke E, Copray S (2006) Deficient p75 low-affinity neurotrophin receptor expression does alter the composition of cellular infiltrate in experimental autoimmune encephalomyelitis in C57BL/6 mice. *J Neuroimmunol* 174:92–100 .
<https://doi.org/10.1016/j.jneuroim.2006.01.020>

Laverdet B, Danigo A, Girard D, Magy L, Demiot C, Desmoulière A (2015) Skin innervation: Important roles during normal and pathological cutaneous repair. *Histol. Histopathol.* 30:875–892

Lee P, Zhuo H, Helke CJ (2001) Axotomy alters neurotrophin and neurotrophin receptor mRNAs in the vagus nerve and nodose ganglion of the rat. *Brain Res Mol Brain Res* 87:31–41 .
[https://doi.org/10.1016/s0169-328x\(00\)00277-1](https://doi.org/10.1016/s0169-328x(00)00277-1)

- Leon A, Buriani A, Dal Toso R, Fabris M, Romanello S, Aloe L, Levi-Montalcini R (1994) Mast cells synthesize, store, and release nerve growth factor. *Proc Natl Acad Sci U S A* 91:3739–3743 .
<https://doi.org/10.1073/pnas.91.9.3739>
- Levi-Montalcini R (1997) *The Saga of the Nerve Growth Factor*. WORLD SCIENTIFIC
- Levi-Montalcini R, Hamburger V (1951) Selective growth stimulating effects of mouse sarcoma on the sensory and sympathetic nervous system of the chick embryo. *J Exp Zool* 116:321–361 .
<https://doi.org/10.1002/jez.1401160206>
- Li R, Li D, Wu C, Ye L, Wu Y, Yuan Y, Yang S, Xie L, Mao Y, Jiang T, Li Y, Wang J, Zhang H, Li X, Xiao J (2020) Nerve growth factor activates autophagy in Schwann cells to enhance myelin debris clearance and to expedite nerve regeneration. *Theranostics* 10:1649–1677 . <https://doi.org/10.7150/thno.40919>
- Lumelsky N, O’Hayre M, Chander P, Shum L, Somerman MJ (2018) Autotherapies: Enhancing Endogenous Healing and Regeneration. *Trends Mol. Med.* 24:919–930
- Maniwa S, Iwata A, Hirata H, Ochi M (2003) Effects of neurotrophic factors on chemokinesis of Schwann cells in culture. *Scand J Plast Reconstr Surg Hand Surg* 37:14–17 .
<https://doi.org/10.1080/alp.37.1.14.17>
- Marei HES, Althani A, Afifi N, Abd-Elmaksoud A, Bernardini C, Michetti F, Barba M, Pescatori M, Maira G, Paldino E, Manni L, Casalbore P, Cenciarelli C (2013) Over-expression of hNGF in adult human olfactory bulb neural stem cells promotes cell growth and oligodendrocytic differentiation. *PLoS One* 8:e82206 . <https://doi.org/10.1371/journal.pone.0082206>
- Martin-Zanca D, Barbacid M, Parada LF (1990) Expression of the trk proto-oncogene is restricted to the sensory cranial and spinal ganglia of neural crest origin in mouse development. *Genes Dev* 4:683–694 . <https://doi.org/10.1101/gad.4.5.683>
- Matsuda H, Kannan Y, Ushio H, Kiso Y, Kanemoto T, Suzuki H, Kitamura Y (1991) Nerve growth factor induces development of connective tissue-type mast cells in vitro from murine bone marrow cells. *J Exp Med* 174:7–14 . <https://doi.org/10.1084/jem.174.1.7>
- Matsuoka I, Meyer M, Thoenen H (1991) Cell-type-specific regulation of nerve growth factor (NGF) synthesis in non-neuronal cells: Comparison of Schwann cells with other cell types. *J Neurosci* 11:3165–3177 . <https://doi.org/10.1523/jneurosci.11-10-03165.1991>
- Meberg PJ, Ono S, Minamide LS, Takahashi M, Bamburg JR (1998) Actin depolymerizing factor and cofilin phosphorylation dynamics: response to signals that regulate neurite extension. *Cell Motil*

Cytoskeleton 39:172–90 . [https://doi.org/10.1002/\(SICI\)1097-0169\(1998\)39:2<172::AID-CM8>3.0.CO;2-8](https://doi.org/10.1002/(SICI)1097-0169(1998)39:2<172::AID-CM8>3.0.CO;2-8)

Melville S, Sherburn TE, Coggeshall RE (1989) Preservation of sensory cells by placing stumps of transected nerve in an impermeable tube. *Exp Neurol* 105:311–5 . [https://doi.org/10.1016/0014-4886\(89\)90135-0](https://doi.org/10.1016/0014-4886(89)90135-0)

Mesulam MM, Lalehzari N, Rahmani F, Ohm D, Shahidehpour R, Kim G, Gefen T, Weintraub S, Bigio E, Geula C (2019) Cortical cholinergic denervation in primary progressive aphasia with Alzheimer pathology. *Neurology* 92:E1580–E1588 . <https://doi.org/10.1212/WNL.0000000000007247>

Micera A, Vigneti E, Aloe L (1998) Changes of NGF presence in nonneuronal cells in response to experimental allergic encephalomyelitis in Lewis rats. *Exp Neurol* 154:41–46 . <https://doi.org/10.1006/exnr.1998.6864>

Mietto BS, Mostacada K, Martinez AMB (2015) Neurotrauma and inflammation: CNS and PNS responses. *Mediators Inflamm* 2015: . <https://doi.org/10.1155/2015/251204>

Miron VE, Kuhlmann T, Antel JP (2011) Cells of the oligodendroglial lineage, myelination, and remyelination. *BBA - Mol Basis Dis* 1812:184–193 . <https://doi.org/10.1016/j.bbadis.2010.09.010>

Mitsiadis TA, Pagella P (2016) Expression of nerve growth factor (NGF), TrkA, and p75NTR in developing human fetal teeth. *Front Physiol* 7: . <https://doi.org/10.3389/fphys.2016.00338>

Moscatelli I, Pierantozzi E, Camaioni A, Siracusa G, Campagnolo L (2009) p75 neurotrophin receptor is involved in proliferation of undifferentiated mouse embryonic stem cells. *Exp Cell Res* 315:3220–3232 . <https://doi.org/10.1016/j.yexcr.2009.08.014>

Obreja O, Rukwied R, Nagler L, Schmidt M, Schmelz M, Namer B (2018) Nerve growth factor locally sensitizes nociceptors in human skin. *Pain* 159:416–426 . <https://doi.org/10.1097/j.pain.0000000000001108>

Oderfeld-Nowak B, Zaremba M, Kwiatkowska-Patzer B, Lipkowski AW, Kurkowska-Jastrzębska I, Triaca V, Aloe L (2009) NG2 positive cells of rat spinal cord activated during experimental autoimmune encephalomyelitis are spatially associated with radially oriented astroglia and express p75 receptor: A role for nerve growth factor in oligodendrocyte progenitor migration? *Arch Ital Biol* 147:105–115 . <https://doi.org/10.4449/aib.v147i4.871>

Pannella M, Giardino L, Calzà L, Fernández M (2018) Growth and neurotrophic factors in embryonic stem cells. In: *Methods in Molecular Biology*. Humana Press Inc., pp 275–294

- Park MJ, Kwak HJ, Lee HC, Yoo DH, Park IC, Kim MS, Lee SH, Chang HR, Hong S Il (2007) Nerve growth factor induces endothelial cell invasion and cord formation by promoting matrix metalloproteinase-2 expression through the phosphatidylinositol 3-kinase/Akt signaling pathway and AP-2 transcription factor. *J Biol Chem* 282:30485–30496 . <https://doi.org/10.1074/jbc.M701081200>
- Petratos S, Gonzales MF, Azari MF, Marriott M, Minichiello RA, Shipham KA, Profyris C, Nicolaou A, Boyle K, Cheema SS, Kilpatrick TJ (2004) Expression of the low-affinity neurotrophin receptor, p75NTR, is upregulated by oligodendroglial progenitors adjacent to the subventricular zone in response to demyelination. *Glia* 48:64–75 . <https://doi.org/10.1002/glia.20056>
- Piirsoo M, Kaljas A, Tamm K, Timmusk T (2010) Expression of NGF and GDNF family members and their receptors during peripheral nerve development and differentiation of Schwann cells in vitro. *Neurosci Lett* 469:135–140 . <https://doi.org/10.1016/j.neulet.2009.11.060>
- Pyle AD, Lock LF, Donovan PJ (2006) Neurotrophins mediate human embryonic stem cell survival. *Nat Biotechnol* 24:344–350 . <https://doi.org/10.1038/nbt1189>
- Reichardt LF (2006) Neurotrophin-regulated signalling pathways. *Philos. Trans. R. Soc. B Biol. Sci.* 361:1545–1564
- Reinke JM, Sorg H (2012) Wound repair and regeneration. *Eur. Surg. Res.* 49:35–43
- Richardson PM, McGuinness UM, Aguayo AJ (1980) Axons from CNS neurones regenerate into PNS grafts. *Nature* 284:264–265 . <https://doi.org/10.1038/284264a0>
- Richardson PM, Riopelle RJ (1984) Uptake of nerve growth factor along peripheral and spinal axons of primary sensory neurons. *J Neurosci* 4:1683–1689 . <https://doi.org/10.1523/jneurosci.04-07-01683.1984>
- Richner M, Ulrichsen M, Elmegaard SL, Dieu R, Pallesen LT, Vaegter CB (2014) Peripheral Nerve Injury Modulates Neurotrophin Signaling in the Peripheral and Central Nervous System. *Mol. Neurobiol.* 50:945–970
- Sacchetti M, Lambiase A, Schmidl D, Schmetterer L, Ferrari M, Mantelli F, Allegretti M, Garhofer G (2020) Effect of recombinant human nerve growth factor eye drops in patients with dry eye: A phase IIa, open label, multiple-dose study. *Br J Ophthalmol* 104:127–135 . <https://doi.org/10.1136/bjophthalmol-2018-312470>
- Sen CK, Gordillo GM, Roy S, Kirsner R, Lambert L, Hunt TK, Gottrup F, Gurtner GC, Longaker MT (2009) Human skin wounds: A major and snowballing threat to public health and the economy: PERSPECTIVE

ARTICLE. *Wound Repair Regen.* 17:763–771

Sima AAF (2003) New insights into the metabolic and molecular basis for diabetic neuropathy. *Cell. Mol. Life Sci.* 60:2445–2464

Snider WD, McMahon SB (1998) Tackling pain at the source: New ideas about nociceptors. *Neuron* 20:629–632

Sock E, Wegner M (2019) Transcriptional control of myelination and remyelination. *Glia*

Starkey GD, Petratos S, Shipham KA, Butzkueven H, Bucci T, Lowry K, Cheema SS, Kilpatrick TJ (2001) Neurotrophin receptor expression and responsiveness by postnatal cerebral oligodendroglia. *Neuroreport* 12:4081–4086 . <https://doi.org/10.1097/00001756-200112210-00044>

Sun D (2016) Endogenous neurogenic cell response in the mature mammalian brain following traumatic injury. *Exp. Neurol.* 275:405–410

Takano R, Hisahara S, Namikawa K, Kiyama H, Okano H, Miura M (2000) Nerve growth factor protects oligodendrocytes from tumor necrosis factor- α -induced injury through Akt-mediated signaling mechanisms. *J Biol Chem* 275:16360–5 . <https://doi.org/10.1074/jbc.M910419199>

Taniuchi M, Clark HB, Schweitzer JB, Johnson EM (1988) Expression of nerve growth factor receptors by Schwann cells of axotomized peripheral nerves: ultrastructural location, suppression by axonal contact, and binding properties. *J Neurosci* 8:664–81

Terenghi G (1999) Peripheral nerve regeneration and neurotrophic factors. *J Anat* 194:1–14 . <https://doi.org/10.1046/j.1469-7580.1999.19410001.x>

Tron VA, Coughlin MD, Jang DE, Stanisz J, Sauder DN (1990) Expression and modulation of nerve growth factor in murine keratinocytes (PAM 212). *J Clin Invest* 85:1085–1089 . <https://doi.org/10.1172/JCI114539>

Tuveri M, Generini S, Matucci-Cerinic M, Aloe L (2000) NGF, a useful tool in the treatment of chronic vasculitic ulcers in rheumatoid arthritis. *Lancet* 356:1739–1740 . [https://doi.org/10.1016/S0140-6736\(00\)03212-8](https://doi.org/10.1016/S0140-6736(00)03212-8)

Verge VMK (1996) Neurotrophins and nerve injury in the adult. *Philos Trans R Soc B Biol Sci* 351:423–430 . <https://doi.org/10.1098/rstb.1996.0038>

von Büdingen H-C, Mei F, Greenfield A, Jahn S, Shen Y-AA, Reid HH, McKemy DD, Chan JR (2015) The myelin oligodendrocyte glycoprotein directly binds nerve growth factor to modulate central axon circuitry. *J*

Cell Biol 210:891–898 . <https://doi.org/10.1083/jcb.201504106>

Webber C, Zochodne D (2010) The nerve regenerative microenvironment: Early behavior and partnership of axons and Schwann cells. *Exp. Neurol.* 223:51–59

Wells JM, Watt FM (2018) Diverse mechanisms for endogenous regeneration and repair in mammalian organs. *Nature* 557:322–328

Wiese S, Metzger F, Holtmann B, Sendtner M (1999) The role of p75NTR in modulating neurotrophin survival effects in developing motoneurons. *Eur J Neurosci* 11:1668–76 .
<https://doi.org/10.1046/j.1460-9568.1999.00585.x>

Wiese UH, Ruth JL, Emson PC (1992) Differential expression of growth-associated protein (GAP-43) mRNA in rat primary sensory neurons after peripheral nerve lesion: a non-radioactive in situ hybridisation study. *Brain Res* 592:141–56 . [https://doi.org/10.1016/0006-8993\(92\)91669-6](https://doi.org/10.1016/0006-8993(92)91669-6)

Wislet S, Vandervelden G, Rogister B (2018) From Neural Crest Development to Cancer and Vice Versa: How p75NTR and (Pro)neurotrophins Could Act on Cell Migration and Invasion? *Front. Mol. Neurosci.* 11

Xiao J, Kilpatrick TJ, Murray SS (2009) The Role of Neurotrophins in the Regulation of Myelin Development. *Neurosignals* 17:265–276 . <https://doi.org/10.1159/000231893>

Xu D, Wu D, Qin M, Nih LR, Liu C, Cao Z, Ren J, Chen X, He Z, Yu W, Guan J, Duan S, Liu F, Liu X, Li J, Harley D, Xu B, Hou L, Chen ISY, Wen J, Chen W, Pourtaheri S, Lu Y (2019) Efficient Delivery of Nerve Growth Factors to the Central Nervous System for Neural Regeneration. *Adv Mater* 31:e1900727 .
<https://doi.org/10.1002/adma.201900727>

Yamashita T, Tucker KL, Barde YA (1999) Neurotrophin binding to the p75 receptor modulates Rho activity and axonal outgrowth. *Neuron* 24:585–593 . [https://doi.org/10.1016/S0896-6273\(00\)81114-9](https://doi.org/10.1016/S0896-6273(00)81114-9)

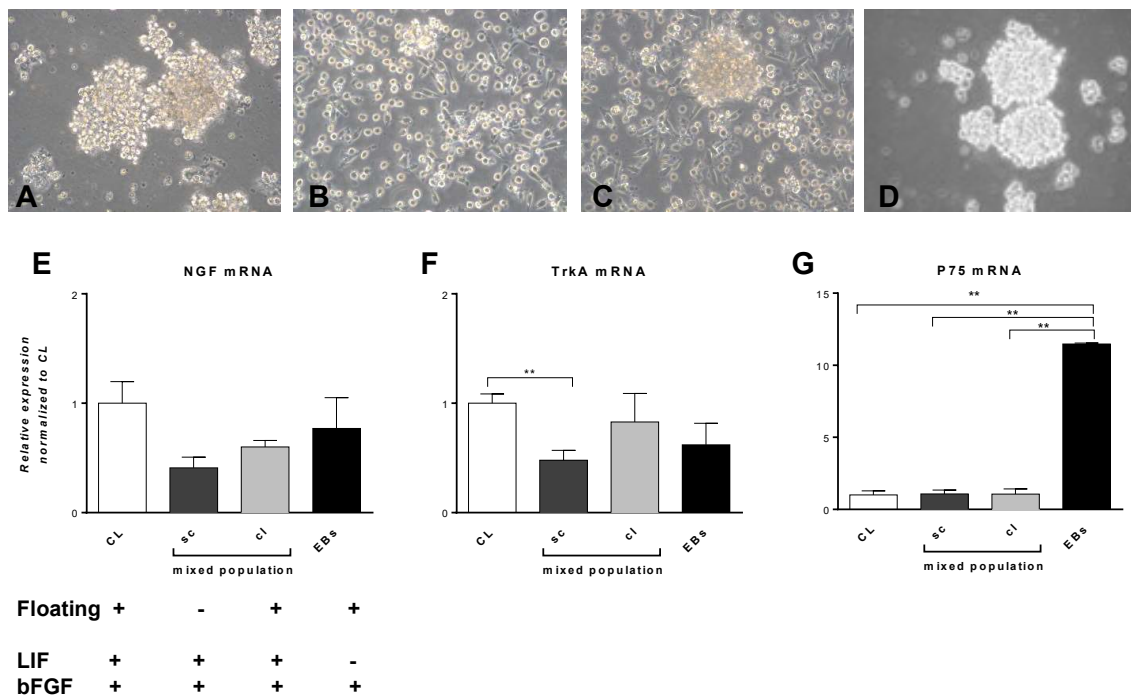
Yu X, Qi Y, Zhao T, Fang J, Liu X, Xu T, Yang Q, Dai X (2019) NGF increases FGF2 expression and promotes endothelial cell migration and tube formation through PI3K/Akt and ERK/MAPK pathways in human chondrocytes. *Osteoarthr Cartil* 27:526–534 . <https://doi.org/10.1016/j.joca.2018.12.007>

Legend

Figure 1.

NGF, *trkA* and *p75* gene expression in RESCs. Representative images of RESCs grown as CLs (A), mixed population of SCs and CLs (B, C) and EBs (D) in the specified culture conditions and mediums containing the mitogens indicated. Graphs show relative mRNA expression of NGF (E) and its receptors, *trkA* (F) and *p75* (G), normalized to CL. Mean values \pm SEM from 3 independent experiments performed in duplicate are included in the graphs. Statistical analysis was performed using 1-way ANOVA and Tukey's multiple comparisons test. Significant results were fixed at $p < 0.05$.

Abbreviations: bFGF, basic fibroblast growth factor; CL, clusters; EBs, embryoid bodies; LIF, Leukemia inhibitory factor; SC, single cells.



5. GENERAL CONCLUSIONS

The complex and evolving context of traumatic spinal cord lesions, significantly the molecular and cellular changes during the onset and progression of secondary degeneration with the aim of defining possible novel therapeutic approaches, was the main focus of this thesis work.

The present work started with the initial need for a standardized animal model of contusive SCI. The severity of the lesion and the functional outcomes were defined with two different types of initial damage. We obtained a severe and mild SCI model. The first is characterized by the complete immobility of the posterior hind limbs, a slow locomotor recovery, and the neurologic bladder's development. The second model showed no neurologic bladder signs and a faster and higher recovery in locomotion after the contusive lesion. We decided to characterize further and test pharmacological intervention in the mild lesion model of SCI for the presence of a more extended pharmacological window, intended as longer spontaneous functional recovery.

We first analyzed the modification in gene expression involved in the formation and maintenance of the ECM in the spinal cord. The data obtained by the gene expression analysis performed in the spinal cord segments surrounding the lesion site and not directly involved in the lesion showed a different modulation of genes after SCI. Bioinformatic analysis revealed a crucial role for Timp1 as a hub gene in the rostral segment from the lesion during the SCI evolution. The importance of Timp1 was confirmed by in-vitro analysis on astrocyte cells stimulated with a pro-inflammatory cytokines mix. Our approach demonstrated a solid data driven approach for the identification of critical pathways involved in secondary neurodegeneration, which could help understand pathological mechanisms and verify regenerative medicine treatments.

We then analyzed synaptic plasticity-related genes in the motor areas of the CNS. We found a different regulation of gene expression between spinal areas and supraspinal regions involved in locomotor function. For the spinal cord, we observed a different modulation between the rostral and caudal segments surrounding the lesion epicenter, confirming the general findings of the ECM analysis. In particular, in the rostral segment, we found an increased expression of early response genes and neurotrophins receptors Fos, Junb, and Ngfr, which was not observed in the caudal segment of the spinal cord. Moreover, the deafferentation of descending motor pathways in the spinal cord also causes gene expression changes in supraspinal areas. We found the motor cortex as the most affected region, especially in the long term, with a consistent downregulation of crucial genes for neuronal survival like Igf1, Ntf3, and Ntrk2. Overall, this analysis suggests that molecular mapping is fundamental to investigate the modification in spinal and supraspinal areas after SCI. Moreover, it could allow to identify specific therapeutic windows for the intervention with regenerative and rehabilitation therapies specifically directed to a class of neurons in the CNS.

The final part of this work demonstrated that effective intervention in the secondary cascade of the SCI could improve the functional outcome of treated animals. In particular, our treatment aims to reduce the inflammatory microenvironment developed in the acute phase of the lesion and increase spontaneous remyelination. The new delivery solution is based on an implantable electrospun PLLA scaffold loaded with ibuprofen and T3, designed for a local and prolonged drug release. This therapeutic solution produced a marked reduction in the principal class of inflammatory cells, the microglia/macrophages, into the lesioned and perilesional spinal tissue and a reduction of glutamate, the main excitotoxic neurotransmitter. The pharmacological regulation of the microenvironment in the lesioned areas improves OPCs and neuron survival. In concomitance, the action of T3 helps the surviving OPCs and stimulates their differentiation in OLs, enhancing the myelination of the segments of the spinal cord surrounding the primary lesion. It is noteworthy that our data demonstrated a long-lasting efficacy in reduction of inflammatory marker and stimulation of neuroprotective effects, thus confirming that an appropriate pharmacological cocktail administered in the therapeutic windows defined by the secondary degeneration progression might help the spontaneous repair of the CNS.

References

1. Scaal, M. Early development of the vertebral column. *Seminars in Cell and Developmental Biology* **49**, 83–91 (2016).
2. Kesseland, M. & Gruss, P. Homeotic transformations of murine vertebrae and concomitant alteration of Hox codes induced by retinoic acid. *Cell* **67**, 89–104 (1991).
3. Mai, J. K. & Paxinos, G. *The Human Nervous System. The Human Nervous System* (Elsevier Inc., 2012). doi:10.1016/C2009-0-02721-4
4. Paxinos, G. *The Rat Nervous System: Fourth Edition. The Rat Nervous System: Fourth Edition* (Elsevier Inc., 2014). doi:10.1016/C2009-0-02419-2
5. Stassart, R. M., Möbius, W., Nave, K. A. & Edgar, J. M. The Axon-Myelin unit in development and degenerative disease. *Frontiers in Neuroscience* **12**, 467 (2018).
6. Cho, T. A. Spinal cord functional anatomy. *CONTINUUM Lifelong Learning in Neurology* **21**, 13–35 (2015).
7. Felten, D. L., O'Banion, M. K. & Maida, M. S. Spinal Cord. in *Netter's Atlas of Neuroscience* 77–83 (Elsevier, 2016). doi:10.1016/B978-0-323-26511-9.00005-9
8. Watson, C., Paxinos, G. & Kayalioglu, G. *The Spinal Cord*. (Academic Press, 2009). doi:10.1016/B978-0-12-801462-2.00001-1
9. Felten, D. L., O'Banion, M. K. & Maida, M. S. Spinal Cord. in *Netter's Atlas of Neuroscience* 233–246 (Elsevier, 2016). doi:10.1016/B978-0-323-26511-9.00010-2
10. Bican, O., Minagar, A. & Pruitt, A. A. The Spinal Cord. A Review of Functional Neuroanatomy. *Neurologic Clinics* **31**, 1–18 (2013).
11. Gofur, E. M. & Singh, P. *Anatomy, Back, Vertebral Canal Blood Supply*. StatPearls (StatPearls Publishing, 2019).
12. Martirosyan, N. L. *et al.* Blood supply and vascular reactivity of the spinal cord under normal and pathological conditions: A review. *J. Neurosurg. Spine* **15**, 238–251 (2011).
13. Rexed, B. The cytoarchitectonic organization of the spinal cord in the cat. *J. Comp. Neurol.* **96**, 415–495 (1952).
14. Heise, C. & Kayalioglu, G. Cytoarchitecture of the Spinal Cord. in *The Spinal Cord* 64–93 (Elsevier Ltd, 2009). doi:10.1016/B978-0-12-374247-6.50010-9
15. Tracey, D. Ascending and Descending Pathways in the Spinal Cord. in *The Rat Nervous System: Fourth Edition* 149–164 (Academic Press, 2004).
16. Conta, A. C. & Stelzner, D. J. The Propriospinal System. in *The Spinal Cord* 180–190 (Elsevier Ltd, 2009). doi:10.1016/B978-0-12-374247-6.50016-X
17. Chung, K., Langford, L. A. & Coggeshall, R. E. Primary afferent and propriospinal fibers in the rat dorsal and dorsolateral funiculi. *J. Comp. Neurol.* **263**, 68–75 (1987).
18. Qin, C., Kranenburg, A. & Foreman, R. D. Descending modulation of thoracic visceroreceptive transmission by C 1-C 2 spinal neurons. *Auton. Neurosci. Basic Clin.* **114**, 11–16 (2004).

19. Cazalets, J. R., Borde, M. & Clarac, F. Localization and organization of the central pattern generator for hindlimb locomotion in newborn rat. *J. Neurosci.* **15**, 4943–4951 (1995).
20. Stroman, P. W. *et al.* The current state-of-the-art of spinal cord imaging: Methods HHS Public Access. *Neuroimage* **84**, 1070–1081 (2014).
21. Welniarz, Q., Dusart, I. & Roze, E. The corticospinal tract: Evolution, development, and human disorders. *Dev. Neurobiol.* **77**, 810–829 (2017).
22. Van Middendorp, J. J., Sanchez, G. M. & Burridge, A. L. The Edwin Smith papyrus: a clinical reappraisal of the oldest known document on spinal injuries. (2010). doi:10.1007/s00586-010-1523-6
23. Bickenbach, J., Officer, A., Shakespeare, T., von Groote, P. & World Health Organization. *International perspectives on spinal cord injury : summary.* (2013).
24. James, S. L. *et al.* Global, regional, and national burden of traumatic brain injury and spinal cord injury, 1990–2016: a systematic analysis for the Global Burden of Disease Study 2016. *Lancet Neurol.* **18**, 56–87 (2019).
25. Alizadeh, A., Dyck, S. M. & Karimi-Abdolrezaee, S. Traumatic Spinal Cord Injury: An Overview of Pathophysiology, Models and Acute Injury Mechanisms. *Front. Neurol.* **10**, 1–25 (2019).
26. Brooks, N. P. Central Cord Syndrome. *Neurosurgery Clinics of North America* **28**, 41–47 (2017).
27. Kunam, V. K. *et al.* Incomplete cord syndromes: Clinical and imaging review. *Radiographics* **38**, 1201–1222 (2018).
28. Eckert, M. J. & Martin, M. J. Trauma: Spinal Cord Injury. *Surg. Clin. North Am.* **97**, 1031–1045 (2017).
29. Kang, Y. *et al.* Epidemiology of worldwide spinal cord injury: a literature review. *J. Neurorestoratology* **Volume 6**, 1–9 (2017).
30. Eldahan, K. C. & Rabchevsky, A. G. Autonomic Dysreflexia after Spinal Cord Injury: Systemic Pathophysiology and Methods of Management. *Aut. Neurosci.* **209**, 59–70 (2018).
31. Arnold, P. M. *et al.* Systematic Review Efficacy, Safety, and Timing of Anticoagulant Thromboprophylaxis for the Prevention of Venous Thromboembolism in Patients With Acute Spinal Cord Injury: A Systematic Review. *Glob. Spine J.* **7**, 138–150 (2017).
32. Hou, S. & Rabchevsky, A. G. Autonomic consequences of spinal cord injury. *Compr. Physiol.* **4**, 1419–1453 (2014).
33. Burke, D., Fullen, B. M., Stokes, D. & Lennon, O. Neuropathic pain prevalence following spinal cord injury: A systematic review and meta-analysis. *Eur. J. Pain* **21**, 29–44 (2017).
34. Finnerup, N. B. Neuropathic pain and spasticity: Intricate consequences of spinal cord injury. *Spinal Cord* **55**, 1046–1050 (2017).
35. Regan, M. A. *et al.* A Systematic Review of Therapeutic Interventions for Pressure Ulcers Following Spinal Cord Injury. *Arch Phys Med Rehabil* **90**, 213–231 (2009).
36. Kirshblum, S. C. *et al.* International standards for neurological classification of spinal cord injury (Revised 2011). *Journal of Spinal Cord Medicine* **34**, 535–546 (2011).
37. Frankel, H. L. *et al.* The value of postural reduction in the initial management of closed injuries of the spine with paraplegia and tetraplegia part I. *Paraplegia* **7**, 179–192 (1969).

38. Chehrazi, B., Wagner, F. C., Collins, W. F. & Freeman, D. H. A scale for evaluation of spinal cord injury. *J. Neurosurg.* **54**, 310–315 (1981).
39. John Klohe, K., Green, B. A., Smith, R. S., Adkins, R. H. & MacDonald, A. M. University of miami neuro-spinal index (UMNI): A quantitative method for determining spinal cord function. *Paraplegia* **18**, 331–336 (1980).
40. Bracken, M. B., Webb, S. B. & Wagner, F. C. Classification of the severity of acute spinal cord injury: Implications for management. *Paraplegia* **15**, 319–326 (1978).
41. Roberts, T. T., Leonard, G. R. & Cepela, D. J. Classifications In Brief: American Spinal Injury Association (ASIA) Impairment Scale. *Clin. Orthop. Relat. Res.* **475**, 1499–1504 (2017).
42. Ditunno, J. F., Young, W., Donovan, W. H. & Creasey, G. The International Standards Booklet for Neurological and Functional Classification of Spinal Cord Injury. *Paraplegia* **32**, 70–80 (1994).
43. Walters, B. C. *et al.* Guidelines for the management of acute cervical spine and spinal cord injuries: 2013 update. in *Neurosurgery* **60**, 82–91 (Neurosurgery, 2013).
44. Hauwe, L. van Den, Sundgren, P. C. & Flanders, A. E. Spinal trauma and spinal cord injury. in *Diseases of the Brain, Head and Neck, Spine 2020–2023* 231–240 (Springer, 2020). doi:10.1007/978-3-319-30081-8_21
45. Granger, N. & Carwardine, D. Acute spinal cord injury. Tetraplegia and paraplegia in small animals. *Veterinary Clinics of North America - Small Animal Practice* **44**, 1131–1156 (2014).
46. Brisson, B. A. Intervertebral disc disease in dogs. *Veterinary Clinics of North America - Small Animal Practice* **40**, 829–858 (2010).
47. Partridge, B. & Rossmeis, J. H. Companion animal models of neurological disease. *Journal of Neuroscience Methods* **331**, (2020).
48. Olby, N. J. *et al.* Development of a functional scoring system in dogs with acute spinal cord injuries. *Am. J. Vet. Res.* **62**, 1624–1628 (2001).
49. Levine, G. J. *et al.* Description and repeatability of a newly developed spinal cord injury scale for dogs. *Prev. Vet. Med.* **89**, 121–127 (2009).
50. Griffin, J., Levine, J. & Kerwin, S. Canine Thoracolumbar Invertebral Disk Disease: Pathophysiology, Neurologic Examination, and Emergency Medical Therapy. *Compend Contin Educ Pr. Vet* **31**, E1–E3 (2009).
51. Park, E. H., White, G. A. & Tieber, L. M. Mechanisms of injury and emergency care of acute spinal cord injury in dogs and cats. *Journal of Veterinary Emergency and Critical Care* **22**, 160–178 (2012).
52. Dumont, R. J. *et al.* Acute spinal cord injury, part I: Pathophysiologic mechanisms. *Clin. Neuropharmacol.* **24**, 254–264 (2001).
53. Ek, C. J., Habgood, M. D., Dennis, R., Dziegielewska, K. M. & Mallard, C. Pathological Changes in the White Matter after Spinal Contusion Injury in the Rat. *PLoS One* **7**, 43484 (2012).
54. Hassenjad, Z. *et al.* Oligodendroglioneogenesis and Axon Remyelination after Traumatic Spinal Cord Injuries in Animal Studies: A Systematic Review. *Neuroscience* **402**, 37–50 (2019).
55. David, G. *et al.* Traumatic and nontraumatic spinal cord injury: pathological insights from neuroimaging. *Nature Reviews Neurology* **15**, 718–731 (2019).

56. Mortazavi, M. M. *et al.* The microanatomy of spinal cord injury: A review. *Clin. Anat.* **28**, 27–36 (2015).
57. Kwon, B. K., Tetzlaff, W., Grauer, J. N., Beiner, J. & Vaccaro, A. R. Pathophysiology and pharmacologic treatment of acute spinal cord injury. *Spine J.* **4**, 451–464 (2004).
58. Klauser, C. K., Rodts-Palenik, S. & Martin, J. N. Acute Spinal Cord Injury. *Crit. Care Obstet. Fifth Ed.* **28**, 228–234 (2011).
59. Couillard-Despres, S., Bieler, L. & Vogl, M. Pathophysiology of traumatic spinal cord injury. in *Neurological Aspects of Spinal Cord Injury* 503–528 (Springer International Publishing, 2017). doi:10.1007/978-3-319-46293-6_19
60. Donnelly, D. J. & Popovich, P. G. Inflammation and its role in neuroprotection, axonal regeneration and functional recovery after spinal cord injury. *Exp. Neurol.* **209**, 378–388 (2008).
61. Pineau, I. & Lacroix, S. Proinflammatory cytokine synthesis in the injured mouse spinal cord: Multiphasic expression pattern and identification of the cell types involved. *J. Comp. Neurol.* **500**, 267–285 (2007).
62. Fernández, M. *et al.* Possible Strategies to Optimize a Biomarker Discovery Approach to Correlate with Neurological Outcome in Patients with Spinal Cord Injury: A Pilot Study. *J. Neurotrauma* **37**, 431–440 (2020).
63. Lewén, A., Matz, P. & Chan, P. H. Free radical pathways in CNS injury. *Journal of Neurotrauma* **17**, 871–890 (2000).
64. Hall, E. D., Wang, J. A., Bosken, J. M. & Singh, I. N. Lipid peroxidation in brain or spinal cord mitochondria after injury. *J. Bioenerg. Biomembr.* **48**, 169–174 (2016).
65. Springer, J. E. *et al.* 4-Hydroxynonenal, a lipid peroxidation product, rapidly accumulates following traumatic spinal cord injury and inhibits glutamate uptake. *J. Neurochem.* **68**, 2469–2476 (1997).
66. Xiong, Y., Rabchevsky, A. G. & Hall, E. D. Role of peroxynitrite in secondary oxidative damage after spinal cord injury. *J. Neurochem.* **100**, 639–649 (2007).
67. Osellame, L. D., Blacker, T. S. & Duchen, M. R. Cellular and molecular mechanisms of mitochondrial function. *Best Practice and Research: Clinical Endocrinology and Metabolism* **26**, 711–723 (2012).
68. Nicholls, D. G. & Budd, S. L. Mitochondria and neuronal survival. *Physiological Reviews* **80**, 315–360 (2000).
69. Duchen, M. R. Ca²⁺-dependent changes in the mitochondrial energetics in single dissociated mouse sensory neurons. *Biochem. J.* **283**, 41–50 (1992).
70. Sullivan, P. G., Rabchevsky, A. G., Waldmeier, P. C. & Springer, J. E. Mitochondrial permeability transition in CNS trauma: Cause or effect of neuronal cell death? in *Journal of Neuroscience Research* **79**, 231–239 (J Neurosci Res, 2005).
71. Pivovarova, N. B. & Andrews, S. B. Calcium-dependent mitochondrial function and dysfunction in neurons: Minireview. *FEBS Journal* **277**, 3622–3636 (2010).
72. Duchen, M. R. Mitochondria, calcium-dependent neuronal death and neurodegenerative disease. *Pflügers Archiv European Journal of Physiology* **464**, 111–121 (2012).
73. Baldassarro, V. A., Marchesini, A., Giardino, L. & Calzà, L. PARP activity and inhibition in fetal and adult oligodendrocyte precursor cells: Effect on cell survival and differentiation. *Stem Cell Res.* **22**,

54–60 (2017).

74. Baldassarro, V. A. *et al.* Cell death in pure-neuronal and neuron-astrocyte mixed primary culture subjected to oxygen-glucose deprivation: The contribution of poly(ADP-ribose) polymerases and caspases. *Microchem. J.* **136**, 215–222 (2018).
75. Kahle, K. T. *et al.* Molecular mechanisms of ischemic cerebral edema: Role of electroneutral ion transport. *Physiology* **24**, 257–265 (2009).
76. Wrathall, J. R., Teng, Y. D. & Choiniere, D. Amelioration of functional deficits from spinal cord trauma with systemically administered NBQX, an antagonist of non-N-methyl-D-aspartate receptors. *Exp. Neurol.* **137**, 119–126 (1996).
77. Panter, S. S., Yum, S. W. & Faden, A. I. Alteration in extracellular amino acids after traumatic spinal cord injury. *Ann. Neurol.* **27**, 96–99 (1990).
78. Farooque, M., Hillered, L., Holtz, A. & Olsson, Y. Changes of extracellular levels of amino acids after graded compression trauma to the spinal cord: An experimental study in the rat using microdialysis. *J. Neurotrauma* **13**, 537–548 (1996).
79. Káradóttir, R. & Attwell, D. Neurotransmitter receptors in the life and death of oligodendrocytes. *Neuroscience* **145**, 1426–1438 (2007).
80. Verkhratsky, A. & Steinhäuser, C. Ion channels in glial cells. *Brain Research Reviews* **32**, 380–412 (2000).
81. Liu, D., Xu, G. Y., Pan, E. & McAdoo, D. J. Neurotoxicity of glutamate at the concentration released upon spinal cord injury. *Neuroscience* **93**, 1383–1389 (1999).
82. Olney, J. W., Ho, L., Rhee, V. & Degubareff, T. Neurotoxic Effects of Glutamate. *New England Journal of Medicine* **289**, 1374–1375 (1973).
83. Epstein, F. H., Lipton, S. A. & Rosenberg, P. A. Excitatory amino acids as a final common pathway for neurologic disorders. *New England Journal of Medicine* **330**, 613–622 (1994).
84. Schanne, F. A. X., Kane, A. B., Young, E. E. & Farber, J. L. Calcium dependence of toxic cell death: A final common pathway. *Science (80-)*. **206**, 700–702 (1979).
85. Cunha, M. I. *et al.* Pro-inflammatory activation following demyelination is required for myelin clearance and oligodendrogenesis. *J. Exp. Med.* **217**, (2020).
86. Sun, X. *et al.* Multiple organ dysfunction and systemic inflammation after spinal cord injury: A complex relationship. *Journal of Neuroinflammation* **13**, (2016).
87. Schnell, L. Acute inflammatory responses to mechanical lesions in the CNS: Differences between brain and spinal cord. *Eur. J. Neurosci.* **11**, 3648–3658 (1999).
88. Gadani, S. P., Walsh, J. T., Lukens, J. R. & Kipnis, J. Dealing with Danger in the CNS: The Response of the Immune System to Injury. *Neuron* **87**, 47–62 (2015).
89. Kwon, B. K. *et al.* Cerebrospinal fluid biomarkers to stratify injury severity and predict outcome in human traumatic spinal cord injury. *J. Neurotrauma* **34**, 567–580 (2017).
90. Zhang, N., Yin, Y., Xu, S. J., Wu, Y. P. & Chen, W. S. Inflammation & apoptosis in spinal cord injury. *Indian Journal of Medical Research* **135**, 287–296 (2012).
91. David, S. & Kroner, A. Repertoire of microglial and macrophage responses after spinal cord injury.

Nature Reviews Neuroscience **12**, 388–399 (2011).

92. Kroner, A. & Rosas Almanza, J. Role of microglia in spinal cord injury. *Neuroscience Letters* **709**, 134370 (2019).
93. Davalos, D. *et al.* ATP mediates rapid microglial response to local brain injury in vivo. *Nat. Neurosci.* **8**, 752–758 (2005).
94. Probert, L. *et al.* *TNFR1 signalling is critical for the development of demyelination and the limitation of T-cell responses during immune-mediated CNS disease.* *Brain* **123**, (2000).
95. Ferguson, A. R. *et al.* Cell death after spinal cord injury is exacerbated by rapid TNF α -induced trafficking of GluR2-lacking AMPARs to the plasma membrane. *J. Neurosci.* **28**, 11391–11400 (2008).
96. Vanegas, H. & Schaible, H. G. Prostaglandins and cyclooxygenases in the spinal cord. *Progress in Neurobiology* **64**, 327–363 (2001).
97. DuBois, R. N. *et al.* Cyclooxygenase in biology and disease. *FASEB J.* **12**, 1063–1073 (1998).
98. Resnick, D. K., Graham, S. H., Dixon, C. E. & Marion, D. W. Role of cyclooxygenase 2 in acute spinal cord injury. *J. Neurotrauma* **15**, 1005–1013 (1998).
99. Jones, T., McDaniel, E. & Popovich, P. Inflammatory-Mediated Injury and Repair in the Traumatically Injured Spinal Cord. *Curr. Pharm. Des.* **11**, 1223–1236 (2005).
100. Taoka, Y. *et al.* Role of neutrophils in spinal cord injury in the rat. *Neuroscience* **79**, 1177–1182 (1997).
101. Neirinckx, V. *et al.* Neutrophil contribution to spinal cord injury and repair. *Journal of Neuroinflammation* **11**, (2014).
102. Pineau, I., Sun, L., Bastien, D. & Lacroix, S. Astrocytes initiate inflammation in the injured mouse spinal cord by promoting the entry of neutrophils and inflammatory monocytes in an IL-1 receptor/MyD88-dependent fashion. *Brain. Behav. Immun.* **24**, 540–553 (2010).
103. Stirling, D. P., Liu, S., Kubes, P. & Yong, V. W. Depletion of Ly6G/Gr-1 leukocytes after spinal cord injury in mice alters wound healing and worsens neurological outcome. *J. Neurosci.* **29**, 753–764 (2009).
104. Popovich, P. G., Wei, P. & Stokes, B. T. Cellular inflammatory response after spinal cord injury in Sprague-Dawley and Lewis rats. *J. Comp. Neurol.* **377**, (1997).
105. Greenhalgh, A. D. & David, S. Differences in the phagocytic response of microglia and peripheral macrophages after spinal cord Injury and its effects on cell death. *J. Neurosci.* **34**, 6316–6322 (2014).
106. Prüss, H. *et al.* Non-resolving aspects of acute inflammation after spinal cord injury (SCI): Indices and resolution plateau. *Brain Pathol.* **21**, 652–660 (2011).
107. Greenhalgh, A. D. *et al.* Peripherally derived macrophages modulate microglial function to reduce inflammation after CNS injury. *PLoS Biol.* **16**, (2018).
108. Garcia, E., Aguilar-Cevallos, J., Silva-Garcia, R. & Ibarra, A. Cytokine and Growth Factor Activation In Vivo and In Vitro after Spinal Cord Injury. (2016). doi:10.1155/2016/9476020
109. Liddelow, S. A. & Barres, B. A. Review Reactive Astrocytes: Production, Function, and Therapeutic Potential. *Immunity* **46**, 957–967 (2017).

110. Williams, A. E. *Immunology*. (John Wiley & Sons, Ltd, 2011). doi:10.1002/9781119998648
111. Ankeny, D. P., Lucin, K. M., Sanders, V. M., McGaughy, V. M. & Popovich, P. G. Spinal cord injury triggers systemic autoimmunity: Evidence for chronic B lymphocyte activation and lupus-like autoantibody synthesis. *J. Neurochem.* **99**, 1073–1087 (2006).
112. Walsh, J. T. *et al.* Regulatory T Cells in Central Nervous System Injury: A Double-Edged Sword. *J. Immunol.* **193**, 5013–5022 (2014).
113. Gensel, J. C. & Zhang, B. Macrophage activation and its role in repair and pathology after spinal cord injury. *Brain Res.* **1619**, 1–11 (2015).
114. Bellver-Landete, V. *et al.* Microglia are an essential component of the neuroprotective scar that forms after spinal cord injury. *Nat. Commun.* **10**, 518–536 (2019).
115. Kigerl, K. A. *et al.* Identification of two distinct macrophage subsets with divergent effects causing either neurotoxicity or regeneration in the injured mouse spinal cord. *J. Neurosci.* **29**, 13435–13444 (2009).
116. Hata, K. *et al.* RGMa inhibition promotes axonal growth and recovery after spinal cord injury. *J. Cell Biol.* **173**, 47–58 (2006).
117. Horn, K. P., Busch, S. A., Hawthorne, A. L., Van Rooijen, N. & Silver, J. Another barrier to regeneration in the CNS: Activated macrophages induce extensive retraction of dystrophic axons through direct physical interactions. *J. Neurosci.* **28**, 9330–9341 (2008).
118. Busch, S. A., Horn, K. P., Silver, D. J. & Silver, J. Overcoming macrophage-mediated axonal dieback following CNS injury. *J. Neurosci.* **29**, 9967–9976 (2009).
119. Arandjelovic, S. & Ravichandran, K. S. Phagocytosis of apoptotic cells in homeostasis. *Nature Immunology* **16**, 907–917 (2015).
120. Neumann, H., Kotter, M. R. & Franklin, R. J. M. Debris clearance by microglia: an essential link between degeneration and regeneration. *Brain* **132**, 288–295 (2009).
121. Broux, B. *et al.* Phagocytosis in the Brain: Homeostasis and Disease. *Front. Immunol.* | www.frontiersin.org **1**, (2019).
122. David, S., Greenhalgh, A. D. & Kroner, A. Macrophage and microglial plasticity in the injured spinal cord. *Neuroscience* **307**, 311–318 (2015).
123. Greenhalgh, A. D. & David, S. Neurobiology of Disease Differences in the Phagocytic Response of Microglia and Peripheral Macrophages after Spinal Cord Injury and Its Effects on Cell Death. (2014). doi:10.1523/JNEUROSCI.4912-13.2014
124. Brown, G. C. & Neher, J. J. *Microglial phagocytosis of live neurons*. *Nature Publishing Group* (2014). doi:10.1038/nrn3710
125. Emery, E. *et al.* Apoptosis after traumatic human spinal cord injury. *J. Neurosurg.* **89**, 911–920 (1998).
126. Crowe, M. J., Bresnahan, J. C., Shuman, S. L., Masters, J. N. & Beattie, M. S. Apoptosis and delayed degeneration after spinal cord injury in rats and monkeys. *Nat. Med.* **3**, 73–76 (1997).
127. Green, D. R. & Llambi, F. Cell Death Signaling. *Cold Spring Harb. Perspect. Biol.* **7**, 1–24 (2015).
128. Fan, H. *et al.* Reactive astrocytes undergo M1 microglia/macrophages-induced necroptosis in spinal

- cord injury. *Mol. Neurodegener.* **11**, 81–89 (2016).
129. Fan, H. *et al.* Quercetin prevents necroptosis of oligodendrocytes by inhibiting macrophages/microglia polarization to M1 phenotype after spinal cord injury in rats. *J. Neuroinflammation* **16**, 1–15 (2019).
 130. Liu, M. *et al.* Necroptosis, a novel type of programmed cell death, contributes to early neural cells damage after spinal cord injury in adult mice. *J. Spinal Cord Med.* **38**, 745–753 (2015).
 131. Pasparakis, M. & Vandenabeele, P. Necroptosis and its role in inflammation. *Nature* **517**, 311–320 (2015).
 132. Abbaszadeh, F., Fakhri, S. & Khan, H. Targeting apoptosis and autophagy following spinal cord injury: Therapeutic approaches to polyphenols and candidate phytochemicals. *Pharmacological Research* **160**, (2020).
 133. McTigue, D. M., Wei, P. & Stokes, B. T. Proliferation of NG2-positive cells and altered oligodendrocyte numbers in the contused rat spinal cord. *J. Neurosci.* **21**, 3392–3400 (2001).
 134. Liu, X. Z. *et al.* Neuronal and glial apoptosis after traumatic spinal cord injury. *J. Neurosci.* **17**, 5395–5406 (1997).
 135. Casha, S., Yu, W. R. & Fehlings, M. G. Oligodendroglial apoptosis occurs along degenerating axons and is associated with FAS and p75 expression following spinal cord injury in the rat. *Neuroscience* **103**, 203–218 (2001).
 136. Wang, J. T., Medress, Z. A. & Barres, B. A. Axon degeneration: Molecular mechanisms of a self-destruction pathway. *Journal of Cell Biology* **196**, 7–18 (2012).
 137. Williams, P. R. *et al.* A recoverable state of axon injury persists for hours after spinal cord contusion in vivo. *Nat. Commun.* **5**, (2014).
 138. Beirowski, B. *et al.* The progressive nature of Wallerian degeneration in wild-type and slow Wallerian degeneration (Wlds) nerves. *BMC Neuroscience* **6**, (2005).
 139. Chaudhry, V. & Cornblath, D. R. Wallerian degeneration in human nerves: Serial electrophysiological studies. *Muscle Nerve* **15**, 687–693 (1992).
 140. Fujita, Y. & Yamashita, T. Axon growth inhibition by RhoA/ROCK in the central nervous system. *Front. Neurosci.* **8**, 1–12 (2014).
 141. Sofroniew, M. V. Dissecting spinal cord regeneration perspective. *Nature* **557**, 343–350 (2018).
 142. Hagg, T. & Oudega, M. Degenerative and spontaneous regenerative processes after spinal cord injury. *Journal of Neurotrauma* **23**, 264–280 (2006).
 143. Pelvig, D. P., Pakkenberg, H., Stark, A. K. & Pakkenberg, B. Neocortical glial cell numbers in human brains. *Neurobiol. Aging* **29**, 1754–1762 (2008).
 144. Sofroniew, M. V. Molecular dissection of reactive astrogliosis and glial scar formation. *Trends Neurosci.* **32**, 638–647 (2009).
 145. Sofroniew, M. V. Multiple roles for astrocytes as effectors of cytokines and inflammatory mediators. *Neuroscientist* **20**, 160–172 (2014).
 146. Sofroniew, M. V. Astrogliosis. *Cold Spring Harb. Perspect. Biol.* **7**, (2015).

147. Anderson, M. A. *et al.* Astrocyte scar formation aids central nervous system axon regeneration. *Nature* **000**, 1–20 (2016).
148. Colombo, E. & Farina, C. Astrocytes: Key Regulators of Neuroinflammation. *Trends in Immunology* **37**, 608–620 (2016).
149. Cekanaviciute, E. & Buckwalter, M. S. Astrocytes: Integrative Regulators of Neuroinflammation in Stroke and Other Neurological Diseases. *Neurotherapeutics* **13**, 685–701 (2016).
150. Bradbury, E. J. & Burnside, E. R. Moving beyond the glial scar for spinal cord repair. *Nat. Commun.* **10**, 3879–3894 (2019).
151. Hara, M. *et al.* Interaction of reactive astrocytes with type I collagen induces astrocytic scar formation through the integrin-N-cadherin pathway after spinal cord injury. *Nat. Med.* **23**, 818–828 (2017).
152. Herrmann, J. E. *et al.* STAT3 is a critical regulator of astrogliosis and scar formation after spinal cord injury. *J. Neurosci.* **28**, 7231–7243 (2008).
153. Wanner, I. B. *et al.* Glial scar borders are formed by newly proliferated, elongated astrocytes that interact to corral inflammatory and fibrotic cells via STAT3-dependent mechanisms after spinal cord injury. *J. Neurosci.* **33**, 12870–12886 (2013).
154. Soderblom, C. *et al.* Perivascular fibroblasts form the fibrotic scar after contusive spinal cord injury. *J. Neurosci.* **33**, 13882–13887 (2013).
155. Filous, A. R. *et al.* Entrapment via synaptic-like connections between NG2 proteoglycan + cells and dystrophic axons in the lesion plays a role in regeneration failure after spinal cord injury. *J. Neurosci.* **34**, 16369–16384 (2014).
156. Hackett, A. R. *et al.* STAT3 and SOCS3 regulate NG2 cell proliferation and differentiation after contusive spinal cord injury. *Neurobiol. Dis.* **89**, 10–22 (2016).
157. Gaudet, A. D. & Popovich, P. G. Extracellular matrix regulation of inflammation in the healthy and injured spinal cord. *Experimental Neurology* **258**, 24–34 (2014).
158. Haggerty, A. E., Marlow, M. M. & Oudega, M. Extracellular matrix components as therapeutics for spinal cord injury. *Neuroscience Letters* **652**, 50–55 (2017).
159. Rowlands, D., Sugahara, K. & Kwok, J. C. F. Glycosaminoglycans and glycomimetics in the central nervous system. *Molecules* **20**, 3527–3548 (2015).
160. Harlow, D. E. & Macklin, W. B. Inhibitors of myelination: ECM changes, CSPGs and PTPs. *Experimental Neurology* **251**, 39–46 (2014).
161. Cooper, J. G. *et al.* Spinal Cord Injury Results in Chronic Mechanical Stiffening. *J. Neurotrauma* **37**, 494–506 (2020).
162. Totoiu, M. O. & Keirstead, H. S. Spinal cord injury is accompanied by chronic progressive demyelination. *J. Comp. Neurol.* **486**, 373–383 (2005).
163. Xu, G. Y., Liu, S., Hughes, M. G. & McAdoo, D. J. Glutamate-induced losses of oligodendrocytes and neurons and activation of caspase-3 in the rat spinal cord. *Neuroscience* **153**, 1034–1047 (2008).
164. Pukos, N., Goodus, M. T., Sahinkaya, F. R. & McTigue, D. M. Myelin status and oligodendrocyte lineage cells over time after spinal cord injury: What do we know and what still needs to be unwrapped? HHS Public Access. *Glia* **67**, 2178–2202 (2019).

165. Baldassarro, V. A., Marchesini, A., Giardino, L. & Calzà, L. Differential effects of glucose deprivation on the survival of fetal versus adult neural stem cells-derived oligodendrocyte precursor cells. *Glia* **68**, 898–917 (2020).
166. James, G. & Butt, A. M. P2Y and P2X purinoceptor mediated Ca²⁺ signalling in glial cell pathology in the central nervous system. *Eur. J. Pharmacol.* **447**, 247–260 (2002).
167. Wang, Y. *et al.* Astrocytes from the Contused Spinal Cord Inhibit Oligodendrocyte Differentiation of Adult Oligodendrocyte Precursor Cells by Increasing the Expression of Bone Morphogenetic Proteins. *J. Neurosci.* **31**, 6053–6058 (2011).
168. Horky, L. L., Galimi, F., Gage, F. H. & Horner, P. J. Fate of Endogenous Stem/Progenitor Cells Following Spinal Cord Injury. *J. Comp. Neurol.* **498**, 525–538 (2006).
169. Shuman, S. L., Bresnahan, J. C. & Beattie, M. S. Apoptosis of microglia and oligodendrocytes after spinal cord contusion in rats. *J. Neurosci. Res.* **50**, (1997).
170. Plemel, J. R. *et al.* Remyelination after spinal cord injury: Is it a target for repair? *Progress in Neurobiology* **117**, 54–72 (2014).
171. Namjoo, Z. *et al.* Targeting axonal degeneration and demyelination using combination administration of 17 β -estradiol and Schwann cells in the rat model of spinal cord injury. *J. Cell. Biochem.* **119**, 10195–10203 (2018).
172. Wu, B. & Ren, X. Promoting axonal myelination for improving neurological recovery in spinal cord injury. *Journal of Neurotrauma* **26**, 1847–1856 (2009).
173. Kuhn, S., Gritti, L., Crooks, D. & Dombrowski, Y. Oligodendrocytes in Development, Myelin Generation and Beyond. *Cells* **8**, (2019).
174. Alizadeh, A., Karimi-Abdolrezaee, S., Alizadeh, A. & Karimi-Abdolrezaee, S. Microenvironmental regulation of oligodendrocyte replacement and remyelination in spinal cord injury. *J. Physiol.* **594**, 3539–3552 (2016).
175. Duncan, G. J. *et al.* The fate and function of oligodendrocyte progenitor cells after traumatic spinal cord injury. *Glia* **68**, 227–245 (2020).
176. Alizadeh, A., Santhosh, K. T., Kataria, H., Gounni, A. S. & Karimi-Abdolrezaee, S. Neuregulin-1 elicits a regulatory immune response following traumatic spinal cord injury. *J. Neuroinflammation* **15**, (2018).
177. Fernández, M., Paradisi, M., Del Vecchio, G., Giardino, L. & Calzà, L. Thyroid hormone induces glial lineage of primary neurospheres derived from non-pathological and pathological rat brain: implications for remyelination-enhancing therapies. *Int. J. Dev. Neurosci.* **27**, 769–778 (2009).
178. Blesch, A. & Tuszynski, M. H. Spinal cord injury: plasticity, regeneration and the challenge of translational drug development. *Trends in Neurosciences* **32**, 41–47 (2009).
179. Fan, H. *et al.* Reactive astrocytes undergo M1 microglia/macrophages-induced necroptosis in spinal cord injury. *Mol. Neurodegener.* **11**, (2016).
180. Anderberg, L., Aldskogius, H. & Holtz, A. Spinal cord injury - Scientific challenges for the unknown future. *Ups. J. Med. Sci.* **112**, 259–288 (2007).
181. Hill, M. D. & Hachinski, V. Stroke treatment: Time is brain. *Lancet* **352**, 10–14 (1998).
182. Badhiwala, J. H., Ahuja, C. S. & Fehlings, M. G. Time is spine: A review of translational advances in

spinal cord injury. *J. Neurosurg. Spine* **30**, 1–18 (2019).

183. Furlan, J. C., Noonan, V., Cadotte, D. W. & Fehlings, M. G. Timing of Decompressive Surgery of Spinal Cord after Traumatic Spinal Cord Injury: An Evidence-Based Examination of Pre-Clinical and Clinical Studies. *J. Neurotrauma* **28**, 1371–1399 (2011).
184. Fehlings, M. G. *et al.* Early versus Delayed Decompression for Traumatic Cervical Spinal Cord Injury: Results of the Surgical Timing in Acute Spinal Cord Injury Study (STASCIS). *PLoS One* **7**, 1–8 (2012).
185. Hall, E. D. & Braughler, J. M. Effects of intravenous methylprednisolone on spinal cord lipid peroxidation and (Na⁺ + K⁺)-ATPase activity. Dose-response analysis during 1st hour after contusion injury in the cat. *J. Neurosurg.* **57**, 247–253 (1982).
186. Badhiwala, J. H., Wilson, J. R., Kwon, B. K., Casha, S. & Fehlings, M. G. A Review of Clinical Trials in Spinal Cord Injury Including Biomarkers. *Journal of Neurotrauma* **35**, 1906–1917 (2018).
187. Lyons, M. K. *et al.* A Randomized, Controlled Trial of Methylprednisolone or Naloxone in the Treatment of Acute Spinal-Cord Injury. *N. Engl. J. Med.* **323**, 1207–1209 (1990).
188. Hugenholtz, H. *et al.* High-dose methylprednisolone for acute closed spinal cord injury - Only a treatment option. *Can. J. Neurol. Sci.* **29**, 227–235 (2002).
189. Yrjänheikki, J., Keinänen, R., Pellikka, M., Hökfelt, T. & Koistinaho, J. Tetracyclines inhibit microglial activation and are neuroprotective in global brain ischemia. *Proc. Natl. Acad. Sci. U. S. A.* **95**, 15769–15774 (1998).
190. Casha, S. *et al.* Results of a phase II placebo-controlled randomized trial of minocycline in acute spinal cord injury. *Brain* **135**, 1224–1236 (2012).
191. Kucher, K. *et al.* First-in-man intrathecal application of neurite growth-promoting anti-nogo- a antibodies in acute spinal cord injury. *Neurorehabil. Neural Repair* **32**, 578–589 (2018).
192. Freund, P. *et al.* Anti-Nogo-A antibody treatment enhances sprouting of corticospinal axons rostral to a unilateral cervical spinal cord lesion in adult macaque monkey. *J. Comp. Neurol.* **502**, 644–659 (2007).
193. Chen, M. S. *et al.* Nogo-A is a myelin-associated neurite outgrowth inhibitor and an antigen for monoclonal antibody IN-1. *Nature* **403**, 434–439 (2000).
194. Grossman, R. G. *et al.* A prospective, multicenter, Phase i matched-comparison group trial of safety, pharmacokinetics, and preliminary efficacy of riluzole in patients with traumatic spinal cord injury. *J. Neurotrauma* **31**, 239–255 (2014).
195. Schwartz, G. & Fehlings, M. G. Evaluation of the neuroprotective effects of sodium channel blockers after spinal cord injury: Improved behavioral and neuroanatomical recovery with riluzole. *J. Neurosurg.* **94**, 245–256 (2001).
196. Agrawal, S. K. & Fehlings, M. G. Mechanisms of secondary injury to spinal cord axons in vitro: Role of Na⁺, Na⁺-K⁺-ATPase, the Na⁺-H⁺ exchanger, and the Na⁺-Ca²⁺ exchanger. *J. Neurosci.* **16**, 545–552 (1996).
197. Lord-Fontaine, S. *et al.* Local inhibition of Rho signaling by cell-permeable recombinant protein BA-210 prevents secondary damage and promotes functional recovery following acute spinal cord injury. *J. Neurotrauma* **25**, 1309–1322 (2008).
198. Fehlings, M. G. *et al.* A phase I/IIa clinical trial of a recombinant Rho protein antagonist in acute

- spinal cord injury. *J. Neurotrauma* **28**, 787–796 (2011).
199. Dubreuil, C. I., Winton, M. J. & McKerracher, L. Rho activation patterns after spinal cord injury and the role of activated Rho in apoptosis in the central nervous system. *J. Cell Biol.* **162**, 233–243 (2003).
 200. Atlas, R. M. One Health: Its Origins and Future. in *Current topics in microbiology and immunology* **365**, 1–13 (Curr Top Microbiol Immunol, 2012).
 201. Ramsey, J. B. G. *et al.* Care of rats with complete high-thoracic spinal cord injury. *J. Neurotrauma* **27**, 1709–22 (2010).
 202. Basso, D. M., Beattie, M. S. & Bresnahan, J. C. A sensitive and reliable locomotor rating scale for open field testing in rats. *J. Neurotrauma* **12**, 1–21 (1995).
 203. Mi, H. *et al.* Protocol Update for large-scale genome and gene function analysis with the PANTHER classification system (v.14.0). *Nat. Protoc.* **14**, 703–721 (2019).
 204. Szklarczyk, D. *et al.* STRING v11: Protein-protein association networks with increased coverage, supporting functional discovery in genome-wide experimental datasets. *Nucleic Acids Res.* **47**, D607–D613 (2019).
 205. Shannon, P. *et al.* Cytoscape: A software Environment for integrated models of biomolecular interaction networks. *Genome Res.* **13**, 2498–2504 (2003).
 206. Enquist, L. W., Husak, P. J., Banfield, B. W. & Smith, G. A. Infection and spread of alphaherpesviruses in the nervous system. *Advances in virus research* **51**, 237–347 (1998).
 207. McCarthy, K. M., Tank, D. W. & Enquist, L. W. Pseudorabies virus infection alters neuronal activity and connectivity in vitro. *PLoS Pathog.* **5**, (2009).
 208. Conn, P. M. *Animal Models for the Study of Human Disease. Animal Models for the Study of Human Disease* (Elsevier Inc., 2013). doi:10.1016/C2011-0-05225-0
 209. Robinson, N. B. *et al.* The current state of animal models in research: A review. *Int. J. Surg.* **72**, 9–13 (2019).
 210. Ericsson, A. C., Crim, M. J. & Franklin, C. L. A brief history of animal modeling. *Mo. Med.* **110**, 201–205 (2013).
 211. Okechukwu, I. B. Introductory Chapter: Animal Models for Human Diseases, a Major Contributor to Modern Medicine. in *Experimental Animal Models of Human Diseases - An Effective Therapeutic Strategy* (InTech, 2018). doi:10.5772/intechopen.70745
 212. Kim, C. K., Adhikari, A. & Deisseroth, K. Integration of optogenetics with complementary methodologies in systems neuroscience. *Nature Reviews Neuroscience* **18**, 222–235 (2017).
 213. Ordaz, J. D., Wu, W. & Xu, X. M. Optogenetics and its application in neural degeneration and regeneration. *Neural Regeneration Research* **12**, 1197–1209 (2017).
 214. Sneddon, L. U., Halsey, L. G. & Bury, N. R. Considering aspects of the 3Rs principles within experimental animal biology. *Journal of Experimental Biology* **220**, 3007–3016 (2017).
 215. Hamers, F. P. T., Koopmans, G. C. & Joosten, E. A. J. CatWalk-Assisted Gait Analysis in the Assessment of Spinal Cord Injury. *J. Neurotrauma* **23**, 537–548 (2006).
 216. Krishna, V. *et al.* A contusion model of severe spinal cord injury in rats. *J. Vis. Exp.* **78**, 1–5 (2013).

217. Mills, C. D., Hains, B. C., Johnson, K. M. & Hulsebosch, C. E. *Strain and Model Differences in Behavioral Outcomes after Spinal Cord Injury in Rat. JOURNAL OF NEUROTRAUMA* **18**, (Mary Ann Liebert, Inc, 2001).
218. Kjell, J., Sandor, K., Josephson, A., Svensson, C. I. & Abrams, M. B. Rat Substrains Differ in the Magnitude of Spontaneous Locomotor Recovery and in the Development of Mechanical Hypersensitivity after Experimental Spinal Cord Injury. *J. Neurotrauma* **30**, 1805–1816 (2013).
219. Chan, W. M., Mohammed, Y., Lee, I. & Pearse, D. D. Effect of Gender on Recovery After Spinal Cord Injury. *Translational Stroke Research* **4**, 447–461 (2013).
220. White, A. & Holmes, G. Investigating neurogenic bowel in experimental spinal cord injury: Where to begin? *Neural Regeneration Research* **14**, 222–226 (2019).
221. de Groat, W. C., Griffiths, D. & Yoshimura, N. Neural control of the lower urinary tract. *Compr. Physiol.* **5**, 327–396 (2015).
222. Scheff, S. W., Rabchevsky, A. G., Fugaccia, I., Main, J. a & Lumpp, J. E. Experimental modeling of spinal cord injury: characterization of a force-defined injury device. *J. Neurotrauma* **20**, 179–193 (2003).
223. Liao, S. *et al.* The 3D characteristics of post-traumatic syringomyelia in a rat model: a propagation-based synchrotron radiation microtomography study. *J. Synchrotron Radiat.* **24**, 1218–1225 (2017).
224. Ward, R. E. *et al.* A characterization of white matter pathology following spinal cord compression injury in the rat. *Neuroscience* **260**, 227–239 (2014).
225. Borrell, J. A., Frost, S., Peterson, J. & Nudo, R. J. A three-dimensional map of the hindlimb motor representation in the lumbar spinal cord in sprague dawley rats HHS Public Access. *J Neural Eng* **14**, 16007 (2017).
226. Nicolopoulos-Stournaras, S. & Iles, J. F. Motor neuron columns in the lumbar spinal cord of the rat. *J. Comp. Neurol.* **217**, 75–85 (1983).